# STUDIES ON THE DEVELOPMENT OF SELECTED CARBON BASED MATERIALS AND THEIR APPLICATION IN WATER TREATMENT

**Thesis submitted for the degree of**

**Doctor of Philosophy (Science) of**

**Jadavpur University**

**by**

**SANDIPAN BHATTACHARYA**

**(Registration Number: SLSBT 1106419)**



**Jadavpur University**

**Kolkata-700032**

**India**

**2023**

# CERTIFICATE FROM THE SUPERVISOR(S)

**This is to certify that the thesis entitled "** Studies on the development of selected carbon based materials and their application in water treatment**" Submitted by Sri / Smt.** Sandipan Bhattacharya **who got his / her name registered on 2nd September, 2019** (Index Number :- 64/19/Life Sc./26) **for the award of Ph. D. (Science) Degree of Jadavpur University, is absolutely based upon his own work under the supervision of** Prof. Papita Das **and** Prof. Abhijit Saha **and that neither this thesis nor any part of it has been submitted for either any degree / diploma or any other academic award anywhere before.**

Papita Das

23/5/2023

Dr. Papita Das

(Signature of the Supervisor(s) date with official seal)

23/5/2023

**THE THESIS IS DEDICATED TO MY PARENTS AND MY LATE GRANDMOTHER.**

**Title of the thesis:**


**STUDIES ON THE DEVELOPMENT OF SELECTED CARBON BASED MATERIALS AND THEIR APPLICATION IN WATER TREATMENT**


**Name, Designation and Institute of the Supervisor/s:**


**1. Name of the Supervisor:**

PROF. DR. PAPITA DAS

**Designation and Institution of the Supervisor :**

Professor, Department of Chemical Engineering, Jadavpur University, Kolkata – 700032, India.

Director, School of Advanced Studies in Industrial Pollution Control Engineering, Jadavpur University, Kolkata – 700032, India.


**2. Name of the Supervisor:**

DR. ABHIJIT SAHA

**Designation and Institution of the Supervisor:**

Former Centre-Director, UGC-DAE Consortium for Scientific Research, Kolkata Centre

Plot 8, Block LB, Sector III, Bidhannagar, Kolkata 700 106

# ACKNOWLEDGEMENT

**'It is God who makes everything possible'- Bhagvad Gita**

Completion of the thesis for the purpose of receiving my Ph.D degree has been the greatest achievement of my life. Though this work bears my name as the author but this has been a collaborative work in every sense of the word. A multitude of people has been responsible behind this work.

First and foremost I would like to express my deepest gratitude towards my supervisors Prof. Papita Das and Dr. Abhijit Saha. Prof. Das was kind enough to provide me with the opportunity to work as a researcher in her laboratory and I was most fortunate to have her as my Ph.D guide. She has guided me in the most diligent manner through each and every aspect of my research work. She was always approachable with any kind of problem pertaining to research work. I consider myself extremely lucky for being able to do my research work under her guidance. I would also like to express my utmost indebtedness towards Dr. Saha. Dr. Saha greatly supported my research efforts and his thoughtful and enlightening suggestions have very much improved my work. Dr. Saha has been most kind in allowing me to have access to his laboratory whenever it was required and he also granted me the permission to use the different advanced, hi-tech instruments that were present in UGC DAE CSR, Kolkata Centre. His guidance greatly facilitated my research work. I would also like to extend my heartiest thanks to Prof. Avijit Bhowal, Chemical Engineering Department, Jadavpur University for his constant support and invaluable suggestion which greatly helped my research work. I am also very much thankful to Dr. Aparna Dutta and Dr. Gautam Pramanik, UGC DAE CSR, Kolkata centre for their guidance and support.

I would also like to convey my thanks to the Department of Chemical Engineering, Jadavpur University. The teachers of the department have been very kind and supportive to me. The technical staff have provided me with assistance regarding various matters of my research. I have done many analysis in the departmental laboratories and would like to take this opportunity to thanks Mr Jyotish Das (UGC SAP lab) and Mr Nayan Mondal (DST Lab) for their co-operation and assistance.

I would also like to extend my gratitude towards the Department of Life Science and Biotechnology for allowing me to get registered for my PhD work.

I am also very much thankful to Prof. Anirudhha Mukhopadhay, Department of Environmental Science, University of Calcutta for his help and support which greatly helped me in my research activities. I would also like to thank Dr. Punarbasu Chaudhuri and Dr. Pritha Bhattacharjee, Department of Environmental Science, University of Calcutta for their support and encouragement.

<div align="right">SANDIPAN BHATTACHARYA</div>

# CONTENT

# ABSTRACT

Trace organic pollutants are emerging as a serious source of water pollution in recent times due to its widespread usage and corresponding ubiquitous presence in the water bodies around the world. Conventional methods of waste water treatment like sewage treatment plants are unable to effectively remove these pollutants from water. Thus alternative methods of water purification have to be investigated. For the present study, four compounds were selected as the target pollutant namely three pharmaceuticals Carbamazepine (CBZ), Naproxen (NPX) and Rantidine (RTN) and one plasticizer Bisphenol A (BPA). The reason for selecting these particular compounds is that they are widely used all over the world in very high quantities. Also, all these chemicals have some reported deleterious effect on the environment, usually on non-target organisms that consumes them directly or indirectly. Therefore, the presence of these chemicals in water can be considered to be a source of considerable concern. In this study various methods have been investigated for removing these pollutants. Firstly the process of adsorption was investigated. Graphene Oxide (GO) was considered to be one of the adsorbents due to its many unique properties like very high surface area, presence of functional groups on its surface, mechanical and chemical stability etc. Other than GO, an activated biochar, synthesized from rice straw and activated by Hummer's method were also used as an adsorbent. The activated biochar was named Activated Rice Straw Biochar (ARSB) and was considered to be a cheaper alternative of GO. Then, the process of photo-catalysis was also investigated with the aim of degrading the pollutants into benign end products. $TiO_2$ was selected as the semiconductor for photo-catalysis due to its chemical stability, non-toxic nature and relative ease of availability. Then it was combined with the previously investigated adsorbents GO and ARSB by a solvo-thermal method in order to increase its adsorption ability, to delay the electron recombination and to decrease the band gap energy. The synthesized nanocomposites were termed GO-$TiO_2$ and ARSB-$TiO_2$ and consisted of nine parts by weight of GO/ARSB and one part by weight of $TiO_2$. The synthesized materials were characterized by different methods like scanning electron microscopy (SEM), Fourier transform infrared spectroscopy (FTIR), X-ray diffractometry (XRD) and Raman spectroscopy. The bands gap of the photo-catalysts were calculated from their Tauc plots. The removal efficacies of the synthesized materials were investigated over a range of experimental parameters by virtue of batch studies and the process was further optimized by the Response Surface Methodology (RSM) study. The ability of the synthesized materials to remove the targeted contaminants by adsorption under a dynamic condition was investigated by a rotating packed bed (RPB) study. From the result of the experiment it was observed that all the synthesized materials were able to remove significant amounts of the targeted pollutants from there aquatic solution, some exhibiting more efficiency than the other. Among the adsorbents GO

exhibited higher efficiency than ARSB. In case of the photo-catalysts, GO-TiO$_2$ exhibited higher efficiency than ARSB-TiO$_2$ although the gap between their efficiency was lesser than that of GO and ARSB. All the synthesized material exhibited reusability up-to a certain degree when treated by the appropriate solution for regeneration. The process of Fenton oxidation was also applied for removing the pollutants followed by adsorption with GO, and this process exhibited very high efficiency. Lastly, the different water treatment techniques investigated so far was tested for the purpose of treating real waste water. Water sample was collected from two places, one being a lake containing water with high pollutant load and the other being the effluent from an industry situated in south of Kolkata, West Bengal. Both the water were treated separately by the different treatment techniques, and among them Fenton oxidation followed by adsorption with GO was most effective for the purpose of reducing the Chemical Oxygen Demand (COD) for the lake water whereas adsorption with GO was able to reduce the COD of the industrial effluent by the highest degree. From the results of the experiment it was observed that, the different treatment techniques investigated in the course of this thesis were able to effectively remove the trace organic pollutants from water and also thus, can be used for the treatment of this kind of pollutants in future. In terms of treating real water, the effectivity of the different treatment processes varied, but still some techniques showed enough efficiency to be considered for future research.

# LIST OF FIGURES

# LIST OF TABLES

# SYMBOLS AND ACRONYMS :-

**List of Symbols:**

A: Arrhenius constant

b: Langmuir constant (mg/L)

$C_o$: Concentration of solvent at time '0' minutes (mg/L)

$C_t$ : Concentration of solvent at time 't' minutes (mg/L)

$C_e$: Equilibrium concentration of pollutant in the solution (mg/L)

g: Gram

$\Delta G°$: Gibbs free energy change (kJ/mole)

$\Delta H°$: Enthalpy of reaction (kJ/mole)

K: Kelvin

$K_f$: Freundlich constant ( mg/g) $(L/g)^{1/n}$

k: Rate constant

$k_1$: Pseudo first order rate constant $(min^{-1})$

$k_2$: Pseudo second order rate constant ( g mg $min^{-1}$)

$k_d$: Equilibrium constant

n: Freundlich adsorption isotherm constant

$q_e$: Equilibrium pollution concentration adsorbent (mg/g)

$q_{max}$: Maximum adsorption capacity (mg/g)

$q_t$: Amount of pollutant adsorbed at time 't' (mg/g)

R: Universal gas constant (8.314 Joule mole Kelvin)

$r^2$: Correlation coefficient

$\Delta S°$: Entropy of reaction (J $mol^{-1}$ $K^{-1}$)

T: Temperature in Kelvin scale

t; Time

$\theta$: Bragg's angle

**<u>List of abbreviation :-</u>**

CBZ: Carbamazepine

NPX: Naproxen

RTN: Rantidine

BPA: Bisphenol A

GO: Graphene Oxide

$TiO_2$: Titanium Dioxide

RPB: Rotating Packed Bed

# CHAPTER 1

# INTRODUCTION

---

## 1.1 GENERAL INTRODUCTION

In recent times, a range of trace pollutants have been detected in the aquatic environment. They are collectively termed as emerging contaminants (EC's) and consists of different groups of chemicals like pharmaceuticals (PHA's), endocrine disputing chemicals (EDC's), nanomaterials, synthesized genetic material, degraded products of EC's etc. (Cheng et al., 2021; Gogoi et al., 2018; Zhou et al., 2020). These EC's are continually released into the environment mainly by anthropogenic activities, due to their wide scale utilization for various purposes (Gogoi et al., 2018). Although these EC's are generally detected in very low concentration (in the ng/L to µg/L range) in the aquatic environment, they can still pose a viable risk to their surrounding environment due to their chemically active and persistent nature (Bhattacharya et al., 2021). Additionally, they are not effectively removed by conventional treatment methods like by wastewater treat plants (WTP) or by sewage treatment plants (STP) (Gogoi et al., 2018). As a consequence of which these EC's pose a serious risk of water contamination in the future times and effective methods for their removal from the aquatic environment should be investigated.

As mentioned above, PHA's form a significant portion of these EC's. PHA's are active material that have been designed to incite a specific response even at a very low concentration (Ebele et al., 2017). As a consequence they can be harmful if they are taken up by a non-target organism even at a very low concentration. PHA's mainly enter the environment as (i) undigested part of the ingested medicine (ii) through improper disposal of expired medicines (iii) as the effluents generated from hospitals and clinics (iv) as the wastes generated from the pharmaceutical industry (Thalla, 2020). As mentioned before, pharmaceuticals are generally present at very low concentration in the environment. At these concentrations, they generally do not pose any acute toxic effect. However, long time exposure to these PHA's can have some chronic effect on some organisms (Ku¨mmerer, 2009). For example it has been observed that pharmaceuticals, typically at concentrations found in sewage treatment plant can have a negative effect on organisms such as Daphnia, Zebrafish, Bacteria and algae etc. (Ku¨mmerer, 2009). Some other toxic effects of pharmaceuticals that has been recorded are, antidepressants affecting the life cycle of clams and fishes , disorienting the learning behaviour of cuttlefish and causing disorder in

the movement of snails (Khan et al., 2017). Sometimes the residues of these PHA's are observed in the downstream of many sewage treatment plants, where they have been detected to cause intersex among different aquatic organisms, leading to their almost extinction (Khan et al., 2017). The pollution caused by the traces of PHA's also affects aquatic flora like green algae, blue green algae and cyanobacteria. Pharmaceuticals like fluoroquinolones have been known to damage the replication of chloroplast due to their homology with bacteria (Khan et al., 2017). Another negative aspect of PHA's as trace pollutants is that, it can cause resistance among the target pathogens. As a consequence of which the pathogen gets accustomed to the PHA's, thereby reducing the efficacy of the pharmaceutical at the intended dosage (Drillia et al., 2005). The widely used PHA's Diclofenac, at concentrations of 5 µg/L-50 µg/L can cause disruption of the normal functioning of gill and kidney and cause immune suppression in some forms of fish (Ebele et al., 2017). In most of the real life scenarios the PHA's are found as mixtures, which in many cases have a greater toxic effect than single compounds. For example a mixture of the two drugs Carbamazepine and Diclofenac can have a greater toxic effect on Daphnia magna than the individual PHA's at the same concentration (Ebele et al., 2017). Also, sometimes the effect of the PHA's can be observed on non-effected organisms. For example the European perch (*Perca fluviatilis*) on being exposed to the 1ow concentration of the psychoactive drug Oxazepam, exhibits an increased feeding rate thereby having a negative influence on its main prey species though the prey species were not (directly) affected by the drug (Richmond et al., 2017). Most of these PHA's which are observed as pollutants are not easily biodegradable (Kanakaraju et al., 2018). This, along with the fact that PHA's are continually being released into the environment due to their wide scale usage makes them pseudo-persistent pollutants (Khan et al., 2017; Ku¨mmerer, 2009). Therefore it can be stated that the pollution caused by PHA's, though generally not resulting in acute toxicity can have a deleterious effect on the environment.

## 1.2 COMPONENTS SELECTED FOR STUDY

For this particular thesis, the focus is on three pharmaceuticals, Carbamazepine (CBZ), Naproxen (NPX) and Rantidine Hydochloride (RTN). All three of these are widely used drugs whose traces have been observed in aquatic environment all across the world (Bhattacharya et al., 2020, 2021; Bhattacharyya et al., 2018; Khan et al., 2017; Ku¨mmerer, 2009; Richmond et al., 2017). As per the Clinical database of USA in the year 2020, NPX was the 91st most used drugs (8,143,638 prescriptions), RTN was the 177th most used drugs (3,260,051 prescription) and CBZ was the 185th most used drugs (2,858,880 prescriptions) (**https://clincalc.com/DrugStats/Top300Drugs.aspx**).

CBZ ($C_{15}H_{12}N_2O$) is a widely consumed antiepileptic drug which is used for treating pain, epilepsy and some mental conditions (Batucan et al., 2022). It was first synthesized in 1960 and it primarily functions by binding to sodium channels and in some cases calcium channels and functions by impeding the action potential and lowering the synaptic transmission. The exact mechanism by virtue of which CBZ

affect the aquatic organism is not clear. However there have been a number of occasions where it has been noted that CBZ affects the aquatic environment (Batucan et al., 2022). The toxic effect of CBZ have been observed in Zebra fish (*Danio rerio*), common carp (*Cyprinus carpio*), Daphnia magna etc. (Ács et al., 2022; Batucan et al., 2022; Tian et al., 2019). CBZ are not effectively removed by traditional methods of waste water treatment like WTP's and STP's and exhibited high level of persistence in the aquatic environment (Batucan et al., 2022; Yongjun Zhang et al., 2008).

RTN ($C_{13}H_{22}N_4O_3S$) is histamine $H_2$ receptor antagonist which is used to reduce the production of acid from the parietal cells of the stomach (Mondal et al., 2015). As mentioned before, it is among the most prescribed drugs in the world. RTN reaches the environment through various sources and had been detected in many aquatic regions of the world (Bergheim et al., 2012). RTN can undergo biotic and abiotic transformation in the environment and can form different types of metabolites. RTN in itself does not possess any acute toxic effects even at very high concentrations (100 mg/L), however its photodegraded by-products can be harmful for many organisms (Isidori et al., 2009). From the work of (Sandip Mondal et al., 2015) RTN was degraded by a photo-simulator and from there two degradation products were observed, they were designated as compound 1 ($C_{12}H_{21}N_3O_2S$) and compound 2 ($C_{12}H_{21}N_3O_2S$). RTN along with these two photo-degraded products were found to exhibit some chronic toxic effect on rotifers and crustaceans, with the compound 1 exhibiting more toxic effect. As a consequence of which, effective methods must be investigated for the proper removal of RTN from the aquatic environment.

NPX ($C_{14}H_{14}O_3$) is a non-steroidal anti-inflammatory drug (NSAID) which is used for the treatment of pain, inflammation or fever. As mentioned above it is one of most widely used medicines in the world. NPX is generally detected at concentrations of ng/L -µg/L in the aquatic environment (Q. Li et al., 2016). Though NPX has a relatively short half-life (27 days), but it is still considered to be pseudo-persistent due to its high rate of usage (Grenni et al., 2013). Naproxen retains its active nature even after being discharged into the environment and can disrupt the health of aquatic animals by impeding with their life style. For example, exposure to 0.1 µg/L of NPX has been known to reduce the egg fertilization of Florida flagfish (Jordonella floridae) over one complete life cycle ( Mondal et al., 2015). NPX also has been known to disrupt the gill tissue of Zebra fish at a concentration of 10 µg/L, thereby signifying that it can cause genetic defect to an aquatic vertebrate at a realistic concentration ( Mondal et al., 2015).

Like PHA's, EDC's are also an important group of emerging pollutants. Chemicals are designated as EDC's if they impersonate the activity of natural hormones such as estrogen, testosterone or thyroid hormone. EDC's are mainly of man-made origin and can be comprised of various classes like synthetic hormones, pharmaceuticals and personal care products (PPCP's), industrial chemicals, pesticides, combustion by-products and surfactants etc. (Chang et al., 2009).

Among the different EDC's, the chemical Bisphenol A (BPA) ($C_{15}H_{16}O_2$) is of special interest due to its high usage and its potency to cause adverse effects. BPA is mainly used as a monomer for the production of polysulfone and polycarbonate polymers, epoxy resins and polyacrylates (Trojanowicz et al., 2020). BPA is also used for the synthesis of flame retardant and thermal papers (Trojanowicz et al., 2020)**.** It has been estimated that 3 million tons of BPA are synthesized on an annual basis and the number is predicted to increase in the future times due to the increment in demand for materials synthesized from BPA (Trojanowicz et al., 2020). Due to its wide scale utilization in plastic manufacturing, BPA are found in plastic food containers, plastic cans, water pipes and bottle caps (Chouhan et al., 2014; Davididou et al., 2018). In the manufactured product, the BPA are joined together by ester bonds which in turn can be hydrolysed at high temperature and at very high and low pH. As a consequence of which, at these extreme conditions the BPA are leached into its surrounding medium, which in many cases is water (Chouhan et al., 2014; Davididou et al., 2018). The conventional WTP's are unable to remove the BPA from the environment. As a result of which, the BPA are ingested by organisms which consumes these contaminated water, including humans ((Chouhan et al., 2014; Davididou et al., 2018). Even low levels of BPA have also been found to cause undesirable biological effects in humans such as problem of reproductive system, and cancer of breast, testes and prostates (Chouhan et al., 2014; Davididou et al., 2018). Along with humans BPA has been found to cause maladies in the reproductive systems of aquatic invertebrates, amphibians, mammals and reptiles (Chouhan et al., 2014).

As has been described above EC's like PHA's and EDC's have a proven degenerative effect on the aquatic environment. Therefore effective methods should be implemented for the efficient removal of these EC's from the aquatic environment. As had been reported in many previous literatures, conventional WTP's and STP's are not sufficient for effectively removing these EC's from water. As a consequence of which alternative, non-conventional tertiary methods of waste water treatment like adsorption and advanced oxidation process (AOP) should be employed for effectively treating these EC's from water (Banerjee et al., 2015a, 2016; Barman et al., 2018; Carabin et al., 2015; P. Das & Das, 2016; Nawaz et al., 2017; Sophia et al., 2016).

## 1.3 VARIOUS TREATMENT PROCEDURES

Carbon based materials have displayed immense promise regarding the removal of EC's from water. Adsorbents that have employed for the removal of these EC's from water have been predominantly carbon based materials like Graphene Oxide (GO), Graphene, Carbon Nanotubes (CNT), Activated Charcoal (AC), biochar etc. (Bhattacharya et al., 2021; Mukherjee et al., 2019; Roy et al., 2018; X. Tan et al., 2015). The same carbonaceous materials can be utilized in the process of photo-catalysis, where they are combined with the semiconductor to form a composite photo-catalyst with greater surface area, lower band gap energy and greater time for electron recombination (Amalraj Appavoo et al., 2014;

Carabin et al., 2015; Fazal et al., 2020; Nawaz et al., 2017; L. Xu et al., 2018; Hanyu Zhang et al., 2017). The adsorbents can also be utilized in combination with some AOP's like Fenton oxidation and ionization radiation in order to remove the intermediate formed during the reaction. Below is a list of methods that can be applied for the removal of trace pollutants like EC's from water and how carbon based materials can be applied in that process :-

Adsorption is a very effective method for the elimination of EC's from there aquatic solution. The main advantages of adsorption are its simplicity in operation and cost effectiveness. Generally no additional energy is necessary for the process of adsorption. Various materials can act as effective adsorbents like activated carbon, graphene oxide, graphene, carbon nanotubes etc. (Tomul et al., 2020).

Graphene oxide (GO) in particular has generated tremendous interest in recent times as an effective form of an adsorbent (Banerjee et al., 2016). GO is mainly synthesized from the oxidation of graphite which can be done by various methods. Hummers and Offeman published a new method in 1958 where they synthesized GO from the oxidation of graphite by sulphuric acid ($H_2SO_4$) and potassium permanganate ($KMnO_4$) (Sophia et al., 2016). This method or some modification of this method is generally used in the synthesis of GO as because it is considered to be safer as compared to the previous methods (Sophia et al., 2016). The main attributes of GO that makes it an effective adsorbents are its high surface area, presence of functional groups on its surface, and good chemical and thermal stability (Bhattacharya et al., 2020).

Like GO, activated carbon and biochar's are also considered to be effective adsorbents (Tan et al., 2015). Biochar's in general have one advantage over GO, that is, it is generally synthesized from a surplus product of organic origin, like an agricultural by-product like rice straw, rice husk, sugarcane bagasse, peanut shell (Bhattacharya et al., 2021; Das et al., 2021; Ganguli et al., 2020; Saha et al., 2021) or an industrial by product like wood shavings or saw dust (Chakraborty & Das, 2021). As a consequence of which the cost of production of biochar is generally lower than that of GO (Bhattacharya et al., 2021; Roy et al., 2018; Tomul et al., 2020). Therefore the synthesis of biochar for the treatment of emerging pollutants can be considered to be advantageous both ways in terms of utilization of an agricultural by-product and the treatment of pollutants in an aquatic ecosystem (X. Tan et al., 2015).

Advanced Oxidation Process (AOP) is also a widely adopted method for the treatment of emerging pollutants from water (Nawaz et al., 2017). One advantage of AOP over adsorption is that, unlike in adsorption where there is only a mass transfer of pollutants from the water to the surface of the adsorbent, in the process of AOP the pollutants are degraded. However, it also happens that sometimes the EC's are degraded to form intermediate products which are more harmful than the parent compounds. Therefore it is more practical to combine the process of AOP with another treatment method that can result in the overall removal of these pollutants from water.

Photo-catalysis is a very effective method of AOP. In this phenomenon, an incident radiation of necessary wavelength is directed on the surface of a semi-conductor. This incident radiation then excites an electron ($e^-$) on the surface of the semi-conductor which then travels to the conduction band from the valance band thereby generating an electron hole ($h^+$) on the surface of the semi-conductor (Yu et al., 2019). This in turn dissociates the water molecule into (OH•) and hydronium ($H^+$) radicals. The free electron on the other hand can reduce the $O_2$ molecules to form $O_2^-$ (Hanyu Zhang et al., 2017). This in turn can split the water molecules to form OH• radical and hydrogen peroxide ($H_2O_2$) molecules (Hassani et al., 2017). Therefore it can be stated that during the process of photo-catalysis, various oxidizing species are generated which can degrade trace organic pollutants like EC's into $CO_2$ and $H_2O$ (Fazal et al., 2020; L. Xu et al., 2018). Different types of semiconductors are used for the purpose of photo-catalysis namely, Titanium Dioxide ($TiO_2$), Zinc Oxide (ZnO), Tin (IV) Oxide ($SnO_2$), Tungsten Trioxide ($WO_3$), Ferric Oxide ($Fe_2O_3$) etc. (H. Kim & Lee, 2014). Among them $TiO_2$ holds a special place of interest due to its chemical stability, non-toxicity and easy availability (Nawaz et al., 2017; Yu et al., 2019; Hanyu Zhang et al., 2017). However, the main drawbacks against the utilization of $TiO_2$ as a semiconductor are the agglomeration of $TiO_2$ nanoparticles among themselves and the quick recombination of $h^+$ and $e^-$, thereby inhibiting the photocatalytic ability of $TiO_2$ (Hanyu Zhang et al., 2017). In order to alleviate this problem, the $TiO_2$ is generally combined with a supporting materials (Yu et al., 2019; Hanyu Zhang et al., 2017). Carbonaceous materials like GO and biochar are a common choice as a supporting material, due to their large surface area, good adsorption capacity and ability to inhibit the recombination of electron-hole pairs (Fazal et al., 2020; Nawaz et al., 2017; Yu et al., 2019). Particularly in case of GO, the functional groups present on its surface acted as an electron absorber, thereby delaying the recombination of the electron on its surface (Yu et al., 2019).

The mechanism by virtue of which various oxidizing species are generated during the reaction of photocatalysis is given as follows:-

$$TiO_2 + Irradiation\ (h\nu) =\ h^+ + e^- \dots\dots\dots\dots\dots\dots\dots\dots\dots\dots\dots\dots\dots\dots\dots\dots\dots\dots\text{(i)}$$

$$h^+ +\ H_2O = \bullet\,OH + H^+ \ \dots\dots\dots\dots\dots\dots\dots\dots\dots\dots\dots\dots\dots\dots\dots\dots\dots\dots\dots\text{(ii)}$$

$$OH^- +\ h^+ = \bullet\,OH\dots\dots\dots\dots\dots\dots\dots\dots\dots\dots\dots\dots\dots\dots\dots\dots\dots\dots\dots\dots..\text{(iii)}$$

$$e^- +\ O_2 =\ O_2{}^- \ \dots\dots\dots\dots\dots\dots\dots\dots\dots\dots\dots\dots\dots\dots\dots\dots\dots\dots\dots\dots..\text{(iv)}$$

$$O_2{}^- +\ H_2O = \bullet\,HO_2 + OH^-\dots\dots\dots\dots\dots\dots\dots\dots\dots\dots\dots\dots\dots\dots\dots\dots..\text{(v)}$$

$$2 \bullet OH_2 =\ O_2 + H_2O_2\dots\dots\dots\dots\dots\dots\dots\dots\dots\dots\dots\dots\dots\dots\dots\dots.....\text{(vi)}$$

$$\bullet OH_2 +\ H_2O\ +\ e^- =\ H_2O_2 +\ OH^-\dots\dots\dots\dots\dots\dots\dots\dots\dots\dots\dots\dots\dots\dots....\text{(vii)}$$
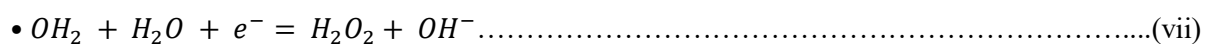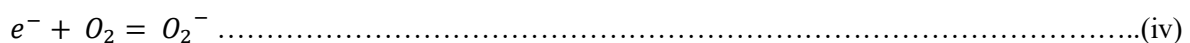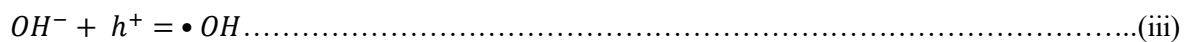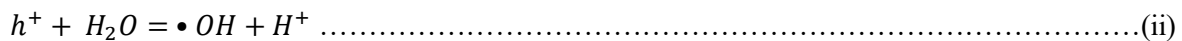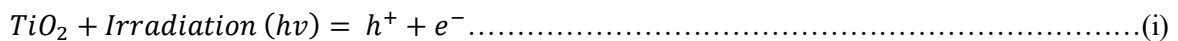
Thus various oxidizing species are generated from the photocatalysis of $H_2O$ by $TiO_2$, which can degrade the organic pollutants into benign products like $CO_2$ and $H_2O$ (Das et al., 2022; Hanyu Zhang et al., 2017; Yu Zhang et al., 2018).

Another common AOP is Fenton Oxidation. Fenton Oxidation was discovered 100 years ago but was utilized for the purpose of the treatment of pollutants about 60 years ago (Neyens & Baeyens, 2003). Fenton oxidation is a homogeneous catalytic reaction where Hydrogen peroxide ($H_2O_2$) is dissociated into •OH (oxidation potential = 2.8 V) in the presence of $Fe^{3+}$ ions which operates as the catalyst. The •OH radicals dissociate the organic pollutants into smaller intermediates and ultimately into benign end products like $CO_2$ and $H_2O$ (Mohammed et al., 2019). The two main mechanisms by which •OH radical decomposes the organic pollutants are (i) hydroxyl addition and (ii) hydrogen abstraction (Mohammed et al., 2019). The hydrogen abstraction is done with unsaturated organic compounds and the hydroxyl addition is done with aromatic compounds or multiple carbon bonds.

The chemical equations describing the Fenton equations is given as follows :-

$$Fe^{2+} + H_2O_2 = Fe^{3+} + OH^{•} + OH^{-}$$...............................................................................(viii)

$$Fe^{3+} + H_2O_2 = Fe^{2+} + OOH^{•} + H^{+}$$.........................................................................(ix)

The rate of equation (viii) (40-80 L/mole sec$^{-1}$) is much higher than that of equation (ix) (9 x 10$^{-7}$) mole per second (Vasquez-Medrano et al., 2018) . Therefore the regeneration of $Fe^{2+}$ becomes rate limiting step of the reaction. Also the Fenton reaction best operates at the lower pH range (3-4), because at the higher pH the $Fe^{2+}$ is precipitated as Fe (OH)$_3$, thereby hindering the Fenton reaction. The concentration and dosage of $H_2O_2$ and $Fe^{2+}$ are also important rate determining factors (Vasquez-Medrano et al., 2018). In the Fenton reaction, the $Fe^{2+}$ ion is mainly supplied in the form of ferrous sulphate (FeSO$_4$) and the $H_2O_2$ is mainly used as a 30-35 % solution. The main advantage of using Fenton reaction for the degradation of EC's is that it is a simple chemical reaction, with relatively cost effective reagents and the rate of the reaction is very rapid (Mohammed et al., 2019). However, studies should be conducted to make the process more economically viable. Also, it's best to combine AOP's like Fenton oxidation with another tertiary mode of treatment so that the intermediates of the reaction can be properly removed from the water. Carbon based adsorbents like GO and biochar can be utilized for adsorbing the intermediates along with the precipitated Fe(OH)$_3$ from the water. The chemically stable nature of the carbon based adsorbents makes them suitable for operating in chemical conditions of the Fenton reaction.

## 1.4 EXPERIMENTAL METHODOLOGY

For this present thesis, the removal of the four above mentioned EC's, i.e., CBZ, NPX, RTN and BPA from their aquatic solution by different carbon based compounds have been investigated. For the

process of adsorption, GO and the activated biochar synthesized from rice straw termed ARSB was used. For the process of photo-catalysis, the semiconductor $TiO_2$ was combined with both GO and ARSB. The removal of the EC's were also investigated with Fenton oxidation reaction. The Fenton reaction was combined with adsorption with GO in order to enhance the removal of the EC's along with the effective removal of the reaction intermediates.

In case of the adsorption study, the optimum conditions under which highest removal was possible were determined by virtue of a batch study. The data were further optimized with Response Surface Methodology (RSM). The data from the batch study of the adsorption was utilized to calculate the adsorption isotherm, adsorption kinetics and adsorption thermodynamics in order to find mechanism of the adsorption reaction, the rate of the adsorption reaction and the nature of the adsorption reaction respectively. In order to evaluate the ability of the adsorbents to remove the EC's under a dynamic condition, a Rotating Packed Bed (RPB) study was performed.

In case of photo-catalysis, the semiconductor $TiO_2$ was chosen for its non-toxic and stable nature along with its ease of availability. The $TiO_2$ was combined with GO and ARSB by a hydrothermal method to form a composite which was utilized in dual role of both an adsorbent and a photo-catalyst. The effectivity of the composite was evaluated under various incident radiations. The radiation which exhibited the highest efficiency was used for further studies. Like in case of adsorption, the experimental conditions under which highest removal of EC's were obtained by the photo-catalyst were determined by virtue of a batch study and further optimization was done with RSM studies.

In case of the Fenton reaction, the source of $Fe^{3+}$ ion were $FeSO_4.7\ H_2O$ and the $H_2O_2$ were added as a 30 % solution.

At the end, the ability of adsorbents and photo-catalyst to treat the real time waste water was also evaluated. Wastewater was collected from two places, namely from a lake with high load of pollutant and the other being the effluent from a pharmaceutical industry situated in Kolkata. The best performing adsorbents and photo-catalyst were used for treating these water and the efficacy of the adsorbent and photo-catalyst were determined by measuring the quantity of COD (mg/L) before and after treatment.

Overall the aim of this thesis was to document the ways by which trace pollutants like EC's that has multiple negative effects on its surroundings can be effectively removed by different methods. The logic behind choosing the methods that were chosen, the process by which the experiments were performed, the outcome of the experiment and the logic behind the result is described in this thesis in detail.

# CHAPTER 2

# LITERATURE REVIEW

---

## 2.1 EMERGING CONTAMINANTS AND THEIR EFFECT ON THE ENVIRONMENT

In the recent period, pollution of the environment by various trace organic pollutants has become a significant nuisance. These pollutants are generally available in the environment in very low concentration (µg/L-ng/L range). However by virtue of their chemically active nature, these trace pollutants have the capacity to impart an adverse effect on organisms even at this trace concentration (Ku¨mmerer, 2009). An important sub-set of these trace pollutants are group of organic trace pollutants termed as "Emerging contaminants" or EC's.

These EC's can be broadly classified into three groups.

　　1.> Cosmetic care items.

　　2.> Pharmaceuticals (PHA's).

　　3.> Endocrine disrupting chemicals (EDC's) (Gogoi et al., 2018).

PHA's are generally released into the environment due to the improper disposal of unused and expired medicine, as undigested part of the human and animal excrement and as effluent from health care facilities and manufacturing plants synthesizing medicines (Thalla, 2020). EDC's are a group of chemicals which can have an adverse effect on human health by altering the physiological functions of the human body by mimicking hormones like estrogen, testosterone and thyroid etc. (H. Chang et al., 2009). EDC's are mainly released into the environment by activities like the discharge of effluents from sewage treatment plants in water, as surface run-off from settlements, road systems and agriculture, direct discharge into water from manufacturing plants, as leachate from mishandling of materials containing EDC's (Burkhardt-Holm, 2010).

In this thesis, emphasis has been given on three PHA's (CBZ, NPX and RTN) and one EDC (BPA). They were chosen by virtue of their wide use, ubiquitous presence and proven adverse effect on the environment.

CBZ ($C_{15}H_{12}N_2O$) is a widely consumed antiepileptic drug which is used for treating pain, epilepsy and some mental conditions (Batucan et al., 2022). It was first synthesized in 1960 and it primarily operates as a sodium chain blocker. CBZ is widely used for the treatment of maladies like seizures, trigeminal neuralgia and mental disorders (Zhang et al., 2008). Among the total CBZ that is consumed, about 72 % is absorbed by the body and the rest of the 28 % is eliminated from the body in the form of faeces (Zhang et al., 2008). CBZ is mainly metabolized in the body by the liver and in the end only about 1 % of the CBZ leaves the body in the unaltered state. CBZ can be termed as a resistant pollutant, which is not entirely degraded even at the modern multistage sewage treatment plants (Batucan et al., 2022). Previous studies have reported a global usage of CBZ at 1.1 kilo-ton. Such substantial usage of CBZ has resulted in its appearance in different sources of water including surface water, ground water, wastewater treatment plants and even drinking water. Therefore, presence of CBZ in different water resources is being considered as an issue of global concern. CBZ reportedly exerts toxic effects on aquatic life including bacteria, algae, invertebrates and fish. The adverse effect of CBZ on the environment have been documented in Zebra fish (*Danio rerio*), common carp (*Cyprinus carpio*), Daphnia magna etc. ((Ács et al., 2022; Batucan et al., 2022; Tian et al., 2019). Permissible limit of CBZ in drinking water sources varies in different countries and is found to be 40 and 100 $\mu g\,L^{-1}$ in Minnesota, U.S.A and Australia respectively. Moreover, use of water containing CBZ for irrigation results in accumulation of the same in soil. The standard concentration of CBZ in soils irrigated using wastewaters has been found to be 0.02–15 $\mu g\,kg^{-1}$. According to the US Food and Drug Administration, an environment assessment should be performed whenever the concentration of the active ingredient of CBZ is equal to or found to exceed 1.0 $\mu g\,L^{-1}$ in aquatic environment. Hence, efficient treatment strategies are required for removal of this pollutant from the aquatic environment (Bhattacharya et al., 2020).

NPX ($C_{14}H_{14}O_3$) is a non-steroidal anti-inflammatory drug (NSAID) which is used for the treatment of pain, inflammation or fever. As mentioned above it is one of most widely used medicines in the world. NPX is generally detected at concentrations of ng/L -μg/L in the aquatic environment (Q. Li et al., 2016). Though NPX has a relatively short half-life (27 days), but it is still considered to be pseudo-persistent due to its high rate of usage (Grenni et al., 2013). Naproxen retains its active nature even after being discharged into the environment and can disrupt the health of aquatic animals by impeding with their life style. For example, exposure to 0.1 μg/L of NPX has been known to reduce the egg fertilization of Florida flagfish (Jordonella floridae) over one complete life cycle (Mondal et al., 2015). NPX also has been known to disrupt the gill tissue of Zebra fish at a concentration of 10 μg/L, thereby signifying that it can cause genetic defect to an aquatic vertebrate at a realistic concentration (Sandip Mondal et al., 2015). The photodegraded by-products of NPX has been found to be more toxic than the original product, with the photodegraded by-product of NPX being harmful to the small aquatic crustaceans like *Ceriodaphnia dubia* and *Daphnia magna* and bacteria's like *Vibrio fischeri*. NPX also had toxic effects

on the two algal species, *Cymbella* and *Scenedesmus quadricauda*, with the toxic effect depending on the concentration and the duration of the exposure (Ding et al., 2017). On being exposed to NPX for a prolonged period, a decrease in the ammonia oxidizing bacteria in the river Tiber was observed (Wojcieszyńska & Guzik, 2020). As a consequence of which, like CBZ it is also necessary to remove NPX from its aqueous solution even if it is present in trace concentrations.
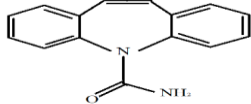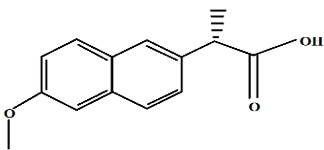
RTN ($C_{13}H_{22}N_4O_3S$) is histamine $H_2$ receptor antagonist which is used to reduce the production of acid from the parietal cells of the stomach (Sandip Mondal et al., 2015). As mentioned before, it is among the most prescribed drugs in the world. RTN reaches the environment through various sources and had been detected in many aquatic regions of the world (Bergheim et al., 2012). RTN can undergo biotic and abiotic transformation in the environment and can form different types of metabolites. RTN in itself does not possess any acute toxic effects even at very high concentrations (100 mg/L), however its photodegraded by-products can be harmful for many organisms (Isidori et al., 2009). From the work of (Sandip Mondal et al., 2015), RTN was degraded by a photo-simulator and from there two degradation products were observed, they were designated as compound 1 ($C_{12}H_{21}N_3O_2S$) and compound 2 ($C_{12}H_{21}N_3O_2S$). RTN along with these two photo-degraded products were found to exhibit some chronic toxic effect on rotifers and crustaceans, with the compound 1 exhibiting more toxic effect. As a consequence of which, effective methods must be investigated for the proper removal of RTN from the aquatic environment.

Like PHA's, EDC's are also an important group of emerging pollutants. Chemicals are designated as EDC's if they impersonate the activity of natural hormones such as estrogen, testosterone or thyroid hormone. EDC's are mainly of man-made origin and can be comprised of various classes like synthetic hormones, pharmaceuticals and personal care products (PPCP's), industrial chemicals, pesticides, combustion by-products and surfactants etc. (H. Chang et al., 2009).

Among the different EDC's, the chemical Bisphenol A (BPA) ($C_{15}H_{16}O_2$) is of special interest due to its high usage and its potency to cause adverse effects. BPA is mainly used as a monomer for the production of polysulfone and polycarbonate polymers, epoxy resins and polyacrylates (Trojanowicz et al., 2020). BPA is also used for the synthesis of flame retardant and thermal papers (Trojanowicz et al., 2020). It has been estimated that 3 million tons of BPA are synthesized on an annual basis and the number is predicted to increase in the future times due to the increment in demand for materials synthesized from BPA (Trojanowicz et al., 2020). Due to its wide scale utilization in plastic manufacturing, BPA are found in plastic food containers, plastic cans, water pipes and bottle caps (Chouhan et al., 2014; Davididou et al., 2018). In the manufactured product, the BPA are joined together by ester bonds which in turn can be hydrolysed at high temperature and at very high and low pH. As a consequence of which, at these extreme conditions the BPA are leached into its surrounding medium, which in many cases is water (Chouhan et al., 2014; Davididou et al., 2018). The conventional WTP's

are unable to remove the BPA from the environment. As a result of which, the BPA are ingested by organisms which consumes these contaminated water, including humans (Chouhan et al., 2014; Davididou et al., 2018). Even low levels of BPA have also been found to cause undesirable biological effects in humans such as problem of reproductive system, and cancer of breast, testes and prostates (Chouhan et al., 2014; Davididou et al., 2018). Along with humans BPA has been found to cause maladies in the reproductive systems of aquatic invertebrates, amphibians, mammals and reptiles (Chouhan et al., 2014). BPA have been found to increase the secretion of hormones like estradiol, progesterone, serum lutenizing hormone and testosterone (Wisniewski et al., 2015). BPA exposure have been known to decrease the sperm count, sexual function and lower fertility in males (Y. Ma et al., 2019). Prenatal exposure to BPA resulted in lower birth weight and lower birth height, organ and neural development in babies (Y. Ma et al., 2019). Exposure to BPA resulted in earlier puberty onset in boys and later puberty onset in girls, thereby reflecting the gender induced effect of BPA (Berger et al., 2019). Also it has been observed, that in case of male offspring in humans, pre-birth exposure of BPA results in anxiety and depression in the male child (Perera et al., 2016). As per one study conducted by (Shu et al., 2018), BPA toxicity results in obesity and type-2 diabetes with insulin resistance. Higher quantity of BPA in urine resulted in higher blood pressure and cardiovascular disease (Shankar & Teppala, 2012). In case of a pregnancy, the level of BPA in serum was positively correlated with preeclampsia  (Y. Ye et al., 2018). BPA can contribute to the formation of non-alcoholic fatty liver disease (NAFLD) and as an enhancer for the onset of allergic diseases like asthma, bronchial hyper-responsiveness and type-1 diabetes (Yu et al., 2019). It has been also found that levels of BPA were associated with some neurodevelopment diseases like autism spectrum disorder (ASD) (Rahbar et al., 2017). BPA has also been observed to be responsible for different types of cancer like cervical cancer and ovarian cancer (Y. Ma et al., 2019).

**Table 2.1**: List of chemicals investigated in this study and their chemical structure.

| Compound | Chemical Formula | Molecular Weight (g/mole) | Structure | Reference |
|---|---|---|---|---|
| CBZ | $C_{15}H_{12}N_2O$ | 236.27 |  | (Khan et al., 2017) |
| NPX | $C_{14}H_{14}O_3$ | 230.26 |  | (Ding et al., 2017) |

| RTN | $C_{13}H_{22}N_4O_3S$ | 314.4 |  | (Bergheim et al., 2012) |
|-----|-----|-----|-----|-----|
| BPA | $C_{15}H_{16}O_2$ | 228.3 |  | (Bhatnagar & Anastopoulos, 2017) |

Therefore, it is very much important to make the necessary arrangements in order to remove the EC's from water at the earliest opportunity. Various methods exists which has been explored for the purpose of removing the EC's from the aquatic environments namely, adsorption, photo-degradation, photo-catalysis, biodegradation, phytoremediation, membrane bioreactor, electrochemical oxidation, Fenton like oxidation, catalytic wet peroxide oxidation, ozonation, sono-catalysis, and biocatalytic degradation etc. (Tomul et al., 2020). Among these methods, the methods that have been selected for the treatment of the EC's in this particular thesis consists of adsorption, photo-catalysis and Fenton oxidation. In a broad sense the processes can be divided into adsorption and AOP. The list of methods along with the materials that have been utilized for treating the designated pollutants is listed below:-

## 2.2 METHODS OF REMEDIATION

### 2.2.1 Adsorption

Adsorption in particular is one of the most effective method due to its simplicity in operation, rapid equilibrium time and cost effective nature (Bhattacharya et al., 2021). There are various adsorbents which are used for the treatment of these EC's from water. Among them carbonaceous adsorbents like Graphene, GO, activated carbon, biochar etc. have gained high popularity due to their mechanical and chemical stability and very high surface area. For treating the above mentioned EC's, two types of adsorbents have been specifically used as reported in this thesis, they are GO and an activated biochar synthesized from rice straw .

#### 2.2.1.1 Graphene Oxide (GO)

GO, are single or multi layered hexagonal sheets of carbon surrounded by oxygen containing functional groups on its side (Tshangana et al., 2021). GO is generally synthesized by the oxidation of graphite. They were first synthesized by Brodie in 1859 in order to find the carbon weight in graphite (Tshangana et al., 2021). Many methods are available for the synthesis of Graphene Oxide, among which the Hummer's method, first published in 1958 is the most popular method (Hummers Jr. & Offeman, 1957). In recent times, there have been renewed interest in the synthesis of GO, due to it being a precursor in

the synthesis of Graphene (Tshangana et al., 2021). The carbon groups in GO are arranged in hexagonal rings to form a honey comb like structure (Tshangana et al., 2021). From this structure of GO, the $sp^2$-hybridized characteristics of GO are born (Tshangana et al., 2021). From the strong oxidation of GO, various functional groups are formed like hydroxyl, epoxyl and carboxyl groups, which lines the surface of GO (Banerjee et al., 2016). The GO consists of 25-30 % of oxygen, which enables it to have a good dispersion in water. The absence of this hydrophilic oxygen functional groups make graphene hydrophobic and the presence of these groups make GO hydrophilic (Banerjee et al., 2016). The electronic properties of GO makes them good adsorbents, enabling them to adsorb organic compounds like EC's by hydrogen bonding, π-π stacking , electrostatic and hydrogen forces (Banerjee et al., 2016). This along with the other properties of GO like very high surface area, good chemical and mechanical stability make them ideal as adsorbents (Bhattacharya et al., 2020) . As such GO have been extensively utilized for treating micro-pollutants from there aquatic solutions.

Banerjee et al., 2016 utilized GO for removing the PHA Ibuprofen from water. Ibuprofen is one of the most utilized group of PHA in the world. The functional groups present on the surface of GO like epoxy, carboxyl and hydroxyl helps in the dispersion of GO in water (Banerjee et al., 2016). These functional groups along with the large surface area of GO resulted in the high removal of the Ibuprofen by GO. As per the results of the paper, the highest removal of Ibuprofen that was observed was 98.17 % and it was obtained at experimental conditions of pH 6, initial concentration of Ibuprofen at 6 mg/L, dosage of GO at 1.00 g/L, solution pH at 6, agitation speed of 180 rotation per minute, temperature of 308 K and contact time of 60 minutes.

 Das & Das, 2016 used GO for removing the PHA RTN from its aquatic solution. The reason for choosing GO as the adsorbent for treating RTN was that, GO had very large surface area, was cost effective, was required in relatively low quantities and was easy to synthesize. Under the optimum conditions (adsorbent dosage 2 g/L, concentration of RTN 10 mg/L, agitation speed 150 rotation per minute (R.P.M), temperature of experimental solution 30°C, experimental time 1 hr) GO was found to be able to remove 99 % of the RTN from its aqueous solution, thereby rendering GO to be an effective adsorbent for the uptake of RTN from its aqueous solution.

Bhattacharya et al., 2020 utilized GO for treating CBZ from its aqueous solution. The reason for choosing GO as the adsorbent was the large surface area and the chemical and thermal stability of GO. GO was able to remove 99 % of the CBZ from its aquatic solution under the experimental conditions of pH 6, adsorbent dosage of 1 g/L and the reaction time of 120 minutes. The adsorption capacity of GO at equilibrium was about 9.2 mg/g. This study reemphasized the point that GO was an efficient adsorbent by virtue of its high surface area and potential to be reused repeatedly without losing its viability.

Bhattacharyyaa et al., 2018 used GO for removing the PHA's RTN and Prednisolone from their aquatic solution. GO was able to effectively remove these two PHA's from their aquatic solution, with the highest removal of RTN being 90.64 % and the highest removal of Prednisolone being 92.68 %. The experimental conditions under which the highest removal of RTN was recorded are initial RTN concentration 10 mg/L, GO dosage of 1 g/L, pH 6, agitation speed of 140 R.P.M, reaction time of 1 hour and temperature of 313 K. The experimental conditions for the highest removal of Prednisolone are initial prednisolone condition 10 mg/L, GO dosage of 2 g/L, pH 6, and agitation speed of 120 R.P.M, reaction time of 1 hour and at a temperature of 313 K. Other than this, the GO also exhibited high level of reusability, thereby making it an effective adsorbent for the purpose of removal of trace pollutants like EC's from water.

Wang et al., 2021 used a composite synthesized by combining GO and ferric oxide ($Fe_2O_3$) by a co-precipitation method. The combination of GO with $Fe_2O_3$ provided the composite with magnetic properties which enabled the effective retrieval of the composite from water after treatment. The GO-$Fe_2O_3$ composite exhibited a removal percentage of 96.4 % of BPA and exhibited a removal efficiency of 11.5 mg/g of BPA from water. The highest removal efficiency that was exhibited by the GO-$Fe_2O_3$ composite was 3293.1 mg/g, which was correspondingly 1.9 and 1.2 times greater than GO and reduced GO respectively. Along with it the composite exhibited higher thermal stability, greater solid/liquid separation performance and greater anti-fouling properties than the original materials. This study demonstrates the attribute of GO to be combined with another material for higher separation ability, all the while maintaining its adsorption ability.

### 2.2.1.2 Biochar

Biochar can be defined as a carbon rich component which is synthesized by high temperature heating of carbon rich compounds (X. Tan et al., 2015). As the name suggests, biochar is mainly synthesized by high temperature treatment of materials of biological origin. A multitude of materials have been utilized for the synthesis of biochar namely, bamboo, Brazilian pepper wood, cattle dung, coconut coir, corn straw, hickory wood, orange peel, rice husk, rice straw, sludge, soybean stover etc. (X. Tan et al., 2015). Due to the relatively low cost of the starting material of biochar (which mainly consists of agricultural waste product or by-products) and straightforward method of synthesis (heating of the biomass at high temperature resulting in the volatilization of the materials as per their stability), the cost of the synthesis of biochar is much less than that of other specialized adsorbents like activated carbon, graphene, GO etc. Moreover, during the synthesis of Biochar, abundant agricultural material are converted into products which is used in the remediation of the environment, thereby resulting in a dual positive outcome (X. Tan et al., 2015). The properties of Biochar which makes them an effective adsorbent are there high surface area, large pore volume availability, high physical strength and chemical stability (Tomul et al., 2020). However, compared to other adsorbents like activated carbon

and GO, un-modified biochar has been shown to exhibit lesser adsorptive ability (Cheng et al., 2021). For example, as per the result of (Hao et al., 2018) the rate of removal of Phenol by biochar was 0.04 g/min whereas the removal of Phenol by activated carbon is 20.575 g/min. Therefore in order to enhance adsorption efficiency of Biochar, it is necessary to activate it by some form. The different methods of the activation of Biochar consist of :-

I.   Chemical Activation of Biochar by :-

a.   Acid-Base Modification

b.   Metal-Metal Oxide Modification

c.   Oxidation

d.   Reduction

II.   Physical Activation of Biochar

a.   Mixing of Biochar with clay

b.   Ball Milling.

Different types of activation have different effects on the surface modification of Biochar. For example, the surface area and pore volume of the synthesized Biochar are supposed to increase by ball-milling method (Cheng et al., 2021). On the other hand, oxygen containing functional groups are incorporated on the surface of the Biochar on being modified by the oxidation method (Goswami et al., 2017). These properties of the biochar make the material more hydrophilic and helps in their greater dispersion and greater adsorption efficiency (Bhattacharya et al., 2021; Goswami et al., 2017).

Ma et al., 2010 utilized activated bamboo charcoal for removing 2,4-dichlorophenol (DCP) from water. Dried strips of moso bamboo (*Phyllostachys heterocycla*) are carbonized in a nitrogenous environment at 850°C for two hours. Followed by this it was cooled down to normal condition. The biochar was then activated by steam at 850°C for 2 hours. Before using, the activated charcoal was further activated by boiling it in distilled water for 2 hours to remove the ash and impurities. Then it was oven dried for 24 hours at 105°C. After that, the material was grounded and was passed through mesh with pore size 0.074 mm followed by which it was stored in a desiccator for future use. The adsorption reaction occurred very quickly and 90 % of the adsorbate were taken up within 5 mins of the start of the reaction (J. Ma et al., 2010). Therefore it can be stated that a chemical like 2,4-DCP with potential toxic effect can be effectively treated with activated Bamboo-charcoal.

In a study conducted by (Tomul et al., 2020), biochar synthesized from peanut shell (termed in the aforementioned paper as Peanut Shell Biochar (PSB)) were utilized to treat NPX from its aqueous solution. The Biochar was synthesized from peanut shells, which were first collected from a local

market after which it was washed at first with tap water, followed by with purified water and then it was dried at 80°C for 24 hours. The dried peanut shells were then ground by a ball mill into uniformly formed powder having a diameter of 0.16 to 0.25 mm. The Biochar were further synthesized by three different methods. In first case, a pure Biochar was synthesized by direct pyrolysis of the peanut shell at 800°C for four hours in a non-circulated air atmosphere. The next set of Biochar was synthesized by first treating the Biochar with water in a Teflon lined autoclave at 190°C for 24 hours. Followed by which the Biochar was pyrolyzed at 800°C for 4 hours in a non-circulated air atmosphere. The third set of Biochar was synthesized by treating the biochar by two cycles of pyrolyzation, during each the Biochar biomass was heated at 800°C for 4 hours in a non-circulated air atmosphere. The three types of Biochar were named 800-PSB, 190-800-PSB and 800-800-PSB respectively. Then in order to elucidate the effect of $\pi$-$\pi$ bonding on the adsorption efficiency of the Biochar, the oxidized biochar were synthesized from these Biochar. Approximately, 0.5 g of the Biochar were added to 100 ml of $H_2O_2$ (35 %) and it was rotated for 24 hours at room temperature. Followed by this the material was washed till it achieved a neutral pH, dried and stored in a desiccator for future application. From the experimental result it was observed that the adsorption ability of the Biochar decreased in the order of 800-800-PSB (324 mg/g) >190-800-PSB (215 mg/g) > 800-PSB (105 mg/g). The micro-pore volume of the adsorbent was the dominant adsorption factor, whereas the $\pi$-$\pi$ interaction, which was supposed to be the dominant form of adsorption mechanism in the oxidized adsorbents, did not play a significant role in the adsorption reaction. As a consequence of which, the oxidized adsorbents was much less effective in the uptake of NPX in comparison to their non-oxidized counterpart.

Naghdi et al., 2019 used a commercially obtained pinewood biochar for eliminating CBZ from aqueous solution. The pinewood biochar was obtained from a commercial vendor. It was synthesized by heating the pine white wood at 525°C +/- 1°C at the rate of 25°C for 20 minutes under atmospheric pressure under a nitrogenous environment. The Biochar was further activated by ball milling technique to convert it into a nano-biochar. Before the ball milling procedure, the biochar was kept in a freezer at -80°C for 24 hour. The ball milling was performed at the agitation speed of 575 rotation per minute for 100 minutes. The corresponding biochar had a particle size of 60 +/- 5 nm and a surface area of 47.25 $m^2$/g. The activated nano-biochar were used to remove very low concentration of CBZ (0.5-25 ppb of CBZ) from the aqueous solution and were able to remove 95 % of CBZ after a period of 3 hours. Thus it can be stated that the pinewood Biochar is an effective adsorbent for the purpose of removing low concentrations of CBZ from its aqueous solution.

Bhattacharya et al., 2021 utilized a biochar synthesized from rice straw and activated it by oxidizing it by following a modified Hummer's method. The **A**ctivated **R**ice **S**traw **B**iochar abbreviated as ARSB, was used for removing NPX from its aqueous solution. A similar product were synthesized by (Goswami et al., 2017) and it was used to remove the dye Crystal Violet from its aqueous solution. First the rice straw was washed with tap water and sundried for a week after which it was cleaned thoroughly

with distilled water for the purpose of removing dirt, dust and any other impurities. The washed rice straw was dried at 80°C for about 48 h for the purpose of removing the moisture. After drying in the oven the rice straw fibres were cut into small pieces. Then the rice straw was heated in an inert atmosphere at high temperature (450 °C) inside a fabricated reactor to form a biochar, which was then homogenised by crushing followed by sieving to get a mixture of uniform particle size (< 50 μm). The biochar thus synthesized was given the name Rice Straw Biomass Biochar (RSBB). Thereafter the RSBB was activated by following a modified Hummer's method. In brief, about 20 mg of the RSBB was mixed with 200 ml of Sulphuric acid ($H_2SO_4$) under continuous stirring. The flask containing the acidic mixture was then transferred to an ice bath after which a fixed amount of KMnO4 was added into this mixture, also under continuous agitation. The whole arrangement was then kept at room temperature for 30 min under rotation. After that, 150 ml of distilled water was slowly added into the mixture, after which it was transferred into an incubator shaker where it was rotated at 45 °C for 3 h. Subsequently, 200 ml of distilled water ($H_2O$) was put inside the reaction mixture followed by 150 ml of 30% Hydrogen Peroxide ($H_2O_2$). After adding the H2O2 the reaction mixture turned yellow thereby denoting the end point of the reaction. The reaction mixture was then placed inside an ultrasonic cleaner (Digital Ultrasonic Cleaner; LMUC-4) for approximately 15 min so that the synthesized ARSB particles attained uniform particle size. After this the ARSB particles was isolated from the suspension by filtration followed by centrifugation and the extracted ARSB particles were then repeatedly washed with distilled water, 30% ethanol ($C_2H_5OH$) and 5% Hydrochloric Acid (HCl) to remove any residual impurities (mainly metallic) from them. Then after sufficient washing when the ARSB had attained neutral pH, they were freeze dried and then stored in an air tight container. The optimized conditions under which the synthesized ARSB exhibited highest removal of NPX was obtained by means of a batch study whereas, the efficacy of the adsorbent to remove NPX under a dynamic condition was determined by virtue of a column study. The highest removal that was obtained was 89.78 % that was obtained at pH 6-7, ARSB dosage 2 g/L, temperature 303 K and NPX concentration. When the concentration was further increased, the removal percentage decreased due to the saturation of the adsorbent surface. In case of the column study, the longest breakthrough times were recorded at highest bed height of 7.62 cm (60 min) and at a NPX concentration of 10 mg/L. Thus it can be concluded that ARSB is an effective adsorbent which could be utilized for the removal of trace pollutants like NPX from their aqueous solution.

In the study conducted by Zhou et al., 2019 a biochar was synthesized from citrus peel and it was combined with GO and $Fe_3O_4$ (Iron Oxide Black) to remove the antibiotics ciprofloxacin and sparfloxacin from water. The addition of GO to the biochar helped to incorporate oxygen containing functional groups which enhanced the dispersion of the Biochar into water along with increasing its adsorption ability. The addition of $Fe_3O_4$ imparts some magnetic properties to the Biochar, so that the materials can be separated out from experimental solution magnetically. The $Fe_2O_3$ was synthesized by

a co-precipitation method. The citrus peel biochar was synthesized by cleaning, drying and grinding to form a powder. Then it was activated with Potassium hydroxide (KOH) by mixing it with KOH (30 %) at a ratio of ½ (W/V) of citrus peel and KOH. After letting the mixture stand for about ½ hour, it was dried at 70°C for 3 hours at an oxygen free environment. In order to prepare the GO suspension, 500 mg of GO was added to ½ litre of distilled water then it was ultra-sonicated for 2 hours. The composite was synthesized by a one-pot hydrothermal method where the materials were heated at 800°C for 2 hours at a heating rate of 5°C min$^{-1}$. The heating was performed at a Nitrogenous atmosphere. The composite containing 1 % GO, termed mGOCP-1% attained very high adsorption capacity for ciprofloxacin (283.44 mg/g) and for sparfloxacin (502.37 mg/g). The adsorption mechanism that was responsible for this high rate of uptake of these pharmaceuticals by the adsorbent were π-π interaction, hydrogen bonding and the hydrophobicity of the pharmaceutical molecules.

## 2.2.2 Photo-catalysis

Among the different methods that have been investigated for the removal of EC's from water, photo-catalysis has been considered to be a very viable option. Photo-catalysis is a combination of two words, denoting a catalysis reaction which is accelerated by light (photon) (Ameta et al., 2018) Therefore, photo-catalysts are material which can accelerate the rate of a reaction on being exposed to light and the phenomenon is known as photo-catalysis (Ameta et al., 2018). In other words, photo-catalysis can be defined as a phenomenon, in which an electron hole pair is generated in a material on being exposed to light (Ameta et al., 2018). Generally all photo-catalysts are semiconductor.

Photo-catalysis reaction can be broadly defined into two types:-

1. Homogeneous Photo-catalysis :- A photocatalytic reaction in which both the photo-catalysts and the reactants are in the same phase.

2. Heterogeneous Photo-catalysis :- A photocatalytic reaction in which the photo-catalysts and the reactants are in different phases.

The difference between the valance band and the conduction band is known as the band gap ($E_g$). When a wavelength of sufficient energy falls on the semi-conducting material, then the electron in the valance band absorbs it and then it travels from the valance band to the conduction band. As a consequence of which, an electron is emitted ($e^-$) and an electron hole is generated in the valance band ($h^+$). The $e^-$ is utilized for the reduction of a compound and the $h^+$ is used for the oxidation of a compound (Ameta et al., 2018). In an aqueous medium, if the recombination of the $h^+$ and $e^-$ ions can be delayed, then the $h^+$ ion can dissociate the $H_2O$ molecules to produce various oxidizing species like hydroxyl ions ($OH^-$) and hydroxyl radicals ($\bullet OH^-$) which can degrade the trace organic pollutants like EC's, preferably into benign materials like $H_2O$ and $CO_2$.

Among the different types of semiconductors that are employed for the treatment of waste water, $TiO_2$ has attained very high acceptability due to its easy availability, chemical and physical stability and non-toxic nature (Bhattacharya et al., 2022). On the other hand, $TiO_2$ has some drawbacks like the relatively high band gap of its two crystal phases Anatase (3.2 eV) and Rutile (3.0 eV). As a consequence of which they can be only activated by UV rays, which has some harmful effect on living organisms (Khalid et al., 2017). Also $TiO_2$ particles on itself has a tendency to agglomerate in aqueous medium, thereby decreasing their photocatalytic activity (Bhattacharya et al., 2022). Most importantly, recombination time of the photo generated electron on the surface of $TiO_2$ is in the range of $10^{-9}$ seconds whereas the time required for the reaction of adsorbed pollutants with the $TiO_2$ is in the range of $10^{-6}$ to $10^{-3}$ seconds (Khalid et al., 2017).

Therefore in order to bypass these problems, $TiO_2$ is generally applied for the treatment of wastewaters in the form of a composite. Carbonaceous materials are widely preferred for synthesizing the composites with $TiO_2$. The addition of the carbonaceous materials enhances the adsorption ability, increases the dispersion of $TiO_2$ in water, lowers down the energy of the band gap due to the formation of a new conduction layer and delays the recombination of the electron hole pair thereby providing more time for the reaction to take place (Khalid et al., 2017; Nawaz et al., 2017). For this particular thesis, $TiO_2$ was combined with GO and the activated Biochar ARSB. The synthesis of the adsorbent was performed by a hydrothermal method. Below is a list of examples where composites of $TiO_2$ and carbonaceous materials were utilized for treating EC's.

### 2.2.2.1 TiO₂ and GO composite

Nawaz et al., 2017 synthesized a 3-dimentional (3D) reduced GO/$TiO_2$ aerogel by a simple one-pot hydrothermal treatment. The GO was synthesized by a modified Hummer's method with $NaNO_3$ (sodium nitrate) and $KMnO_4$ in presence of $H_2SO_4$. Then different ratios of $TiO_2$ was added with respect to the weight of GO in the composite (Weight of GO: Weight of $TiO_2$:-1:1 to 1:4). The GO were present in uniform aqueous dispersion at the concentration of 4 mg/ml at a volume of 10 ml. A certain quantity of L-ascorbic acid was added to the solution, and then the full mixture in a sealed glass vial was kept in an oil bath at 95°C for 1 hour. The synthesized material was washed with distilled water for few times and then it was freeze-dried for future use. During the synthesis of the composite the GO was reduced, therefore the synthesized compound was named RGOT. From the experimental result, it was found that the RGOT composite with ratio 1:2 exhibited the best result which could be attributed to the uniform anchoring of $TiO_2$ particles on the surface of rGO. Lower ratio of $TiO_2$ resulted in greater adsorption but lower photo-degradation rates whereas higher quantity of $TiO_2$ in the composite, resulted in agglomeration of $TiO_2$ particles, lessening the contact between the pollutant and $TiO_2$ and also the GO and $TiO_2$. Also at the higher concentration, the $TiO_2$ particles agglomerated among themselves, thereby hindering the entry of UV light inside the composite. The combination of GO with $TiO_2$ resulted in

greater adsorption of the pollutants and delayed the recombination of the photo-generated electrons, which is adsorbed on the surface of RGO which functions as the electron sink. The electron holes in the VB either directly degrades the pollutants, or results in the formation of oxidizing radicals like $OH^-$, $O_2^{\cdot-}$ and $\cdot OH$ which oxidizes the pollutants. The 1:2 RGOT reduced aerogel was able to degrade 99 % of a 10 mg/L CBZ solution under 90 minutes thereby denoting that a composite formed with GO and $TiO_2$ was successful in degrading recalcitrant trace pollutants like PHA's from water.

Appavoo et al., 2014 synthesized a $TiO_2$-GO nanocomposite with 2 % GO. In order to synthesize the nanocomposite, first the GO was dispersed in a solution of ethanol and distilled water which was then ultra-sonicated for 1 hour. Then 200 mg of P25 (a type of $TiO_2$ powder), was added to this solution and then it was stirred for 1 hour in order to obtain a uniform dispersion. After that the suspension was transferred to 100 ml Teflon lined autoclave, where it was heated for 180°C for 1 hour. After that the composite was washed with distilled water and rinsed with ethanol and then it was dried at 80°C for 6 hours. The synthesized composite consisted of reduced Graphene and P25 and thus was named Graphene-P25 or Gr-P25. Five different types of Gr-P25 were synthesized with different quantities of GO namely, Gr-P25 1 %, 1.5 %, 2 %, 5 % and 10 % where the numerical with % denote the quantity of GO. The synthesized composite were used to remove the pharmaceutical CBZ from water. The composite were taken in a concentration of 10 mg/L and the concentration of CBZ was 200 ppb and the volume was 300 ml. The illumination intensity if the UV lamp was 1.8 mW/cm$^2$. From the screening process it was found that 2Gr-P25 had the greatest pseudo-first order degradation rate (0.4686 min$^{-1}$) followed by 1.5Gr-P25 (0.4478 min$^{-1}$) and 1Gr-P25 (0.3959 min$^{-1}$). The degradation rate decreased significantly for 5Gr-P25 (0.1340 min$^{-1}$) and 10Gr-P25 (0.1040 min$^{-1}$). Clearly, when the concentration of GO in Gr-P25 was around 2 %, it facilitated the photo degradation of CBZ by increasing the surface area of the composite and entrapping the pollutant molecules on the surface of the composite. However, when the quantity of GO increased beyond 2 % then it decreased the rate of pseudo-first order degradation reaction. This could be attributed to the interference of photons by the GO molecules, leading to the lesser adsorption of the photons molecules by $TiO_2$. In this particular study, the determination of the optimum conditions were investigated by a Central Composite Design (CCD) model of RSM. The optimum conditions under which 100 % removal of CBZ was obtained by the 2Gr-P25 composite were 5 minute UVA irradiation, 25.14 mg/L Gr-P25 dosage, 1.35 mW/cm$^2$ and 167.68 ppb initial CBZ condition. From this particular study it was found the effect of GO dosage on the effective activity of Gr-P25 composite.

Bhattacharya et al., 2022 synthesized a nanocomposite with GO and $TiO_2$ combined in a ratio of 1:1 which was used for the degradation of CBZ in an aquatic solution. The GO was synthesized by a modified Hummer's method. Then it was dispersed in a solution of water and ethanol, which was then ultra-sonicated. Then equal quantity of $TiO_2$ (a combination of 3 part anatase and 1 part rutile) was added to this suspension which was then magnetically stirred for 30 minutes. Then it was hydrothermally

treated for 12 hours at 120°C. After the hydrothermal reaction, the synthesized nanocomposite was extracted by centrifugation followed by which it was washed with deionised water and alcohol. Then it was dried. The degradation potential of the synthesized nanocomposite was detected under five different kinds of radiations namely UVA, UVB, UVC, visible light and sunlight. The composite exhibited highest removal under UVA radiations. Therefore that radiation was used for future application. The optimum conditions under which the highest removal of CBZ was obtained was determined by virtue of a batch study. The highest removal was obtained at 5 mg/L concentration of CBZ, at a photo-catalyst dosage of 2 g/L and agitation speed 100 R.P.M. For the 10 mg/L concentration of CBZ, the highest removal was found to be 91.18 %, which was achieved at pH 4, $TiO_2$-GO dosage of 2 g/L and agitation speed of 100 R.P.M. The process was further optimized with the RSM study, where the optimum removal was found to be 91.7 % which was obtained at the experimental parameters of photocatalyst dosage of 1.12 g/L, pH of 4.11 and agitation speed of 97.93 R.P.M. The process was also further optimized with Artificial Neural Network which also exhibited close interaction with the experimental result.

Xu et al., 2018 synthesized a $TiO_{2-x}$/rGO composite to remove BPA from its aqueous solution. The $TiO_{2-x}$/rGO composite was synthesized by a hydrothermal method followed by calcination. Firstly, into 50 ml of isopropyl alcohol 50 mg of GO was added which was then ultra-sonicated for 1 hour. Then to it 10 ml of Titanium Butoxide was added and then it was strongly stirred for 30 minutes to yield a uniform solution. Then to this solution, 2 ml of water was added and this was stirred for 30 minutes. Then the solution was transferred to a 100 ml Teflon lined autoclave, where it was heated at 180°C for 8 hours. Then the substrates were washed with absolute ethyl alcohol and distilled water for several times, then it was freeze dried overnight. After that the $TiO_{2-x}$/rGO composite were synthesized by calcined at 300°C for 3 hours at a heating rate of 3°C per minute, under an Argon atmosphere. These results in the introduction of $Ti^{3+}$ and oxygen vacancies ($Ti^{3+}/O_v$ ) in the $TiO_{2-x}$/rGO composite. The introduction of ($Ti^{3+}/O_v$ ) shifts the adsorption edge of the $TiO_{2-x}$/rGO composite into the visible adsorption band. Due to the formation of $Ti^{3+}$ impurity level in the $TiO_{2-x}$/rGO composite due to calcination, a narrower band gap is formed. From the Tauc plot analysis, the bandgap of $TiO_{2-x}$/rGO were obtained to be 2.86 eV. As a consequence of which, the composite was able to be activated by visible light. Therefore, the combined effect of $TiO_{2-x}$/rGO ensured a lowered band gap along with higher surface area, greater adsorption and longer time for the recombination of the photo-generated electron. As a consequence of which the $TiO_{2-x}$/rGO composite exhibited greater photo-degradation rate as compared to only $TiO_2$, $TiO_2$/rGO and $TiO_{2-x}$ respectively.

Lin et al., 2016 synthesized GO-$TiO_2$ coated side glowing optical fibres (SOFs) which were synthesized by a polymer assisted hydrothermal deposition method (PAHD). Briefly, the GO were synthesized by a modified Hummer's method. The titanium solution was prepared by dropping titanium tetrachloride into 30 % $H_2O_2$ solution. The titanium solution was then added inside a solution containing 2 g of 50 wt % polyethylenimine, 1 g of ethylenediaminetetraacetic acid (EDTA) and 40 ml of distilled water. The

solution has a bright orange colour. Different solutions of GO and $TiO_2$ were synthesized with GO percentages of 0.1 %, 0.3 %, 0.5 %, 0.8 %, 1.4 %, 2.1 %, 2.7 %, 4.0 % , 5.0 % and 10 % respectively. Then this were added to the bright orange solution and then the whole solution was transferred to a Teflon lined acid digester vessel, which was then placed in a stainless steel autoclave. The SOF's were then dipped inside the solution containing the Teflon lined autoclave which was then hydrothermally treated at 200°C for 8 hours. After which the SOH's coated with GO-$TiO_2$ were taken out and cleaned with deionized water and were dried at 40°C. From the Fourier Transform Infrared Spectroscopy (FTIR) of the synthesized nanocomposite it was obtained that the GO was reduced during the synthesis of GO-$TiO_2$. From the X-ray Diffraction analysis it was obtained that the $TiO_2$ was present as anatase, rutile and brookite forms. From the UV-vis absorbance spectroscopy it was obtained that the rGO-$TiO_2$ had reduced band gap as compared to pristine $TiO_2$ and therefore could operate at lower energy radiation. The photocatalytic efficiency of the rGO-$TiO_2$ coated SOF's was determined by these factors namely, the adsorption of pollutants on the surface of composite (though this was not the main determining factor), the lowering of bad gap of $TiO_2$ and the formation of heterojunction between GO and $TiO_2$ composite which delays the recombination of the photo-generated electron. And finally the optimum percentage of GO is also important as greater quantity of GO might cover the $TiO_2$ molecules, thereby inhibiting the photons from reaching them. From the experimental results it was obtained that the rGO-$TiO_2$ composite with 2.7 % GO exhibited the highest photocatalytic activity. Under UV-light, the 2.7 % rGO-$TiO_2$ coated SOF's exhibited 54 % degradation of CBZ, 81 % degradation of Ibuprofen and 92 % degradation of sulfamethoxazole after 180 min of UV radiation. The effectivity of the rGO-$TiO_2$ coated SOF's under visible light was performed with 2.7 % rGO-$TiO_2$ and Ibuprofen. From the experimental result it was obtained that 2.7 % rGO-$TiO_2$ coated SOF's removed 18 % of Ibuprofen under visible light, as compared to 41 % under low pressure UV light and 81 % under high pressure UV light. Although the efficiency of rGO-$TiO_2$ under visible light was 1/4th of that of under high pressure UV and ½ of that under low pressure UV but still it was greater than that degraded by $TiO_2$ under high pressure UV. As $TiO_2$ can only be activated by UV light, the result of this experiment proves that combination of GO with $TiO_2$ reduced the band gap of $TiO_2$. Also, rGO-$TiO_2$ composite exhibited an almost linear correlation between quantum flux and photodegradation rate. Therefore it can be presumed that the rGO-$TiO_2$ composite will function more properly under a greater quantum flux, like under sunlight. Thus, Lin et al., 2016 synthesized a procedure where a rGO-$TiO_2$ composite can be immobilized on a support (SOF) which can be utilized for degrading trace pollutants PHA's from there aqueous solution under visible light.

### 2.2.2.2 TiO₂ and Biochar Composite

Luo et al., 2015 synthesized a composite consisting of $TiO_2$ and wood charcoal synthesized from Chinese honeylocust pine wood. The $TiO_2$/ WC (Wood Charcoal) composite was synthesized by a dip-sol-gel method which was followed by calcination. Firstly, the Chinese honeylocust were cut into small pieces.

Then they were soaked in 2 mol/L $HNO_3$ solution at 60°C for half a day in order to remove pollutants like metal ions followed by which they were soaked in absolute alcohol and deionized water at 60°C for another half day to leach out the other pollutants like pigments. The process was repeated twice followed and then the wood was dried at 60°C for 12 hours. The composite was prepared with this pre-treated wood charcoal and used tetrabutyl titanate (TBOT) as the titanium source. 14 ml of TBOT was added to 64 ml of absolute ethanol in order to obtain a yellow coloured precursor solution. Then wood charcoal was added to this precursor solution and it was dipped into this solution for 12 hours at room temperature. A solution consisting of 64 ml of absolute ethanol, 5.4 ml of acetic acid and 14 ml of deionized water was adjusted at pH 2 using 1 mole/L $HNO_3$. This solution was dropped into the mixture containing the titanium and honeylocust pine wood at a rate of 3 ml/min for 2 hours while it was kept at 40°C. Then the substrate containing honeylocust pine wood infused with titanium was taken out and dried at 80°C for 12 hours. Then the mixture were calcined at 400°C, 450° C and 500°C to synthesize composites termed $TiO_2$-WC-400, $TiO_2$-WC-450 and $TiO_2$-WC-500. A pure $TiO_2$ was synthesized at 450°C which was termed $TiO_2$-450. A commercial $TiO_2$ was obtained named AEROXIDE $TiO_2$ (P25 ca.80 % anatase, 20 % rutile; BET area ca.50 $m^2$/g, Evonik Corp., Germany) was used as the reference photocatalyst. Batch experiments were performed inside a photochemical reactor. The removal of BPA were investigated by both adsorption and photodegrdation. For photo-degradation, the ultra violet light were provided by a 20 W lamp (254 nm). The photochemical reactor were at room temperature by passing water through the system. For a typical experiment, 0.025 g of the photocatalyst were added to 50 ml of a 20 mg/L BPA solution. First the experiment were continued in the dark for 9 hours for the adsorption desorption reaction to reach equilibrium. Then the light were turned on. The remaining BPA was measured by HPLC. $TiO_2$-WC-400 exhibited the highest removal of BPA at 58.67 % at the end of the equilibrium period followed by $TiO_2$-WC-450 at 24.96 % due to availability of greater surface area and charcoal quantity in them. The highest photocatalytic degradation was exhibited by $TiO_2$-WC-500 at 54.6 % followed by $TiO_2$-WC-450 at 53.4 %. The higher photocatalytic removal by $TiO_2$-WC-500 can be attributed to the optimum ratio of rutile and anatase 40 % and 60 %. Also, the $TiO_2$-WC-500 had a homologous structure to that of Chinese honeylocust pine wood, which attributed to the retaining of anatase and rutile $TiO_2$ within them, resulting in better electron transform within them. That in turn resulted in the superior photocatalytic performance of $TiO_2$-WC-500. The higher photocatalytic degradation by $TiO_2$-WC-450 can be attributed to the higher adsorption of BPA by the composite. Cumulatively, $TiO_2$-WC-400 and $TiO_2$-WC-450 exhibited almost similar removal of BPA at 80.08 % and 78.32 % respectively. Therefore (Luo et al., 2015) synthesized a composite which could operate both as an adsorbent and as a photocatalyst and can result in the effective removal of BPA (20 mg/L) from its aqueous solution at a very reasonable dosage.

Silva et al., 2021 synthesized a biochar-$TiO_2$ magnetic nanocomposite for the purpose of removal of antibiotics used in aquaculture, Oxolinic acid (OXA) and Sulfadiazine (SDZ). The biochar was

synthesized by conventional pyrolysis method and the precursor was the paper mill sludge, which was collected from a plant working with eucalyptus wood (*Eucalyptus globulus*). First the sludge was dried for 24 hours at 105°C followed by which it was grounded by a blade mill. Then it was heated at 800°C for 150 minutes under a $N_2$ controlled atmosphere. The resulting Biochar was washed with 1.2 M HCl followed by distilled water. The process was continued till the washing leachate reached neutral pH and the ashes and the other components were washed out. Then the Biochar was again oven dried at 105°C for 24 hours and sieved at <180 μm and stored in an air dry container for future use. The magnetic nanoparticles were synthesized by a co-precipitation method involving a mixture of $Fe^{2+}$ and $Fe^{3+}$ salts in which a basic solution (KOH 0.5 M) were added dropwise. The magnetic particles were collected as a dark precipitate and were magnetically separated and were washed and stored for future use. The Biochar-$TiO_2$ composites were synthesized by a solvothermal method. The Biochar was dispersed in a solution of ethanol. The precursor of $TiO_2$, Titanium Butoxide ($Ti(BuO)_4$) was dispersed in another solution of ethanol. Then second solution was added dropwise to the first solution, and then a solution of ethanol and water was added dropwise to this solution. Then they were hydrothermally treated. The Biochar-$TiO_2$ magnetic composites were synthesized by both *in-situ* method and *ex-situ* method. In *in-situ* method, the Biochar-$TiO_2$ were added to the ferrous salt before the addition of KOH whereas in the ex-situ method, the Biochar-$TiO_2$ was mixed with the magnetic particle under a $N_2$ atmosphere, and were mixed together by adjusting the pH between the $pH_{pzc}$ of Biochar-$TiO_2$ and magnetic nanoparticle, thereby promoting surface attraction. Eventually four different composites were synthesized, magnetized biochar (BC_Mag), Magnetized biochar functionalized with $TiO_2$ (BCMag_$TiO_2$), Bichar-$TiO_2$ magnetized by in-situ method (BC_$TiO_2$_MagIn) and Bichar-$TiO_2$ magnetized by ex-situ method (BC_$TiO_2$_MagEx). The photo-catalysis was performed by a solar stimulator. The removal of the antibiotics OXA and SDZ were observed to be maximum for the BCMag_$TiO_2$ at a dosage of 100 mg/L, resulting in 87 % photo-degradation of SDZ and 98 % photo-degradation of OXA. The second best removal was by 100 mg/L dosage of BC_$TiO_2$_MagEx with 76 % removal of SDZ and 69 % removal of OXA. From the kinetics study it was observed that the half -life of SDZ was achieved 3-4 times faster and that of OXA 2 times faster in presence of these materials than in their absence. Thus from this study, it can be inferred that a cost effective waste material (paper mill sludge) can be used for enhancing the photo-degradation ability of $TiO_2$ which in turn can be used for degrading trace pollutants like antibiotics from water.

Kim & Kan, 2016 synthesized a Biochar supported $TiO_2$ photo-catalyst which was used for removing Sulfamethoxazole (SMX) from its aqueous solution. The Biochar was used for the support of $TiO_2$ as because it was an easy and low cost support system of $TiO_2$. The Biochar was combined with $TiO_2$ by a sol-gel method. Combination of the Biochar with $TiO_2$ is supposed to increase the surface area of the photo-catalyst enabling the higher adsorption of the pollutant, to prolong the recombination time of the photo-generated electron and enabled the easier separation of the photo-catalyst after the treatment. The

Biochar-$TiO_2$ exhibited higher adsorption as compared to only $TiO_2$. However, the Biochar-$TiO_2$ showed lesser photocatalytic efficiency as compared to only $TiO_2$ and UVC reaction. However the mineralization of SMX by Biochar-$TiO_2$ as measured in terms of Chemical Oxidation Demand (COD) was four times greater as compared to direct photolysis by UVC radiation. This could be attributed to the delay of the photoelectron recombination on the surface of $TiO_2$ made possible by the Biochar. The mineralization of SMX by direct $TiO_2$ was also less than that of Biochar-$TiO_2$ which could be attributed to the rapid recombination of photo-generated electron on the surface of $TiO_2$. At optimum conditions (6h irradiation, Biochar-$TiO_2$ dosage 5 g/L, pH 4) it led to high removal and correspondingly high mineralization of SMX, 91 % and 81 % respectively. The bio-toxicity test with *Daphnia magna* and *E.coli* expressing β-galactosidase exhibited negligible toxicity on exposure to SMX after photo-degradation and the intermediates formed after photo-degradation with Biochar-$TiO_2$ were also found to be of benign in nature. Therefore it can be stated that the Biochar-$TiO_2$ composite synthesized by Kim and Kan, 2016 was a cost-effective and efficient photo-catalyst that could be used for the photo-degradation of recalcitrant pollutants like SMX into benign and harmless products.

Zhang et al., 2018 synthesized a composite where $TiO_2$ was supported on a Reed straw biochar and it was used for the removal of SMX by adsorption and photocatalysis. The Biochar was synthesized by heating the raw material (Reed straw) at 500°C for 6 hours followed by treating it with acid. The finished product was named acid pretreated biochar, abbreviated to pBC. The $TiO_2$/pBC composite was synthesized by sol-gel method with tetrabutyl titanate $Ti(C_4H_9O)_4$ being utilized as the precursor of $TiO_2$. After the synthesis of the composite, the materials were calcined at the temperatures 300°C, 400°C and 500°C inside a muffle furnace for 2 hours. The composite were correspondingly named $TiO_2$/pBC (300), $TiO_2$/pBC (400) and $TiO_2$/pBC (500) respectively. $TiO_2$ was also synthesized from tetrabutyl titanate $Ti(C_4H_9O)_4$ and calcined at 300°C. During the adsorption study highest removal of SMX was observed by the $TiO_2$/pBC (300) composite. During the photocatalysis reaction it was observed that the removal of SMX by $TiO_2$/300 was 91.27 % which was much higher than that by only TiO (58.47 %). The COD reduction of SMX under by $TiO_2$/pBC (300) was 57.44 %, which was more than that by $TiO_2$. Although the presence of impurities like nitrate and bicarbonate ions, which are commonly found in Yellow river, had an antagonistic effect on the removal efficacy of $TiO_2$/pBC (300) but still it was able to remove 65.7 % SMX from the river water. The higher photocatalytic ability of $TiO_2$/pBC (300) as compared to only $TiO_2$ could be attributed to the delay in recombination of the photogenerated $e^-$ with the $h^+$ hole, thereby enabling the hydrolysis of the $H_2O$ molecules resulting in the generation of oxidizing species which in turn degraded the organic pollutant. The $TiO_2$/pBC (300) composite also exhibited high regeneration ability, removing 85 % of SMX in its fifth cycle. Therefore it can be stated that $TiO_2$/pBC (300) was a cost effective material with sufficient regeneration ability, which could be utilized for efficient removal of SMX from its aqueous solution without producing any harmful intermediates. Thus, $TiO_2$/pBC (300) could be used for the effective removal of recalcitrant pollutant from there aquatic solution.

Lazarotto et al., 2020 synthesized a composite with coffee ground biochar and $TiO_2$ in order to remove Diclofenac (DCF) from its aqueous solution. Coffee ground is a widely available by-product of coffee cultivation, where in order to manufacture 1 kg of soluble coffee, 2 kg of coffee ground is produced. By synthesizing a biochar from the coffee ground, a waste material is being turned to a product of environmental remediation. The biochar-$TiO_2$ composite was synthesized by mixing dried coffee ground with $TiO_2$ in porcelain mortar by manual mechanical mixing, followed by pyrolysis in a $N_2$ atmosphere at 650°C for 2 hours. Two composites were synthesized, one with a ratio of 1 part biochar and 1 part $TiO_2$ termed B1T1 and another with a ratio of 2 part biochar and 1 part $TiO_2$ termed B2T1. The photo-catalysis reaction was performed with a Mercury vapour lamp of 125 W with incident radiation $\lambda < 400$ nm. With 20 mg/L concentration of DCF and 1 g/L dosage of B1T1, about 90 % removal of DCF was possible in about 120 minutes of reaction time. The removal capacity of B2T1 was even more. This high degradation of DCF could be accounted to the delay in electron recombination, which is made possible by the biochar. The synthesized composites showed high efficiency even after five cycles of reuse. Thus it can be stated that the biochar-$TiO_2$ composites synthesized by (Lazarotto et al., 2020) was a cost efficient material that can be effectively used for the removal of trace pollutants like DCF from the aquatic solution.

## 2.2.3 Fenton Oxidation

Another AOP that is widely utilized for the treatment of trace organic pollutants in water in the Fenton's oxidation process. Fenton's oxidation process was discovered by Henry John Horstman Fenton in the late 1890's. In this reaction a mixture of $Fe^{2+}$ (generally obtained from $FeSO_4.7\,H_2O$) and $H_2O_2$ react to emit hydroxyl radicals. The reaction denoting the Fenton reaction can be stated as follows :-

$$Fe^{2+} + H_2O_2 = Fe^{3+} + OH^{\bullet} + OH^{-} \dots\dots\dots\dots\dots\dots\dots\dots\dots\dots\dots\dots\dots\dots\dots\dots\dots(x)$$

$$Fe^{3+} + H_2O_2 = Fe^{2+} + OOH^{\bullet} + H^{+} \dots\dots\dots\dots\dots\dots\dots\dots\dots\dots\dots\dots\dots\dots\dots(xi)$$

The decomposition of the hydrogen peroxide molecule can be given as follows:-

$$2H_2O_2 = HOO \bullet + HO \bullet + H_2O \dots\dots\dots\dots\dots\dots\dots\dots\dots\dots\dots\dots\dots\dots\dots\dots\dots(xii)$$
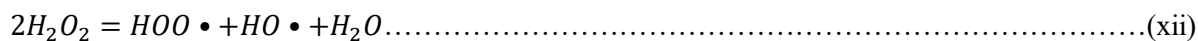
The hydroxyl radicals being strong and non-selective oxidizing agents can degrade the EC's in their aquatic solution (Sun et al., 2009). The Fenton reaction is preferably performed at acidic pH as because at the alkaline pH, the ferrous ions that are formed during the reaction are precipitated as ferrous hydroxide, thereby extinguishing the source of $Fe^{2+}$ in the solution and slowing the pace of the reaction (Mirzaei et al., 2017). The first part of the reaction accelerates rapidly due to rapid generation of OH• radical from $H_2O_2$ due to the presence of $Fe^{2+}$ (Eq(x)). However in the second part of the reaction, where $Fe^{3+}$ ions react with $H_2O_2$ to form $Fe^{2+}$ ions and HO2• that the reaction slows down as because the HO2• have lower oxidation potential (E°=1.65 V) as compared to OH• (E°=2.8 V) and have a lower rate of

production (Mirzaei et al., 2017). Generally the rate of the reaction as depicted in Eq (x) is much higher than the rate of the reaction depicted in Eq (xi). Therefore regeneration of $Fe^{2+}$ ion from the $Fe^{3+}$ ion becomes the rate limiting step of the reaction (Vasquez-Medrano et al., 2018).

Fenton being an advanced oxidation process generates reaction intermediates which in themselves can be harmful for the environment. In order to mitigate that problem it is advisable to combine the Fenton reaction with another method of waste water treatment like adsorption. In that way, the Fenton reaction would be able to rapidly degrade the pollutants, followed by which the reaction intermediates can be adsorbed by an efficient adsorbent (Della-flora et al., 2021).

A study conducted by Velásquez et al., 2014 reported the use of Fenton and Photo-Fenton reaction for the purpose of removal of Sulfathiazole from water. The optimization of the reaction was done by the CCD design of RSM. From there it was observed that 90 % of Sulfathiazole was removed by Fenton and Photo-Fenton reaction after 8 minutes, with reagent concentration of 192 µmol/L for $Fe^{2+}$ ion and 1856 µmol/L for $H_2O_2$ in case of the Fenton reaction and 157 µmol/L for $Fe^{2+}$ ion and 1219 µmol/L for $H_2O_2$ in case of the Photo-Fenton reaction. The removal of Total Organic Carbon (TOC) after the degradation of Sulfathiazole by Fenton and Photo-Fenton process were found to be 30 % and 75 % respectively. Acetic acid, maleic acid, oxamic acid and succinic acid were found to be reaction intermediates. As was observed, the Photo-Fenton reaction exhibited a greater efficiency as compared to only the Fenton process.

As per the findings of Dwivedi et al., 2018, Fenton oxidation was able to effectively remove high concentrations of the pharmaceutical Carbamazepine (CBZ) that was found in the waste water of a pharmaceutical industry. After initial studies to optimize experimental parameters, it was observed that pH, Fenton Dose and experimental time were the preliminary factors which significantly affected the Fenton reaction process. Then the whole process was then optimized by the CCD in RSM tool in MINITAB 16. The optimized conditions under these model was found to be pH = 3.5 and $H_2O_2$ concentration of 8.5 g/L, which was able to remove 49.39 +/- 0.93 % of CBZ from a very high concentration (442.08 +/- 2.58 mg/L). After Fenton oxidation, the waste water was filtered through granulated activated carbon (GAC) which was subsequently able to remove 99.51 +/- 0.02 % of CBZ. The toxicity assessment of the treated waste water was done with the germination assay of plant seeds Pisum sativum and Vigna radiate. From the result of the test it was found that, the treated wastewater (after both Fenton oxidation and GAC filtration) exhibited a lesser toxicity as compared to untreated waste water. Therefore it can be stated that Fenton oxidation followed by Granular Activated filtration served as an effective method for the purpose of treating pharmaceutical wastewater at the source, thereby subsequently resulting in zero discharge from the source.

Della-flora et al., 2021 conducted a study in which a combined process of Solar Photo Fenton and adsorption was used to remove PHA's. For this study, nine different pharmaceuticals were taken

namely, Chloramphenicol, Fluconazole, Flutamide, Furosemide, Gemfibrozil, Ibuprofen, Losartan, Nimesulide and Paracetamol. The pharmaceuticals were dissolved in a hospital wastewater as the solvent matrix, at an environmentally relevant concentration of 500 µg/L. An avocado seed activated carbon was utilized as the adsorbent. Four different modules of Solar Photo Fenton process were studied and among them, the best result were exhibited by $H_2O_2$ concentration of 100 mg/L and multiple additions of $Fe^{2+}$ ions at 5 mg/L concentrations at reaction times of 0 min, 5 min and 10 min in the multiple pharmaceutical and hospital waste water matrix. As per the experimental results, all the pharmaceuticals exhibited 99% removal except for Fluconazole which exhibited 80 % of removal. In case of the Solar Photo Fenton process, a maximum of 28 transformation products were obtained at the end of 15 minutes. In order to remove these transformation products along with the residual pharmaceuticals, 20 ml of the experimental solution was mixed with 14 mg dosage of avocado seed activated carbon and the reaction was continued for 15 minutes. At the end of this adsorption study, 30 of the 36 compounds, including all the trace of the pharmaceuticals and transformation products were removed. All the compounds with a closed chain, aromatic ring structure were removed at 99-100 %, with the π-π bonds being the main mechanism of adsorption. Only, the two transformation products of Flutamide with open chain structure were removed at a relatively lower percentage of 50 % and 60 %. Thus it can be stated that Solar Photo Fenton process combined with adsorption was an efficient method for the removal of PHA's at an environmentally relevant concentration dissolved in a real time waste water matrix.

Katsumata et al., 2004 used Photo-Fenton oxidation for the purpose of degrading BPA from its aqueous solution. Ferrous sulphate heptahydrate ($FeSO_4.7H_2O$) was used as the source for $Fe^{2+}$ ions. A Xe lamp with 990 W was used as the light source with the vessel wall absorbing the UV radiations of short wavelengths (λ <300 nm). The range of the radiation in which reaction was carried out was 320-410 nm with a light intensity of 0.5 mW/cm$^2$. For a 10 mg/L concentration of BPA, under optimum conditions ($4 \times 10^{-4}$ mole/L of $H_2O_2$; $4 \times 10^{-5}$ mole/L of $Fe^{2+}$ ions ; pH 4 and temperature 25°C) complete degradation of BPA was observed under 9 minutes. The reaction kinetics was found to follow the pseudo-first order reaction rates. BPA was converted to $CO_2$ during the mineralization of BPA by the Photo-Fenton reaction. Under the same conditions at which 100 % degradation of BPA was obtained under 9 minutes, it was observed that 54 % of BPA was converted to $CO_2$ after 24 hours. After increasing the concentration of the reagents by 10 times ($4 \times 10^{-3}$ mole/L of $H_2O_2$; $4 \times 10^{-4}$ mole/L of $Fe^{2+}$), it was observed that 93 % of BPA was converted to $CO_2$ after 36 hours. Under the same conditions 13 % of TOC was left in the experimental solution after 36 hours. 6 types of intermediates were formed from the degradation of BPA. Overall, inferring from the degradation and mineralization rate of BPA as obtained from the experimental result, it can be stated that Photo-Fenton reaction is an effective process for the purpose of removing BPA from wastewater.

Guo et al., 2014 investigated the degradation of the antibiotic Amoxicillin by a Fenton oxidation method, along with an activated sludge treatment method and a combined method of Fenton oxidation and activated sludge treatment. Different parameters were tested for the removal of Amoxicillin like the effect of $H_2O_2/Fe^{2+}$ molar ratio, effect of reaction time, effect of temperature and effect of initial pH. From there the optimal conditions for the maximal removal of Amoxicillin were found to be 4 mL $FeSO_4.7H_2O$ solution (20.43 g/L), 6 mL of $H_2O_2$ solution (3%) and temperature of 40 °C. Under this condition, a 1 g/L concentration of Amoxicillin were degraded by 80 % in 70 min. The activated sludge process in itself was unable to sufficiently degrade Amoxicillin in a sufficiently short period, due to the toxic effect of the antibiotic Amoxicillin on the microorganisms of the activated sludge. The highest degradation of Amoxicillin by the activated sludge treatment was in the range of 69.04 %-88.79% with the concentration of Amoxicillin being less than 350 mg/L. But the combined effect of Fenton degradation followed by activated sludge treatment was very effective for degrading Amoxicillin, with complete degradation being observed for concentration less than 500 mg/L. When the concentration of Amoxicillin was increased up-to 1000 mg/L, the removal rate was obtained as 85.13 %. It was inferred that the Fenton reaction disintegrated the Amoxicillin, as a consequence of which its toxic effect on the microorganisms of the activated sludge were decreased, resulting in its greater decomposition by the activated sludge process. Thus it can be stated that Fenton reaction can be utilized to decompose the antibiotic followed by its complete degradation by the activated sludge process. In that way, the reagents required for the Fenton reaction can be decreased, and the efficiency of the activated sludge process can also be increased.

Given above are the list of methods by which the removal of four EC's (CBZ, NPX, RTN and BPA) were investigated. The aim of the research work as presented in this thesis, was to evaluate the conditions under which the optimal removal of the pollutants by the above mentioned methods were possible. Making the process as effective as possible along with being cost effective was another aim of this undertaking. Lastly, the best performing method was utilized for treating two real-time waste waters selected from two different spots. The research methodologies for the respective processes along with their corresponding results and their explanation is presented in the respective chapters.

# CHAPTER 3

# OBJECTIVES OF THE PRESENT RESEARCH STUDY

## 3.1 OBJECTIVES OF THE PRESENT STUDY

From the literature review, the following objectives were selected for the present research work

1.> To synthesize carbonaceous based materials to remove emerging contaminants (ECs) present in solution

2.> To study the Advanced Oxidation followed by adsorption for the removal of EC present in solution

3.> To investigate the effects of different parameters on the removal of the EC using composite materials in batch and optimization method

4.> Utilization of Rotating packed bed reactor to find the efficacy of the synthesized materials to remove the EC's under a dynamic system by adsorption.

5.> Testing the efficacy of the investigated systems for the purpose of treating real water.

## 3.2 NOVELTY OF THE PRESENT STUDY

In the present study both GO, which was a premium carbon compound synthesized from commercial grade graphite and ARSB, an activated biochar synthesized from rice straw were used for removing the EC's from water. From the result of their respective experiments, a comparison of their efficacy for the purpose of removing the different kind of EC's can be conducted. The same logic can also be applied in case of the GO-TiO$_2$ and the ARSB-TiO$_2$ composite. As a matter of fact, from the set of experiments carried out as a whole, comparison can be made between all the treatment methods and from there a conclusion can be reached as to which method is more effective. In case of the treatment methods involving the photo-catalyst GO-TiO$_2$ and ARSB-TiO$_2$, different types of incident radiations (UVA, UVB, UVC and visible radiation) were utilized for activation of the photo-catalyst. In the end, the incident radiation which exhibited the highest efficiency were utilized for further studies. Also in case of the RPB study, the adsorbents and photo-catalyst were directly applied to the solution tank rather than forming a packed bed. Also another method was investigated where an advanced oxidation process Fenton oxidation was used for degrading the EC's, followed by adsorption with GO to remove all the products. In this method, the advanced oxidation process was followed by adsorption. And at last, the experimental methods explored in this thesis were used for treating water samples collected from two sites, one being a lake with polluted water and the other being the effluent from an industry.

# CHAPTER 4

# SYNTHESIS OF GO AND ITS UTILIZATION FOR REMOVING EC'S FROM THE AQUATIC SYSTEM

## 4.1 INTRODUCTION

Trace organic pollutants like residual PHA's present in the effluents are rapidly becoming issues of immense concern on a global scale. Wide use and disposal of these products have resulted in a rapid rate of accumulation of the same in adjacent aquatic (Bhattacharya et al., 2020). CBZ, NPX and RTN are among the most widely used PHA's and hence are also among those that are most frequently encountered in the aquatic ecosystem. CBZ is generally prescribed as a medicine for neurological syndromes like depression, post-traumatic stress disorder, restless leg syndrome, diabetes insipidus etc. Global annual usage of CBZ range around 1.01 Kilo-Ton. As a consequence of utilization of such high quantity of CBZ, its presence has been detected in almost all sources of water viz., surface water, ground water, wastewater treatment plants and even drinking water. Thus presence of CBZ in aquatic environment has emerged as a cause of Global concern. The toxic effect of CBZ has been observed on various forms of aquatic life including bacteria, algae, invertebrates and fish. The permissible limit of CBZ in potable water varies across different countries and is reported to be in the range of 40 and 100 μg/L in developed countries such as U.S.A and Australia (Hai et al., 2018). Also, utilization of CBZ containing water for agricultural purposes results in the accumulation of CBZ in the soil. The standard concentration of CBZ in soils irrigated using contaminated water has been found to be in the range of 0.02–15 μg/kg (F. Chen et al., 2011). According to the US Food and Drug Administration (USFDA), an environment assessment should be performed whenever the concentration of the active ingredient of CBZ is equal to or found to exceed 1.0 μg/L in aquatic environment (Bhattacharya et al., 2020). NPX ($C_{14}H_{14}O_3$) is a well-known and widely used broad range, NSAID (non-steroidal anti-inflammatory drug) which is generally prescribed for the treatment of pain and swelling. As per ClinCalc, NPX was the 67th most prescribed drug in USA in 2011 with 11,942,765 annual prescription. As a result of its widespread utilization, NPX has been found in a range of locations consisting of both natural and man-made aquatic environments and thereby poses a health risk to any organisms which consumes water

from these resources, including the organisms that live in these ecosystems (Bhattacharya et al., 2021). Also in reference to previous literature regarding the toxicity of NPX, it was noted that NPX was capable of causing some oxidative stress and genotoxic effect in microorganisms (Ahmed & Haider, 2018; Górny et al., 2019). RTN ($C_{13}H_{22}N_4O_3S$) is a histamine $H_2$ receptor antagonist, which is used in order to block the action of the biogenic amine on the parietal cells of the stomach, in order to decrease the acid production from these cells (Isidori et al., 2009). As is common in case of the widely utilized pharmaceuticals, traces of RTN have also been found observed in different water bodies. In a study conducted by (Isidori et al., 2009), RTN was found in nine sewage water treatment plants (STP's) in Italy and was also present in the surface waters in North Italy. RTN was also found in trace quantities in 1.2 % of US streams and in the downstream of several of STP's in Italy (Isidori et al., 2009; Kolpin et al., 2002). RTN is excreted in about (6-39)% of its parent compound. Upon reaching the aquatic ecosystem, it can have some unintended effects on non-target organisms (Isidori et al., 2009). Although RTN is comparatively less toxic as compared to other PHA's like CBZ and NPX, but still RTN and some of its photodegraded by-products are able to exert some measure of toxicity on unintended targets (Bergheim et al., 2012; Sandip Mondal et al., 2015). Thus it can be unilaterally agreed upon that, efficient treatment strategies are required for removing this type of trace pollutants like PHA's from the aquatic environment.

Like PHA's, another important source of trace organic pollutants are EDC's. EDC's are chemical compounds which share a chemical structure analogues to that of hormones, therefore they can mimic the functioning of the hormone, and thus can dis-balance the normal functioning of the human body (Chouhan et al., 2014). A well-known example of an EDC is BPA ($C_{15}H_{16}O_2$). BPA is mainly synthesized by the combination and condensation of two parts of phenol with one part of acetone in the presence of a promoter and a catalyst. The synthesis process takes place at high temperature and low pH. It mainly exists as a white solid in room temperature (Chouhan et al., 2014). BPA exhibits high resistance and physical stability. BPA is generally used as a plasticizer, for the synthesis of products like plolycarbonate plastics and epoxy raisins and is one of the most widely used chemicals in the world (Bhatnagar & Anastopoulos, 2017). Humans are mainly exposed to BPA through their diet. When plastic containers containing BPA are exposed to high heat or extreme pH (high or low), then the "esters bonds" holding the BPA to the plastics are hydrolysed, leading to the leaching of the plastics into the food or drinks (Chouhan et al., 2014). As mentioned before, BPA is an EDC, and it mimics the action of the female hormone estrogen, and is known as a xenoestrogen (Chouhan et al., 2014). BPA can cause multiple disorders to the Human body namely, decrease in sperm counts, hormone related cancer, brain damage etc. Moreover it can cross over the placental barrier in the body of the mother, and can concentrate inside the foetus (Chouhan et al., 2014). Thus it can be stated that unintended intake of BPA can have serious consequences for humans.

Hence, efficient treatment strategies are required for removal of this type of EC's from the aquatic environment.

However, conventional treatment processes practised in wastewater treatment plants (WWTPs) are incapable of sufficiently removing these trace pollutants from the aquatic ecosystem (Jinfeng Wang et al., 2012). Recent studies have reported the process of adsorption as an efficient and cost-effective process for persistent contaminant treatment (Banerjee et al., 2015b, 2016; L. Liu et al., 2012). A wide variety of materials such as clays, polymers and several carbon-based materials (like fly-ash or charcoal) have been investigated for adsorption of different types of aqueous pollutants (Banerjee et al., 2016). Of all other types of carbonaceous adsorbents reported in contemporary studies, GO has received significant attention due to its mechanical and chemical stabilities as well as high specific surface area (Banerjee et al., 2016). Carbonaceous nanomaterial like GO has been widely investigated as an adsorbent due to its convenient process of synthesis, efficient pollutant removal in significantly low dosage and cost effectiveness (Banerjee, Mukhopadhyay, et al., 2017; M. Li & Liu, 2013; Mukherjee et al., 2019). Moreover, GO surfaces bear large quantities of oxygen rich epoxy, hydroxyl, and carboxyl groups (Banerjee et al., 2016). Presence of these functional groups render GO hydrophilic and therefore, suitable for adsorption of trace organic pollutants like EC's from their aqueous solutions (Banerjee et al., 2016). The present study investigated the potential of GO for efficient removal of the four EC's CBZ, NPX, RTN and BPA. Morphology, chemical nature and crystalline properties of GO particles used in this study were analysed with scanning electron microscopy (SEM), Fourier transform infrared (FTIR) spectroscopy, X-ray diffractometry (XRD) and Raman spectrometry respectively. Batch studies were carried out for elucidating the effect of significant experimental parameters on the process of adsorption. Results obtained in batch studies were further investigated for determining the isotherm and kinetic models guiding the concerned process. Process optimization was carried out by performing a RSM study. Other than the batch study, a RPB study was also conducted in order to intensify the process of adsorption of the EC's by GO (A. Das et al., 2008). The centrifugal force exerted by the RPB was much more intense than in batch study or in column study. In order to determine the reusability of GO, a consecutive adsorption-desorption cycles were also performed for determining the reusability potential of the GO reported in this study.

## 4.2 MATERIALS AND METHODS :-

### 4.2.1 Materials required

The pharmaceuticals were brought from M.P Biomedicals (CBZ, NPX), Sigma-Aldrich (RTN) and Merck (BPA). The Graphite and $KMnO_4$ were brought from Merck, the $H_2SO_4$ were brought from Emplura and the $H_2O_2$ (30%) were brought from Emplura. All the materials were obtained in laboratory grade and were used as received without further purification.

### 4.2.2 Synthesis of GO

For this experiment, the GO was synthesized by using the modified **Hummer's method** (Banerjee et al., 2015b; P. Das & Das, 2016). In this experimental study, firstly, 3 g of graphite powder was suspended in 120 ml of concentrated $H_2SO_4$ while keeping the experimental apparatus in an ice bath. Then 8 g of potassium permanganate $KMnO_4$, which acts as an oxidizing agent was added to the above mixture in a controlled manner under constant stirring condition. After the complete addition of the $KMnO_4$, the experimental apparatus was kept at 45 °C for 3 h at constant stirring. Then, $H_2O_2$ was added to the experimental mixture followed by water. The synthesized GO was then washed three times, with HCl, ethanol and distilled water to remove any other metal impurities that may be present in the solution. Finally, the GO was extracted from the solution by centrifugation, after which it was freeze dried and stored in a cool place for future use.

### 4.2.3 Characterization

Characterization of the synthesized GO particles were done by Scanning Electron Microscopy (SEM), Raman Spectroscopy, Fourier transform infrared spectroscopy (FT-IR) and X-ray Diffractometry (XRD).

The structural and morphological properties of GO was analysed by means of Scanning Electron Microscope (SEM) from ZEISS EVO MA-10 Germany. Before performing the SEM analysis, the sample was made conductive by covering it with a coat of Platinum under vacuum condition by a sputter coater (Bhattacharya et al., 2021).

The GO was analysed by a FT-IR spectrometer in order to elucidate the chemical bonds and functional groups that were present in the GO. The FT-IR analysis was carried out by a Perkin Elmer instrument, USA, in the range of wavelength 400–4500 $cm^{-1}$ at a transmission rate of 4 cm $sec^{-1}$. For the FT-IR analysis, the GO was cast into pellets with KBr as the background material, with the ratio of sample and KBr being about 1: 100 in terms of weight (Ganguly et al., 2020).

The XRD analysis of ARSB was done in order to find crystal lattice of ARSB. The XRD was performed by an X-ray diffractometer from Malvern, Pananalytical, UK having a Cu-$K\alpha$ radiation operating at a voltage of 40 kV, current flow of 40 mA over an intensity range ($2\theta$) of 5–80°.

The Raman Spectral measurement of the GO were taken using a Lab Ram HR Model: 800 (Horiba Jobin Yuvon) spectrometer. Datwere recorded over the range of 200–3500 $cm^{-1}$ with the exposure time of 5 s. The operating wavelength of the He-Ne laser was 632.8 nm and the laser power was 17 mW.

The spectral detection was obtained through an air-cooled charge-coupled device were recorded over the range of 200–3500 cm$^{-1}$ with the exposure time of 5 s. The operating wavelength of the Helium-Neon laser was 632.8 nm and the laser power was 17 mW. The spectral detection was obtained through an air-cooled charge-coupled device. The spectral detection was obtained through an air-cooled charge-coupled device.

## 4.2.4 Preparation of the Experimental Solution

RTN was directly mixed with double distilled water. NPX, CBZ and BPA were first dissolved in $C_2H_5OH$ followed by which they were diluted to their required concentration by dilution with double distilled water.

## 4.2.5 Batch study

A batch study was performed in order to find the experimental conditions under which the highest removal of the EC's by the GO was possible. The set of parameters and there variation remained constant for every EC. The experimental parameters that were considered for the batch study were initial adsorbate concentration (5 mg/L – 20 mg/L), adsorbent dosage (0.5 g/L – 2 g/L), pH of the experimental solution (2–10), and temperature (298 K- 313 K). A 0.1 M NaOH solution and a 0.1 N HCl solution was utilized for regulating the pH of the experimental mixture wherever required. For each individual batch experiment, experimental solution was taken in an Erlenmeyer flask. All the experiments were done inside an incubator under constant rotation. Samples were extracted at predetermined timeslots. The samples were passed through a 0.22 μm syringe filter followed by centrifugation at 15,000 rpm for 15 min in order to separate out the very fine GO particles from the extracted samples. Analysis of the remaining EC's in the solution after treating with GO was spectrophotometrically by analysing them in a UV–Vis Spectrophotometer (Perkin Elmer Lambda 360). The $\lambda_{max}$ of the different adsorbates are given as follows:-

**Table 4.1**: The $\lambda_{max}$ of the different EC's.

| Chemical | $\lambda_{max}$ | Reference |
|---|---|---|
| CBZ | 283 nm | (Bhattacharya et al., 2020) |
| NPX | 230 nm | (Bhattacharya et al., 2021) |
| RTN | 313 nm | (B. Singh & Sharma, 2008) |
| BPA | 228 nm | (Brugnera et al., 2010) |

Each experiment were conducted thrice and average value was considered.

## 4.2.6 Process optimization with RSM

The process of adsorption of the EC's by GO was optimised with the help of the central composite design (CCD) model of RSM. The RSM was done with the software Design Expert Version 7.0 (Stat-Ease, USA). The RSM can be defined as a mathematical and statistical tool used for the purpose of optimizing a particular process operation. RSM also helps to explain the effect that the parameters of a concerned operation have on one another and on the process as a whole. For the purpose of process optimization, a number of experiments as recommended by the software (denoted as runs) had to be performed. For each of these experimental runs, a specific set of experimental conditions is laid out by the software known as input variables. The outcome obtained after performing the experiments with these input variables is known as the output response which has to be re-entered into the software for the purpose of calculating and plotting out the optimization study (Banerjee, Mukhopadhyay, et al., 2017; Ganguly et al., 2020). For the current set of studies, the experimental parameters that were chosen as the input variable are pH of the experimental solution, dose of adsorbent (mg/100 ml) and the time of treatment (minutes). The concentration of the EC's were kept constant for the RSM experiment at 10 mg/L. The output responses were determined to be in terms of the percentage removal of the EC's by GO. With reference to conditions and range of parameters provided to the software, it recommended 20 experiments, with 6 replications for each set of pollutants. The runs recommended by the software along with their corresponding outcome, and the statistical outcome of the RSM process is provided in tabular form in the result section.

## 4.2.7 Process Intensification with Rotating Packed Bed (RPB) study

It has been widely reported that GO is an effective adsorbent for the purpose of removing trace pollutants from their aquatic solutions (Banerjee et al., 2016; Banerjee, Roy Barman, et al., 2017; Bhattacharya et al., 2020; Bhattacharyyaa et al., 2018; P. Das & Das, 2016). There also exists many different methods by virtue of which the adsorption capacity of GO can be further increased. One such method of process intensification is the utilization of a Rotating Packed Bed (RPB) method. RPB is a high throughput setup where the gravitational force is replaced by centrifugal force, which is quite a few times higher in magnitude. RPB contractors were first designed by Collin Ramshaw and Roger H Mallison in the year 1981 for effective mass transformation between two fluid phases. A doughnut shaped packed bed is present inside the setup which is rotated at a high speed and solution is sprayed on the inner edge of an RPB and is thrown outward by centrifugal force. Concurrently, gas is introduced from the outer edge of the bed and flows inwards relatively counter-currently to the liquid by pressure gradient. Under this thorough centrifugal field, thin liquid films and tiny liquid droplets are generated resulting in dramatic increase in mass transfer. Therefore RPB is generally applied to increase the order of magnitude of a mass transfer process (A. Das et al., 2008; Hashim et al., 2019). Some of the variables

that can regulated in the RPB system are the materials with which the packed beds are formed, the speed at which the RPB is rotated, the rate of flow of the solution and general experimental parameters like, pH, temp etc. (Hashim et al., 2019).

RPB has been extensively utilized for the purpose of removing pollutants from their aqueous systems. (A. Das et al., 2008) utilized the dried scales of *Catla catla* fish in an RPB system for the purpose of adsorbing Cu(II) from the aqueous solution. In four different independent studies (B. Li et al., 2018), (C. Chang & Lee, 2012), (Kundu et al., 2015) and (Hashim et al., 2019) utilized activated carbon as the packing material inside a RPB for the purpose of removing phenol, methomyl (a widely used pesticide), Direct 23 dye and Arsenic from water respectively. In case of the study of (Kundu et al., 2015) it was observed that 93 % of dye was removed by the RPB as compared to 55 % removed by a shake flask, with in a time period of 5 hours with other factors such as dose of adsorbent and volume of reactant remaining constant. From the experimental outcome of (Kundu et al., 2015) it was observed that rotor speed and flow rate were two important factors in controlling the efficiency of the RPB with the highest removal being observed at 628 RPM agitation speed and 40 L/hour flow rate. In case of the study by (Hashim et al., 2019), activated carbon was used for removing Arsenic from water. The process was optimized by the Taguchi method and from the experimental result it was observed that the highest removal of Arsenic was observed at the experimental conditions of initial concentration of Arsenic 150 mg/L, pH 3, packing density 510 kg/m$^3$, feed rate of 50 L/h and rotation speed of 1600 RPM. (Mosleh et al., 2018) utilized a photocatalyst consisting of CuO/CuO$_2$/Cu nanoparticles synthesized by a sonochemical combined thermal synthesis method for the simultaneous degradation of Safranin O (SO) and Methylene Blue (MB). Unlike the previous example where the adsorbent was utilized to form a packing bed, in case of the study by (Mosleh et al., 2018) the photocatalyst CuO/CuO$_2$/Cu was directly added to the experimental solution containing the dye. The process was optimized by the CCD model of RSM and from there the parameters for the maximum removal of the dyes were found to be 0.3 g/L of CuO/CuO$_2$/Cu photocatalyst, pH 6, RPM of 600, dye concentration of 10 mg/L, flow rate of 0.3 ml/L and reaction time of 90 minutes. Under this condition 98.01 % of SO and 91.91 % of MB were removed. The Langmuir-Hinshelwood kinetic model best described the degradation of the dyes by the CuO/CuO$_2$/Cu photocatalyst.

Similarly, like in the experiment of (Mosleh et al., 2018), in this experiment also GO was directly added to the experimental reservoir containing the solution of EC's. The name and dimensions of the different parts of the RPB that is used in this experimented are given as follows, outer casing (diameter = 20 cm), the inner rotating disk (diameter = 15 cm), the wire mesh and a cylindrical distributor having 9 column of 4 rows, separated from each other by a distance of 5 mm. A schematic diagram showing the RPB and its different parts is given in **Fig. 4.1** and the different parts of RPB are shown in **Fig. 4.2 (a)-(d)**. The experimental solution containing the EC's were kept in a container known as a reservoir. The

volume of the solution was kept fixed at 2 L. During the experiment, the experimental solution was pumped up by an electric motor inside the Rotating Packed Bed (RPB). The flow rate was kept constant at 0.2 L/min. The dosage of GO was also kept constant at 2 g/L. The rotors were moved by a shaft motor. The rotor speed was kept constant at around 150 R.P.M. With all the other experimental parameters remaining constant, the parameter that was varied was the solution of the adsorbate. For each EC, three concentration were tested 2.5 mg/L, 5 mg/L and 10 mg/L. In the functioning of the RPB, the liquid flew outwards through the distributor resulting in the formation of thin films and small dots. As mentioned before the GO was applied directly inside the reservoir. The formation of thin films and small dots reduces the mass transfer barrier thereby enhancing the adsorption. After treatment, the samples were collected, pre-treated and spectrophotometrically detected using the same techniques as described in case of batch studies, in **Section 4.2.4 *Batch Studies***. The result of the experiment is presented in the form of line graph with percentage removal against time. Every experiment was carried out three times, and the mean value with the respective standard deviation is given.
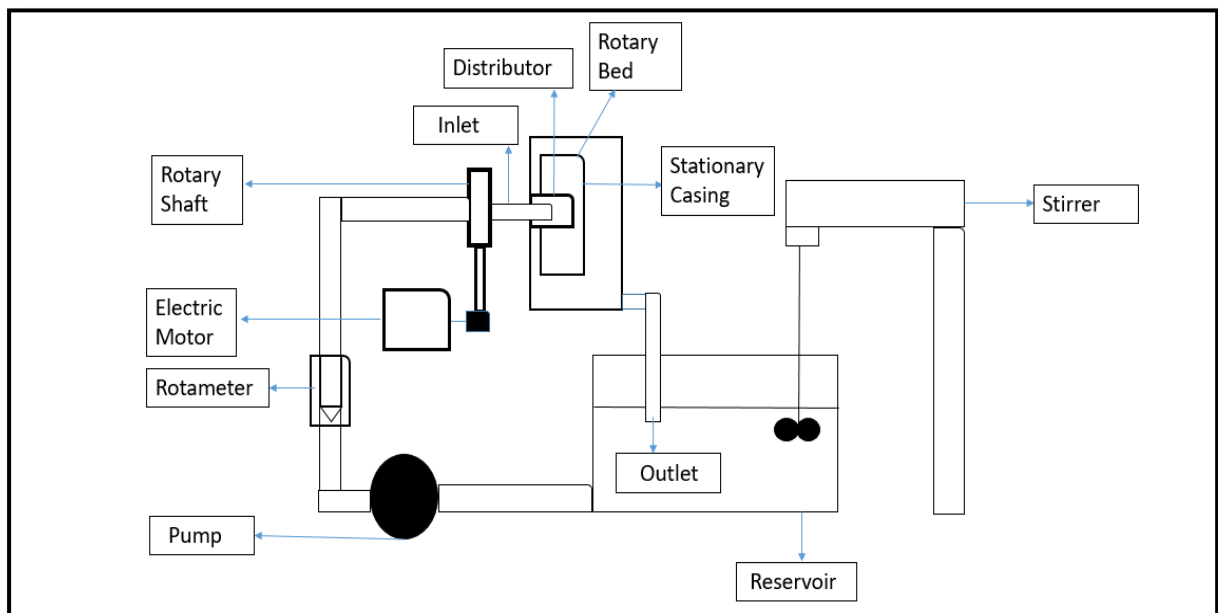


**Fig. 4.1**:- Schematic diagram of RPB.

**Fig. 4.2(a)** - RPB Casing :- Diameter 20 cm



**Fig. 4.2(b)**- RPB Distributor :- 36 pores
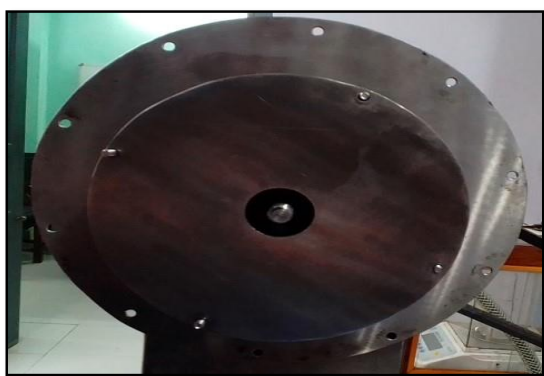


**Fig. 4.2(c)** - Rotating Disc :- Diameter 15 cm
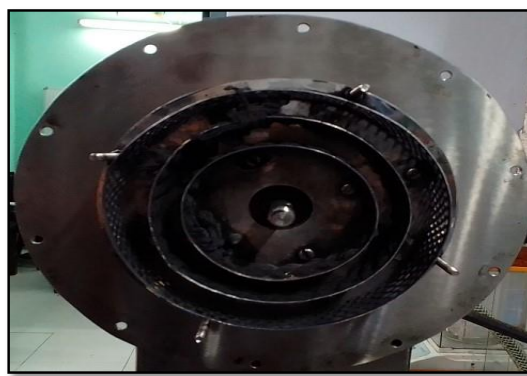


**Fig. 4.2(d)** - Wire Mesh for holding

packing material

## 4.2.8 Reusability study of GO

In case of the adsorption study, the reusability of the adsorbent is a critical determinant in terms of determining the feasibility of the adsorbent for future applications. In this study GO used in the batch study was utilised for assessing the reusability capacity and it was evaluated by successive adsorption-desorption cycles with different proposed desorbing mediums, namely distilled water, boiling (distilled) water, 10% HCl solution, 10% NaCl solution, 10% NaOH solution and 10% ethanol solution. After the completion of the batch study, the GO was retrieved for the reusability study. Then the GO was dried and was treated separately with each of these five desorbing solution for a fixed time (1 hr). After each desorption study, the regenerated GO was subsequently utilised for another cycle of adsorption study. In this way, the adsorption-desorption study was continued for about 5 cycles. The concentration of the adsorbate was kept at 10 mg/L for all the cycles and the dose of GO was kept fixed at 2 g/L (Banerjee et al., 2015b; Goswami et al., 2017).

## 4.3 CALCULATIONS :-

### 4.3.1 Percentage removal and adsorption capacity

The percentage removal of the EC's by GO during the batch study is calculated by the following equation.

$$Removal \% = \frac{C_0 - C_t}{C_0} \times 100 \dots\dots\dots\dots\dots\dots\dots\dots\dots\dots\dots\dots\dots\dots\dots\dots (xiii)$$

Where $C_0$ and $C_t$ represent the Concentration of adsorbate in the experimental solution at time 0 mins (mg/L) and Concentration of the adsorbate in the experimental solution at equilibrium time '$t$' (mg/L), respectively.

The adsorption capacity of the adsorbent GO after a pre-determined time interval (t) can be calculated with the following equation.

$$q_e = \frac{(C_0 - C_t) \times V}{m} \dots\dots\dots\dots\dots\dots\dots\dots\dots\dots\dots\dots\dots\dots\dots\dots (xiv)$$

$C_0$ and $C_t$ are same as in Eq-(xiii), $V$ (L) = Volume of the experimental solution used during the batch study and $m$ (g) = Mass of adsorbent used during the experiment. And $q_e$ (mg/g) = maximum adsorption capacity at equilibrium time $t$.

### 4.3.2 Adsorption Isotherm

Adsorption isotherm is performed to describe the equilibrium performance of the adsorbents when the temperature is constant (Al-ghouti & Da, 2020). From the batch study data, the result obtained from the study conducted over the variable adsorbent dose at constant temperature was utilized for calculating the different adsorption isotherms. In total four isotherm models were investigated namely the Langmuir model, the Freundlich model, the Temkin model and the Dubinin-Radushkevich model.

> **The Langmuir Isotherm Model**

The Langmuir model of isotherm is an empirical model which assumes that the thickness of the layer of adsorbed molecules is one molecule (unimolecular adsorption). As per the assumptions of Langmuir isotherm model, the adsorption occurs at identical site and the adsorption is homogeneous and equal sorption activation energy and constant enthalpies are possessed by each molecule (Al-ghouti & Da, 2020). The linear form of the Langmuir Isotherm equation is given as follows:-

$$\frac{C_e}{q_e} = \frac{1}{Q_0 b} + \frac{C_e}{Q_0} \dots\dots\dots\dots\dots\dots\dots\dots\dots\dots\dots\dots\dots\dots\dots\dots (xv)$$

Where, $C_e$ (mg/L) denotes equilibrium PHA concentration in solution , $q_e$ (mg g$^{-1}$) denotes theoretical maximum adsorption capacity, $Q_0$ (mg g$^{-1}$) denotes maximum monolayer coverage capacity calculated

from slope of $C_e/q_e$ vs. $C_e$ plot, $b$ (L mg$^{-1}$) denotes Langmuir coefficient of energy of adsorption calculated from intercept of $C_e/q_e$ vs. $C_e$ plot. The correlation of coefficient of the $C_e/q_e$ vs. $C_e$ plot (as reported) is denoted by $R^2$.

## ➤ The Freundlich Isotherm Model

In case of the Freundlich isotherm model, the adsorption layer is not considered to consist of a single layer of molecules. In Freundlich adsorption model, the adsorption is considered to be multi-layered and the adsorption heat and affinities are not considered to be evenly distributed on the heterogeneous surface of the adsorbent. Thus in other words, the Freundlich isotherm model defines the heterogeneity of the adsorbent surface as well as the exponential distribution of the active site and active site energies (Al-ghouti & Da, 2020). As per Freundlich model, the adsorption can be multi-layered, with uniform energy and reversible action (Gimbert et al., 2008). The non-linear form of the Freundlich isotherm model is given as follows:-

$$\ln q_e = \frac{1}{n_f} \ln C_e + \ln K_f \quad \dots\dots\dots\dots\dots\dots\dots\dots\dots\dots\dots\dots\dots\dots\dots\dots\dots\dots\dots\dots(xvi)$$

Where $C_e$, and $q_e$ denotes the same as mentioned in equation (xv). $n_f$ (no unit) denotes Adsorption intensity calculated from slope of $ln\ q_e$ vs. $ln\ C_e$ plot and $K_f$ (mg/g) denotes Freundlich coefficient of adsorption capacity calculated from intercept of $ln\ q_e$ vs. $ln\ C_e$ plot.

## ➤ The Temkin Isotherm Model

The Temkin isotherm model assumes the adsorption heat to be a function of temperature. Tempkin model considers that the heat of adsorption of all molecules in the layer decreases linearly due to the increase in surface coverage (Al-ghouti & Da, 2020; Gimbert et al., 2008). Another assumption of the Tempkin isotherm model is that the energy is evenly distributed (Al-ghouti & Da, 2020). A linear form of the Tempkin isotherm model is shown as follows :-

$$q_e = B_T \ln C_e + B_T \ln K_T \dots\dots\dots\dots\dots\dots\dots\dots\dots\dots\dots\dots\dots\dots\dots\dots\dots\dots\dots\dots\dots(xvii)$$

Where $C_e$, $q_e$ and $R^2$ denotes the same as mentioned in equation (xv). $B_T$ (J mole-1) denotes coefficients of heat of adsorption calculated from slope of $qe$ vs. $ln\ Ce$ plot at operational temperature $T$ (303 K). $K_T$ (L g$^{-1}$) denotes Temkin equilibrium binding constant calculated from intercept of $q_e$ vs. $ln\ C_e$ plot at operational temperature $T$ (303 K).

## ➤ The Dubinin-Radushkevich Isotherm Model

The Dubinin-Radushkevich model is a semi-empirical model which follows the mechanism of pore-filling. The Dubinin-Radushkevich describes a multi-layer adsorption involving Van der Waals forces. The Dubinin-Radushkevich model can be assigned to physical adsorption (Al-ghouti & Da, 2020). The linear equation representing the Dubinin-Radushkevich model is given as follows :-

$$\ln q_e = \ln Q_s - B\varepsilon^2 \dots\dots\dots\dots\dots\dots\dots\dots\dots\dots\dots\dots\dots\dots\dots\dots\dots\dots\dots\dots\dots\text{(xviii)}$$

Where $q_e$ denotes the same as mentioned in equation (xv). $B$ (mole $^2$ KJ$^{-2}$) denotes Dubinin–Radushkevich constant calculated from slope of $ln\ q_e$ vs. $\varepsilon^2$ plot. $Q_s$ (mg g$^{-1}$) denotes theoretical isotherm saturation capacity calculated from intercept of $ln\ q_e$ vs. $\varepsilon^2$ plot. $E$ (kJ mole$^{-1}$) denotes mean sorption energy.

In case of the Dubinin-Radushkevich isotherm model the parameter ε is denoted as the Polanyi potential and was evaluated from the Dubinin- Raudushkevich model with following equation.

$$\varepsilon = RT \ \ln\left(1 + \frac{1}{c_e}\right) \dots\dots\dots\dots\dots\dots\dots\dots\dots\dots\dots\dots\dots\dots\dots\dots\dots\dots\text{(xix)}$$

Where, $T$ = Temperature in Kelvin (which in case of the dose variation study was 303 ∘ K), $R$ (8.314 J $m^{-1}K^{-1}$) = universal gas constant and $Ce$ (mg/L) = concentration of adsorbate in experimental solution under equilibrium condition (Bhattacharya et al., 2021).

For each respective batch study of CBZ, NPX, RTN and BPA, the respective adsorption isotherm study result was presented in a tabular form. On being fitted with the experimental data, the adsorption isotherm for which the R$^2$ value was maximum was considered to best describe the adsorption process.

### 4.3.3 Adsorption Kinetics

From the analysis of Adsorption kinetics, the rate of the adsorption reaction can be determined thereby providing an idea about time required for the adsorption to reach equilibrium. Information regarding adsorption pathway and mechanism can also be obtained from the adsorption kinetics analysis (Sahoo & Prelot, 2020). The mechanism of the adsorption at the solid-liquid interface can be explained in the following four steps :-

1. Bulk diffusion, where the adsorbate is transferred from the bulk of the solution to the liquid film surrounding the adsorbate molecules.

2. External Diffusion, is the phase where the adsorbate molecules has to be diffused through the surface liquid films surrounding the solid particles.

3. Internal diffusion of the adsorbate molecules where they are transferred from the liquid film to the surface of the adsorbent through. This is also known as Intraparticle Diffusion. Intraparticle diffusion are mainly controlled by two mechanism (i) pore diffusion and (ii) surface diffusion.

4. Interaction of the adsorbate molecules with the surface sites, either through physisorption or chemisorption. Desorption is also a part of this step in case of reversible adsorption.

The overall rate of the adsorption reaction is determined by the slowest of the four steps. The first and fourth steps are fast whereas the second and third step are slow. In order to determine the reaction

kinetics of the adsorption of EC's on the surface of GO, five kinetic models were adopted namely Pseudo-first order reaction, pseudo-second order reaction, Elovich model, Intraparticle Diffusion model and Liquid film diffusion model.

➢ **Pseudo-first order kinetic model**

Pseudo-first order kinetic model was first proposed by **Lagergren** in 1898. The pseudo first order model is based on the assumption that, the rate of change of solute uptake with time is directly proportional to difference in saturation concentration and the amount of solid uptake with time (Sahoo & Prelot, 2020). Some other assumptions of the pseudo-first order kinetic models are, Sorption only occurs on the localized sites and there is no interaction between sorped molecules, the surface coverage does not affect the adsorption energy, the concentration of adsorbate is considered to be constant during the adsorption reaction, the adsorbed molecules forms a monolayer on the surface of the adsorbent (Largitte & Pasquier, 2016). The linear form of the pseudo-first order model is described as follows :-

$$\log(q_e - q_t) = [\log q_e - \frac{k_1}{2.303}t] \dots\dots\dots\dots\dots\dots\dots\dots\dots\dots\dots\dots\dots\dots\dots(xx)$$

Where, $k_1$ denotes Pseudo-1$^{st}$ order rate constant obtained from linear plots of *log ($q_e - q_t$)* vs. *t (min)*. $q_e$ (mg g$^{-1}$) denotes quantity of adsorbate adsorbed at equilibrium. $q_t$ denotes quantity of adsorbate adsorbed at time 't'.

➢ **Pseudo-second order kinetic model**

The pseudo-second order kinetic model is based on the assumption that, the rate limiting step is the chemical adsorption or chemisorption and the adsorption rate is dependent on the adsorption capacity of the adsorbent and not on the concentration of the adsorbate. The linear equation describing the Pseudo-second order kinetic model is described as follows :-

$$\frac{t}{q_t} = \frac{1}{k_2 q_e^2} + \frac{t}{q_e} \dots\dots\dots\dots\dots\dots\dots\dots\dots\dots\dots\dots\dots\dots\dots\dots\dots\dots\dots(xxi)$$

Where, $k_2$ denotes Pseudo-2$^{nd}$ order rate constant obtained from linear plots of *log (t/$q_t$)* vs. *t (min)*. $q_e$ (mg g$^{-1}$) denotes quantity of adsorbate adsorbed at equilibrium. $q_t$ denotes quantity of adsorbate adsorbed at time 't'.

➢ **Elovich model**

Elovich model is used to describe second-order kinetics assuming that the surface is energetically heterogeneous (Sahoo & Prelot, 2020). Some of the other assumptions of the Elovich models are, the sorption occurs on localized sites and there is interaction between the sorbed ions, with the increase in surface coverage the energy of adsorption also increases linearly and as per the Elovich model, the concentration of adsorbate molecules remains constant.

$$q_t = \frac{1}{\beta}\ln(\alpha\beta) + \frac{1}{\beta}\ln(t) \dots\dots\dots\dots\dots\dots\dots\dots\dots\dots\dots\dots\dots\dots\dots\dots\dots\dots\dots\text{(xxii)}$$

Where $\alpha$ (mg g$^{-1}$ min) denotes initial adsorption rate calculated from the intercept of liner plot of $q_t$ vs. *ln t*. $\beta$ (mg g$^{-1}$) denotes initial desorption rate calculated from the slope$^{-1}$ of liner plot of $q_t$ vs. *ln t*.

> **Intraparticle diffusion model**

The Intraparticle diffusion model was proposed by Webber and Morris. The linear equation representing the Intraparticle diffusion model is given as follows :-

$$q_t = K_{diff}\, t^{1/2} + C \dots\dots\dots\dots\dots\dots\dots\dots\dots\dots\dots\dots\dots\dots\dots\dots\dots\dots\dots\dots\dots\dots\text{(xxiii)}$$

Where, K$_{diff}$ (mg g$^{-1}$ min$^{-1/2}$) denotes intra-particle diffusion rate constant calculated from the slope of regression plot of $q_t$ vs. $t^{1/2}$ where $t$ is time (min). C (mg g$^{-1}$) denotes Constant calculated from the intercept of regression plot of $q_t$ vs. $t^{1/2}$ where $t$ is time (min).

On fitting the Intraparticle model with the experimental data, if a straight line is obtained on plotting $q_t$ vs. $t^{1/2}$, then Intraparticle diffusion is considered to be the main mechanism controlling the adsorption process (Sahoo & Prelot, 2020). However, if non-linearity is observed on plotting $q_t$ vs. $t^{1/2}$, then it can be assumed that other factors are also involved in the rate-controlling step of the adsorption process (Sahoo & Prelot, 2020). The constant 'C' denotes the thickness of the boundary layer, with greater value of C denoting greater effect of the boundary layer.

> **Liquid film diffusion model**

The Liquid film diffusion model is represented by the following linear equation :-

$$\ln(1 - \frac{q_t}{q_e}) = -Rt \dots\dots\dots\dots\dots\dots\dots\dots\dots\dots\dots\dots\dots\dots\dots\dots\dots\dots\dots\dots\dots\text{(xxiv)}$$

Where R denotes the rate of the reaction and 't' denotes the reaction time in minutes. The value $q_e$ and $q_t$ are the same as in equation (xx). The kinetic model is plotted as $\ln(1 - \frac{q_t}{q_e})$ vs t (Qiu et al., 2009).

## 4.3.4 Adsorption thermodynamics and Activation Energy

The activation energy (Ea) for the adsorption of the EC's on the surface of GO is determined by the Arrhenius equation which can be described as:-

$$\ln K = \frac{E_a}{R\,T} \dots\dots\dots\dots\dots\dots\dots\dots\dots\dots\dots\dots\dots\dots\dots\dots\dots\dots\dots\dots\dots\dots\dots\dots\dots\text{(xxv)}$$

Where K, A, R and T represents the kinetic constant (rate constant of the kinetic model which best described the adsorption process), pre-exponential factor, universal gas constant and temperature in Kelvin respectively. The value of E$_a$ for the process operation can be deduced from (ln K Vs $T^{-1}$), which is the slope of the Arrhenius plot (Banerjee et al., 2016).

The thermodynamics of the process of adsorption of EC's on GO was determined by the changes in the Gibbs free energy ($\Delta$ G°; kJ mol$^{-1}$), change in the enthalpy ($\Delta$ H°; kJ mol$^{-1}$) and the change in the entropy ($\Delta$ S°; J$^{-1}$ mol$^{-1}$ K$^{-1}$). The thermodynamic variables were calculated by utilizing the following three equations.

$$K_c = \frac{C_a}{C_e} \quad \dots\dots\dots\dots\dots\dots\dots\dots\dots\dots\dots\dots\dots\dots\dots\dots\dots\dots\dots\dots\dots\dots\text{(xxvi)}$$

$$\Delta G = RT \ln Kc \quad \dots\dots\dots\dots\dots\dots\dots\dots\dots\dots\dots\dots\dots\dots\dots\dots\dots\dots\dots\text{(xxvii)}$$

$$\ln K_c = -\left(\frac{\Delta H}{\Delta R}\right)\left(\frac{1}{T}\right) + \left(\frac{\Delta S}{R}\right)\dots\dots\dots\dots\dots\dots\dots\dots\dots\dots\dots\dots\dots\dots\text{(xxviii)}$$

Where $K_c$, $C_a$ and T denotes the distribution coefficient of adsorption, the quantity of EC's adsorbed by a unit mass of GO and the absolute operational temperature in Kelvin respectively. The intercept and slope of the $\ln K_c$ vs (1/T) plot was utilized to calculate the value of $\Delta S°$ and $\Delta H°$ respectively (Banerjee et al., 2017).

## 4.3.5. Optimization using RSM

For the RSM process, a quadratic polynomial model was derived by analysis of variance and it was utilized for the purpose of maximizing the optimization for the process operation of adsorption of EC's on the surface of GO. The association between the three independent experimental parameters that were selected for this study (dose of the adsorbent GO, pH of the experimental solution and reaction time of the experiment) was empirical in nature and it was derived from the polynomial quadratic equation (Bhattacharya et al., 2020).

# 4.4  RESULTS :-

## 4.4.1 Characterization

### *4.4.1.1 SEM analysis of GO*

**Fig. 4.3 (a)** exhibits the surface morphology of GO as recorded using SEM. The SEM images of GONP revealed that it is composed of thin, closely associated and highly overlapping platelet-like carbon sheets. The rough surfaces of these crumpled GO reportedly facilitate efficient adsorption (Goswami et al., 2017; Mukherjee et al., 2019). These wrinkled and layered structures of GO are reportedly formed as a result of interactions between oxygen containing functional groups (Bhattacharya et al., 2020).
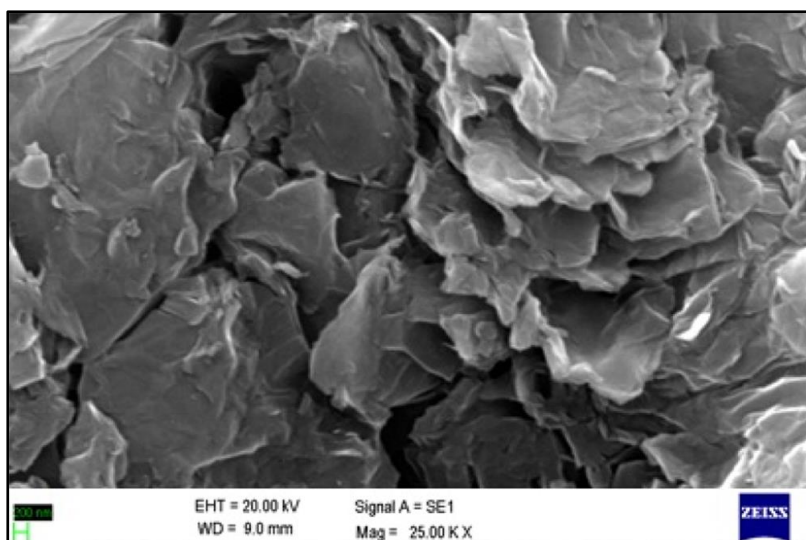
**Fig. 4.3 (a)** :- SEM image of GO

### 4.4.1.2 FTIR analysis of GO

The FTIR spectra of GO is shown in **Fig. 4.3(b),** from there it was observed that GO exhibited points at 3400 cm$^{-1}$, 2900 cm$^{-1}$, 1550-1600 cm$^{-1}$ and 1385 cm$^{-1}$ which denotes the functional groups C=O, O-H, C=H, C-H and C-O respectively. Thereby it can be inferred that the GO synthesized from graphite by Hummers method was sufficiently oxidized. Moreover these peaks are denoted as the characteristic peaks of GO (Banerjee et al., 2016).
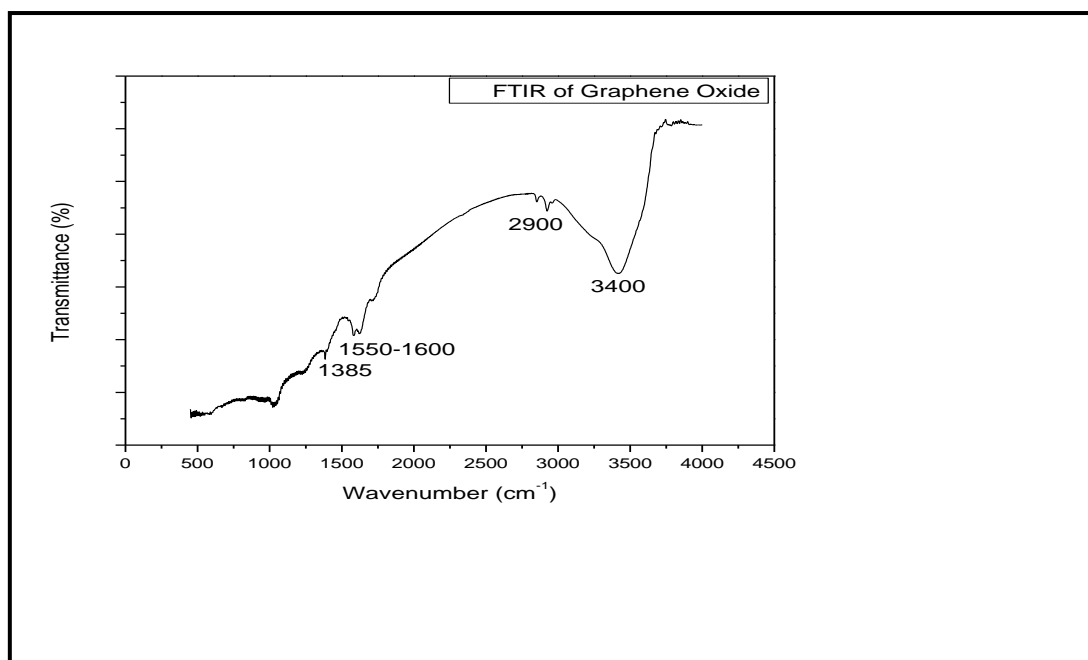


**Fig. 4.3 (b)** :- FT-IR spectra image of GO

*4.4.1.3 XRD analysis of GO*

The XRD spectra shown in **Fig. 4.3(c)** exhibit three prominent peaks at 12.7°, 25.6° and 42.6°. The peak at 12.7° is the characteristic peak of GO (L. Liu et al., 2012; Nawaz et al., 2017) whereas the peaks at 25.6 ° and 42.6 ° are due to unreacted graphite (Ganguly et al., 2020). These are denoted as the characteristic peaks of GO as per previous literature thereby denoting that GO was successfully synthesized from graphite by the Hummers method.
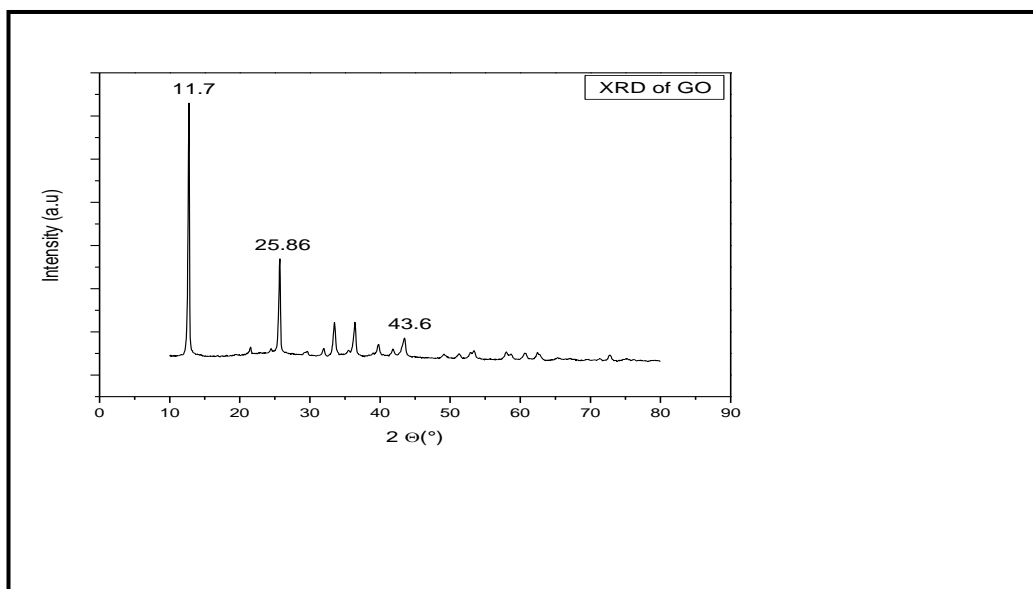


**Fig. 4.3 (c)** :- XRD image of GO

*4.4.1.4 Raman Spectroscopy of G*

The Raman Spectroscopy of GO is shown in **Fig. 4.3 (d)**, from there it can observed it has two main peaks the peak at 1341.64 is known as the D-band and is marked as $I_D$ in the figure and the peak at 1587.66 is known as the G-band and is marked as $I_G$. The D band denotes dis-ordered carbon structure due to structural defect caused by the attachment of hydroxyl and epoxide groups on the carbon basal plane whereas the peak present at the G-band denote the tangential C-C vibration (Nawaz et al., 2017; Wang et al., 2014). The ratio between and $I_D/I_G$ denotes the ratio between $sp^2$ hybridized carbon atoms and $sp^3$ hybridized carbon atoms, with high $I_D/I_G$ values denoting greater defects in the $sp^3$ carbon structure, denoting smaller size of $sp^2$ hybridized carbon molecules thereby denoting reduction of the GO molecules (Nawaz et al., 2017). From the Raman Spectra it can be seen that the ration of $I_D$ and $I_G$ is near about 1 (length wise) with $I_D$ being slightly bigger than $I_G$, denoting the almost equal number of $sp^2$ and $sp^3$ hybridized carbon atoms, thereby denoting successful oxidation of graphite into GO molecules .
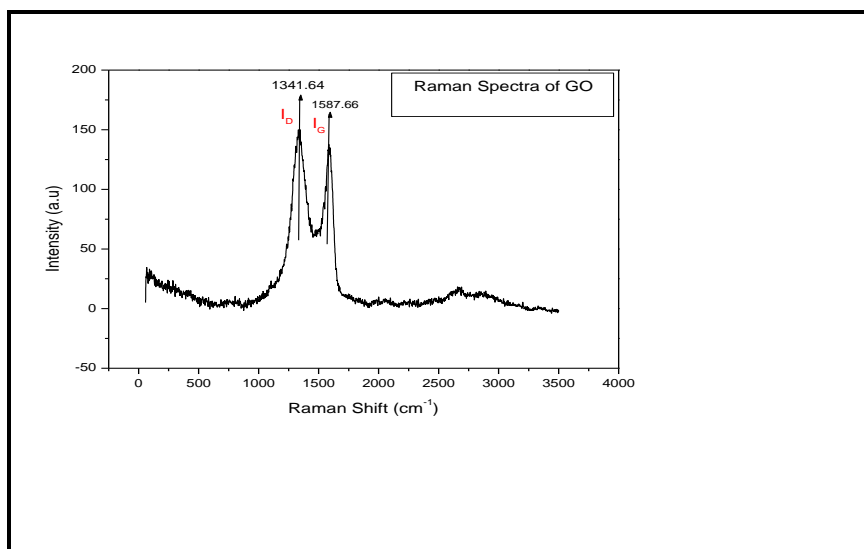
**Fig. 4.3 (d)** :- Raman Spectra of GO

## 4.4.2 Batch Study Results

### 4.4.2.1 Effect of concentration of adsorbate on the removal efficacy of GO

In order to investigate the effect of the concentration of the adsorbate on the removal efficacy of GO, four concentration (5 mg/L, 10 mg/L, 15 mg/L and 20 mg/L) were taken in case of each of the EC's . The dose of GO, pH of the experimental solution and temperature were all kept constant at 2 g/L, pH 7 and 303 K respectively. The result of the experiment is shown in **Fig. 4.4 (a-d)**, and from there it was observed that the removal of CBZ and NPX by GO (**Fig. 4.4(a)** and **Fig. 4.4(b)**) decreased with the increase in concentration of the adsorbate (Bhattacharya et al., 2020). This phenomenon could be attributed to the fact that, with the dosage of GO remaining constant, the active sites available on the surface of the adsorbent got saturated with the increase in adsorbate concentration. As a consequence of which the removal of CBZ and NPX by GO, also decreased with the increase in concentration of CBZ and NPX (Banerjee et al., 2017). In case of CBZ, the highest removal was observed at the 5 mg/L concentration (99.18%) followed by the 10 mg/L concentration (97.74%). However, for the 15 mg/L concentration of CBZ the removal decreased to 94.38 % followed by a significant decrease in case of the 20 mg/L concentration of CBZ (84.88 %). For NPX, the highest removal was observed at the 5 mg/L concentration (85.27 %) followed by the 10 mg/L concentration (80.58 %) followed by the 15 mg/L concentration of NPX (68.52 %) and lastly the lowest removal was observed for the 20 mg/L concentration of NPX (63.76 %).

In case of the removal of RTN and BPA by GO (**Fig. 4.4(c)** and **Fig. 4.4 (d)**) it was observed that the removal of the EC's by GO increased when the concentration increased from 5 mg/L to 10 mg/L. This could to ascribed to the gradient based transfer of adsorbate molecules from the solution to the surface of GO (Bhattacharya et al., 2021). However, when the concentration increased beyond the 10 mg/L

mark, the removal of the adsorbates by GO again decreased. This could be ascribed to the fact that with the dosage of GO remaining constant, beyond the optimum concentration the surface of GO was saturated by the adsorbent molecules leading to decreased adsorption beyond a particular point (Banerjee et al., 2016; Bhattacharya et al., 2021). In case of RTN, the highest removal was observed at the 10 mg/L concentration (97.3 %) followed by the 5 mg/L concentration (95.14 %) followed by the 15 mg/L concentration of RTN (88.11 %) and lastly the lowest removal was observed for the 20 mg/L concentration of RTN (86.35 %). In case of BPA, the highest removal was observed at the 10 mg/L concentration (86.92 %) followed by the 5 mg/L concentration (84.48 %) followed by the 15 mg/L concentration of BPA (80.14 %) and lastly the lowest removal was observed for the 20 mg/L concentration of BPA (54.33 %).
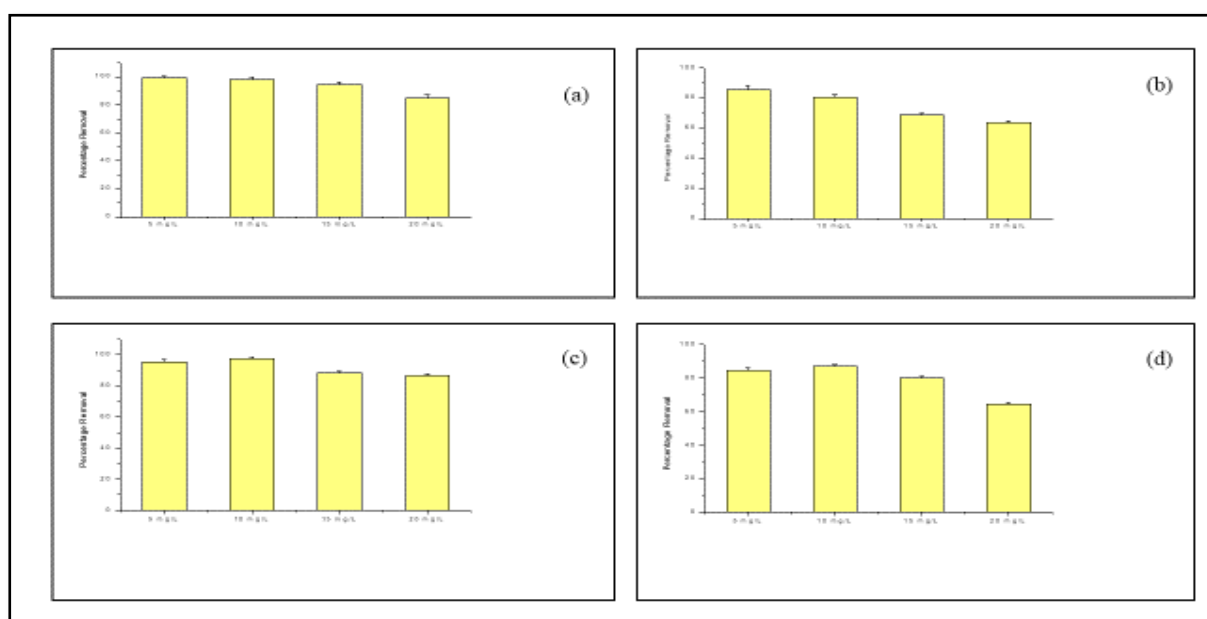


**Fig. 4.4:-** Effect of concentration on removal of **(a)** CBZ **(b)** NPX **(c)** RTN **(d)** BPA by GO

### 4.4.2.2 Effect of dosage of adsorbent on the removal efficacy of GO

The effect of the dosage of the adsorbent on its removal efficacy was investigated over four different dosage of GO i.e., 0.5 g/L, 1 g/L, 1.5 g/L and 2 g/L. The concentration of EC's were kept constant at 10 mg/L. The pH of the solution was kept at neutral and the temperature was kept at 303 K. The result of the experiment is given shown in (**Fig. 4.5(a)-(d)**). A similar trend was observed in case of each of the dosage study and that was, the removal of each of the EC's (CBZ, NPX, RTN and BPA) increased with increase in dosage of GO. This outcome could be attributed to the fact that with the increase in dosage of GO, the number of active sites available increases leading to greater uptake of the EC's by GO (Banerjee et al., 2016; Bhattacharya et al., 2020, 2021; Mukherjee et al., 2019). As a consequence of which the removal of the EC's were directly proportional to the dosage of GO. For CBZ , the removal

at the 0.5 g/L dose of GO was observed to be 89.51 %, the removal at 1 g/L dosage was found to be 94.86 %, at 1.5 g/L dosage was found to be 96.09 % and at the 2 g/L dosage was 97.5 % respectively. For NPX, the removal at the 0.5 g/L dose of GO was observed to be 62.94 %, the removal at 1 g/L dosage was found to be 73.52 %, at 1.5 g/L dosage was found to be 76.07 % and at the 2 g/L dosage was 80.99 % respectively. For RTN, the removal at the 0.5 g/L dose of GO was observed to be 73.78 %, the removal at 1 g/L dosage was found to be 78.11 %, at 1.5 g/L dosage was found to be 86.22 % and at the 2 g/L dosage was 97.57 % respectively. For BPA, the removal at the 0.5 g/L dose of GO was observed to be 66.88 %, the removal at 1 g/L dosage was found to be 76.51 %, at 1.5 g/L dosage was found to be 82.99 % and at the 2 g/L dosage was 86.16 % respectively. In case of each of the EC, the highest removal was achieved for the 2 g/L dosage of GO therefore this dosage of GO was utilized for further studies.
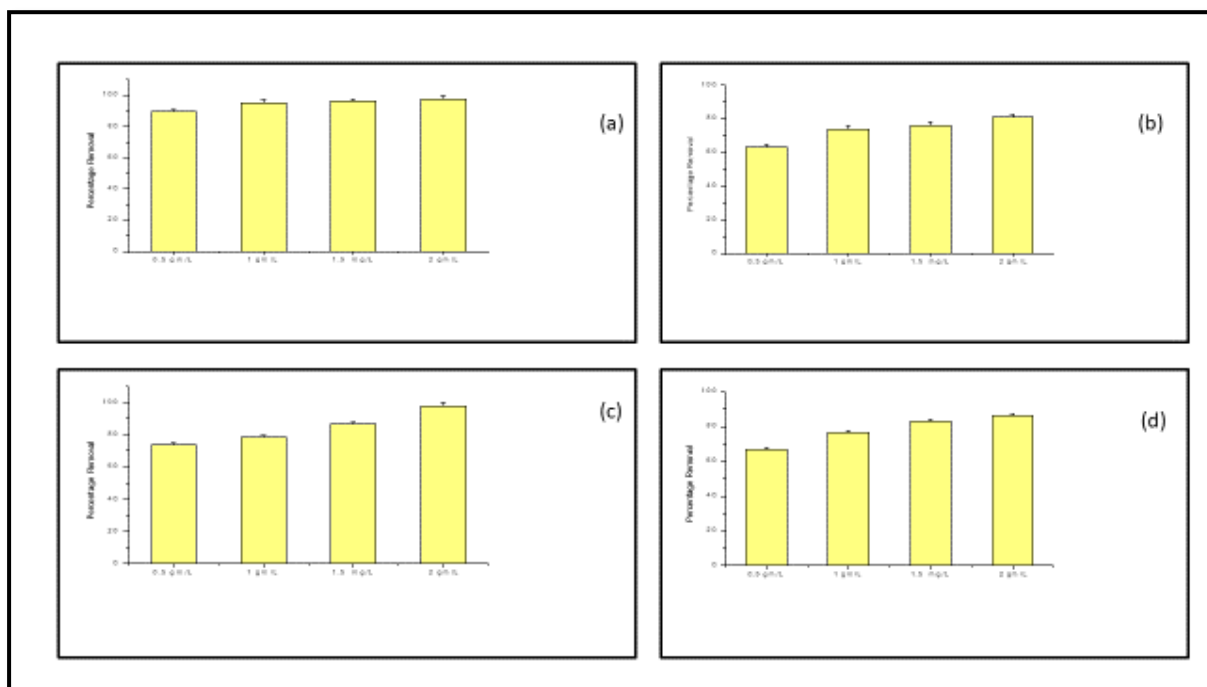


**Fig. 4.5:-** Effect of GO dosage on removal of **(a)** CBZ **(b)** NPX **(c)** RTN **(d)** BPA by GO

### *4.4.2.3 Effect of pH of the experimental solution on the removal efficacy of GO*

The effect of pH on the removal of EC's by GO was investigated under five different pH of the experimental solution, viz., pH 2, pH 4, pH 6, pH 8 and pH 10. The concentration of CBZ was kept constant at 10 mg/L and the dosage of GO was kept fixed at 2 g/L. The result of the experiment is shown in **Fig. 4**.**6(a)-(d)**. From the result of the experimental study shown in **Fig. 4.6(a)** it was observed that the removal of CBZ by GO decreased with the increase in pH of the experimental solution. The highest removal was observed at pH 2 (99.38 %) followed by pH 4 (98.15 %) and pH 6 (97.74 %). The lowest

removal was observed for pH 10 (86.21 %). Similar results were observed in the works of (Bhattacharya et al., 2020; A. M. E. Khalil et al., 2020) and (Delhiraja et al., 2019) . The logic behind this phenomenon can be given as, CBZ adsorption by GO particles is reportedly mediated via π-π interactions, electrostatic interactions and hydrophobic effects depending on the proximity of the bonding molecules (Bhattacharya et al., 2020). The $pK_a$ value of CBZ is 13.9 (Al-hamadani et al., 2018). Therefore, under pH values lower than $pK_a$ values, CBZ is presented in protonated form which reportedly facilitates uptake of the same by the adsorbent particles. The pH of the experimental solutions also influences functional groups present on the surface of both CBZ ($-NH_2$) and GO ($-OH$, $-COOH$, $-C-O$, $-C=O$) (Al-hamadani et al., 2018). The $pH_{pzc}$ of GO is $4.87 \pm 0.26$ (Banerjee et al., 2016). At pH values lower than $pH_{pzc}$, the surface of GO reportedly acquires positive charge (Banerjee et al., 2016) and is therefore capable of efficient removal of neutral CBZ moieties from aqueous solutions. According to similar studies, the decline in percentage removal of CBZ recorded at higher pH had resulted from hydrophobicity of CBZ exhibited at these pH conditions.

From the result of the experimental study shown in **Fig. 4.6(b)** it was observed that the removal of NPX by GO decreased with the increase in pH of the experimental solution. The highest removal was observed at pH 4 (90.93 %) followed by pH 2 (85.98 %), pH 6 (81.84 %) and pH 8 (70.41 %). The lowest removal was observed for pH 10 (62 %). Similar results were observed in the works of (Mondal et al., 2020) and (Ciğeroğlu et al., 2020). The logic behind this phenomenon can be given as, NPX adsorption by GO particles is reportedly mediated via π-π interactions, electrostatic interactions and hydrogen (H-H) bonding (Mondal et al., 2020). As stated earlier, the $pH_{pzc}$ of GO is 4.87 +/- 0.26 (Banerjee et al., 2016) and the $pK_a$ value of NPX is 4.2 (Reynel-Avila et al., 2015). Therefore at pH below 4.15 the molecules of NPX are neutrally charged whereas above pH 4.15 the molecules of NPX are negatively charged. Similarly, the surface of GO are positive below there $pH_{pzc}$ (4.87 +/- 0.26) and negative above the $pH_{pzc}$ (Banerjee et al., 2016). Therefore at the lower pH range the adsorption of NPX by GO is enhanced due to van der Waal's interaction and hydrogen bonding (I˙lbay et al., 2015) whereas at the higher pH range, the adsorption of NPX by GO is reduced due to the repulsion between negative surface of GO and the anionic form of NPX (Mondal et al., 2020). As ionic interaction is not feasible at pH under 4.2, therefore the highest removal was observed at pH 4  (Mondal et al., 2020). Thus, the highest removal of NPX was observed at pH 4 and thereafter the removal of NPX by GO decreased with the increase in pH of the experimental solution (Bhattacharya et al., 2020).

From the result of the experiment as shown in **Fig. 4.6 (c)** it was observed that the removal of RTN by GO increased with the increase in pH of the experimental solution till pH 6. With further increase in pH, a decline in the removal of RTN was observed. The reason behind this observation can be explained as, RTN has two $pK_a$ values 2.7 and 8.2 (Kortejarvi et al., 2005) and RTN remains in a protonated, cationic stage at pH below 2.7 and it remains in an anionic stage at pH greater than 8.2 (Al-rub et al.,

2020). On the other hand, as mentioned before the pH$_{pzc}$ of GO is 4.87 +/- 0.26  (Bhattacharya et al., 2020) meaning the surface of GO will be positively charged at pH less than ~5 and will be negatively charged at pH greater than ~ 5. Therefore at the lower pH range, the removal of RTN will be affected due to the repulsion of the positives charges between the molecules of RTN and the surface of GO. Similarly, at the higher pH range the adsorption will be affected due to the accumulation of negative charges on the surface of GO and the anionic molecules of RTN (Al-rub et al., 2020). As a result the highest removal of RTN by GO was observed at pH 6, where the charge of the RTN molecules were neutral and the surface of GO was negatively charged (Al-rub et al., 2020). The adsorption of RTN molecules on the surface of GO might have been due to H-bonding and dipole-dipole interactions (Al-rub et al., 2020)**.** Similar results were observed in the studies of (Bhattacharyya et al., 2019) and (Bhattacharyyaa et al., 2018) where RTN was removed from water by GO and an activated carbon synthesized from lemon peel respectively.

From the result of the experiment as shown in **Fig. 4.6(d)** it was observed that the removal of BPA by GO varied very little with the change in pH from pH 2 – pH 6, exhibiting a slight decrease in removal with the increase in pH from pH 2 (87.54 %) to pH 6 (86.6 %). However, with the increase in pH to pH 8 a significant decrease was observed in the adsorption of BPA by GO as the removal percentage fell down from 86.2 % to 78.74 % which further fell down to 70.79 % at pH 10. The reason behind this phenomenon can be described as follows, the pK$_a$ value of BPA is 9.6, and beyond this pH the BPA molecules dissociate to form bis-phenolate anions (L. Xu et al., 2018). As a consequence of which, at the higher pH range, the removal of BPA by GO is drastically reduced due to the accumulation of negative charges on the surface of GO and in the BPA molecules. Thus the removal of BPA by GO was found to be at a higher range at the acidic neutral pH range (pH 4 – pH 6) and followed by which it decreased drastically at the higher basic pH range (pH 8 – pH 10). Similar result have been observed in the work of **Chang et al., 2013**(Chang et al., 2012) and **Xu et al., 2012**(J. Xu et al., 2012).
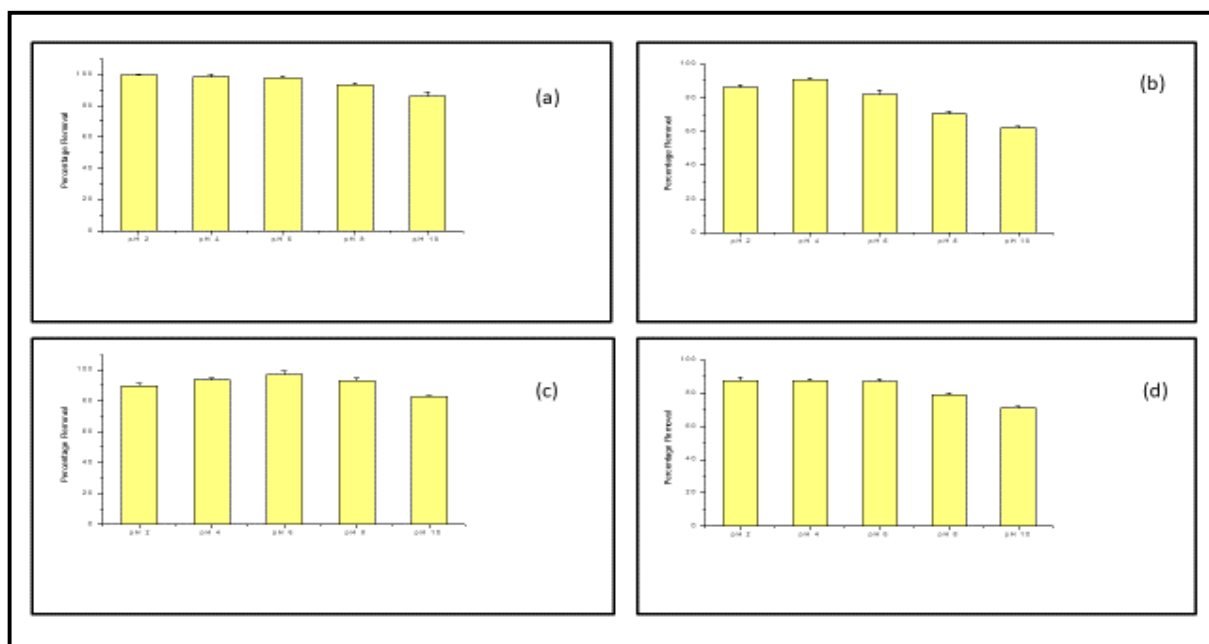
**Fig. 4.6:-** Effect of pH on the removal of **(a)** CBZ **(b)** NPX **(c)** RTN **(d)** BPA by GO

### *4.4.2.4 Effect of temperature on the removal efficacy of GO*

The effect of temperature on the removal of the EC's by GO was detected at four temperatures 298 K, 303 K, 308 K and 313 K. For every experiment, the dosage of GO was kept constant at 2 g/L and the concentration of EC's was kept constant at 10 mg/L and pH of the experimental solution was kept neutral. The result of the experiment is shown in (**Fig. 4.7(a)-(d)**)**.** From there it was observed that the removal of CBZ and NPX by GO (**Fig. 4**.**7(a)** and **Fig. 4.7(b)** respectively) increased with the increase in temperature. For CBZ the removal was 93.62 % at 298 K, 97.12 % at 303 K, 98.15 % at 308 K and 99.18 % at 313 K. For NPX the removal was 77.25 % at 298 K, 79.81 % at 303 K, 80.63 % at 308 K and 83.63 % at 313 K. As observed in both the cases the highest removal was observed at 313 K (99.18 % for CBZ and 83.63 % for NPX). This could be attributed to the widening of the pores of the GO at the higher temperature thereby leading to higher adsorption (Bhattacharya et al., 2020). The increase in temperature also increased the number of collision between the surface of adsorbent and the adsorbate molecules thereby resulting in greater adsorption of adsorbate molecules by GO (Bhattacharya et al., 2021). From the nature of the reaction it can also be stated that the adsorption of CBZ and NPX molecules on the surface of GO was endothermic in nature (Banerjee et al., 2016; Bhattacharya et al., 2020).

In case of the removal of RTN by GO (**Fig. 4.7 (c)**) it was observed that the removal of RTN by GO increased from 91.89 % to 96.49 % on increasing the temperature from 298 K to 303 K. After that the removal of RTN decreased with increase in temperature. This can be attributed to the fact that on increasing the temperature to the point of 303 K, the interaction between the molecules of RTN and the surface of GO increased resulting in greater adsorption of RTN molecules on the surface of GO

(Bhattacharya et al., 2021). The increase in porosity of GO might have also contributed to the higher adsorption of RTN molecules (Banerjee et al., 2016). However, on increasing the temperature beyond 303 K, the removal of RTN decreased, which could be attributed to the increased kinetic energy of the surface of GO and the RTN molecules resulting in the breakage of the adsorbate adsorbent bonds (Al-rub et al., 2020). The removal of RTN by GO decreased to 93.51 % on increasing the temperature to 308 K and to 88.11 % on increasing the temperature to 313 K.  Thus from the experimental result it was inferred that 303 K was the most optimum temperature for the adsorption of RTN by GO.

From the result of the experiment as showed in **Fig. 4.7(d),** it was observed that the removal of BPA by GO remained almost constant at the temperature range of 298 K to 308 K, with 85.34 % removal at 298 K, 86.37 % removal at 303 K and 85.41 % removal at 308 K. On increasing the temperature further to 313 K, the removal percent decreased slightly to 82.92 %. This could be attributed to the tendency of the adsorbate molecules to be transformed from the solid phase to the bulk solution due to the increase in temperature (Chang et al., 2012). Similar results were observed in the studies of (Chang et al., 2012; Kwon & Lee, 2015; Phatthanakittiphong & Seo, 2016; Xu et al., 2012).
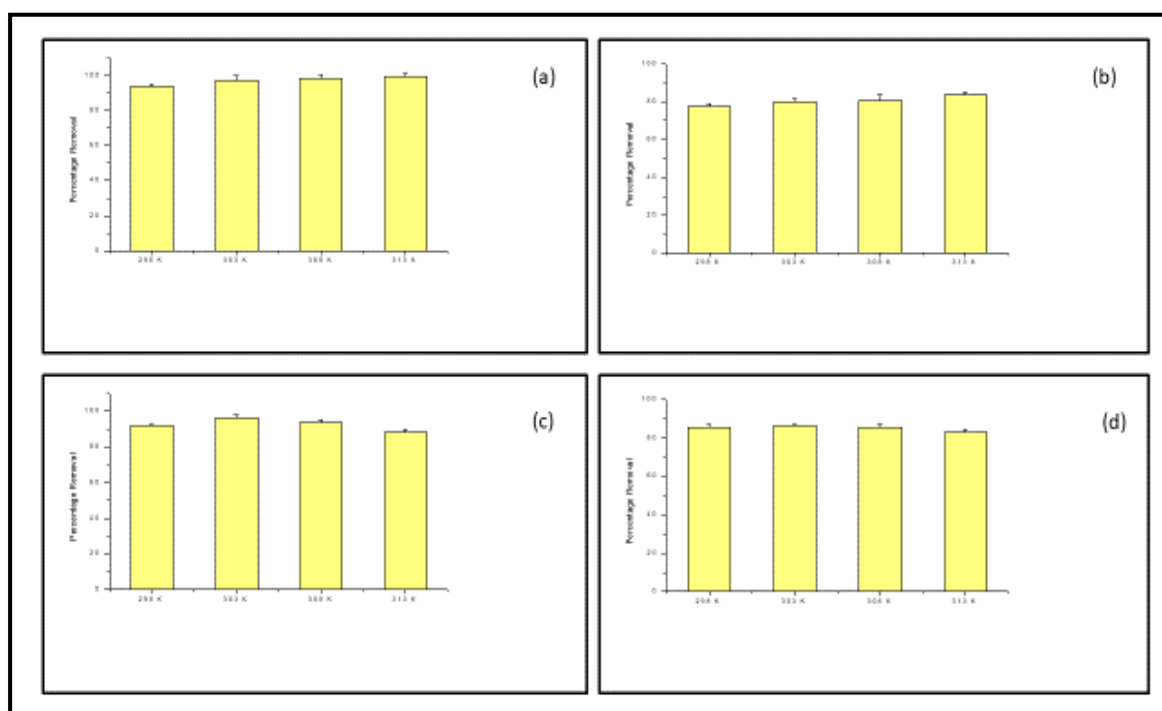


**Fig. 4.7:-** Effect of temperature on the removal of **(a)** CBZ **(b)** NPX **(c)** RTN **(d)** BPA by GO

## 4.4.3 Adsorption Isotherm

The dose variation data (0.5 g/L-2 g/L) from the batch study was used for calculating the adsorption isotherm. The result of the isotherm study is given in the following tables.

### 4.4.3.1 Adsorption Isotherm for the adsorption of CBZ by GO

The result of the experiment is given in **Table 4.2** and from there it was observed that the adsorption of CBZ on the surface of GO was best described by the Langmuir isotherm model ($R^2$=0.97) denoting that the adsorption of CBZ on the surface of GO was uniform and monolayer in nature and the binding energy of each adsorbed molecule on the surface of GO was uniform in nature (Banerjee et al., 2016).

**Table 4.2**:- Investigating different isotherm parameters for CBZ adsorption by GO

| Models | Parameters | Description | Unit | Adsorbent Dosage (g/L) | | | |
|---|---|---|---|---|---|---|---|
| | | | | 0.5 g/L | 1 g/L | 1.5 g/L | 2 g/L |
| Langmuir | $C_e$ | Equilibrium pharmaceutical concentration in solution | mg L$^{-1}$ | 1.04 | 0.51 | 0.39 | 0.25 |
| | $q_e$ | Theoretical maximum adsorption capacity | mg g$^{-1}$ | 17.9 | 9.49 | 6.41 | 4.88 |
| | $Q_0$ | Maximum monolayer coverage capacity calculated from slope of $C_e/q_e$ vs. $C_e$ plot. | mg g$^{-1}$ | 5.22 | 6.19 | 4.29 | 3.29 |
| | $b$ | Langmuir coefficient of energy of adsorption calculated from intercept of $C_e/q_e$ vs. $C_e$ plot. | L mg$^{-1}$ | 7.84 | 3.56 | 4.46 | 5.64 |
| | $R^2$ | Correlation coefficient | | 0.89 | 0.99 | 0.99 | 0.99 |
| Freundlich | $n_f$ | Adsorption intensity calculated from slope of $ln\ q_e$ vs. $ln\ C_e$ plot | | 1.91 | 5.31 | 6.47 | 7.36 |
| | $K_f$ | Freundlich coefficient of adsorption capacity calculated from intercept of $ln\ q_e$ vs. $ln\ C_e$ plot | mg g$^{-1}$ | 20.47 | 8.68 | 5.72 | 4.25 |
| | $R^2$ | Correlation coefficient | | 0.83 | 0.91 | 0.88 | 0.85 |
| Temkin | $B_T$ | Coefficients of heat of adsorption calculated from slope of $q_e$ vs. $ln\ C_e$ plot at operational temperature $T$ (303K ) | J mol$^{-1}$ | 5.92 | 1.51 | 0.85 | 0.5624 |
| | $K_T$ | Temkin equilibrium binding constant calculated from intercept of $q_e$ vs. $ln\ C_e$ plot at operational temperature $T$ (303 K) | L g$^{-1}$ | 24.85 | 328.83 | 903.96 | 2063.97 |
| | $R^2$ | Correlation coefficient | | 0.93 | 0.94 | 0.92 | 0.88 |
| Dubinin-Radushkevich | $B$ | Dubinin–Radushkevich constant calculated from slope of $ln\ q_e$ vs. $\varepsilon^2$ plot. | mole$^2$ KJ$^{-2}$ | 0.0000003 | 0.00000004 | 0.00000003 | 0.00000002 |
| | $Q_s$ | Theoretical isotherm saturation capacity calculated from intercept of $ln\ q_e$ vs. $\varepsilon^2$ plot. | mg g$^{-1}$ | 8.91 | 7.21 | 3.66 | 3.94 |
| | $E$ | Mean sorption energy | kJ mole$^{-1}$ | 1290.99 | 3535.53 | 4082.48 | 5000 |
| | $R^2$ | Correlation coefficient | | 0.57 | 0.69 | 0.67 | 0.54 |
| | $\varepsilon$ | Polanyi Potential | | 1686.15 | 2720.09 | 3197.22 | 4079.47 |

### 4.4.3.2 Adsorption Isotherm for the adsorption of NPX by GO

The result of the experiment is given in **Table 4.3** and from there it was observed that the adsorption of NPX on the surface of GO was best described by the Tempkin isotherm model ($R^2$=0.98) denoting that the adsorption of NPX on the surface of GO was uniform in nature and the heat of adsorption of the adsorbent moieties decreased in a linear fashion as the reaction increased (Bhattacharya et al., 2020).

**Table 4.3**:- Investigating different isotherm parameters for NPX adsorption by GO

| Models | Parameters | Description | Unit | Adsorbent Dosage (g/L) | | | |
|---|---|---|---|---|---|---|---|
| | | | | 0.5 g/L | 1 g/L | 1.5 g/L | 2 g/L |
| Langmuir | $C_e$ | Equilibrium pharmaceutical concentration in solution | mg L$^{1}$ | 3.71 | 2.65 | 2.39 | 1.9 |
| | $q_e$ | Theoretical maximum adsorption capacity | mg g$^{-1}$ | 12.59 | 7.35 | 5.07 | 4.05 |
| | $Q_0$ | Maximum monolayer coverage capacity calculated from slope of $C_e/q_e$ vs. $C_e$ plot. | mg g$^{-1}$ | 2.71 | 2.67 | 1.78 | 1.56 |
| | $b$ | Langmuir coefficient of energy of adsorption calculated from intercept of $C_e/q_e$ vs. $C_e$ plot. | L mg$^{-1}$ | 0.29 | 0.51 | 0.55 | 0.71 |
| | R$^2$ | Correlation coefficient | | 0.92 | 0.95 | 0.96 | 0.98 |
| Freundlich | $n_f$ | Adsorption intensity calculated from slope of $ln\ q_e$ vs. $ln\ C_e$ plot | | 0.69 | 1.28 | 1.32 | 1.55 |
| | $K_f$ | Freundlich coefficient of adsorption capacity calculated from intercept of $ln\ q_e$ vs. $ln\ C_e$ plot | mg g$^{-1}$ | 92.92 | 16.66 | 10.53 | 6.56 |
| | R$^2$ | Correlation coefficient | | 0.95 | 0.94 | 0.94 | 0.96 |
| Temkin | $B_T$ | Coefficients of heat of adsorption calculated from slope of $q_e$ vs. $ln\ C_e$ plot at operational temperature $T$ (303K ) | J mol$^{-1}$ | 11.21 | 4.19 | 2.72 | 1.85 |
| | $K_T$ | Temkin equilibrium binding constant calculated from intercept of $q_e$ vs. $ln\ C_e$ plot at operational temperature $T$ (303 K) | L g$^{-1}$ | 11.81 | 15.93 | 16.33 | 0.055 |
| | R$^2$ | Correlation coefficient | | 0.99 | 0.98 | 0.98 | 0.98 |
| Dubinin-Radushkevich | $B$ | Dubinin–Radushkevich constant calculated from slope of $ln\ q_e$ vs. $\varepsilon^2$ plot. | mole$^{2}$ KJ$^{-2}$ | 0.000004 | 0.000001 | 0.000001 | 0.0000007 |
| | $Q_s$ | Theoretical isotherm saturation capacity calculated from intercept of $ln\ q_e$ vs. $\varepsilon^2$ plot. | mg g$^{-1}$ | 3.62 | 3.63 | 0.79 | 0.37 |
| | $E$ | Mean sorption energy | kJ mole$^{-1}$ | 1118.03 | 2236.07 | 2236.07 | 2672.61 |
| | R$^2$ | Correlation coefficient | | 0.85 | 0.81 | 0.78 | 0.83 |
| | $\varepsilon$ | Polanyi Potential | | 3.71 | 2.65 | 2.39 | 1.9 |

### 4.4.3.3 *Adsorption Isotherm for the adsorption of RTN by GO*

The result of the experiment is given in **Table 4.4** and from there it was observed that the adsorption of RTN on the surface of GO was best described by the Langmuir isotherm model ($R^2$=0.97) denoting that the adsorption of RTN on the surface of GO was unimolecular and the GO particles did not interact with each other. It also implied that the binding energy of every RTN molecule binding to the surface of GO was the same (Banerjee et al., 2016).

**Table 4.4:- Investigating different isotherm parameters for RTN adsorption by GO**

| Models | Parameters | Description | Unit | Adsorbent Dosage (gm/L) | | | |
|---|---|---|---|---|---|---|---|
| | | | | 0.5 g/L | 1 g/L | 1.5 g/L | 2 g/L |
| Langmuir | $C_e$ | Equilibrium pharmaceutical concentration in solution | mg L$^1$ | 2.6 | 2.19 | 1.39 | 0.24 |
| | $q_e$ | Theoretical maximum adsorption capacity | mg g$^{-1}$ | 14.76 | 7.81 | 5.75 | 4.87 |
| | $Q_0$ | Maximum monolayer coverage capacity calculated from slope of $C_e/q_e$ vs. $C_e$ plot. | mg g$^{-1}$ | 5.12 | 3.08 | 2.92 | 2.63 |
| | $b$ | Langmuir coefficient of energy of adsorption calculated from intercept of $C_e/q_e$ vs. $C_e$ plot. | L mg$^{-1}$ | 0.49 | 0.64 | 1.18 | 3.75 |
| | R$^2$ | Correlation coefficient | | 0.95 | 0.98 | 0.98 | 0.98 |
| Freundlich | $n_f$ | Adsorption intensity calculated from slope of $ln\ q_e$ vs. $ln\ C_e$ plot | | 1.21 | 1.68 | 2.45 | 5.08 |
| | $K_f$ | Freundlich coefficient of adsorption capacity calculated from intercept of $ln\ q_e$ vs. $ln\ C_e$ plot | mg g$^{-1}$ | 34.7 | 14.1 | 6.84 | 4 |
| | R$^2$ | Correlation coefficient | | 0.95 | 0.97 | 0.94 | 0.87 |
| Temkin | $B_T$ | Coefficients of heat of adsorption calculated from slope of $q_e$ vs. $ln\ C_e$ plot at operational temperature $T$ (303K ) | J mol$^{-1}$ | 8.62 | 3.86 | 1.8416 | 0.7381 |
| | $K_T$ | Temkin equilibrium binding constant calculated from intercept of $q_e$ vs. $ln\ C_e$ plot at operational temperature $T$ (303 K) | L g$^{-1}$ | 15.18 | 17.49 | 6.4878 | 262.77 |
| | R$^2$ | Correlation coefficient | | 0.99 | 0.99 | 0.97 | 0.9 |
| Dubinin-Radushkevich | $B$ | Dubinin–Radushkevich constant calculated from slope of $ln\ q_e$ vs. $\varepsilon^2$ plot. | mole$^2$ KJ$^{-2}$ | 0.0000001 | 0.00000009 | 0.00000003 | 0.000000003 |
| | $Q_s$ | Theoretical isotherm saturation capacity calculated from intercept of $ln\ q_e$ vs. $\varepsilon^2$ plot. | mg g$^{-1}$ | 6.6 | 1.35 | 1.29 | 1.7 |
| | $E$ | Mean sorption energy | kJ mole$^{-1}$ | 2236.07 | 2357.02 | 4082.48 | 12909.94 |
| | R$^2$ | Correlation coefficient | | 0.85 | 0.87 | 0.79 | 0.54 |
| | $\varepsilon$ | Polanyi Potential | | 814.00 | 947.79 | 1374.22 | 4109.77 |

### 4.4.3.4 Adsorption Isotherm for the adsorption of BPA by GO

The result of the experiment is given in **Table 4.5** and from there it was observed that the adsorption of BPA on the surface of GO was best described by the Temkin isotherm model ($R^2$=0.97) denoting that the adsorption of BPA on the surface of GO was uniform in nature and the heat of adsorption of the adsorbent moieties decreased in a linear fashion as the reaction proceeded (Bhattacharya et al., 2020).

**Table 4.5**:- Investigating different isotherm parameters for BPA adsorption by GO

| Models | Parameters | Description | Unit | Adsorbent Dosage (gm/L) | | | |
|---|---|---|---|---|---|---|---|
| | | | | 0.5 g/L | 1 g/L | 1.5 g/L | 2 g/L |
| Langmuir | $C_e$ | Equilibrium pharmaceutical concentration in solution | mg L$^1$ | 3.31 | 2.35 | 1.7 | 1.38 |
| | $q_e$ | Theoretical maximum adsorption capacity | mg g$^{-1}$ | 13.38 | 7.65 | 5.53 | 4.31 |
| | $Q_0$ | Maximum monolayer coverage capacity calculated from slope of $C_e/q_e$ vs. $C_e$ plot. | mg g$^{-1}$ | 2.99 | 2.27 | 1.8 | 2.03 |
| | $b$ | Langmuir coefficient of energy of adsorption calculated from intercept of $C_e/q_e$ vs. $C_e$ plot. | L mg$^{-1}$ | 0.324 | 0.46 | 0.63 | 1.05 |
| | R$^2$ | Correlation coefficient | | 0.88 | 0.89 | 0.94 | 0.98 |
| Freundlich | $n_f$ | Adsorption intensity calculated from slope of $ln\ q_e$ vs. $ln\ C_e$ plot | | 0.819 | 1.23 | 1.5 | 2.23 |
| | $K_f$ | Freundlich coefficient of adsorption capacity calculated from intercept of $ln\ q_e$ vs. $ln\ C_e$ plot | mg g$^{-1}$ | 63.88 | 11.18 | 6.65 | 10.59 |
| | R$^2$ | Correlation coefficient | | 0.9 | 0.87 | 0.91 | 0.94 |
| Temkin | $B_T$ | Coefficients of heat of adsorption calculated from slope of $q_e$ vs. $ln\ C_e$ plot at operational temperature $T$ (303K ) | J mol$^{-1}$ | 10.217 | 4.15 | 2.4501 | 1.4666 |
| | $K_T$ | Temkin equilibrium binding constant calculated from intercept of $q_e$ vs. $ln\ C_e$ plot at operational temperature $T$ (303 K) | L g$^{-1}$ | 12.75 | 15.83 | 0.0549 | 28.88 |
| | R$^2$ | Correlation coefficient | | 0.97 | 0.96 | 0.96 | 0.97 |
| Dubinin-Radushkevich | $B$ | Dubinin–Radushkevich constant calculated from slope of $ln\ q_e$ vs. $\varepsilon^2$ plot. | mole$^2$ KJ$^{-2}$ | 0.000003 | 0.000001 | 0.0000006 | 0.0000003 |
| | $Q_s$ | Theoretical isotherm saturation capacity calculated from intercept of $ln\ q_e$ vs. $\varepsilon^2$ plot. | mg g$^{-1}$ | 4.85 | 1.87 | 1.02 | 2.56 |
| | $E$ | Mean sorption energy | kJ mole$^{-1}$ | 408.25 | 707.11 | 912.88 | 1290.99 |
| | R$^2$ | Correlation coefficient | | 0.73 | 0.71 | 0.67 | 0.76 |
| | $\varepsilon$ | Polanyi Potential | | 664.72 | 893.63 | 1165.13 | 1370.27 |

**4.4.4 Adsorption Kinetics**

The temperature variation data (298 K – 313 K) from the batch study was used for calculating the adsorption kinetics. The result of the adsorption kinetics is given in the following tables.

*4.4.4.1 Adsorption Kinetics for the adsorption of CBZ by GO*

The result of the experiment is given in **Table 4.6** and from there it was observed that the adsorption of CBZ on the surface of GO was best described by the pseudo second order kinetic model ($R^2 = 0.98$) (Banerjee et al., 2016).

**Table 4.6**:- Investigating different kinetics parameters for adsorption of CBZ on GO

| Models | Parameters | Description | Units | Temperatures (° K) | | | |
|---|---|---|---|---|---|---|---|
| | | | | 298 K | 303 K | 308 K | 313 K |
| Pseudo first order | $k_1$ | Pseudo-1$^{st}$order rate constant obtained from linear plots of $log\ (q_e - q_t)$ vs. $t$. | min$^{-1}$ | 0.06 | 0.041 | 0.06 | 0.07 |
| | $q_e$ (cal) | Quantity of adsorbate adsorbed at equilibrium | mg g$^{-1}$ | 7.67 | 4.45 | 10.99 | 12.2 |
| | $R^2$ | Correlation coefficient | | 0.91 | 0.92 | 0.96 | 0.94 |
| Pseudo second order | $k_2$ | Pseudo-2$^{nd}$order rate constant determined from plot of $t/q_t$ vs. $t$. | mg g$^{-1}$ min$^{-1}$ | 0.004 | 0.011 | 0.008 | 0.011 |
| | $q_e$ | Quantity of adsorbate adsorbed at equilibrium | mg g$^{-1}$ | 6.37 | 5.58 | 5.9 | 5.69 |
| | $R^2$ | Correlation coefficient | | 0.95 | 0.99 | 0.99 | 0.99 |
| Intraparticle diffusion | $K_{diff}$ | Intra-particle diffusion rate constant calculated from the slope of regression plot of $q_t$vs. $t^{1/2}$ where $t$ is time (min). | mg g$^{-1}$ min$^{-1/2}$ | 0.4328 | 0.303 | 0.3629 | 0.376 |
| | C | Constant calculated from the intercept of regression plot of $q_t$vs. $t^{1/2}$ where $t$ is time (min). | mg g$^{-1}$ | 0.4952 | 1.8 | 1.3653 | 1.0016 |
| | $R^2$ | Correlation coefficient | | 0.82 | 0.89 | 0.8 | 0.88 |
| Elovich Istherm | α | Initial adsorption rate calculated from the intercept of liner plot of $q_t$ vs. $ln\ t$ | mg g$^{-1}$ min | 4.93 | 0.001 | 0.8 | 0.032 |
| | β | Initial desorption rate calculated from the slope$^{-1}$ of liner plot of $q_t$ vs. $ln\ t$. | mg g$^{-1}$ | 0.64 | 0.94 | 0.75 | 0.86 |
| | $R^2$ | Correlation coefficient | | 0.91 | 0.93 | 0.9 | 0.92 |
| Liquid film diffusion model | R | Liquid film diffusion constant | | 0.0597 | 0.0573 | 0.0649 | 0.0701 |
| | $R^2$ | Correlation coefficient | | 0.91 | 0.92 | 0.96 | 0.94 |

### 4.4.4.2 Adsorption Kinetics for the adsorption of NPX by GO

The result of the experiment is given in **Table 4.7** and from there it was observed that the adsorption of NPX on the surface of GO was best described by the Elovich kinetic model ($R^2$ = 0.97) thereby signifying that the adsorption of NPX on the surface of GO was chemical in nature (Wang et al., 2019).

**Table 4.7**:- Investigating different kinetics parameters for adsorption of NPX on GO

| Models | Parameters | Description | Units | Temperatures (° K) | | | |
|--------|-----------|-------------|-------|------|------|------|------|
| | | | | 298 K | 303 K | 308 K | 313 K |
| Pseudo first order | $k_1$ | Pseudo-1st order rate constant obtained from linear plots of $log\,(q_e - q_t)$ vs. $t$. | $min^{-1}$ | 0.015 | 0.014 | 0.074 | 0.019 |
| | $q_e$ (cal) | Quantity of adsorbate adsorbed at equilibrium | $mg\,g^{-1}$ | 4.24 | 3.82 | 17.90 | 2.82 |
| | $R^2$ | Correlation coefficient | | 0.99 | 0.96 | 0.83 | 0.95 |
| Pseudo second order | $k_2$ | Pseudo-2nd order rate constant determined from plot of $t/q_t$ vs. $t$. | $mg\,g^{-1}\,min^{-1}$ | 0.0019 | 0.003 | 0.0059 | 0.0089 |
| | $q_e$ | Quantity of adsorbate adsorbed at equilibrium | $mg\,g^{-1}$ | 6.54 | 5.98 | 5.035 | 5.01 |
| | $R^2$ | Correlation coefficient | | 0.95 | 0.94 | 0.99 | 0.99 |
| Intraparticle diffusion | $K_{diff}$ | Intra-particle diffusion rate constant calculated from the slope of regression plot of $q_t$ vs. $t^{1/2}$ where $t$ is time (min). | $mg\,g^{-1}\,min^{-1/2}$ | 0.4084 | 0.39 | 0. 33 | 0.35 |
| | C | Constant calculated from the intercept of regression plot of $q_t$ vs. $t^{1/2}$ where $t$ is time (min). | $mg\,g^{-1}$ | 0.3768 | 0.0058 | 0.7507 | 0.4 |
| | $R^2$ | Correlation coefficient | | 0.96 | 0.91 | 0.88 | 0.89 |
| Elovich Istherm | α | Initial adsorption rate calculated from the intercept of liner plot of $q_t$ vs. $ln\,t$ | $mg\,g^{-1}\,min$ | 9.81 | 7.04 | 1.87 | 0.84 |
| | β | Initial desorption rate calculated from the slope$^{-1}$ of liner plot of $q_t$ vs. $ln\,t$. | $mg\,g^{-1}$ | 0.70 | 0.72 | 0.85 | 0.89 |
| | $R^2$ | Correlation coefficient | | 0.99 | 0.98 | 0.96 | 0.95 |
| Liquid film diffusion model | R | Liquid film diffusion constant | | 0.0151 | 0.0147 | 0.0163 | 0.0193 |
| | $R^2$ | Correlation coefficient | | 0.99 | 0.96 | 0.94 | 0.95 |

### 4.4.4.3 Adsorption Kinetics for the adsorption of RTN by GO

The result of the experiment is given in **Table 4.8** and from there it was observed that the highest $R^2$ value was exhibited by the pseudo second order kinetic model. From the pseudo-second order kinetic model, high similarity between the experimentally obtained adsorption equilibrium value and theoretically obtained adsorption equilibrium value were obtained. Thus keeping these points in consideration, it can be stated that the adsorption of RTN on the surface of GO was best described by the Pseudo second order kinetic model ($R^2 = 0.99$) (Banerjee et al., 2016; Bhattacharya et al., 2021).

**Table 4.8**:- Investigating different kinetics parameters for adsorption of RTN on GO

| Models | Parameters | Description | Units | Temperatures (° K) | | | |
|---|---|---|---|---|---|---|---|
| | | | | 298 K | 303 K | 308 K | 313 K |
| Pseudo first order | $k_1$ | Pseudo-1st order rate constant obtained from linear plots of $log\,(q_e - q_t)$ vs. $t$. | $min^{-1}$ | 0.044 | 0.026 | 0.039 | 0.056 |
| | $q_e$ (cal) | Quantity of adsorbate adsorbed at equilibrium | $mg\,g^{-1}$ | 3.87 | 1.76 | 2.82 | 9.62 |
| | $R^2$ | Correlation coefficient | | 0.95 | 0.86 | 0.91 | 0.87 |
| Pseudo second order | $k_2$ | Pseudo-2nd order rate constant determined from plot of $t/q_t$ vs. $t$. | $mg\,g^{-1}\,min^{-1}$ | 0.0136 | 0.024 | 0.018 | 0.0094 |
| | $q_e$ | Quantity of adsorbate adsorbed at equilibrium | $mg\,g^{-1}$ | 5.19 | 5.12 | 5.13 | 5.08 |
| | $R^2$ | Correlation coefficient | | 0.99 | 0.99 | 0.99 | 0.97 |
| Intraparticle diffusion | $K_{diff}$ | Intra-particle diffusion rate constant calculated from the slope of regression plot of $q_t$ vs. $t^{1/2}$ where $t$ is time (min). | $mg\,g^{-1}\,min^{-1/2}$ | 0.1915 | 0.2032 | 0.2464 | 0.2214 |
| | C | Constant calculated from the intercept of regression plot of $q_t$ vs. $t^{1/2}$ where $t$ is time (min). | $mg\,g^{-1}$ | 2.6402 | 2.7834 | 2.2685 | 1.5566 |
| | $R^2$ | Correlation coefficient | | 0.84 | 0.8 | 0.79 | 0.82 |
| Elovich Istherm | $\alpha$ | Initial adsorption rate calculated from the intercept of liner plot of $q_t$ vs. $ln\,t$ | $mg\,g^{-1}\,min$ | $3.42 \times 10^{-7}$ | 4.2 | 0.281 | $83 \times 10^{-4}$ |
| | $\beta$ | Initial desorption rate calculated from the slope$^{-1}$ of liner plot of $q_t$ vs. $ln\,t$. | $mg\,g^{-1}$ | 0.99 | 1.35 | 1.11 | 1.13 |
| | $R^2$ | Correlation coefficient | | 0.94 | 0.91 | 0.9 | 0.87 |
| Liquid film diffusion model | R | Liquid film diffusion constant | | 0.0438 | 0.0265 | 0.0531 | 0.056 |
| | $R^2$ | Correlation coefficient | | 0.95 | 0.86 | 0.93 | 0.87 |

### 4.4.4.4 Adsorption Kinetics for the adsorption of BPA by GO

The result of the experiment is given in **Table 4.9** and from there it was observed that the highest $R^2$ value was exhibited by the pseudo second order kinetic model. From the pseudo-second order kinetic model, high similarity between the experimentally obtained adsorption equilibrium value and theoretically obtained adsorption equilibrium value were obtained. Thus keeping these points in consideration, it can be stated that the adsorption of BPA on the surface of GO was best described by the Pseudo second order kinetic model ($R^2 = 0.99$) (Banerjee et al., 2016; Bhattacharya et al., 2021).

**Table 4.9**:- Investigating different kinetics parameters for adsorption of BPA on GO

| Models | Parameters | Description | Units | Temperatures (° K) | | | |
|--------|-----------|-------------|-------|------|------|------|------|
| | | | | 298 K | 303 K | 308 K | 313 K |
| Pseudo first order | $k_1$ | Pseudo-1st order rate constant obtained from linear plots of $log (q_e - q_t)$ vs. $t$. | $min^{-1}$ | 0.05 | 0.05 | 0.04 | 0.05 |
| | $q_e$ (cal) | Quantity of adsorbate adsorbed at equilibrium | $mg\ g^{-1}$ | 3.24 | 3.24 | 1.34 | 5.74 |
| | $R^2$ | Correlation coefficient | | 0.87 | 0.83 | 0.85 | 0.9 |
| Pseudo second order | $k_2$ | Pseudo-2nd order rate constant determined from plot of $t/q_t$ vs. $t$. | $mg\ g^{-1}\ min^{-1}$ | 0.03 | 0.05 | 0.06 | 0.017 |
| | $q_e$ | Quantity of adsorbate adsorbed at equilibrium | $mg\ g^{-1}$ | 4.84 | 4.46 | 4.38 | 4.56 |
| | $R^2$ | Correlation coefficient | | 0.99 | 0.99 | 0.99 | 0.99 |
| Intraparticle diffusion | $K_{diff}$ | Intra-particle diffusion rate constant calculated from the slope of regression plot of $q_t$ vs. $t^{1/2}$ where $t$ is time (min). | $mg\ g^{-1}\ min^{-1/2}$ | 0.133 | 0.0943 | 0.1042 | 0.1881 |
| | C | Constant calculated from the intercept of regression plot of $q_t$ vs. $t^{1/2}$ where $t$ is time (min). | $mg\ g^{-1}$ | 2.8981 | 3.3141 | 3.2174 | 1.9482 |
| | $R^2$ | Correlation coefficient | | 0.87 | 0.97 | 0.69 | 0.94 |
| Elovich Istherm | α | Initial adsorption rate calculated from the intercept of liner plot of $q_t$ vs. $ln\ t$ | $mg\ g^{-1}\ min$ | 28.05 | 112.99 | 61.42 | 1.49 |
| | β | Initial desorption rate calculated from the slope$^{-1}$ of liner plot of $q_t$ vs. $ln\ t$. | $mg\ g^{-1}$ | 2.17 | 3.13 | 2.6 | 1.47 |
| | $R^2$ | Correlation coefficient | | 0.89 | 0.94 | 0.81 | 0.94 |
| Liquid film diffusion model | R | Liquid film diffusion constant | | 0.0504 | 0.0097 | 0.0112 | 0.057 |
| | $R^2$ | Correlation coefficient | | 0.87 | 0.98 | 0.78 | 0.95 |

### 4.4.5 Activation Energy and Adsorption Thermodynamics

The activation energy for the adsorption of the adsorbates on the surface of GO was calculated by Arrhenius equation and the adsorption thermodynamics were calculated by the van't Hoff equation. The result of the experiments is given as follows.

*4.4.5.1 Activation Energy and Adsorption Thermodynamics for the adsorption of CBZ by GO*

The result of the study is given in **Table 4.10**. From there it was observed that the activation energy was 39.1 kJ/mole. As the activation energy value was less than 40 kJ/mole then it was observed that the adsorption of CBZ on the surface of GO was physical in nature (Banerjee et al., 2016; Bhattacharya et al., 2020).

From the thermodynamic study, it was observed that the Gibbs value was negative across the temperature range and decreased with increase in temperature (-4938.2 kJ/mole - 10665.46 kJ/mole) thereby signifying that the adsorption of CBZ on the surface of GO was spontaneous in nature. The positive value of $\Delta H°$ signified that the adsorption of CBZ on the surface of GO was endothermic in nature and the reaction went ahead by consuming energy from the concerned system (Banerjee et al., 2015b, 2016). The positive $\Delta S°$ meant that the GO and CBZ both underwent active site interaction during the adsorption process (Balasubramani, Sivarajasekar, & Naushad, 2020; Bhattacharya et al., 2021).

**Table 4.10**:- Analysis of thermodynamic parameters and activation energy for CBZ adsorption by GO.

| Temperature (K) | $\Delta G$ (kJ/mole) | $\Delta H$ (kJ/mole) | $\Delta S$ (joule/mole/kelvin) | $E_a$ ( kJ/mole) |
|---|---|---|---|---|
| 298 K | -4938.20 | 104.96 | 369.04 | 39.1 |
| 303 K | -7116.01 | | | |
| 308 K | -8391.82 | | | |
| 313 K | -10665.46 | | | |

*4.4.5.2 Activation Energy and Adsorption Thermodynamics for the adsorption of NPX by GO*

The rate of the Elovich kinetic model reaction was used as the rate constant for the calculation of activation energy for the adsorption of NPX by GO. From there it was observed that the activation energy was 80.69 kJ/mole. As the activation energy value was more than 40 kJ/mole then it was observed that the adsorption of NPX on the surface of GO was chemisorption in nature (Banerjee et al., 2016; Bhattacharya et al., 2020).

From the thermodynamic study, it was observed that the Gibbs value was negative across the temperature range and decreased with increase in temperature (-1311.85 kJ/mole – - 2439.74 kJ/mole) thereby signifying that the adsorption of NPX on the surface of GO was spontaneous in nature. The

positive value of ΔH° signified that the adsorption of NPX on the surface of GO was endothermic in nature and the reaction went ahead by consuming energy from the concerned system (Banerjee et al., 2015b, 2016). The positive ΔS° meant that the GO and NPX both underwent active site interaction during the adsorption process (Balasubramani, Sivarajasekar, & Naushad, 2020; Bhattacharya et al., 2021). The result of the study is given in **Table 4.11**.

**Table 4.11:-** Analysis of thermodynamic parameters and activation energy for the NPX adsorption by GO

| Temperature (K) | ΔG (kJ/mole) | Δ H (kJ/mole) | ΔS (joule/mole/kelvin) | $E_a$ ( kJ/mole) |
|---|---|---|---|---|
| 298 K | -1311.85 | 19.76 | 70.7 | 80.69 |
| 303 K | -1715.97 | | | |
| 308 K | -1877.30 | | | |
| 313 K | -2439.74 | | | |

### 4.4.5.3 Activation Energy and Adsorption Thermodynamics for the adsorption of RTN by GO

The rate of the pseudo-second order kinetics were used for calculating the activation energy. From the result there it was observed that the activation energy was 21.18 kJ/mole. As the activation energy value was less than 40 kJ/mole then it can be stated that the adsorption of RTN on the surface of GO was physical in nature (Al-rub et al., 2020; Banerjee et al., 2016; Bhattacharya et al., 2020).

From the thermodynamic study, it was observed that the Gibbs value was negative across the temperature range (-4297.59 kJ/mole – 3407.85 kJ/mole for 298 K to 313 K) thereby signifying that the adsorption of RTN on the surface of GO was spontaneous in nature. The negative value of ΔH° signified that the adsorption of RTN on the surface of GO was exothermic in nature (Ciğeroğlu et al., 2020; İlbay et al., 2015). The negative ΔS° value meant that when the equilibrium was reached for the adsorption of RTN by GO, the randomness on the surface of GO decreased (Ciğeroğlu et al., 2020; İlbay et al., 2015). The result of the activation energy and thermodynamics study is given in **Table 4.12**.

**Table 4.12**:- Analysis of thermodynamic parameters and activation energy for RTN adsorption by GO

| Temperature (K) | ΔG (kJ/mole) | Δ H (kJ/mole) | Δ S (joule/mole/kelvin) | $E_a$ ( kJ/mole) |
|---|---|---|---|---|
| 298 K | -4297.59 | -28.97 | -78.99 | 21.18 |
| 303 K | -6599.24 | | | |
| 308 K | -5058.02 | | | |
| 313 K | -3407.85 | | | |

### 4.4.5.4 Activation Energy and Adsorption Thermodynamics for the adsorption of BPA by GO

The rate of the pseudo-second order kinetic model reaction was used as the rate constant. From there it was observed that the activation energy was 26.3 kJ/mole. As the activation energy value was less than 40 kJ/mole then it can be stated that the adsorption of BPA on the surface of GO was physical in nature (Kwon & Lee, 2015; Phatthanakittiphong & Seo, 2016; Xu et al., 2012).

From the thermodynamic study, it was observed that the Gibbs value was negative across the temperature range (-2647.27 kJ/mole –2308.62 kJ/mole for 298 K to 313 K) thereby signifying that the adsorption of BPA on the surface of GO was spontaneous in nature. The negative value of $\Delta H°$ signified that the adsorption of BPA on the surface of GO was exothermic in nature (Kwon & Lee, 2015; Phatthanakittiphong & Seo, 2016; Xu et al., 2012). The negative $\Delta S°$ value meant that when the equilibrium was reached for the adsorption of BPA by GO, the randomness on the surface of GO decreased (Kwon & Lee, 2015; Phatthanakittiphong & Seo, 2016; Xu et al., 2012). The result of the activation energy and thermodynamics study is given in **Table 4.13**.

**Table 4.13:-** Analysis of thermodynamic parameters and Activation energy for BPA adsorption by GO

| Temperature (K) | $\Delta G$ (kJ/mole) | $\Delta H$ (kJ/mole) | $\Delta S$ (joule/mole/kelvin) | $E_a$ ( kJ/mole) |
|---|---|---|---|---|
| 298 K | -2647.27 | -84.35 | -19.07 | 26.3 |
| 303 K | -2722.01 | | | |
| 308 K | -2750.47 | | | |
| 313 K | -2308.62 | | | |

### 4.4.6 Optimization of the process operation by RSM

*4.4.6.1 Optimization of the adsorption of CBZ by GO by RSM method*

The RSM was performed with the aim of understanding the effect of inter parameter interaction on the experimental outcome. In **Table 4.14**, the outcome of the 20 experiments as proposed by the software for the CCD model of the RSM is given and in **Table 4.15** the result of the ANOVA of the RSM model is provided. From there it is observed that the $R^2$ value of the model was 0.95 and the adjusted $R^2$ value was 0.91 which propounded the fact that the polynomial model suggested by RSM was appropriate for predicting the outcome of this adsorption reaction. The high value of F (22.65, much greater than unity) and the low value of P ($< 0.0001$) meant that the optimizing model was highly significant, with the experimental data points exhibiting a high degree of correlation with the predicted data points (Bhattacharya et al., 2021). **Fig. 4.8** shows the relation between the experimentally determined data points and the predicted data points and there also it can be noted that the experimental data points exhibits a high degree of correlation with the predicted data points. The real equation which was used to predict the effect of the input variables on the response output is presented as follows.

$Removal \% = -80.90116 + 13.47165 \times pH + 0.24793 \times Dose + 1.76177 \times Time - 0.040667 \times pH \times Dose - 0.096500 \times pH \times Time - 4.45556 \times 10^{-4} \times Dose \times Time - 0.25861 \times pH^2 - 2.87609 \times 10^{-4} \times Dose^2 - 4.93567 \times 10^{-3} * Time$ ……………..(xxix)

As per the RSM model the optimized conditions under which maximum removal of CBZ (95 %) was possible were: adsorbent dosage of 2.5 g/L, pH value of 4 and reaction time of 120 minutes. For this RSM model, the interaction between the experimental parameters (input variables) and their outcome on the percentage removal of CBZ (response variable) is illustrated by the contour plots shown in **Fig. 4.9-4.11**.

> **Effect of GO dosage and solution pH on CBZ removal by GO**

The interaction in between the pH of the experimental solution and the dosage of GO and its effect on the removal of CBZ is conveyed in the contour plot of **Fig. 4.9**. From there it was observed that the removal of CBZ by GO increased with the increase in dosage of GO. The higher removal of CBZ at the higher dose of GO was due to the availability of greater surface area for the purpose of adsorption and consequently the highest removal value was observed around the highest dosage of 2.5 g/L (Banerjee et al., 2016; Bhattacharya et al., 2021). In case of the variation of pH of the experimental solution, it was observed that the higher removal of CBZ by GO was obtained at the lower pH range and consequently the removal of CBZ by GO decreased at the higher pH range. This was identical to the result obtained from the batch study. With the pH$_{pzc}$ value of GO being $4.87 \pm 0.26$ and the pKa value of CBZ being 13.9 (Al-hamadani et al., 2018; Banerjee et al., 2016), at the lower pH range the positively

charge surface of GO adsorb the neutral molecules. However, at the higher pH range, the CBZ molecules become hydrophobic thereby decreasing their adsorption by the molecules of GO. As a consequence of which the highest removal of CBZ by GO occurred at the lower pH range and at the higher dose range.

➤ **Effect of solution pH and contact time on CBZ removal by GO**

The interaction in between the pH of the experimental solution and contact time and its effect on the removal of CBZ by GO is conveyed in the contour plot of **Fig. 4.10**. From there it was observed that within in the neutral pH range (pH 4- pH 7) the removal of CBZ by GO increased with the increase in contact time (Bhattacharya et al., 2020). This phenomenon is in accordance with the data observed during the batch study that GO particles are more proficient in adsorbing CBZ molecules in the lower pH range and its adsorption efficiency decreases at the higher pH range (Al-Hamadani et al., 2018; Chen et al., 2020). The higher removal of CBZ by GO with the increase in contact time can be attributed to the increased interaction between the molecules of CBZ and GO with the increase in contact time (Banerjee et al., 2016; Bhattacharya et al., 2021). However, the removal of CBZ by GO decreased with the increase in pH beyond the neutral range which could be attributed to the hydrophobicity of the CBZ molecules at the higher pH (Bhattacharya et al., 2020). The optimum removal of CBZ by GO was obtained for the higher range of contact time (105-120 minutes) and for the lower pH range (pH 4-pH 6).

➤ **Effect of contact time and GO dosage on CBZ removal by GO**

The interaction in between the contact time and dosage of adsorbent and its effect on the removal of CBZ by GO is conveyed in the contour plot of **Fig. 4.11**. From there it was observed that the removal of CBZ by GO increased with the increase in contact time and also with the increase of adsorbent dosage. That is because, with the increase in contact time the interaction between the molecules of CBZ and the particles of GO increases resulting in greater adsorption of the CBZ molecules by the GO particles (Bhattacharya et al., 2021). On the other hand, the removal of CBZ by GO increases with the increase in adsorbent dosage due to the greater availability of active sites for the uptake of the molecules (Banerjee et al., 2015b, 2016; Bhattacharya et al., 2020). As a consequence of which the highest removal of CBZ by GO was observed at the highest dose range of GO and at the highest contact time.

**Table 4.14** :- The table showing the 20 different set of parameters (runs) along with their corresponding outcome as proposed by CCD model of RSM for optimization of CBZ removal by GO

| Run | Block | Factor 1 A:pH | Factor 2 B:Dose g/L | Factor 3 C:Time min | Response 1 Percentage Removal |
|-----|-------|------|--------|--------|-------------------|
| 1 | Block 1 | 6.00 | 175.00 | 90.00 | 78.26 |
| 2 | Block 1 | 6.00 | 48.87 | 90.00 | 74.98 |
| 3 | Block 1 | 9.36 | 175.00 | 90.00 | 81.00 |
| 4 | Block 1 | 6.00 | 175.00 | 90.00 | 78.26 |
| 5 | Block 1 | 6.00 | 175.00 | 90.00 | 78.26 |
| 6 | Block 1 | 8.00 | 100.00 | 60.00 | 81.37 |
| 7 | Block 1 | 2.64 | 175.00 | 90.00 | 78.68 |
| 8 | Block 1 | 6.00 | 175.00 | 90.00 | 78.26 |
| 9 | Block 1 | 4.00 | 100.00 | 60.00 | 50.00 |
| 10 | Block 1 | 6.00 | 175.00 | 39.55 | 50.1 |
| 11 | Block 1 | 6.00 | 301.13 | 90.00 | 88.00 |
| 12 | Block 1 | 8.00 | 250.00 | 120.00 | 78.81 |
| 13 | Block 1 | 4.00 | 250.00 | 60.00 | 78.53 |
| 14 | Block 1 | 8.00 | 250.00 | 60.00 | 78.93 |
| 15 | Block 1 | 6.00 | 175.00 | 140.45 | 78.6 |
| 16 | Block 1 | 4.00 | 250.00 | 120.00 | 95.00 |
| 17 | Block 1 | 6.00 | 175.00 | 90.00 | 78.26 |
| 18 | Block 1 | 4.00 | 100.00 | 120.00 | 77.05 |
| 19 | Block 1 | 8.00 | 100.00 | 120.00 | 78.69 |
| 20 | Block 1 | 6.00 | 175.00 | 90.00 | 78.26 |

**Table 4.15** :- ANOVA analysis for the RSM for the process operation of CBZ adsorption by GO

| $R^2$ Value | Adjusted $R^2$ Value | f- value | Probability Value P |
|-------------|---------------------|----------|---------------------|
| 0.95 | 0.91 | 22.65 (>1) | 0.0001 (<0.05)  Significant |
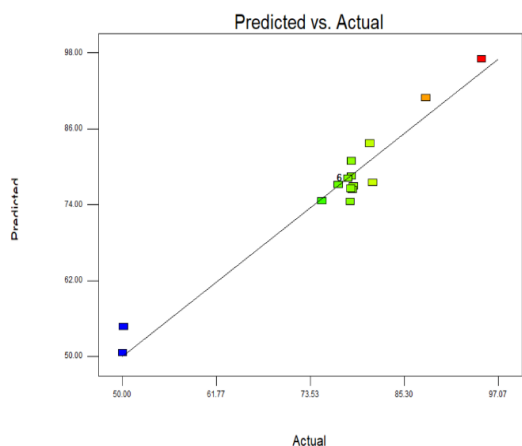
**Fig. 4.8**:- Relation between the predicted data points and the experimental data points as per the RSM model.



**Fig. 4.9**:- Interaction between the pH of the experimental solution and the dose of the GO and their effect on the percentage removal of CBZ.



**Fig. 4.10**- The interaction between the pH of the experimental solution and the contact time (in minutes) and their effect on the percentage removal of CBZ by GO.



**Fig. 4.11**:- The plot showing the interaction between the dose of the GO and the contact time (in minutes) as per the RSM model and their effect on the % removal of CBZ.

*4.4.6.2 Optimization of the adsorption of NPX by GO by RSM method*

The Response Surface Methodology was performed with the aim of understanding the effect of inter parameter interaction on the experimental outcome. In **Table 4.16**, the outcome of the 20 experiments as proposed by the software for the CCD model of the RSM is given and in **Table 4.17** the result of the ANOVA of the RSM model is provided. From there it is observed that the $R^2$ value of the model was 0.93 and the adjusted $R^2$ value was 0.88 which propounded the fact that the polynomial model suggested by RSM was appropriate for predicting the outcome of this adsorption reaction. The high value of F (15.95, greater than unity) and the low value of P ($< 0.0001$) meant that the optimizing model was very much significant, with the experimental data points exhibiting a high degree of correlation with the predicted data points (Bhattacharya et al., 2021). **Fig. 4.12** shows the relation between the experimentally determined data points and the predicted data points and there also it can be noted that the experimental data points exhibits a high degree of correlation with the predicted data points. The real equation which was used to predict the effect of the input variables on the response output is presented as follows.

$$Removal\ \% = 182.80051 - 30.40884 \times pH - 5.54508 \times Dose - 0.88144 \times Time - 2.23333 \times pH \times Dose + 0.015167 \times pH \times Time + 0.088222 \times Dose \times Time + 2.47450 \times pH^2 + 6.10743 \times Dose^2 + 4.10288 \times 10^{-3} \times Time \quad \dots\dots\dots\dots\dots\dots\dots\dots\dots\dots\dots..(xxx)$$

As per the RSM model the optimized conditions under which maximum removal of NPX (92.67%) was possible were: adsorbent dosage of 2.5 g/L, pH value of 4 and reaction time of 120 minutes. For this RSM model, the interaction between the experimental parameters (input variables) and their outcome on the percentage removal of NPX (response variable) is illustrated by the contour plots shown in **Fig. 4.13-4.15**.

➢ **Effect of GO dosage and solution pH on NPX removal by GO**

The interaction in between the pH of the experimental solution and the dosage of GO and its effect on the removal of NPX is conveyed in the contour plot of **Fig. 4.13**. From there it was observed that the removal of NPX by GO increased with the increase in dosage of GO. The higher removal of NPX at the higher dose of GO was due to the availability of greater surface area for the purpose of adsorption and the consequently the highest removal value was observed around the highest dosage of 2.5 g/L (Banerjee et al., 2016; Bhattacharya et al., 2021). In case of the variation of pH of the experimental solution, it was observed that the higher removal of NPX by GO was obtained at the lower pH range and consequently the removal of NPX by GO decreased at the higher pH range. This was similar to the result obtained from the batch study. With the pH$_{pzc}$ value of GO being $4.87 \pm 0.26$ and the pKa value of NPX being 4.15 (Ciğeroğlu et al., 2020; Reynel-avila et al., 2015), at the lower pH range the positively charged surface of GO adsorbs the neutral molecules of NPX by hydrogen bonding and van

deer Waals force (I˙lbay et al., 2015). Subsequently, when the pH value is increased (beyond pH 4.15 for NPX and pH 5 for GO) the surface of GO and the NPX molecules both acquire negative charge (I˙lbay et al., 2015; Mondal et al., 2020). As a consequence of which the removal of NPX by GO decreases with the increase in pH of the experimental solution. However, in **Fig. 4.13** one point was observed at the higher pH range where the removal of NPX was higher than the lower pH. Incidentally this point was also present at the higher dose range. Thus, it can inferred that due to the high dosage of GO, the removal of NPX was also higher at the higher pH range.

➢ **Effect of solution pH and contact time on NPX removal by GO**

The interaction in between the pH of the experimental solution and contact time and its effect on the removal of NPX by GO is conveyed in the contour plot of **Fig. 4.14**. From there it was observed that removal of NPX by GO increased with the increase in contact time due to higher number of interaction between the NPX molecules and the surface of GO resulting in greater adsorption of NPX molecules by GO (Bhattacharya et al., 2021). Similarly, in case of pH value it was observed that higher adsorption of NPX by GO took place in lower pH range which is attributed to the adsorption of NPX molecules by GO by van deer Waal's force and hydrogen bonding (I˙lbay et al., 2015). Thus the highest removal of NPX by GO took place at the higher contact time range and at the lower pH range.

➢ **Effect of contact time and GO dosage on NPX removal by GO**

The interaction in between the contact time and dosage of adsorbent and its effect on the removal of NPX by GO is conveyed in the contour plot of **Fig. 4.15**. From there it was observed that the removal of NPX by GO increased with the increase in contact time and also with the increase of adsorbent dosage. That is because, with the increase in contact time the interaction between the molecules of NPX and the particles of GO increases resulting in greater adsorption of the NPX molecules by the GO particles (Bhattacharya et al., 2021). On the other hand, the removal of NPX by GO increases with the increase in adsorbent dosage due to the greater availability of active sites for the uptake of the NPX molecules (Bhattacharya et al., 2021; I˙lbay et al., 2015). As a consequence of which the highest removal of NPX by GO was observed at the highest dose range of GO and at the highest contact time.

**Table 4.16** :- The table showing the 20 different set of parameters (runs) along with their corresponding outcome as proposed by CCD model of RSM for optimization of NPX removal by GO

| Run | Block | Factor 1 | Factor 2 | Factor 3 | Response 1 |
|---|---|---|---|---|---|
| | | A:pH | B:Dose | C:Time | Percentage Removal |
| | | | g/L | min | |
| 1 | Block 1 | 8.00 | 1.00 | 60.00 | 58.23 |
| 2 | Block 1 | 9.36 | 1.75 | 90.00 | 63.88 |
| 3 | Block 1 | 8.00 | 2.50 | 120.00 | 71.77 |
| 4 | Block 1 | 6.00 | 1.75 | 90.00 | 51.22 |
| 5 | Block 1 | 6.00 | 1.75 | 39.55 | 49.93 |
| 6 | Block 1 | 8.00 | 2.50 | 60.00 | 64.34 |
| 7 | Block 1 | 6.00 | 1.75 | 90.00 | 51.22 |
| 8 | Block 1 | 4.00 | 1.00 | 120.00 | 65.22 |
| 9 | Block 1 | 6.00 | 1.75 | 90.00 | 51.22 |
| 10 | Block 1 | 8.00 | 1.00 | 120.00 | 63.33 |
| 11 | Block 1 | 6.00 | 1.75 | 90.00 | 51.22 |
| 12 | Block 1 | 4.00 | 2.50 | 60.00 | 83.27 |
| 13 | Block 1 | 4.00 | 1.00 | 60.00 | 69.37 |
| 14 | Block 1 | 4.00 | 2.50 | 120.00 | 92.67 |
| 15 | Block 1 | 6.00 | 1.75 | 140.45 | 64.32 |
| 16 | Block 1 | 6.00 | 0.49 | 90.00 | 41.42 |
| 17 | Block 1 | 6.00 | 3.01 | 90.00 | 71.32 |
| 18 | Block 1 | 6.00 | 1.75 | 90.00 | 51.22 |
| 19 | Block 1 | 6.00 | 1.75 | 90.00 | 51.22 |
| 20 | Block 1 | 2.64 | 1.75 | 90.00 | 85.34 |

**Table 4.17**:- ANOVA analysis for the RSM for the process operation of NPX adsorption by GO

| $R^2$ Value | Adjusted $R^2$ Value | f- value | Probability Value P |
|---|---|---|---|
| 0.93 | 0.88 | 15.95 (>1) | <0.0001 (<0.05) Significant |
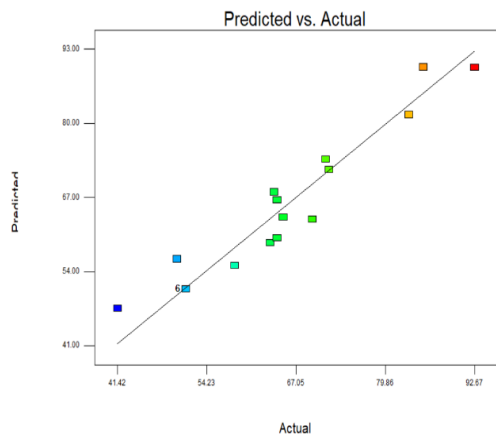
**Fig. 4.12**:- Relation between the predicted data points and the experimental data points as per the RSM model.



**Fig. 4.13**:- Interaction between the pH of the experimental solution and the dose of the GO and their effect on the percentage removal of NPX



**Fig. 4.14**:- The interaction between the pH of the experimental solution and the contact time (in minutes) and their effect on the percentage removal of NPX by GO.



**Fig. 4.15**:- The plot showing the interaction between the dose of the GO and the contact time (in minutes) as per the RSM model and their effect on the percentage removal of NPX.

### 4.4.6.3 Optimization of the adsorption of RTN by GO by RSM method

The RSM was performed with the aim of understanding the effect of inter parameter interaction on the experimental outcome. In **Table 4.18**, the outcome of the 20 experiments as proposed by the software for the CCD model of the RSM is given and in **Table 4.19** the result of the ANOVA of the RSM model is provided. From there it is observed that the $R^2$ value of the model was 0.99 and the adjusted $R^2$ value was 0.98 which propounded the fact that the polynomial model suggested by RSM was appropriate for predicting the outcome of this adsorption reaction. The high value of F (164.77, much greater than unity) and the low value of P ($< 0.0001$) meant that the optimizing model was very much significant, with the experimental data points exhibiting a high degree of correlation with the predicted data points (Bhattacharya et al., 2021). **Fig. 4.16** shows the relation between the experimentally determined data points and the predicted data points and there also it can be noted that the experimental data points exhibits a high degree of correlation with the predicted data points. The real equation which was used to predict the effect of the input variables on the response output is presented as follows.

$$Removal\,\% = -80.97324 + 13.33293 \times pH + 59.13523 \times Dose + 0.88087 \times Time - 0.13 \times pH \times Dose - 1.66667 \times 10^{-4} \times pH \times Time + 0.035556 \times Dose \times Time - 1.11688 \times pH^2 - 10.10083 \times Dose^2 - 5.02979 \times 10^{-3} * Time^2$$ ………………………………..(xxxi)

As per the RSM model the optimized conditions under which maximum removal of RTN (89.17%) was possible were: adsorbent dosage of 3.01 g/L, pH value of 6 and reaction time of 90 minutes. For this RSM model, the interaction between the experimental parameters (input variables) and their outcome on the percentage removal of RTN (response variable) is illustrated by the contour plots shown in **Fig. 4.17-4.19**.

➤ **Effect of GO dosage and solution pH on RTN removal by GO**

The interaction in between the pH of the experimental solution and the dosage of GO and its effect on the removal of RTN is conveyed in the contour plot of **Fig. 4.17**. From there it was observed that the removal of RTN by GO increased with the increase in dosage of GO. This could be attributed to the higher availability of active sites for the uptake of RTN at the higher dosage of GO and consequently the highest removal value was observed around the highest dosage of 2.5 g/L (Banerjee et al., 2016; Bhattacharya et al., 2021). In case of the variation of pH of the experimental solution, it was observed that the highest removal of RTN was observed at around pH 6. This could be attributed to the fact that around the neutral pH range, the molecules of RTN were neutral (Kortejarvi et al., 2005) and the surface of GO are negatively charged and as a result of which maximum adsorption of RTN molecules takes place on the surface of GO at this pH (Al-rub et al., 2020). At the lower pH range both RTN molecules and the surface of GO acquire positive charge whereas at the higher pH range both of these acquire negative charge (Al-rub et al., 2020). As a consequence of which at the higher and lower pH range, the

RTN molecules and GO surface experience repulsion from each other thereby decreasing the adsorption of RTN by GO at this pH. Thus highest removal of RTN is observed at the neutral pH range and at the high adsorbent dosage (Banerjee et al., 2016; Bhattacharyya et al., 2019).

➢ **Effect of solution pH and contact time on RTN removal by GO**

The interaction in between the pH of the experimental solution and contact time and its effect on the removal of RTN by GO is shown in the contour plot of **Fig. 4.18**. From there it was observed that removal of RTN by GO initially increased with the increase in contact time due to higher number of interaction between the RTN molecules and the surface of GO resulting in greater adsorption of RTN molecules by GO (Bhattacharya et al., 2021). However, beyond the optimum contact time, (around 90-105 minutes mark), a slight decrease in the removal of RTN by GO was observed in the contour plot, which could be attributed to desorption due to the physical nature of the adsorption reaction. In case of pH variation it was observed, that highest removal of RTN was around the neutral pH range, which could be attributed to the attraction between the neutral molecules of RTN and the negatively charged surface of GO (Al-rub et al., 2020)**.**

➢ **Effect of contact time and GO dosage on RTN removal by GO**

The interaction in between the contact time and dosage of adsorbent and its effect on the removal of RTN by GO is shown in the contour plot of **Fig. 4.19**. From there it was observed that the removal of RTN by GO increased with the increase in dosage which could be ascribed to the availability of greater surface for the uptake of RTN molecules (Banerjee et al., 2016; Bhattacharya et al., 2021). On the other hand, the adsorption of RTN molecules by GO increased with the increase in contact time till the optimum time range (95-105 minutes), followed by which a slight decrease in the removal of RTN by GO was observed in the contour plot. This could be attributed to the desorption of RTN molecules from the surface of GO due to the physical nature of the adsorption. Thus highest removal of RTN was observed for the highest dosage and for the optimum contact time.

**Table 4.18** :- The table showing the 20 different set of parameters (runs) along with their corresponding outcome as proposed by CCD model of RSM for optimization of RTN removal by GO

| Run | Block | Factor 1 | Factor 2 | Factor 3 | Response 1 |
|-----|-------|----------|----------|----------|------------|
| | | A:pH | B:Dose | C:Time | Percentage Removal |
| | | | g/L | min | |
| 1 | Block 1 | 6 | 1.75 | 90 | 74.14 |
| 2 | Block 1 | 8 | 1 | 60 | 38.33 |
| 3 | Block 1 | 8 | 2.5 | 120 | 80.54 |
| 4 | Block 1 | 4 | 1 | 120 | 38.42 |
| 5 | Block 1 | 9.36 | 1.75 | 90 | 61.40 |
| 6 | Block 1 | 6 | 1.75 | 90 | 74.14 |
| 7 | Block 1 | 4 | 1 | 60 | 37.74 |
| 8 | Block 1 | 6 | 1.75 | 90 | 74.14 |
| 9 | Block 1 | 6 | 1.75 | 90 | 74.14 |
| 10 | Block 1 | 6 | 3.01 | 90 | 89.17 |
| 11 | Block 1 | 6 | 1.75 | 90 | 74.14 |
| 12 | Block 1 | 6 | 0.32 | 90 | 19.20 |
| 13 | Block 1 | 8 | 2.5 | 60 | 76.70 |
| 14 | Block 1 | 8 | 1 | 120 | 36.40 |
| 15 | Block 1 | 2.64 | 1.75 | 90 | 63.84 |
| 16 | Block 1 | 4 | 2.5 | 120 | 80.77 |
| 17 | Block 1 | 6 | 1.75 | 39.55 | 59.11 |
| 18 | Block 1 | 6 | 1.75 | 90 | 74.14 |
| 19 | Block 1 | 6 | 1.75 | 140.45 | 65.74 |
| 20 | Block 1 | 4 | 2.5 | 60 | 79.46 |

**Table 4.19**:- ANOVA analysis for the RSM for the process operation of RTN adsorption by GO

| $R^2$ Value | Adjusted $R^2$ Value | f- value | Probability Value P |
|-------------|----------------------|----------|---------------------|
| 0.99 | 0.98 | 164.77 (>>1) | <0.0001 (<0.01)  Significant |
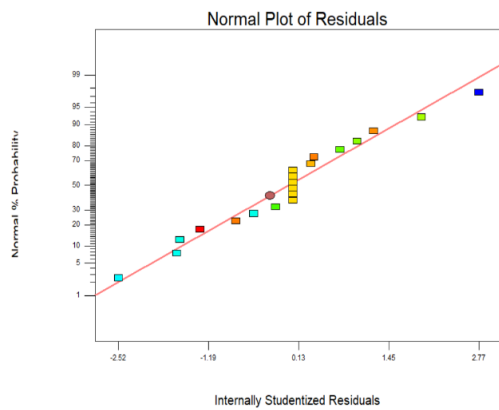
**Fig. 4.16**:- Relation between the predicted data points and the experimental data points as per the RSM model.
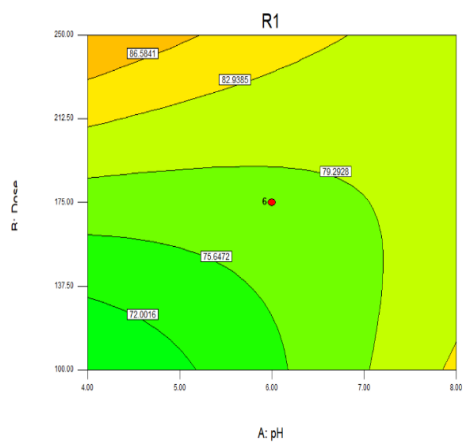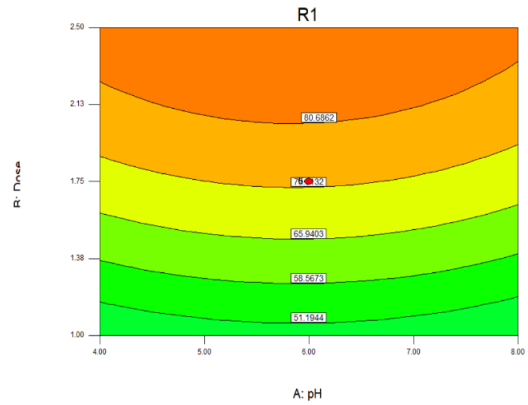


**Fig. 4.17**:- Interaction between the pH of the experimental solution and the dose of the GO and their effect on the percentage removal of RTN
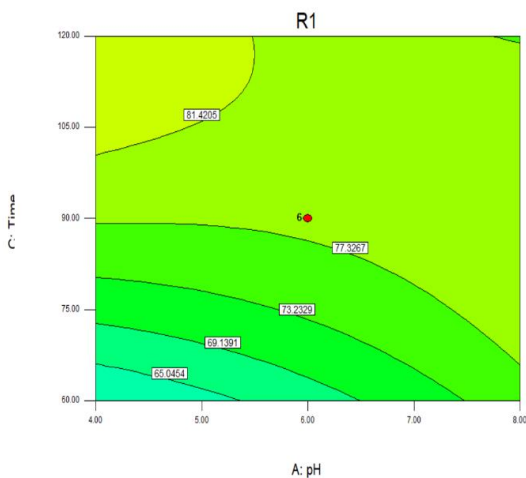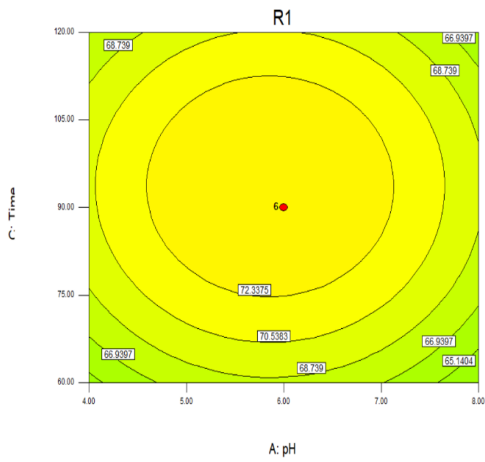


**Fig. 4.18:**- The interaction between the pH of the experimental solution and the contact time (in minutes) and their effect on the percentage removal of RTN by GO.
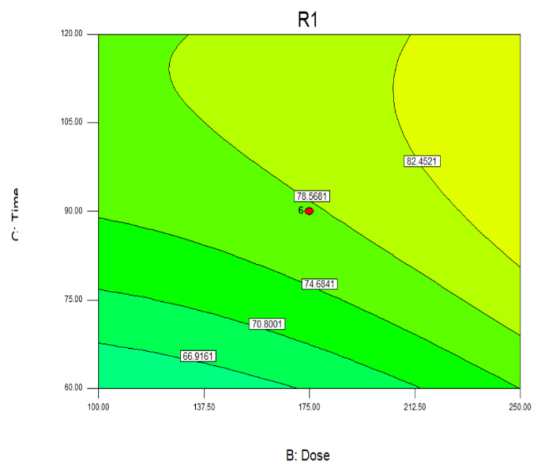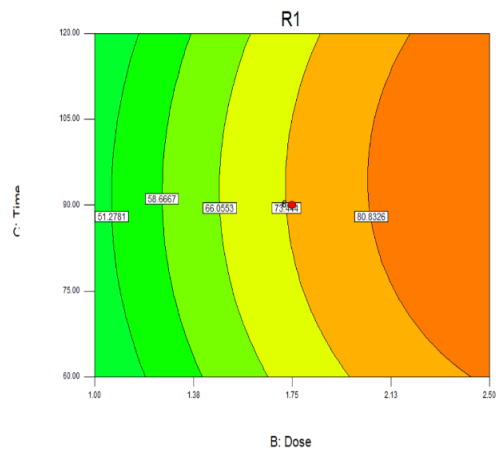


**Fig. 4.19**:- The plot showing the interaction between the dose of the GO and the contact time (in minutes) as per the RSM model and their effect on the percentage removal of RTN by GO.

### 4.4.6.4 Optimization of the adsorption of BPA by GO by RSM method

The RSM was performed with the aim of understanding the effect of inter parameter interaction on the experimental outcome. In **Table 4.20**, the outcome of the 20 experiments as proposed by the software for the CCD model of the RSM is given and in **Table 4.21** the result of the ANOVA of the RSM model is provided. From there it is observed that the $R^2$ value of the model was 0.97 and the adjusted $R^2$ value was 0.95 which propounded the fact that the polynomial model suggested by RSM was appropriate for predicting the outcome of this adsorption reaction. The high value of F (39.35, much higher than unity) and the low value of P ($< 0.0001$) meant that the optimizing model was very much significant, with the experimental data points exhibiting a high degree of correlation with the predicted data points (Bhattacharya et al., 2021). **Fig. 4.20** shows the relation between the experimentally determined data points and the predicted data points and there also it can be noted that the experimental data points exhibits a high degree of correlation with the predicted data points. The real equation which was used to predict the effect of the input variables on the response output is presented as follows.

$$Removal\,\% = -3.87573 + 11.67013 \times \text{pH} + 54.20779 \times \text{Dose} + 0.23592 \times \text{Time} - 1.61705 \times pH \times \text{Dose} + 1.67834 \times 10^{-3} \times pH \times Time - 0.061101 \times \text{Dose} \times \text{Time} - 1.19397 \times pH^2 - 8.80085 \times Dose^2 - 1.89310 \times 10^{-4} \times Time^2 \quad \dots\dots\dots\dots\dots\dots\dots\dots\dots\dots\dots(xxxii)$$

As per the RSM model the optimized conditions under which maximum removal of BPA (89.17%) was possible were: adsorbent dosage of 1.75 g/L, pH value of 2.64 and reaction time of 90 minutes. For this RSM model, the interaction between the experimental parameters (input variables) and their outcome on the percentage removal of BPA (response variable) is illustrated by the contour plots shown in **Fig. 4.21-4.23**.

➢ **Effect of GO dosage and solution pH on BPA removal by GO**

The interaction in between the pH of the experimental solution and the dosage of GO and its effect on the removal of BPA is conveyed in the contour plot of **Fig. 4.21**. From there it was observed that the removal of BPA by GO increased with the increase in dosage of GO. This could be attributed to the higher availability of active sites for the uptake of BPA at the higher dosage of GO and as a result of which the highest percentage removal value was obtained around the highest dosage of 2.5 g/L (Banerjee et al., 2016; Bhattacharya et al., 2021). In case of the variation of pH of the experimental solution, it was observed that the highest removal of BPA was observed at the lower pH range of the experimental solution and the removal percentage decreased with the increase in pH of the experimental solution. This could be attributed to the fact that the $pK_a$ value of BPA is 9.6 (Xu et al., 2018), and at around pH 8 the deprotonation of BPA starts by virtue of which it acquires a negative charge and is dissociated to form negatively charged bis-phenolate monoanions (Chang et al., 2012). On the other hand, the $pH_{pzc}$ of GO is 4.87 +/- 0.26, as a consequence of which at pH higher than 5, the surface of

GO also acquires a negative charge (Banerjee et al., 2016; Bhattacharya et al., 2020). Thus as a result of which, at the higher pH range the adsorption of BPA by GO is obstructed by the electrostatic force of repulsion acting between the negatively charged BPA molecules and the negative surface of GO (Chang et al., 2012; Kwon & Lee, 2015; Phatthanakittiphong & Seo, 2016; Xu et al., 2012). Therefore, the highest removal percentage was observed for the higher dosage of GO and for the lower pH range of the experimental solution.

➢ **Effect of solution pH and contact time on BPA removal by GO**

The interaction in between the pH of the experimental solution and contact time and its effect on the removal of BPA by GO is shown in the contour plot of **Fig. 4.22**. From there it was observed that the removal of BPA by GO increased with the increase in contact time which could be attributed to the higher number of interaction between the BPA molecules and the surface of GO resulting in greater adsorption of BPA molecules by GO (Bhattacharya et al., 2021). In case of pH variation it was observed, that highest removal of BPA was in the acidic pH range, as because at higher pH range in the basic medium both the surface of GO and the molecules of BPA acquire a negative charge (Banerjee et al., 2016; Chang et al., 2012; Xu et al., 2012). The $pK_a$ value of BPA is 9.6, and at around pH 8, the BPA molecules dissociate to form bis-phenolate monoanion (Chang et al., 2013). On the other hand, the $pH_{pzc}$ of GO is 4.87 +/- 0.26 (Banerjee et al., 2016), therefore at the higher pH range the surface of GO also acquires a negative charge. As a result of which at the higher pH range, the adsorption of BPA by GO is obstructed due to the electrostatic force of repulsion acting between the molecules of BPA and the surface of GO (Chang et al., 2012; Kwon & Lee, 2015; Phatthanakittiphong & Seo, 2016; Xu et al., 2012). The highest removal of BPA by GO was therefore observed at the highest contact time and at the lowest pH range.

➢ **Effect of contact time and GO dosage on BPA removal by GO**

The interaction in between the contact time and dosage of adsorbent and its effect on the removal of BPA by GO is shown in the contour plot of **Fig. 4.23**. From there it was observed that the removal of BPA by GO increased with the increase in dosage which could be ascribed to the availability of greater surface for the uptake of BPA molecules (Banerjee et al., 2016; Bhattacharya et al., 2021). On the other hand, the adsorption of BPA molecules by GO increased with the increase in contact time which could be attributed to the greater interaction between the BPA molecules and the surface of GO leading to the greater uptake of BPA by GO. From the analysis of the activation energy it was found that the adsorption of BPA on the surface of GO was physical in nature ($E_a$ = 26.3 kJ/mole < 40 kJ/mole), and as physical adsorption increases with contact time therefore the adsorption of BPA by GO also increased with increase in contact time (Bhattacharya et al., 2021; Mukherjee et al., 2019). Therefore, adsorption of BPA by GO was found to be highest at the highest dosage of GO and at the highest contact time.

**Table 4.20** :- The table showing the 20 different set of parameters (runs) along with their corresponding outcome as proposed by CCD model of RSM for optimization of BPA removal by GO

| Run | Block | Factor 1 | Factor 2 | Factor 3 | Response 1 |
|---|---|---|---|---|---|
| | | A:pH | B:Dose | C:Time | Percentage Removal |
| | | | g/L | min | |
| 1 | Block 1 | 4 | 1 | 60 | 71.96 |
| 2 | Block 1 | 4 | 2.5 | 60 | 90.04 |
| 3 | Block 1 | 4 | 1 | 120 | 82.57 |
| 4 | Block 1 | 8 | 2.5 | 120 | 69.00 |
| 5 | Block 1 | 6 | 1.75 | 90 | 84.89 |
| 6 | Block 1 | 6 | 3.01 | 90 | 87.02 |
| 7 | Block 1 | 6 | 0.31 | 90 | 52.91 |
| 8 | Block 1 | 2.64 | 1.75 | 90 | 92.57 |
| 9 | Block 1 | 8 | 2.5 | 60 | 63.49 |
| 10 | Block 1 | 6 | 1.75 | 90 | 84.89 |
| 11 | Block 1 | 6 | 1.75 | 140.45 | 91.02 |
| 12 | Block 1 | 4 | 2.5 | 120 | 92.10 |
| 13 | Block 1 | 6 | 1.75 | 90 | 84.89 |
| 14 | Block 1 | 8 | 1 | 60 | 58.16 |
| 15 | Block 1 | 6 | 1.75 | 90 | 84.89 |
| 16 | Block 1 | 9.36 | 1.75 | 90 | 53.45 |
| 17 | Block 1 | 6 | 1.75 | 90 | 84.89 |
| 18 | Block 1 | 8 | 1 | 120 | 66.13 |
| 19 | Block 1 | 6 | 1.75 | 39.55 | 81.00 |
| 20 | Block 1 | 6 | 1.75 | 90 | 84.89 |

**Table 4.21**:- ANOVA analysis for the RSM for the process operation of BPA adsorption by GO

| $R^2$ Value | Adjusted $R^2$ Value | f- value | Probability Value P |
|---|---|---|---|
| 0.97 | 0.95 | 39.35 (>1) | <0.0001 Significant |
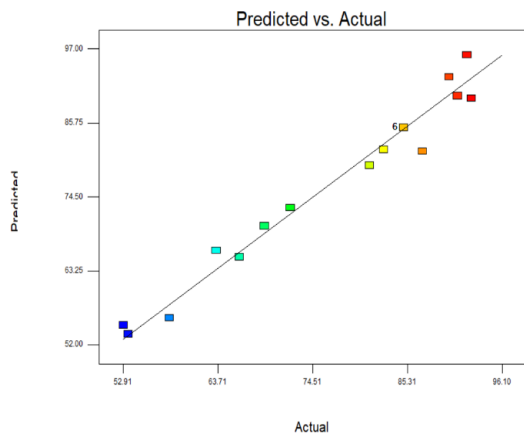
**Fig. 4.20**: Relation between the predicted data points and the experimental data points as per the RSM model.
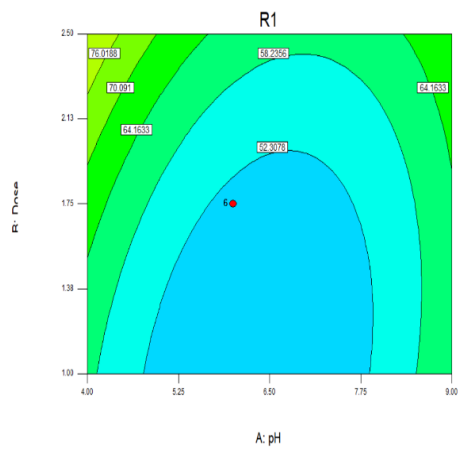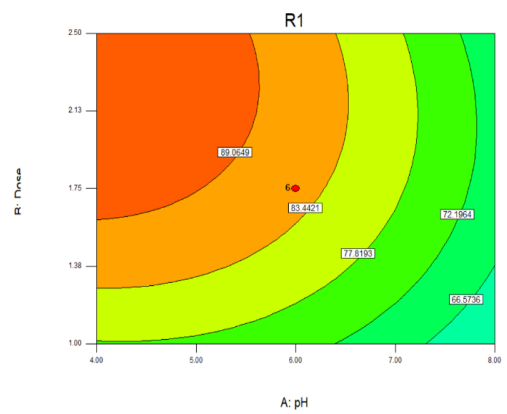


**Fig. 4.21**:- Interaction between the pH of the experimental solution and the dose of the GO and their effect on the percentage removal of BPA
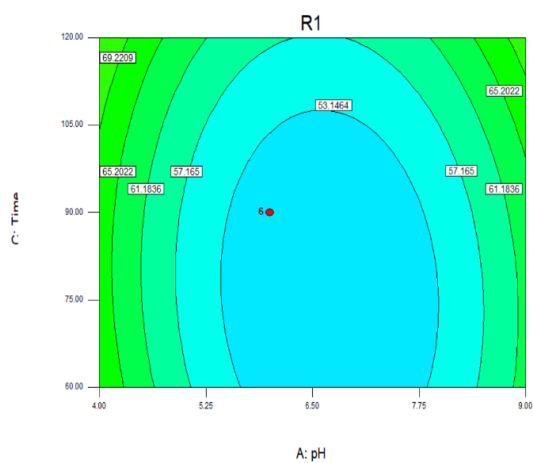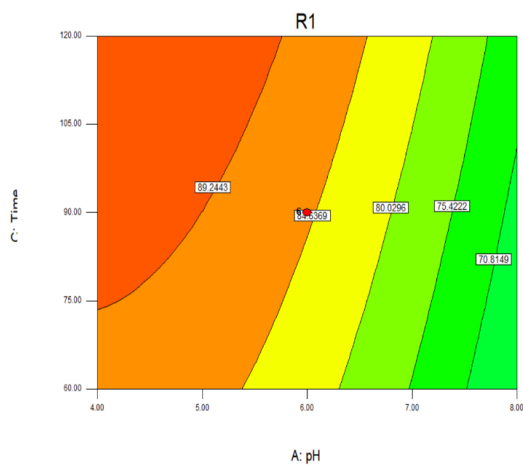


**Fig. 4.22**:- The interaction between the pH of the experimental solution and the contact time (in minutes) and their effect on the percentage removal of BPA by GO.
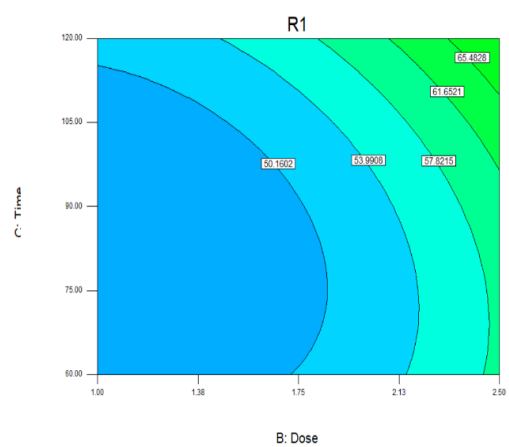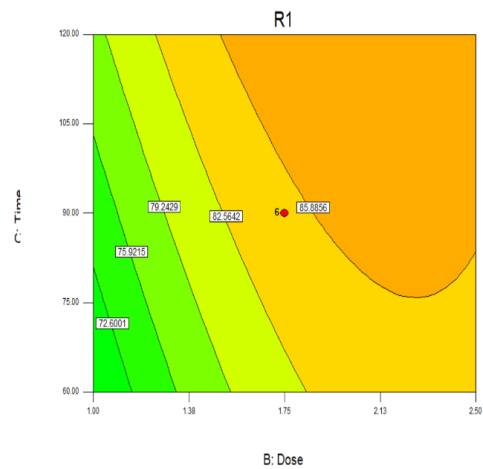


**Fig. 4.23**:- The plot showing the interaction between the dose of the GO and the contact time (in minutes) as per the RSM model and their effect on the percentage

## 4.4.7 Removal of the EC's by RPB

The adsorption efficacy of GO for the purpose of removing the EC's were also checked in a RPB. The application of RPB was for intensifying the adsorption process (Das et al., 2008). Rather than using the GO as a packing material, it was directly added to the experimental solution. For each of the EC's, three concentrations were taken namely 10 mg/L, 5 mg/L and 2.5 mg/L. The result of the experiment is given in (**Fig. 4.24 (a-d)**). From there it was observed that the removal of EC's decreased with the increase in the concentration. The removal of CBZ (**Fig. 4.24 (a)**) for the 10 mg/L concentration of CBZ at the point of equilibrium was 84.53 %, for the 5 mg/L concentration was 90.94% and for the 2.5 mg/L concentration was 94.49 %. The removal of NPX (**Fig. 4.24 (b)**) for the 10 mg/L concentration of NPX at the point of equilibrium was 78.59 %, for the 5 mg/L concentration was 85.55% and for the 2.5 mg/L concentration was 88.18 %. From the removal of RTN (**Fig. 4.24 (c)**) it was observed that the highest removal of RTN was 99.68 % which was observed for the 2.5 mg/L concentration, followed by 96.73 % removal for the 5 mg/L concentration and lastly, 95.38 % removal for the 10 mg/L concentration of RTN. From the result of BPA (**Fig. 4.24(d)**) it was observed that the highest removal of BPA was 92.68 % which was observed for the 2.5 mg/L concentration, followed by 86.6 % removal for the 5 mg/L concentration and lastly, 85.62 % removal for the 10 mg/L concentration of BPA. The logic behind this experimental outcome is that on increasing the concentration of the EC's, the surface of GO was saturated by the molecules of EC's. As a consequence of which the removal of EC's by GO in a RPB decreased with the increase in concentration of EC's. Similarly the equilibrium for the lower concentration was achieved under the fastest time and the equilibrium for the highest concentration was achieved at the slowest time (Banerjee et al., 2016; Bhattacharya et al., 2020).
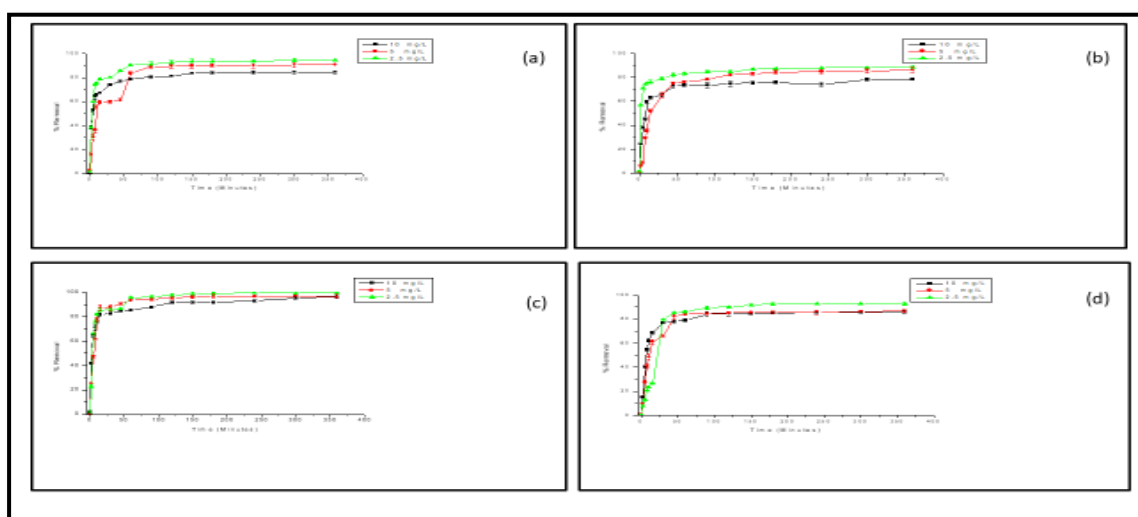


**Fig. 4.24 (a)** Removal of different concentration of CBZ  by GO in a RPB **(b)** Removal of different concentration of NPX  by GO in a RPB **(c)** Removal of different concentration of RTN  by GO in a RPB **(d)** Removal of different concentration of BPA by GO in a RPB.

**4.4.8 Reusability Study**

*4.4.8.1 Reusability Study of GO after treating CBZ*

Out of the six solutions that were used for the regeneration of used GO after treating CBZ, the greatest effectivity was exhibited by the 10% NaOH solution. By treating the CBZ with the 10 % NaOH solution, it was observed that the removal capacity of GO for the purpose of treating CBZ remained over 90 % for the first three cycles. A slight decrease (88.62 %) was observed in case of the fourth cycle followed by a 78.99 % removal in case of the fifth cycle. The reusability study was not performed beyond the fifth cycle due to the loss in the mass of adsorbent and the decreased adsorption ability of GO. Thus, it can be inferred from the reusability study that a certain mass of GO can be effectively used for at least three times for the purpose of removing trace pollutants like CBZ from its aqueous solution (Bhattacharya et al., 2020). The result of the experiment is given in **Fig. 4.25**.
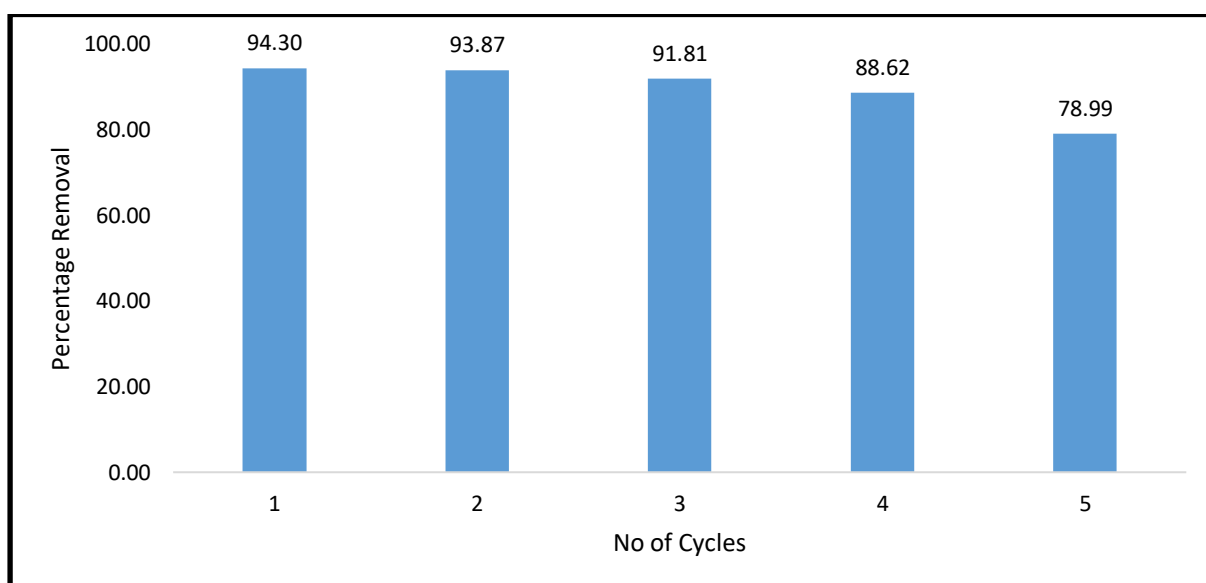


**Fig. 4.25**:- Removal of CBZ by GO in different steps of the reusability cycle.

*4.4.8.2 Reusability Study of GO after treating NPX*

Out of the six solutions that were used for the regeneration of used GO after treating NPX, the greatest effectivity was exhibited by the 10 % HCl solution, therefore further reusability study was performed by this solution only. By treating the GO with the 10 % HCl solution after each adsorption cycle, it was observed that the removal capacity of GO for the purpose of treating NPX remained over 75 % for the first three cycles. A decrease of about 4 % was observed in case of the fourth cycle (71.92 %) followed by which adsorption ability of the GO for the purpose of removing NPX decreased to 63.08 % for the fifth cycle beyond which the reusability study was not extended due to the loss of mass of GO. Thus from the reusability study it was inferred that by washing GO with 10 % HCl solution, it could be used

for 3-4 times with significant adsorption efficacy for the purpose of removing NPX from its aqueous solution (Bhattacharya et al., 2020). The result of the experiment is given in **Fig. 4.26**.
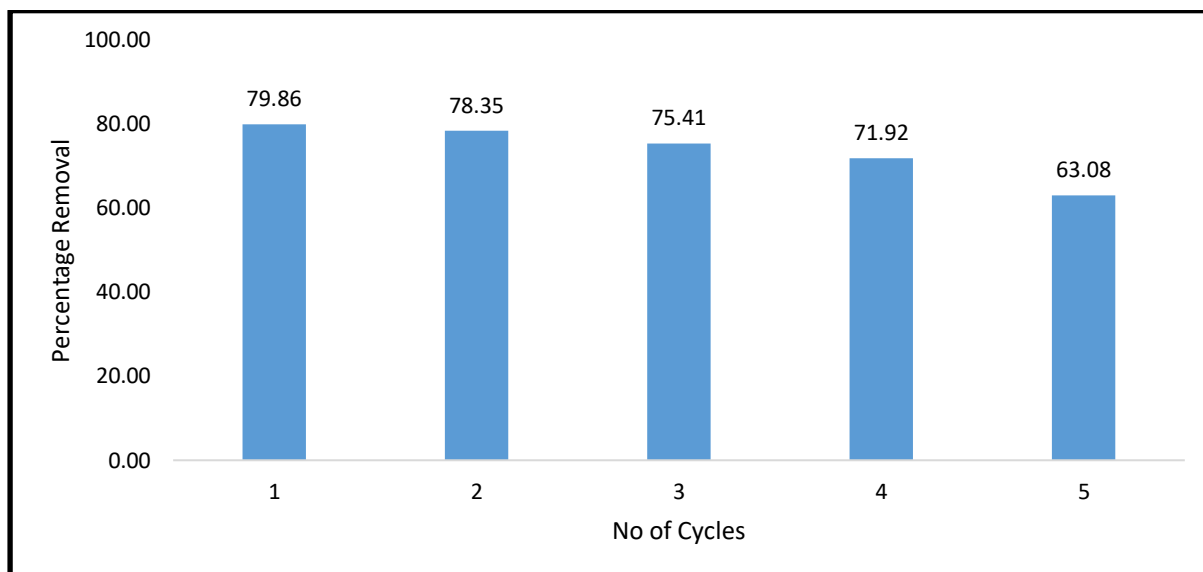


**Fig. 4.26**:- Removal of NPX by GO in different steps of the reusability cycle.

### 4.4.8.3 Reusability Study of GO after treating RTN

Out of the six solutions that were used for the regeneration of used GO after treating RTN, the greatest effectivity was exhibited by the $H_2O$ solution, therefore further reusability study was performed by this solution only. This could be attributed to the high hydrophilicity of RTN molecules (Siew et al., 2012). By treating the GO with the water after each adsorption cycle, it was observed that the removal capacity of GO for the purpose of treating RTN remained over 90 % for the first four cycles followed by a slight decrease in case of the fifth cycle. Thus it can be stated that on washing a particular mass of GO by water, it could effectively reused for the purpose of removing RTN from the aqueous solution for multiple cycles (Bhattacharya et al., 2020). The result of the experiment is given in **Fig. 4.27**.
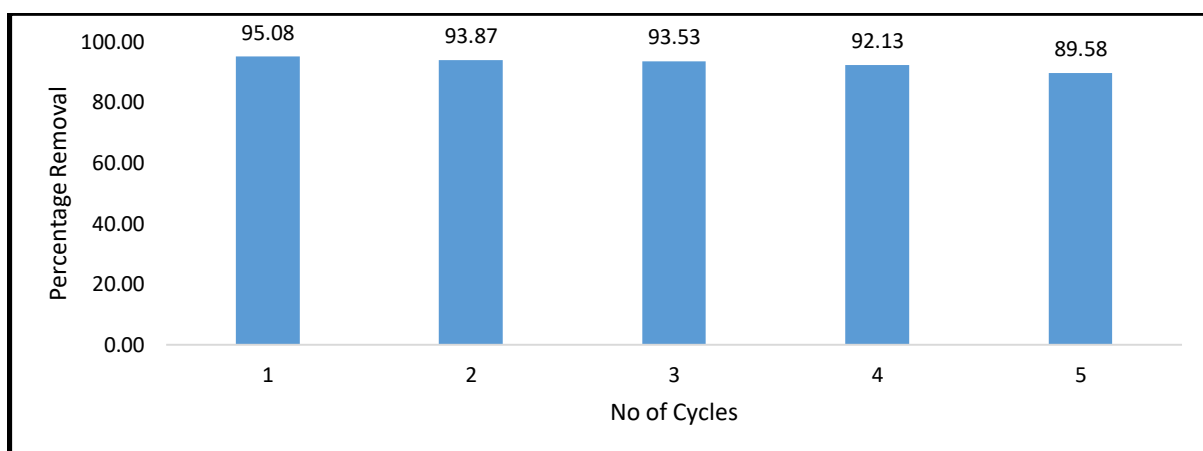


**Fig. 4.27**:- Removal of RTN by GO in different steps of the reusability cycle

### 4.4.8.3 Reusability Study of GO after treating BPA

Out of the six solutions that were used for the regeneration of used GO after adsorbing BPA, the greatest effectivity was exhibited by the 10% ethanol solution, therefore further reusability study was performed by this solution only. The reason for the effectivity of the 10 % ethanol solution for the purpose of regenerating GO after adsorption of BPA can be ascertained to the fact that, BPA is readily soluble in ethanol. By treating the GO with the 10 % ethanol solution after each adsorption cycle, it was observed that the removal capacity of GO for the purpose of treating BPA was 85.45 % for the first cycle, which was similar to the removal obtained from the batch study result. For the second cycle of treatment the adsorption efficiency of GO decreased a bit, and the removal percentage decreased to 82.87 %, and for the third cycle it decreased to 75.34 %. The removal of BPA by GO in the last two cycles were 73.36 % and 67.71 % respectively. Thus from the result of the regeneration study it can be inferred that, on washing with 10 % ethanol solution, the same mass of GO can be used for two to three times for the purpose of removing BPA from its aqueous solution (Bhattacharya et al., 2020). The result of the experiment is given in **Fig. 4.28**.
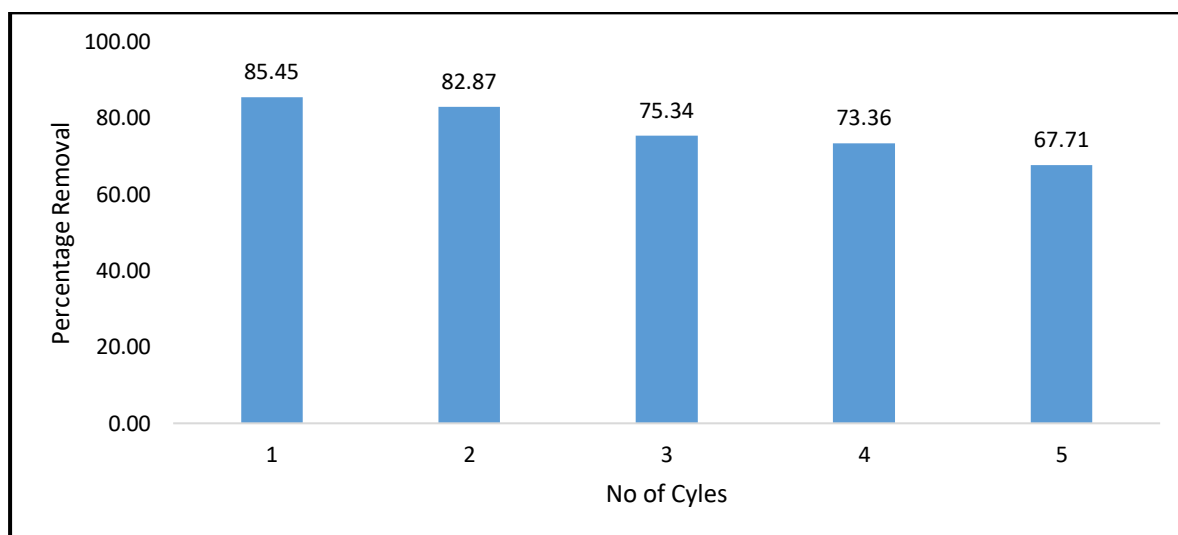


**Fig. 4.28**:- Removal of BPA by GO in different steps of the reusability cycle.

## 4.5 CONCLUSION :-

In the above study, GO was utilized for the adsorption of four trace pollutants viz., the three PHA compound CBZ, RTN, NPX and the EDC, BPA from there aqueous solution. The synthesis of GO was performed with a modified Hummer's method, and from the characterization it was confirmed that GO was successfully synthesized from the oxidation of graphite. From the result of the experimental study it was observed that GO was effective in adsorbing all the four types of pollutants from their aqueous solution. The percentage of removal, however varied with the different pollutants. The highest removal of CBZ was found to be 99.38 % which was obtained at pH 2, GO dosage of 2 g/L, CBZ concentration of 10 mg/L and temperature of 303 K. The highest removal for NPX was observed to be 90.93 % which was obtained at pH 4, GO dosage of 2 g/L, NPX concentration of 10 mg/L and temperature of 303 K. The highest removal for RTN was observed to be 97.52 % which was obtained at pH 6, GO dosage of 2 g/L, RTN concentration of 10 mg/L and temperature of 303 K. The highest removal of BPA was observed to be 87.55 % which was obtained at pH 2, GO dosage of 2 g/L, BPA concentration of 10 mg/L and temperature of 303 K. From the experimental result it can be deduced that variation in pH played a major role in the adsorption efficacy of GO. The $pH_{pzc}$ value of GO has been found to be 4.87 +/- 0.27 from the previous literatures. And the $pK_a$ values of CBZ is 13.9, NPX is 4.15, RTN is 2.7 and 8.2 and BPA is 9.6. Depending on the suitable pH, neutral or oppositely charged EC molecules were adsorbed on the surface of GO. Other than the pH it was observed that on increasing the concentration of the EC's, there removal percentage decreased due to saturation of the adsorbent surface. The removal percentage increased on every occasion on the increase of the adsorbent dosage due to greater availability of active sites. The effect of temperature on the adsorption efficacy of GO generally varied with the change of adsorbate molecules. The process was further optimized with RSM. In RSM, the effect of interaction of multiple parameters on the adsorption capacity of GO was observed. As per RSM, the highest removal of CBZ was 95 % which was attained at GO dosage of 2.5 g/L, pH value of 4 and reaction time of 120 minutes. For NPX the highest removal was 92.67% which was possible at adsorbent dosage of 2.5 g/L, pH value of 4 and reaction time of 120 minutes. For RTN the highest removal was 89.17% which was possible at adsorbent dosage of 3.01 g/L, pH value of 6 and reaction time of 90 minutes. For BPA the highest removal was 89.17% which were possible at adsorbent dosage of 1.75 g/L, pH value of 2.64 and reaction time of 90 minutes. The removal of the EC's by GO was also investigated in the RPB setup, which was used to intensify the adsorption process. As per the result of the experiment, it was observed that the adsorption equilibrium was reached quite rapidly (around the 100 minute) mark of the RPB study. The highest removal was obtained for lowest concentration, which was 2.5 mg/L in each case. The highest removal for CBZ was 94.5 %, for NPX was 88.18%, for RTN was 99.68 % and for BPA was 92.68 %. Lastly, through the reusability of the GO was investigated through the regeneration process and from the result it was observed that GO, on being treated/washed with the proper reagent can be reused for at least 2-3 times with the same efficacy of the pristine

material. Thus from the result of the experiment it was inferred that GO was effective in adsorbing the designated compounds from their aqueous solution. The chemical and physical stability of GO ensured that the experimental parameters can be sufficiently varied for the optimized removal of the EC molecules from water.

# CHAPTER 5

# SYNTHESIS OF ACTIVATED RICE STRAW BIOCHAR (ARSB) AND ITS UTILIZATION FOR REMOVING EC'S FROM THE AQUATIC SYSTEM

## 5.1 INTRODUCTION

Among the various types of adsorbents that have been utilized for waste water treatment, carbonaceous adsorbents has always remained a viable and popular choice by virtue of their physical, chemical and structural characteristics (Reynel-avila et al., 2015). Different carbonaceous adsorbents have been synthesized from different antecedent and they have been efficaciously applied for removing a large variety of pollutants like pesticides, dyes, heavy metals, fluoride, arsenic, pharmaceuticals and other organic and inorganic compounds (Al-hamadani et al., 2018; Barman et al., 2018; Bhattacharya et al., 2020; Khalil et al., 2020; Nawaz et al., 2017; Shukla et al., 2019; Tan et al., 2016) . For instance (Shukla et al., 2019) synthesized a rice husk biochar from microwave pyrolysis method by which it was able to adsorb 65% and 75% of Phosphate and Nitrate respectively. (Khalil et al., 2020) synthesized tea waste biochar and rice husk biochar which were able to remove 99.3% and 96.8% of hexavalent Chromium (Cr(VI)) from water respectively. (Tan et al., 2018) fabricated a rice straw magnetic biochar which was able to remove 91% of Cadmium from water under optimum conditions. (Barman et al., 2018) synthesized a $H_3PO_4$ activated biochar from waste wood fillings and successfully used it to remove Poly Aromatic Hydrocarbons (PAHs) like acenapthene and naphthalene from water. Among these different types of carbonaceous components that have been utilized as an adsorbent for water treatment, one that have generated a lot of interest in recent times is biochar, by virtue of its high porosity and high pore volume, high chemical stability and high physical hardness number and large specific surface area (Barman et al., 2018; Khalil et al., 2020). Also, unlike other carbonaceous adsorbents like activated carbon and GO, biochar are comparatively easier to synthesize and cheaper to manufacture, as the precursors for biochar tend to be plentiful and low-cost agricultural by-products

(Tan et al., 2015). Many studies have reported biochar to be a very efficacious adsorbents for the purpose of removing an array of different pollutants from water (Nawaz et al., 2017;  Tan et al., 2018; Tomul et al., 2020). Biochar can be synthesized from a wide number of precursors and many different methods are available for synthesizing and activating the biochar (Roy et al., 2018; Tan et al., 2018; Tomul et al., 2020). Consequently, the nature of the material used for the synthesis of the biochar and the subsequent method applied for its activation has been known to exhibit a significant impact on the characteristics and thus the effectivity of the biochar (Roy et al., 2018). Therefore selection of the correct precursor and appropriate activation method for the purpose of synthesizing the biochar is of paramount importance for its optimum functionality. For this study, rice straw was chosen as the raw material for the synthesis of the biochar (Goswami et al., 2017; Tan et al., 2018). The reason behind the selection of rice straw is that, rice straw is an agricultural by-product produced in abundance therefore it is a cheap and readily available lignocellulosic material (Dai et al., 2020; Goswami et al., 2017; Tan et al., 2018; Tan et al., 2016). The biochar from rice straw was synthesized by treating the biochar at a high temperature and in inert atmosphere and the biochar thus synthesized was given the name Rice Straw Biomass Biochar (RSBB) (Goswami et al., 2017). It has been reported in previous literatures that the presence of functional groups on the surface of the biochar enhanced the surface reactivity of the biochar (Roy et al., 2018; Tomul et al., 2020). As a consequence of which, the activation of the synthesized RSBB was done with a surface oxidation method (Roy et al., 2018), with a combination of sulphuric acid ($H_2SO_4$) and potassium permanganate ($KMnO_4$), by following a modified Hummers method and ultra-sonication force to increase the surface area and activity as adsorbent. The resultant product was given the name as activated rice straw biochar (ARSB). This ARSB thus synthesized was used for removing EC's from water by adsorption. The synthesized ARSB was characterised by various characterization tools namely SEM, Raman spectroscopy, FTIR spectroscopy and X-ray diffractometry. In this experimental study, the efficacy of ARSB for the purpose of removing EC's from water was evaluated by means of both a batch study and a continuous column study. The data from the batch study was used for determining the adsorption isotherm and rate order kinetics of the concerned process. The isotherm and kinetic model which exhibited the highest correlation value was considered to best describe the adsorption of EC's by ARSB. Optimization of the process was done with RSM. Along with the batch study, the adsorption process was intensified by an RPB study. The reusability potential of the adsorbent ARSB was also evaluated by means of a consecutive adsorption-desorption study.

The RPB study was conducted to intensify the adsorption of EC's by the ARSB. However, rather than using three concentration of the EC's in the RPB, one concentration (10 mg/L) of each of the EC's were taken and they were treated by 2 g/L of ARSB which was directly added to the experimental apparatus.

The aim of this present study was to synthesize an efficient adsorbent from an easily available and cheap raw material (rice straw) and to evaluate the ability of the adsorbent to eliminate a group of recalcitrant

and trace pollutant, individually from there aqueous solution. The optimized conditions under which highest removal of the EC's were possible were deduced by a batch study followed by which the optimization was done with RSM. The process intensification of the removal of EC's by ARSB was done by a RPB study.

## 5.2 MATERIALS AND METHODS :-

### 5.2.1 Materials required

The rice straw was collected from a local vendor and was used after washing and drying. The rest of the materials was collected in the same manner as mentioned in the previous chapter, **Chapter 4, Section 4.2.1.**

### 5.2.2 Synthesis of ARSB from the rice straw

First the rice straw was washed with tap water and sundried for a week after which it was cleaned thoroughly with distilled water for the purpose of removing dirt, dust and any other impurities. The washed rice straw was dried at 80°C for about 48 h for the purpose of removing the moisture. After drying in the oven the rice straw fibres were cut into small pieces. Then the rice straw was heated in an inert atmosphere at high temperature (450°C) inside a fabricated reactor to form a biochar, which was then homogenised by crushing followed by sieving to get a mixture of uniform particle size ($< 50$ μm). The biochar thus synthesized was given the name Rice Straw Biomass Biochar (RSBB). Thereafter the RSBB was activated by following a modified Hummer's method. In brief, about 20 mg of the RSBB was mixed with 200 ml of Sulphuric acid ($H_2SO_4$) under continuous stirring. The flask containing the acidic mixture was then transferred to an ice bath after which a fixed amount of $KMnO_4$ was added into this mixture, also under continuous agitation. The whole arrangement was then kept at room temperature for 30 min under rotation. After that, 150 ml of distilled water was slowly added into the mixture, after which it was transferred into an incubator shaker where it was rotated at 45 °C for 3 h. Subsequently, 200 ml of distilled water ($H_2O$) was put inside the reaction mixture followed by 150 ml of 30% Hydrogen Peroxide ($H_2O_2$). After adding the $H_2O_2$ the reaction mixture turned yellow thereby denoting the end point of the reaction. The reaction mixture was then placed inside an ultrasonic cleaner (Digital Ultrasonic Cleaner; LMUC-4) for approximately 15 min so that the synthesized ARSB particles attained uniform particle size. After this the ARSB particles was isolated from the suspension by filtration followed by centrifugation and the extracted ARSB particles were then repeatedly washed with distilled water, 30% ethanol ($C_2H_5OH$) and 5% Hydrochloric Acid (HCl) to remove any residual impurities (mainly metallic) from them. Then after sufficient washing when the ARSB had attained neutral pH, they were freeze dried and then stored in an air tight container for future use (Banerjee et al., 2016; Goswami et al., 2017).

### 5.2.3 Characterization

Characterization of the synthesized ARSB particles were done by Scanning Electron Microscopy (SEM), Raman Spectroscopy, Fourier transform infrared spectroscopy (FT-IR) and X-ray Diffraction (XRD).

The particulars are the same as mentioned in **Chapter 4, Section 4.2.3.**

### 5.2.4 Preparation of the Experimental Solution.

Using the same process as mentioned **Chapter 4, Section 4.2.4.**

### 5.2.5 Batch study

A batch study was performed in order to find the experimental conditions under which the highest removal of the EC 's by the ARSB was possible. The set of parameters and there variation remained constant for every EC.

The experimental parameters, the range of variables, the time of taking samples, the method of pre-treatment, the mode of detection of EC's in the experimental solution before and after the treatment of the sample by ARSB and the representation of the experiment sample were same as mentioned in **Chapter 4, Section 4.2.5**.

### 5.2.6 Process optimization with RSM

Same theory as mentioned in **Chapter 4, Section 4.2.6**.

### 5.2.7 Process Intensification with Rotating Packed Bed (RPB) study

As mentioned before, in case of the RPB study, one concentration (10 mg/L) of each of the EC's were taken and the dose of ARSB were kept fixed at 2 g/L. The result of the experiment is presented in the form of line graph with percentage removal against time, with the removal of all four of the EC's presented at the same time. The rest of the experimental detail is the same as presented in **Chapter 4, Section 4.2.8**.

### 5.2.8 Reusability study of the ARSB

Following the same procedure as mentioned in **Chapter 4, Section 4.2.9**.

## 5.3 CALCULATIONS :-

### 5.3.1 Percentage removal and adsorption capacity

Same as mentioned in **Chapter 4, Section 4.3.1**.

### 5.3.2 Adsorption Isotherm

Same as mentioned in **Chapter 4, Section 4.3.2**.

### 5.3.3 Adsorption Kinetics

Same as mentioned in **Chapter 4, Section 4.3.3.**

### 5.3.4 Adsorption thermodynamics and Activation Energy

Same as mentioned in **Chapter 4, Section 4.3.4.**

### 5.3.5. Optimization using RSM

Same as mentioned in **Chapter 4, Section 4.3.5.**

## 5.4 RESULTS :-

### 5.4.1 Characterization

#### *5.4.1.1 SEM analysis of ARSB*

From the SEM analysis (**Fig. 5.1(a)**) of ARSB it was observed that the surface of ARSB is composed of thin, overlapping, creased sheets of carbon (Goswami et al., 2017). The uneven, rough structures observed on the surface of ARSB reportedly enhances its adsorption ability. The layers and wrinkles observed in between the layers of ARSB have likely been formed due to the interconnection between the oxygen containing functional groups, analogues to what is observed in case of GO synthesized from graphite by Hummers method (Mukherjee et al., 2019). Therefore, it can be said that the ARSB thus synthesized may have resembled GO is some aspects of its surface morphology (Goswami et al., 2017).
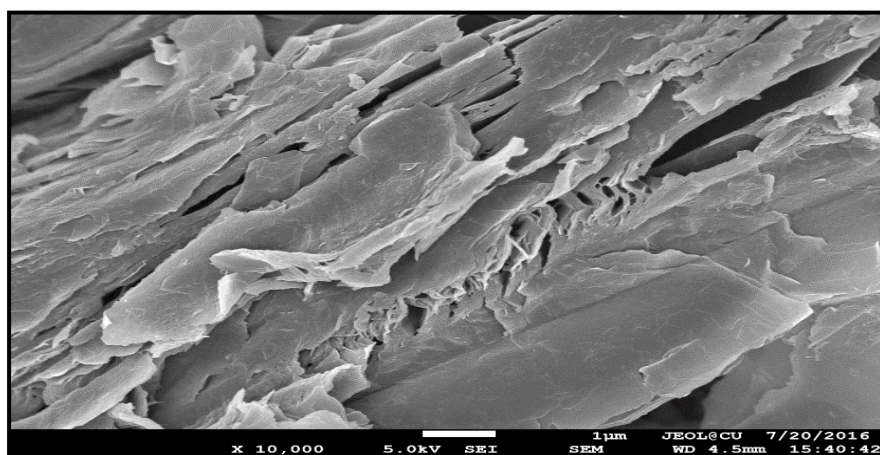


**Fig. 5.1 (a)** :- SEM image of ARSB

### 5.4.4.2 FTIR analysis of ARSB

The FTIR spectrum of ARSB is shown in **Fig. 5.1 (b)**. It was observed from there that prominent peaks are shown at the points 1090 cm$^{-1}$, 1620 cm$^{-1}$, 1732 cm$^{-1}$, 3506 cm$^{-1}$ which denotes the C–O bond, $C = C$ bond, $C = O$ bond and O–H bond respectively (Banerjee et al., 2015b). The peaks denoted at 1396.5 cm$^{-1}$, 1462 cm$^{-1}$, 2924.7 cm$^{-1}$ and 2854 cm$^{-1}$ denotes the C–H bond respectively (Balasubramani, Sivarajasekar, & Naushad, 2020; Bhattacharyyaa et al., 2018). This peaks are comparable to the ones observed in case of GO (Banerjee, et al., 2017; Bhattacharya et al., 2020). Therefore from the FT-IR analysis it can be said that, the adsorbent ARSB synthesized for this study contained various functional groups on its surface comparable to that of GO. This result was desirable, as because these functional groups would ultimately facilitate the surface adsorption of ARSB (Roy et al., 2018).
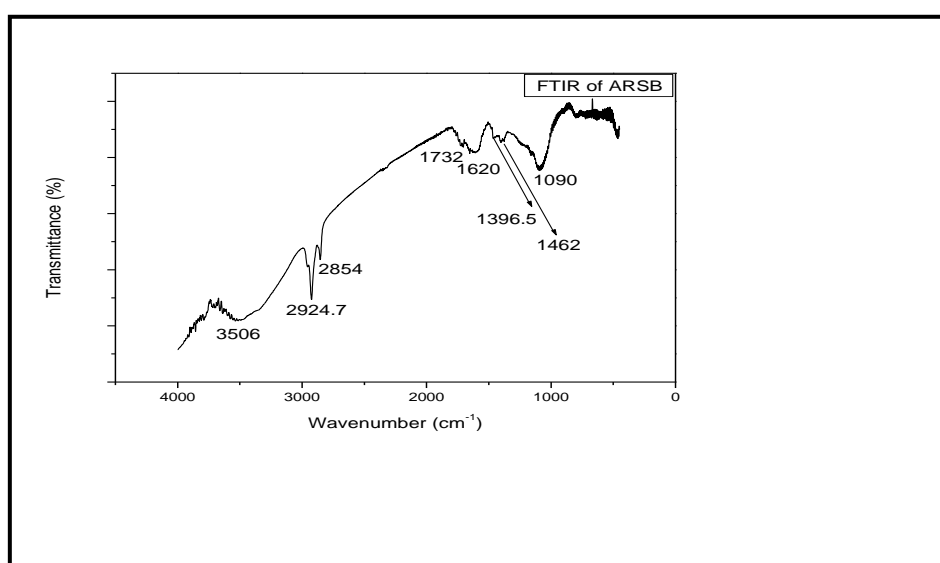


**Fig. 5.1 (b)** :- FT-IR spectra image of ARSB

### 5.4.4.3 XRD analysis of ARSB

The XRD spectrum of ARSB is shown in **Fig. 5.1 (c)**. The prominent peaks in the spectrum are exhibited at the points 13.7° and 27.5°. The presence of the XRD peak at 13.7° can be attributed to the presence of the functional groups on the surface of ARSB (Sharma et al., 2020) thereby reconfirming the successful oxidation of the biochar (RSBB) by Hummers method. The presence of the peak at 27.5° can be ascribed to the un-oxidized graphitic carbon layers present in the ARSB (Saleem et al., 2018). Therefore from the XRD analysis it can be inferred that ARSB synthesized was partially oxidized and had both oxidized and un-oxidized carbon layers in them. Thus it can be said that the synthesized ARSB shared some morphological similarity with reduced GO.
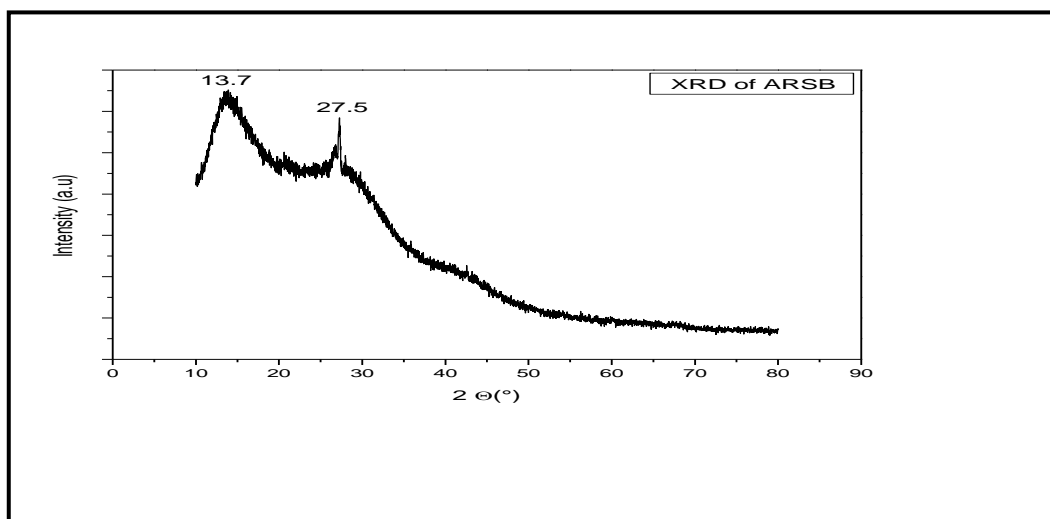
**Fig. 5.1 (c)** :- XRD image of ARSB

## *5.4.4.4 Raman Spectroscopy of ARSB*

From the Raman Spectra of ARSB as shown in **Fig. 5.1 (d)**, the D-band and the G-band were observed at 1332.75 $cm^{-1}$ and 1587.67 $cm^{-1}$ respectively. The D-band denotes the $sp^2$ carbon atom with structural defect proportional to the extent of oxidation and the G-band denoted the in-plane vibration of $sp^2$ bonded graphitic structure (Zhang et al., 2018). From the Raman Spectra of ARSB, it was found that the ratio of D-band to G-band, i.e., $I_D$ /$I_G$ as per their respective peak intensities was 1.19, thereby denoting large number of structural defects in the $sp^3$ hybridized carbon atoms of ARSB (Nawaz et al., 2017). As the ratio of $I_D/I_G$ ~ 1, therefore it was designated that the structure of ARSB was highly graphitized (Liu et al., 2020).
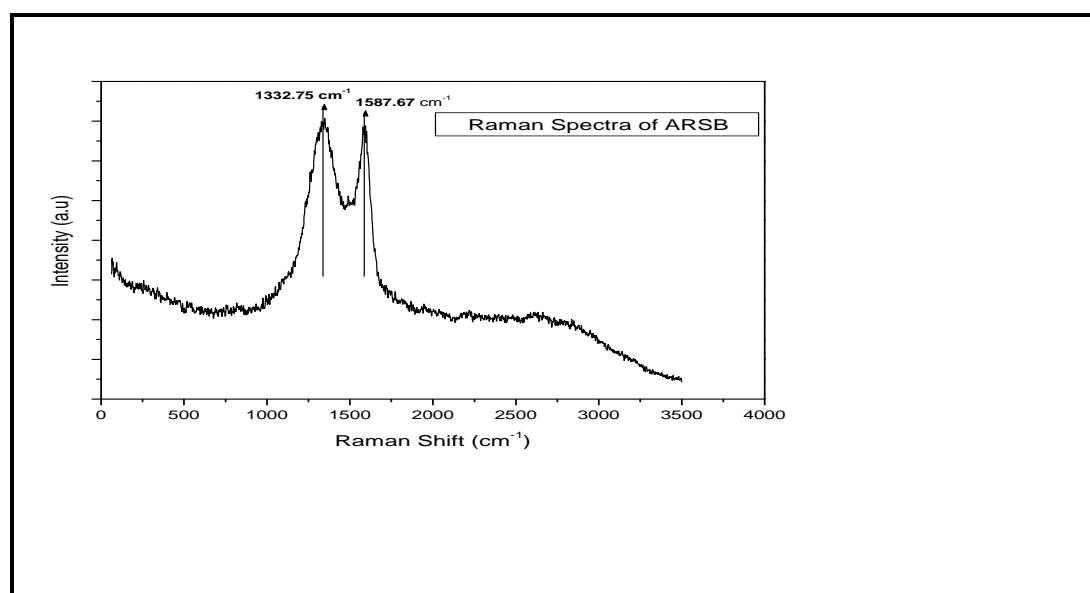


**Fig. 5.1 (d)** :- Raman Spectra of GO

104

### 5.4.2 Batch Study Results

#### *5.4.2.1 Effect of concentration of adsorbate on the removal efficacy of ARSB*

In order to investigate the effect of the concentration of the adsorbate on the removal efficacy of ARSB, four concentration of each of the EC's were taken namely 5 mg/L, 10 mg/L, 15 mg/L and 20 mg/L. The dose of ARSB, pH of the experimental solution and temperature were kept constant at 2 g/L, pH 7 and 303 K respectively. The result of the experiment is given in **Fig. 5.2 ((a)-(d)).** From there it was observed the removal of CBZ by ARSB (**Fig. 5.2 (a)**) increased with the increase in concentration of CBZ from 5 mg/L to 15 mg/L. This could be attributed to the gradient based transfer of the CBZ molecules from the solution to the surface of the adsorbent (Banerjee et al., 2016). When the concentration of CBZ increased from 5 mg/L to 15 mg/L, the percentage removal increased from 49.54 % to 60.56 %. However, when the concentration was increased to 20 mg/L, the removal of CBZ by ARSB decreased to 56.01%. This could be attributed to the saturation of the active sites on the surface of the adsorbent (Bhattacharya et al., 2021). A similar observation was made in case of the removal of BPA by ARSB (**Fig. 5.2 (d)**), where the removal increased with the increase in concentration from 5 mg/L – 10 mg/L. However, when the concentration was increased beyond the 10 mg/L point, the adsorption of BPA by ARSB decreased which could be attributed to the saturation of ARSB surface by BPA molecules.

In case of the removal of NPX and RTN by ARSB a similar trend was observed. That is the removal of the adsorbate by ARSB decreased with the increase in concentration of the adsorbate. For the removal of NPX by ARSB (**Fig. 5.2(b)**) the highest removal was observed at the 5 mg/L concentration (83.19 %) followed by the 10 mg/L concentration (72.66 %) followed by the 15 mg/L concentration of NPX (67.47 %) and lastly the lowest removal was observed for the 20 mg/L concentration of NPX (55.93 %). Similarly, for the removal of RTN by ARSB (**Fig. 5.2(c)**) the highest removal was observed at 5 mg/L (74.69 %), followed by at 10 mg/L (58.42 %), 15 mg/L (46.1 mg/L) and lastly by 20 mg/L (35.64 %). The reason behind this phenomenon can be given as, with the dosage of ARSB remaining constant, the surface of ARSB got saturated with the increase in the concentration of the EC's. As a consequence of which the uptake of the EC's by ARSB decreases with the increase in concentration (Banerjee et al., 2017; Bhattacharya et al., 2021).
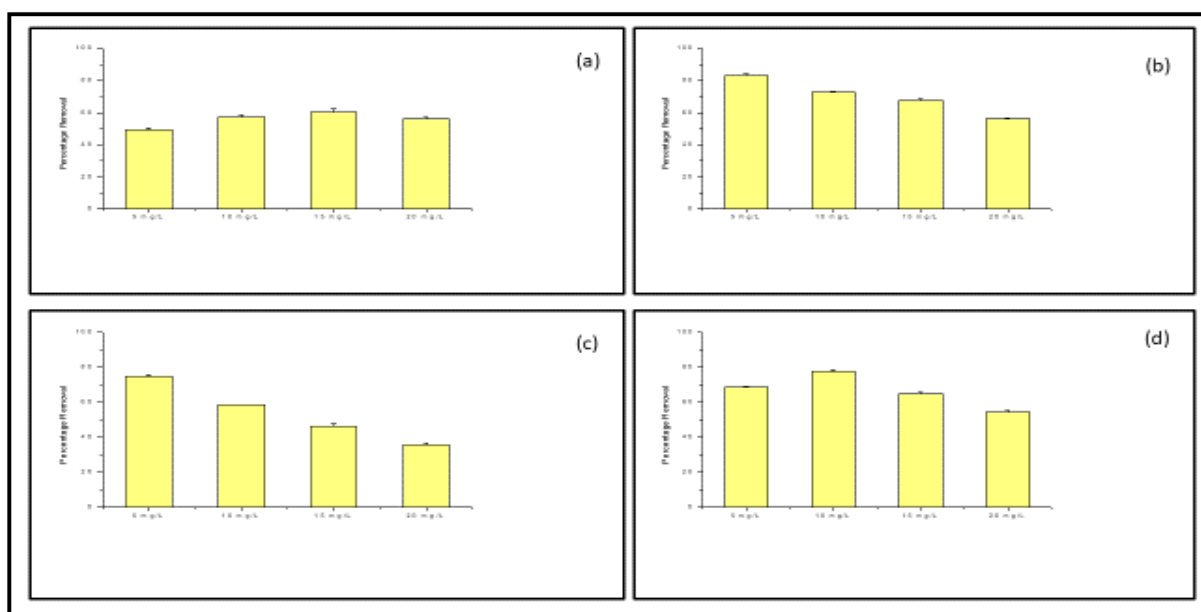
**Fig. 5.2:-** Effect of concentration on the removal of **(a)** CBZ **(b)** NPX **(c)** RTN **(d)** BPA by ARSB

### 5.4.2.2 Effect of dosage of adsorbent (ARSB) on the removal efficacy of ARSB

The effect of the dosage of the adsorbent on its removal efficacy was investigated over four different dosage of ARSB i.e., 0.5 g/L, 1 g/L, 1.5 g/L and 2 g/L. The concentration of EC's were kept constant at 10 mg/L. The pH of the solution was kept at neutral and the temperature was kept at 303 K. The result of the experiment is shown in (**Fig. 5.3 (a)-(d)).** From there it was observed that the removal of EC's by ARSB exhibited a similar trend, that is the percentage removal of the EC's increased with increase in dose of ARSB. This outcome could be attributed to the greater availability of active sites at higher dosage of ARSB which facilitates the higher uptake of EC's (Banerjee et al., 2016; Bhattacharya et al., 2020, 2021; Mukherjee et al., 2019). As a consequence of which the removal of the EC's increased with the increase in dosage of ARSB and in each case the highest removal was observed at 2 g/L dosage of ARSB. In case of the removal of CBZ by ARSB, as shown in **Fig. 5.3(a)**, the removal at the 0.5 g/L dose of ARSB was observed to be 39.56 %, the removal at 1 g/L dosage was found to be 43.66 %, at 1.5 g/L dosage was found to be 48.93 % and at the 2 g/L dosage was 57.84 % respectively. In case of the case of the removal of NPX by ARSB (**Fig. 5.3(b)**), it was observed that the removal at the 0.5 g/L dose of ARSB was 50.11 %, the removal at 1 g/L dosage was 66.9 %, at 1.5 g/L dosage was 68.27 % and at the 2 g/L dosage was 73.16 % respectively. In case of the removal of RTN by ARSB (**Fig. 5.3(c)**) it was observed that the removal at the 0.5 g/L dose of ARSB was 25.18 %, at 1 g/L dosage was 37.59 %, at 1.5 g/L dosage was 47.26 % and at the 2 g/L dosage was 58.3 % respectively. In case of the removal of BPA by ARSB (**Fig. 5.3(d)**) it was observed that the removal at the 0.5 g/L dose of ARSB

was 47 %, at 1 g/L was 62.5 %, at 1.5 g/L dosage was 69.82 % and at the 2 g/L dosage was 75.34 % respectively
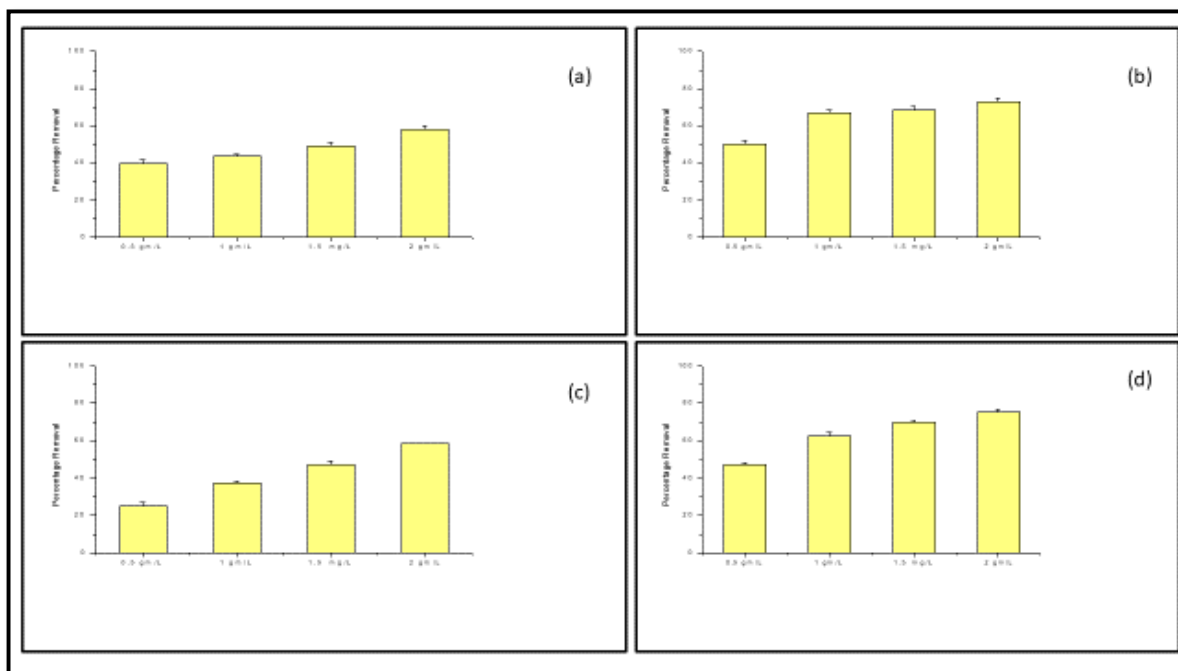


**Fig. 5.3:-** Effect of ARSB dosage on the removal of **(a)** CBZ **(b)** NPX **(c)** RTN **(d)** BPA by ARSB

### *5.4.2.3 Effect of pH of the experimental solution on the removal efficacy of ARSB*

The effect of pH on the removal of EC's by ARSB was investigated under five different pH of the experimental solution, viz., pH 2, pH 4, pH 6, pH 8 and pH 10. The concentration of EC's were kept constant at 10 mg/L and the dosage of ARSB was kept fixed at 2 g/L. The result of the experiment is given in (**Fig. 5.4(a)-(d)**). From **Fig. 5.4(a)** it was observed that the removal of CBZ by ARSB did not differ significantly with the variation of pH. On increasing the pH from pH 2- pH 6, the removal of CBZ by ARSB increased from 58.13 % to 60.19 % and with further increase in pH from pH 6-10 the removal percentage decreased to 57.02 %. The $pH_{pzc}$ of ARSB was found to be 4.5 (Bhattacharya et al., 2021), and the dissociation constant of CBZ is 13.9 (Bhattacharya et al., 2020). Thus, under the detected pH range the CBZ molecules were neutral in nature and on the other hand, at pH less than 4.5 the surface of ARSB was positively charged and it might have experienced some electrostatic force of repulsion from the experimental solution resulting in reduced adsorption of CBZ. When the pH was increased beyond 4.5, the surface of ARSB became positive whereas the experimental solution was neutral in nature, thereby resulting in highest adsorption of CBZ by ARSB. Then when the pH of the experimental solution increased beyond pH 7, and the solution become basic then the surface of ARSB experienced a force of repulsion from the experimental solution thereby leading to decreased adsorption of CBZ by

ARSB. However, as it can be observed from the result of the adsorption reaction, the effect of pH on the removal of CBZ by ARSB was not very significant. In other words, ARSB could adsorb CBZ equally effectively over a long range of pH.

From the removal of NPX by ARSB as shown in **Fig. 5.4(b)** it was observed that the removal of NPX by ARSB decreased with the increase in pH of the experimental solution. The highest removal was observed at pH 2 (80.02%) followed by pH 4 (77.97 %), pH 6 (72.86 %) and pH 8 (64.62 %). The lowest removal was observed for pH 10 (60.41 %). Similar results were observed in the works of (Mondal et al., 2020) and (Ciğeroğlu et al., 2020). The logic behind this phenomenon can be given as, NPX adsorption by ARSB particles is reportedly mediated via $\pi$-$\pi$ interactions, electrostatic interactions and hydrogen (H-H) bonding (Mondal et al., 2020). The $pH_{pzc}$ of ARSB is 4.5 (Bhattacharya et al., 2021) and the $pK_a$ value of NPX is 4.2 (Reynel-avila et al., 2015). Therefore at pH below 4.2 the molecules of NPX are neutrally charged whereas above pH 4.2 the molecules of NPX are negatively charged. Similarly, the surface of ARSB are positive below the $pH_{pzc}$ 4.5 and negative above it (Banerjee et al., 2016). Therefore at the lower pH range the adsorption of NPX by ARSB is enhanced due to van der Waal's interaction and hydrogen bonding (I˙lbay et al., 2015) whereas at the higher pH range, the adsorption of NPX by ARSB is reduced due to the repulsion between negative surface of ARSB and the anionic form of NPX (Mondal et al., 2020). Thus, the highest removal of NPX was observed at pH 2 and the removal of NPX by ARSB decreased with the increase in pH of the experimental solution (Bhattacharya et al., 2021).

The removal of RTN by ARSB also exhibited a similar trend as the adsorption of CBZ by ARSB. From the result of the experiment as shown in **Fig. 5.4(c)** it was observed that the removal of RTN by ARSB increased with the increase in pH of the experimental solution till pH 6. With further increase in pH, a decline in the removal of RTN was observed. The removal at pH 2 was 46.52 %, the removal at pH 4 was 52 %, the removal at pH 6 was 55.33 %, the removal at pH 8 was 53.3 % and the removal at pH 10 was 45.95 %. The logic behind this observation can be attributed to the fact that, RTN has two $pK_a$ values at pH 2.7 and pH 8.2 (Kortejarvi et al., 2005) and RTN remains in a protonated, cationic stage at pH below 2.7 and it remains in an anionic stage at pH greater than 8.2 (Al-rub et al., 2020). On the other hand, as mentioned before the $pH_{pzc}$ of ARSB is 4.5 (Bhattacharya et al., 2021) meaning the surface of ARSB will be positively charged at pH less than 4.5 and will be negatively charged at pH greater than 4.5. Therefore at the lower pH range, the removal of RTN will be affected due to the repulsion of the positives charges between the molecules of RTN and the surface of ARSB. Similarly, at the higher pH range the adsorption will be affected due to the accumulation of negative charges on the surface of ARSB and the anionic molecules of RTN (Al-rub et al., 2020). As a result removal of RTN by ARSB was observed to be highest at pH 6, where the charge of the RTN molecules were neutral and the surface of ARSB was negatively charged (Al-rub et al., 2020). The adsorption of RTN

molecules on the surface of ARSB might have been due to H-bonding and dipole-dipole interactions (Al-rub et al., 2020). Similar results were observed in the studies of (Bhattacharyya et al., 2018) and (Bhattacharyya et al., 2019) where RTN was removed from water by ARSB and an activated carbon synthesized from lemon peel respectively.

The removal of BPA by ARSB at different pH of the experimental solution is shown in (**Fig. 5.4 (d)**). From there it was observed that the removal of BPA by ARSB decreased with the increase in pH, with the highest removal being observed at pH 2 (82.63 %), followed by pH 4 (77.13 %), followed by pH 6 (76.27 %), followed by pH 8 (72.56 %) and lastly, for pH 10 (67.17 %). The reason behind this observation can be attributed to the fact that, the pKa of BPA is 8.96 (Phatthanakittiphong & Seo, 2016). At a pH around 8, the molecules of BPA dissociate to form monovalent bisphenolate anions. On the other hand, the $pH_{pzc}$ of ARSB is 4.5 (Bhattacharya et al., 2021). As a consequence of which at the higher pH range, both the surface of ARSB and the molecules of BPA acquire a negative charge, resulting in the creation of an electrostatic force of repulsion. As a consequence of which, the adsorption of BPA by ARSB is decreased at the higher pH range. Similar result have been observed in the work of (Chang et al., 2012) and (Xu et al., 2012).
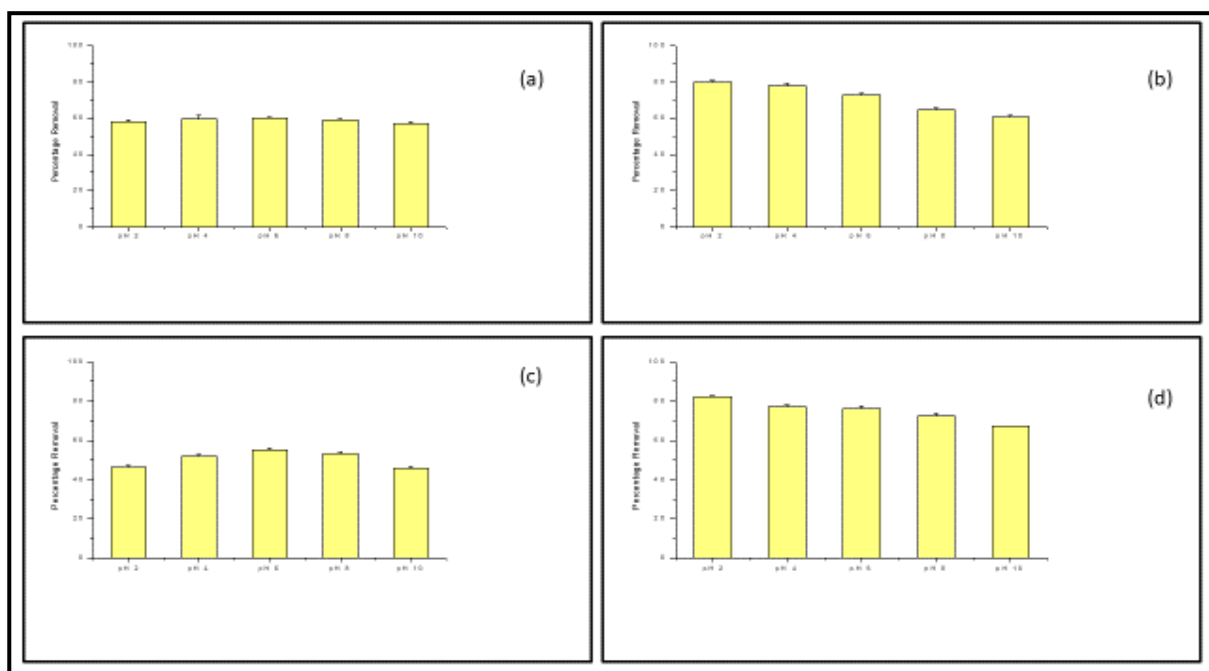


**Fig. 5.4:- E**ffect of pH on the removal of **(a)** CBZ **(b)** NPX **(c)** RTN **(d)** BPA by ARSB

.

### 5.4.2.4 Effect of temperature on the removal efficacy of ARSB

The effect of temperature on the removal of the EC's by ARSB was detected at four temperatures 298 K, 303 K, 308 K and 313 K. The dosage of ARSB was kept constant at 2 g/L and the concentration of

EC's were kept constant at 10 mg/L. The result of the experiment as showed in **Fig. 5.5(a)-(d),** and from there it was observed that the removal of CBZ by ARSB (**Fig. 5.5(a)**) increased with the increase in temperature. The highest removal was observed at 313 K (61.51 %) and the lowest removal was observed at 298 K (57.61 %). The increase in adsorption with increase in temperature could be attributed to the greater interaction between the CBZ molecules and the surface of ARSB and to the widening of the pores on the surface of the ARSB (Bhattacharya et al., 2020, 2021). The increase in adsorption of CBZ molecules by ARSB with increasing temperature denote the endothermic nature of the reaction.

From **Fig. 5.5(b)** it was observed that the removal of NPX by ARSB increased with the increase in temperature upto the optimum temperature point of 308 K. The removal of NPX by ARSB was 68.85 % at 298 K, 72.58 % at 303 K, 73.6 % at 308 K and 65.71 % at 313 K. The increase in adsorption of NPX by the surface of ARSB with the increase in temperature up-to 308 K could be attributed to the increased interactions between the ARSB particles and the NPX molecules and to the widening of the pores on the surface of ARSB thereby resulting in greater uptake of NPX molecules by ARSB (Banerjee et al., 2015b, 2016). However, when the temperature of the experimental solution was increased beyond 308 K to 313 K, the formation of bonds between the surface of ARSB and the NPX molecules is disfavoured resulting in decreased uptake of NPX molecules by the surface of ARSB (Banerjee et al., 2015b). As a consequence of which at this highest temperature, the adsorption of NPX by the surface of ARSB is reduced. Similar results have been reported in previous literatures (Banerjee et al., 2015b; Mukherjee et al., 2019).

From **Fig. 5.5(c),** it was observed that the removal of RTN by ARSB followed a similar trend to the removal of NPX by ARSB, i.e., it increased with increase in temperature from 298 K – 308 K (43.87 % - 62.14 %). This could be attributed to the widening of pore size and the increased interaction between the RTN molecules and the surface of ARSB with the increase in temperature (Banerjee et al., 2016; Bhattacharya et al., 2021). However when the temperature was increased to 313 K, a slight decrease in the removal percentage of RTN was observed (59.76 %). This could be attributed to the increased kinetic energy of the surface of ARSB and the RTN molecules with the increase in temperature resulting in the breakage of the adsorbate adsorbent bonds (Al-rub et al., 2020). Out of the four temperature tested, the highest removal was observed at 308 K (62.14 %), signifying it to be optimum temperature for the adsorption of RTN molecules by ARSB.

From **Fig. 5.5 (d)** the effect of temperature on the removal of BPA by ARSB was detected at four temperatures at 298 K, 303 K, 308 K and 313 K. The dosage of ARSB was kept constant at 2 g/L and the concentration of BPA was kept constant at 10 mg/L. From the result of the experiment as observed in **Fig. 5.5 (d),** it was observed that the removal of BPA by ARSB decreased with the increase in temperature, with the highest removal being observed at 298 K (77.18 %), followed by at 303 K (76.95 %), followed by at 308 K (74.76 %) and lastly at 313 K (71.24 %). The decreased removal of BPA by

ARSB with the subsequent increase in temperature denotes the exothermic nature of the adsorption reaction. Similar results have been observed in the work of (Phatthanakittiphong & Seo, 2016) and (Kwon & Lee, 2015).
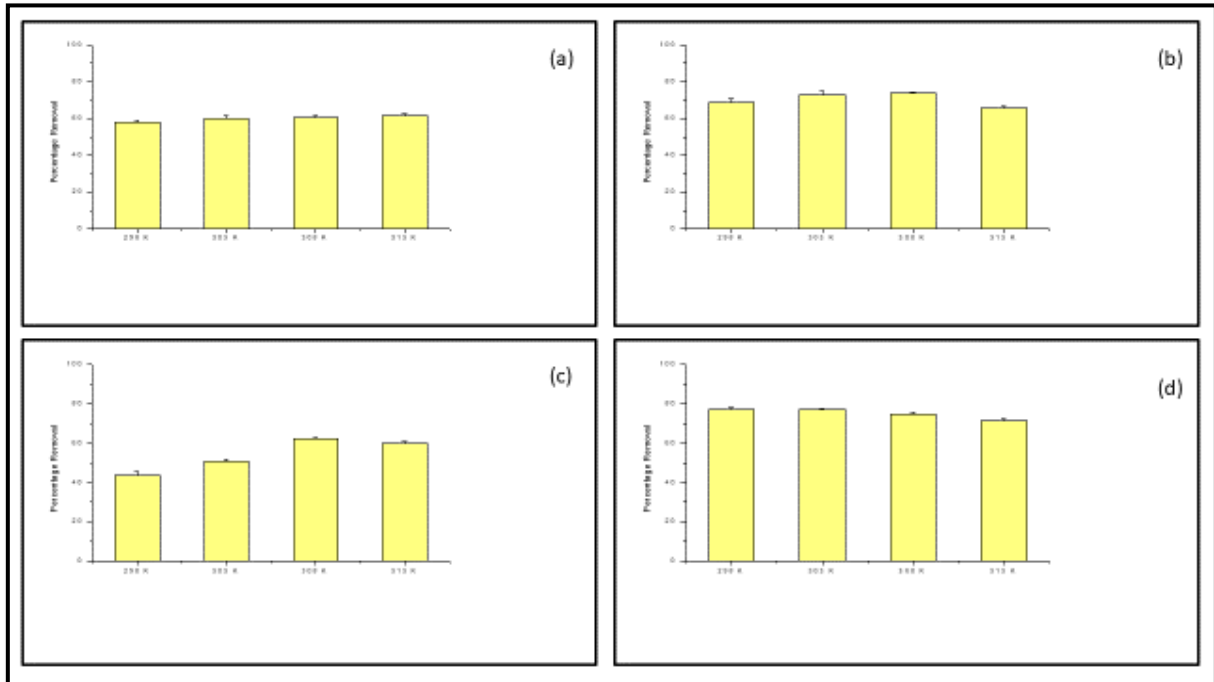


**Fig. 5.5:-** Effect of temperature on the removal of **(a)** CBZ **(b)** NPX **(c)** RTN **(d)** BPA by ARSB

### 5.4.3 Adsorption Isotherm

The dose variation data (0.5 g/L-2 g/L) from the batch study was used for calculating the adsorption isotherm. The result of the isotherm is given in the following tables.

#### 5.4.3.1 Adsorption isotherm for the adsorption of CBZ by ARSB

The result of the experiment is given in **Table 5.1** and from there it was observed that the adsorption of CBZ on the surface of ARSB was best described by the Tempkin isotherm model ($R^2$=0.99) denoting that the adsorption of CBZ on the surface of ARSB was uniform in nature and the heat of adsorption of the adsorption moieties decreased in a linear pattern as the reaction proceeded (Bhattacharya et al., 2020).

**Table 5.1**:- Investigating different isotherm parameters for CBZ adsorption by ARSB

| Models | Parameters | Description | Unit | Adsorbent Dosage (gm/L) | | | |
|---|---|---|---|---|---|---|---|
| | | | | 0.5 g/L | 1 g/L | 1.5 g/L | 2 g/L |
| Langmuir | $C_e$ | Equilibrium pharmaceutical concentration in solution | mg L$^1$ | 6.04 | 5.63 | 5.11 | 4.22 |
| | $q_e$ | Theoretical maximum adsorption capacity | mg g$^{-1}$ | 7.91 | 4.37 | 3.26 | 2.89 |
| | $Q_0$ | Maximum monolayer coverage capacity calculated from slope of $C_e/q_e$ vs. $C_e$ plot. | mg g$^{-1}$ | 1.29 | 0.94 | 0.32 | 0.37 |
| | $b$ | Langmuir coefficient of energy of adsorption calculated from intercept of $C_e/q_e$ vs. $C_e$ plot. | L mg$^{-1}$ | -0.19 | -0.22 | -0.19 | -0.24 |
| | R$^2$ | Correlation coefficient | | 0.98 | 0.96 | 0.82 | 0.92 |
| Freundlich | $n_f$ | Adsorption intensity calculated from slope of $ln\ q_e$ vs. $ln\ C_e$ plot | | 0.36 | 0.47 | -0.36 | -0.48 |
| | $K_f$ | Freundlich coefficient of adsorption capacity calculated from intercept of $ln\ q_e$ vs. $ln\ C_e$ plot | mg g$^{-1}$ | 1147.68 | 116.14 | 244 | 135.69 |
| | R$^2$ | Correlation coefficient | | 0.99 | 0.98 | 0.91 | 0.92 |
| Temkin | $B_T$ | Coefficients of heat of adsorption calculated from slope of $q_e$ vs. $ln\ C_e$ plot at operational temperature $T$ (303K ) | J mol$^{-1}$ | -14.375 | -6.67 | -4.57 | -3.12 |
| | $K_T$ | Temkin equilibrium binding constant calculated from intercept of $q_e$ vs. $ln\ C_e$ plot at operational temperature $T$ (303 K) | L g$^{-1}$ | 0.095 | 0.092 | 15.15 | 0.09 |
| | R$^2$ | Correlation coefficient | | 0.99 | 0.99 | 0.99 | 0.99 |
| Dubinin-Radushkevich | $B$ | Dubinin–Radushkevich constant calculated from slope of $ln\ q_e$ vs. $\varepsilon^2$ plot. | mole KJ$^{-2}$ | 0.00001 | 0.000009 | 0.00001 | 0.000006 |
| | $Q_s$ | Theoretical isotherm saturation capacity calculated from intercept of $ln\ q_e$ vs. $\varepsilon^2$ plot. | mg g$^{-1}$ | 0.1439 | 6.7 x 10$^{-8}$ | 0.801 | 0.58 |
| | $E$ | Mean sorption energy | kJ mole$^{-1}$ | 223.61 | 235.7 | 223.61 | 288.68 |
| | R$^2$ | Correlation coefficient | | 0.99 | 0.96 | 0.84 | 0.77 |
| | $\varepsilon$ | Polanyi Potential | | 385.7 | 411.57 | 450.47 | 536.14 |

### 5.4.3.2 Adsorption isotherm for the adsorption of NPX by ARSB

The dose variation data (0.5 g/L-2 g/L) from the batch study was used for calculating the adsorption isotherm. The result of the experiment is given in **Table 5.2** and from there it was observed that the adsorption of NPX on the surface of ARSB was best described by the Tempkin isotherm model ($R^2$=0.99) denoting that the adsorption of NPX on the surface of ARSB was uniform in nature and the heat of adsorption of the adsorbent moieties decreased in a linear fashion as the reaction increased (Bhattacharya et al., 2021).

**Table 5.2**:- Investigating different isotherm parameters for NPX adsorption by ARSB

| Models | Parameters | Description | Unit | Adsorbent Dosage (gm/L) | | | |
|---|---|---|---|---|---|---|---|
| | | | | 0.5 g/L | 1 g/L | 1.5 g/L | 2 g/L |
| Langmuir | $C_e$ | Equilibrium pharmaceutical concentration in solution | mg L$^1$ | 4.99 | 3.31 | 3.17 | 2.77 |
| | $q_e$ | Theoretical maximum adsorption capacity | mg g$^{-1}$ | 10.02 | 6.69 | 4.55 | 3.66 |
| | $Q_0$ | Maximum monolayer coverage capacity calculated from slope of $C_e/q_e$ vs. $C_e$ plot. | mg g$^{-1}$ | 2.4 | 2.16 | 1.69 | 1.36 |
| | $b$ | Langmuir coefficient of energy of adsorption calculated from intercept of $C_e/q_e$ vs. $C_e$ plot. | L mg$^{-1}$ | 0.25 | 0.4 | 0.46 | 0.54 |
| | R$^2$ | Correlation coefficient | | 0. 96 | 0.97 | 0.99 | 0.99 |
| Freundlich | $n_f$ | Adsorption intensity calculated from slope of $ln\ q_e$ vs. $ln\ C_e$ plot | | 0.57 | 0.97 | 1.11 | 1.22 |
| | $K_f$ | Freundlich coefficient of adsorption capacity calculated from intercept of $ln\ q_e$ vs. $ln\ C_e$ plot | mg g$^{-1}$ | 179.02 | 24.42 | 13.41 | 8.4 |
| | R$^2$ | Correlation coefficient | | 0.97 | 0.97 | 0.98 | 0.98 |
| Temkin | $B_T$ | Coefficients of heat of adsorption calculated from slope of $q_e$ vs. $ln\ C_e$ plot at operational temperature $T$ (303K ) | J mol$^{-1}$ | 12.036 | 4.9 | 3.0729 | 2.1367 |
| | $K_T$ | Temkin equilibrium binding constant calculated from intercept of $q_e$ vs. $ln\ C_e$ plot at operational temperature $T$ (303 K) | L g$^{-1}$ | 11.56 | 13.43 | 14.35 | 0.07 |
| | R$^2$ | Correlation coefficient | | 0.99 | 0.99 | 0.99 | 0.99 |
| Dubinin-Radushkevich | $B$ | Dubinin–Radushkevich constant calculated from slope of $ln\ q_e$ vs. $\varepsilon^2$ plot. | mole$^2$ KJ$^{-2}$ | 0.000006 | 0.000002 | 0.000002 | 0.000001 |
| | $Q_s$ | Theoretical isotherm saturation capacity calculated from intercept of $ln\ q_e$ vs. $\varepsilon^2$ plot. | mg g$^{-1}$ | 2.83 | 2.79 | 0.43 | 0.16 |
| | $E$ | Mean sorption energy | kJ mole$^{-1}$ | 912.87 | 1581.14 | 1581.14 | 707.11 |
| | R$^2$ | Correlation coefficient | | 0.92 | 0.88 | 0.92 | 0.91 |
| | $\varepsilon$ | Polanyi Potential | | 460.22 | 664.94 | 690.12 | 797.77 |

### 5.4.3.3 Adsorption Isotherm for the adsorption of RTN by ARSB

The dose variation data (0.5 g/L-2 g/L) from the batch study was used for calculating the adsorption isotherm. The result of the experiment is given in **Table 5.3** and from there it was observed that the adsorption of RTN on the surface of ARSB was best described by the Tempkin isotherm model ($R^2$=0.99) signifying that the adsorption of RTN on the surface of ARSB was uniform in nature and the heat of the adsorption of the adsorbent moieties decreased linearly as the reaction increased (Bhattacharya et al., 2020).

**Table 5.3**:- Investigating different isotherm parameters for RTN adsorption by ARSB

| Models | Parameters | Description | Unit | Adsorbent Dosage (gm/L) | | | |
|---|---|---|---|---|---|---|---|
| | | | | 0.5 g/L | 1 g/L | 1.5 g/L | 2 g/L |
| Langmuir | $C_e$ | Equilibrium pharmaceutical concentration in solution | mg $L^1$ | 7.48 | 6.24 | 5.27 | 4.17 |
| | $q_e$ | Theoretical maximum adsorption capacity | mg $g^{-1}$ | 5.04 | 3.76 | 3.15 | 2.92 |
| | $Q_0$ | Maximum monolayer coverage capacity calculated from slope of $C_e/q_e$ vs. $C_e$ plot. | mg $g^{-1}$ | 0.57 | 0.98 | 0.97 | 1.15 |
| | $b$ | Langmuir coefficient of energy of adsorption calculated from intercept of $C_e/q_e$ vs. $C_e$ plot. | L $mg^{-1}$ | -0.15 | -0.21 | -0.27 | -0.38 |
| | $R^2$ | Correlation coefficient | | 0.95 | 0.98 | 0.98 | 0.99 |
| Freundlich | $n_f$ | Adsorption intensity calculated from slope of $ln\ q_e$ vs. $ln\ C_e$ plot | | -0.21 | -0.46 | -0.63 | -0.96 |
| | $K_f$ | Freundlich coefficient of adsorption capacity calculated from intercept of $ln\ q_e$ vs. $ln\ C_e$ plot | mg $g^{-1}$ | 61882.49 | 197.87 | 43.92 | 13.19 |
| | $R^2$ | Correlation coefficient | | 0.98 | 0.99 | 0.99 | 0.99 |
| Temkin | $B_T$ | Coefficients of heat of adsorption calculated from slope of $q_e$ vs. $ln\ C_e$ plot at operational temperature $T$ (303K ) | J $mol^{-1}$ | -16.285 | -6.8 | -4.04 | -2.53 |
| | $K_T$ | Temkin equilibrium binding constant calculated from intercept of $q_e$ vs. $ln\ C_e$ plot at operational temperature $T$ (303 K) | L $g^{-1}$ | 0.098 | 0.09 | 0.087 | 0.075 |
| | $R^2$ | Correlation coefficient | | 0.99 | 0.99 | 0.99 | 0.99 |
| Dubinin-Radushkevich | $B$ | Dubinin–Radushkevich constant calculated from slope of $ln\ q_e$ vs. $\varepsilon^2$ plot. | mole $KJ^{-2}$ | 0.00003 | 0.00001 | 0.000006 | 0.000003 |
| | $Q_s$ | Theoretical isotherm saturation capacity calculated from intercept of $ln\ q_e$ vs. $\varepsilon^2$ plot. | mg $g^{-1}$ | 0.31 | 0.99 | 0.0002 | 0.044 |
| | $E$ | Mean sorption energy | kJ $mole^{-1}$ | 129.11 | 707.11 | 288.68 | 408.25 |
| | $R^2$ | Correlation coefficient | | 0.96 | 0.98 | 0.97 | 0.96 |
| | $\varepsilon$ | Polanyi Potential | | 316.01 | 374.89 | 437.4 | 541.55 |

### 5.4.3.4 Adsorption Isotherm for the adsorption of BPA by ARSB

The dose variation data (0.5 g/L-2 g/L) from the batch study was used for calculating the adsorption isotherm. The result of the experiment is given in **Table 5.4** and from there it was observed that the adsorption of BPA on the surface of ARSB was best described by the Temkin isotherm model ($R^2$=0.99) denoting that the adsorption of BPA on the surface of ARSB was uniform in nature and the heat of adsorption of the adsorbent moieties decreased in a linear fashion as the reaction proceeded (Bhattacharya et al., 2020).

**Table 5.4**:- Investigating different isotherm parameters for BPA adsorption by ARSB

| Models | Parameters | Description | Unit | Adsorbent Dosage (gm/L) | | | |
|---|---|---|---|---|---|---|---|
| | | | | 0.5 g/L | 1 g/L | 1.5 g/L | 2 g/L |
| Langmuir | $C_e$ | Equilibrium pharmaceutical concentration in solution | mg L$^1$ | 5.3 | 3.75 | 3.02 | 2.46 |
| | $q_e$ | Theoretical maximum adsorption capacity | mg g$^{-1}$ | 9.4 | 6.25 | 4.65 | 3.77 |
| | $Q_0$ | Maximum monolayer coverage capacity calculated from slope of $C_e/q_e$ vs. $C_e$ plot. | mg g$^{-1}$ | 1.31 | 0.96 | 0.96 | 1.26 |
| | $b$ | Langmuir coefficient of energy of adsorption calculated from intercept of $C_e/q_e$ vs. $C_e$ plot. | L mg$^{-1}$ | -0.204 | -0.267 | -0.334 | -0.49 |
| | R$^2$ | Correlation coefficient | | 0.86 | 0.86 | 0.88 | 0.93 |
| Freundlich | $n_f$ | Adsorption intensity calculated from slope of $ln\ q_e$ vs. $ln\ C_e$ plot | | -0.408 | -0.588 | -0.81 | -1.26 |
| | $K_f$ | Freundlich coefficient of adsorption capacity calculated from intercept of $ln\ q_e$ vs. $ln\ C_e$ plot | mg g$^{-1}$ | 606.43 | 45.8 | 15.74 | 16.52 |
| | R$^2$ | Correlation coefficient | | 0.94 | 0.92 | 0.90 | 0.93 |
| Temkin | $B_T$ | Coefficients of heat of adsorption calculated from slope of $q_e$ vs. $ln\ C_e$ plot at operational temperature $T$ (303K) | J mol$^{-1}$ | -13.558 | -5.8223 | -3.392 | -2.0836 |
| | $K_T$ | Temkin equilibrium binding constant calculated from intercept of $q_e$ vs. $ln\ C_e$ plot at operational temperature $T$ (303 K) | L g$^{-1}$ | 0.093 | 0.088 | 15.14 | 0.063 |
| | R$^2$ | Correlation coefficient | | 0.99 | 0.98 | 0.98 | 0.98 |
| Dubinin-Radushkevich | $B$ | Dubinin–Radushkevich constant calculated from slope of $ln\ q_e$ vs. $\varepsilon^2$ plot. | mole$^2$ KJ$^{-2}$ | 0.00001 | 0.000005 | 0.000006 | 0.000001 |
| | $Q_s$ | Theoretical isotherm saturation capacity calculated from intercept of $ln\ q_e$ vs. $\varepsilon^2$ plot. | mg g$^{-1}$ | 1.57 | 0.065 | 0.11 | 1.77 |
| | $E$ | Mean sorption energy | kJ mole$^{-1}$ | 223.61 | 316.23 | 500 | 707.11 |
| | R$^2$ | Correlation coefficient | | 0.87 | 0.79 | 0.73 | 0.78 |
| | $\varepsilon$ | Polanyi Potential | | 435.46 | 595.56 | 721.05 | 858.09 |

### 5.4.4  Adsorption Kinetics

The adsorption kinetics were calculated with the temperature study data (298 K-303 K) and the results of the study is shown as follows.

#### *5.4.4.1 Adsorption Kinetics for the adsorption of CBZ on the surface of ARSB*

The temperature variation data (298 K – 313 K) from the batch study was used for calculating the adsorption kinetics. The result of the experiment is given in **Table 5.5** and from there it was observed that the adsorption of CBZ on the surface of ARSB was best described by the pseudo second order kinetic model ($R^2$ = 0.98) (Banerjee et al., 2016).

**Table 5.5**:- Investigating different kinetics parameters for adsorption of CBZ on ARSB

| Models | Parameters | Description | Units | Temperatures (° K) | | | |
|---|---|---|---|---|---|---|---|
| | | | | 298 K | 303 K | 308 K | 313 K |
| Pseudo first order | $k_1$ | Pseudo-1st order rate constant obtained from linear plots of $log\ (q_e - q_t)$ vs. $t$. | $min^{-1}$ | 0.06 | 0.04 | 0.09 | 0.04 |
| | $q_e$ (cal) | Quantity of adsorbate adsorbed at equilibrium | $mg\ g^{-1}$ | 4.77 | 2.27 | 13.78 | 2.37 |
| | $R^2$ | Correlation coefficient | | 0.98 | 0.94 | 0.95 | 0.85 |
| Pseudo second order | $k_2$ | Pseudo-2nd order rate constant determined from plot of $t/q_t$ vs. $t$. | $mg\ g^{-1}\ min^{-1}$ | 0.019 | 0.014 | 0.019 | 0.025 |
| | $q_e$ | Quantity of adsorbate adsorbed at equilibrium | $mg\ g^{-1}$ | 3.35 | 3.92 | 3.48 | 3.4 |
| | $R^2$ | Correlation coefficient | | 0.99 | 0.97 | 0.99 | 0.99 |
| Intraparticle diffusion | $K_{diff}$ | Intra-particle diffusion rate constant calculated from the slope of regression plot of $q_t$ vs. $t^{1/2}$ where $t$ is time (min). | $mg\ g^{-1}\ min^{-1/2}$ | 0.191 | 0.2325 | 0.1994 | 0.2287 |
| | C | Constant calculated from the intercept of regression plot of $q_t$ vs. $t^{1/2}$ where $t$ is time (min). | $mg\ g^{-1}$ | 1.054 | 1.1506 | 1.1389 | 0.7244 |
| | $R^2$ | Correlation coefficient | | 0.78 | 0.61 | 0.68 | 0.72 |
| Elovich Istherm | α | Initial adsorption rate calculated from the intercept of liner plot of $q_t$ vs. $ln\ t$ | $mg\ g^{-1}\ min$ | 0.046 | 0.27 | 0.06 | 0.005 |
| | β | Initial desorption rate calculated from the slope$^{-1}$ of liner plot of $q_t$ vs. $ln\ t$. | $mg\ g^{-1}$ | 1.43 | 1.13 | 1.34 | 1.52 |
| | $R^2$ | Correlation coefficient | | 0.89 | 0.75 | 0.81 | 0.74 |
| Liquid film diffusion model | R | Liquid film diffusion constant | | -0.0631 | -0.047 | -0.0975 | -0.0321 |
| | $R^2$ | Correlation coefficient | | 0.98 | 0.94 | 0.95 | 0.87 |

### 5.4.4.2 Adsorption Kinetics for the adsorption of NPX on the surface of ARSB

The temperature variation data (298 K – 313 K) from the batch study was used for calculating the adsorption kinetics. The result of the experiment is given in **Table 5.6** and from there it was observed that the adsorption of NPX on the surface of ARSB was best described by the Pseudo-second order kinetic model ($R^2$ = 0.985) (Bhattacharya et al., 2021).

**Table 5.6**: Investigating different kinetics parameters for adsorption of NPX on ARSB

| Models | Parameters | Description | Units | Temperatures (° K) | | | |
|---|---|---|---|---|---|---|---|
| | | | | 298 K | 303 K | 308 K | 313 K |
| Pseudo first order | $k_1$ | Pseudo-1st order rate constant obtained from linear plots of $log\,(q_e - q_t)$ vs. $t$. | $min^{-1}$ | 0.051 | 0.05 | 0.05 | 0.05 |
| | $q_e$ (cal) | Quantity of adsorbate adsorbed at equilibrium | $mg\,g^{-1}$ | 4.48 | 4.18 | 2.95 | 7.69 |
| | $R^2$ | Correlation coefficient | | 0.93 | 0.97 | 0.93 | 0.75 |
| Pseudo second order | $k_2$ | Pseudo-2nd order rate constant determined from plot of $t/q_t$ vs. $t$. | $mg\,g^{-1}\,min^{-1}$ | 0.015 | 0.015 | 0.03 | 0.006 |
| | $q_e$ | Quantity of adsorbate adsorbed at equilibrium | $mg\,g^{-1}$ | 3.99 | 4.19 | 3.99 | 4.24 |
| | $R^2$ | Correlation coefficient | | 0.99 | 0.99 | 0.99 | 0.97 |
| Intraparticle diffusion | $K_{diff}$ | Intra-particle diffusion rate constant calculated from the slope of regression plot of $q_t$ vs. $t^{1/2}$ where $t$ is time (min). | $mg\,g^{-1}\,min^{-1/2}$ | 0.2255 | 0.2326 | 0.1743 | 0.2425 |
| | C | Constant calculated from the intercept of regression plot of $q_t$ vs. $t^{1/2}$ where $t$ is time (min). | $mg\,g^{-1}$ | 1.2205 | 1.3685 | 2.0389 | 0.1116 |
| | $R^2$ | Correlation coefficient | | 0.99 | 0.85 | 0.68 | 0.93 |
| Elovich Istherm | α | Initial adsorption rate calculated from the intercept of liner plot of $q_t$ vs. $ln\,t$ | $mg\,g^{-1}\,min$ | 0.03 | 0.008 | 1.1 | 3.06 |
| | β | Initial desorption rate calculated from the slope$^{-1}$ of liner plot of $q_t$ vs. $ln\,t$. | $mg\,g^{-1}$ | 1.24 | 1.2 | 1.53 | 1.04 |
| | $R^2$ | Correlation coefficient | | 0.9 | 0.92 | 0.82 | 0.97 |
| Liquid film diffusion model | R | Liquid film diffusion constant | | 0.0509 | 0.05 | 0.0532 | 0.0088 |
| | $R^2$ | Correlation coefficient | | 0.93 | 0.97 | 0.93 | 0.95 |

## 5.4.4.3 Adsorption Kinetics for the adsorption of RTN on the surface of ARSB

The temperature variation data (298 K – 313 K) from the batch study was used for calculating the adsorption kinetics. The result of the experiment is given in **Table 5.7** and from there it was observed that the adsorption of RTN molecules on the surface of ARSB was best described by the pseudo – second order kinetic model which exhibited the highest $R^2 = 0.99$ value (Banerjee et al., 2016; Bhattacharya et al., 2021).

**Table 5.7**: Investigating different kinetics parameters for adsorption of RTN on ARSB

| Models | Parameters | Description | Units | Temperatures (° K) | | | |
|---|---|---|---|---|---|---|---|
| | | | | 298 K | 303 K | 308 K | 313 K |
| Pseudo first order | $k_1$ | Pseudo-1st order rate constant obtained from linear plots of $log\,(q_e - q_t)$ vs. $t$. | $min^{-1}$ | 0.052 | 0.024 | 0.03 | 0.059 |
| | $q_e$ (cal) | Quantity of adsorbate adsorbed at equilibrium | $mg\,g^{-1}$ | 4.27 | 1.02 | 2.32 | 7.15 |
| | $R^2$ | Correlation coefficient | | 0.92 | 0.86 | 0.94 | 0.88 |
| Pseudo second order | $k_2$ | Pseudo-2nd order rate constant determined from plot of $t/q_t$ vs. $t$. | $mg\,g^{-1}\,min^{-1}$ | 0.008 | 0.04 | 0.017 | 0.014 |
| | $q_e$ | Quantity of adsorbate adsorbed at equilibrium | $mg\,g^{-1}$ | 3.05 | 2.72 | 3.51 | 3.5 |
| | $R^2$ | Correlation coefficient | | 0.97 | 0.99 | 0.99 | 0.99 |
| Intraparticle diffusion | $K_{diff}$ | Intra-particle diffusion rate constant calculated from the slope of regression plot of $q_t$ vs. $t^{1/2}$ where $t$ is time (min). | $mg\,g^{-1}\,min^{-1/2}$ | 0.1501 | 0.0923 | 0.1742 | 0.1927 |
| | C | Constant calculated from the intercept of regression plot of $q_t$ vs. $t^{1/2}$ where $t$ is time (min). | $mg\,g^{-1}$ | 0.6472 | 1.548 | 1.2617 | 0.7575 |
| | $R^2$ | Correlation coefficient | | 0.91 | 0.89 | 0.98 | 0.96 |
| Elovich Istherm | α | Initial adsorption rate calculated from the intercept of liner plot of $q_t$ vs. $ln\,t$ | $mg\,g^{-1}\,min$ | 2.7 | 8.2 | 0.058 | 0.055 |
| | β | Initial desorption rate calculated from the slope$^{-1}$ of liner plot of $q_t$ vs. $ln\,t$. | $mg\,g^{-1}$ | 1.36 | 3.24 | 1.69 | 1.45 |
| | $R^2$ | Correlation coefficient | | 0.96 | 0.84 | 0.96 | 0.99 |
| Liquid film diffusion model | R | Liquid film diffusion constant | | -0.0518 | -0.0243 | -0.0544 | -0.0593 |
| | $R^2$ | Correlation coefficient | | 0.92 | 0.86 | 0.88 | 0.88 |

### 5.4.4.4 Adsorption Kinetics for the adsorption of BPA on the surface of ARSB

The temperature variation data (298 K – 313 K) from the batch study was used for calculating the adsorption kinetics. The result of the experiment is given in **Table 5.8** and from there it was observed that the highest $R^2$ value was exhibited by the pseudo second order kinetic model. Thus, it can be stated that the adsorption of BPA on the surface of ARSB was best described by the Pseudo second order kinetic model ($R^2 = 0.96$) (Banerjee et al., 2016; Bhattacharya et al., 2021).

**Table 5.8**: Investigating different kinetics parameters for adsorption of BPA on ARSB

| Models | Parameters | Description | Units | Temperatures (° K) | | | |
|---|---|---|---|---|---|---|---|
| | | | | 298 K | 303 K | 308 K | 313 K |
| Pseudo first order | $k_1$ | Pseudo-1$^{st}$order rate constant obtained from linear plots of $log\ (q_e - q_t)$ vs. $t$. | min$^{-1}$ | 0.07 | 0.036 | 0.06 | 0.051 |
| | $q_e$ (cal) | Quantity of adsorbate adsorbed at equilibrium | mg g$^{-1}$ | 17.24 | 5.66 | 15.89 | 10.17 |
| | $R^2$ | Correlation coefficient | | 0.87 | 0.97 | 0.79 | 0.87 |
| Pseudo second order | $k_2$ | Pseudo-2$^{nd}$order rate constant determined from plot of $t/q_t$ vs. $t$. | mg g$^{-1}$ min$^{-1}$ | 0.005 | 0.004 | 0.0038 | 0.0032 |
| | $q_e$ | Quantity of adsorbate adsorbed at equilibrium | mg g$^{-1}$ | 5.07 | 5.29 | 5.25 | 5.29 |
| | $R^2$ | Correlation coefficient | | 0.98 | 0.98 | 0.98 | 0.91 |
| Intraparticle diffusion | $K_{diff}$ | Intra-particle diffusion rate constant calculated from the slope of regression plot of $q_t$vs. $t^{1/2}$ where $t$ is time (min). | mg g$^{-1}$ min$^{-1/2}$ | 0.3309 | 0.3518 | 0.3474 | 0.3063 |
| | C | Constant calculated from the intercept of regression plot of $q_t$vs. $t^{1/2}$ where $t$ is time (min). | mg g$^{-1}$ | 0.4453 | 0.1852 | 0.0317 | 0.1966 |
| | $R^2$ | Correlation coefficient | | 0.96 | 0.97 | 0.99 | 0.92 |
| Elovich Istherm | α | Initial adsorption rate calculated from the intercept of liner plot of $q_t$ vs. $ln\ t$ | mg g$^{-1}$ min | 2.52 | 4.22 | 0.00002 | 2.1 |
| | β | Initial desorption rate calculated from the slope$^{-1}$ of liner plot of $q_t$ vs. $ln\ t$. | mg g$^{-1}$ | 0.88 | 0.83 | 1.131 | 0.85 |
| | $R^2$ | Correlation coefficient | | 0.95 | 0.97 | 0.95 | 0.92 |
| Liquid film diffusion model | R | Liquid film diffusion constant | | 0.0697 | 0.0612 | 0.0618 | 0.0512 |
| | $R^2$ | Correlation coefficient | | 0.87 | 0.85 | 0.79 | 0.87 |

## 5.4.5 Activation Energy and Adsorption Thermodynamics

The activation energy for the adsorption of the EC's on the surface of ARSB was calculated by Arrhenius equation and the result of the thermodynamics was calculated by the van't Hoff equation. The result of the experiment is given as follows.

### 5.4.5.1 Activation Energy and Adsorption Thermodynamics for the adsorption of CBZ by ARSB

The result of the study is given in **Table 5.9**. The rate of the pseudo-second order kinetic model reaction was used as the rate constant. From there it was observed that the activation energy was 11.65 kJ/mole. As the activation energy value was less than 40 kJ/mole then it was observed that the adsorption of CBZ on the surface of ARSB was physical in nature (Banerjee et al., 2016; Bhattacharya et al., 2020).

From the thermodynamic study, it was observed that the Gibbs value was positive across the temperature range and decreased with increase in temperature (921.47 kJ/mole – 583.52 kJ/mole) thereby signifying that the adsorption of CBZ on the surface of ARSB was non-spontaneous in nature and required the help of external energy (Ali et al., 2016; Hossain et al., 2012; Prado et al., 2004). The positive value of $\Delta H°$ signified that the adsorption of CBZ on the surface of ARSB was endothermic in nature and the reaction went ahead by consuming energy from the concerned system (Banerjee et al., 2016; P. Das et al., 2015). The positive $\Delta S°$ meant that the ARSB and CBZ both underwent active site interaction during the adsorption process (Balasubramani et al., 2020; Bhattacharya et al., 2021).

**Table 5.9**. Analysis of thermodynamic parameters and Activation energy for CBZ adsorption by ARSB

| Temperature (K) | $\Delta G$ (kJ/mole) | $\Delta H$ (kJ/mole) | $\Delta S$ (joule/mole/kelvin) | $E_a$ ( kJ/mole) |
|---|---|---|---|---|
| 298 K | 921.47 | 7.3 | 21.48 | 11.65 |
| 303 K | 751.15 | | | |
| 308 K | 694.01 | | | |
| 313 K | 583.52 | | | |

### 5.4.5.2 Activation Energy and Adsorption Thermodynamics for the adsorption of NPX by ARSB

The result of the experiment is given in **Table 5.10**. The rate of the pseudo-second order kinetic model reaction was used as the rate constant. From there it was observed that the activation energy was 54.67 kJ/mole. As the activation energy value was more than 40 kJ/mole then it was observed that the adsorption of NPX on the surface of ARSB was chemisorption in nature (Banerjee et al., 2016; Bhattacharya et al., 2020).

From the thermodynamic study, it was observed that the Gibbs value was negative across the temperature range (-6818.88 kJ/mole – -6937.52 kJ/mole) thereby signifying that the adsorption of NPX on the surface of ARSB was spontaneous in nature. The positive value of $\Delta H°$ signified that the

adsorption of NPX on the surface of ARSB was endothermic in nature and the reaction went ahead by consuming energy from the concerned system (Banerjee et al., 2015b, 2016). The positive $\Delta S°$ meant that the ARSB and NPX both underwent active site interaction during the adsorption process (Balasubramani et al., 2020; Bhattacharya et al., 2021).

**Table 5.10**. Analysis of thermodynamic parameters and Activation energy for NPX adsorption by ARSB

| Temperature (K) | $\Delta G$ (kJ/mole) | $\Delta H$ (kJ/mole) | $\Delta S$(joule/mole/kelvin) | $E_a$ ( kJ/mole) |
|---|---|---|---|---|
| 298 K | -6818.88 | 14.07 | 70.21 | 54.67 |
| 303 K | -7288.59 | | | |
| 308 K | -7518.36 | | | |
| 313 K | -6937.52 | | | |

### 5.4.5.3 Activation Energy and Adsorption Thermodynamics for the adsorption of RTN by ARSB

The result of the experiment is given in **Table 5.11**. The rate of the pseudo-second order kinetic model reaction was used as the rate constant. From there it was observed that the activation energy was 13.79 kJ/mole. As the activation energy value was less than 40 kJ/mole then it can be stated that the adsorption of RTN on the surface of ARSB was physical in nature (Al-rub et al., 2020; Banerjee et al., 2016; Bhattacharya et al., 2020).

From the thermodynamic study, it was observed that the Gibbs value was positive across the temperature range (2327.99 kJ/mole –774.42 kJ/mole for 298 K to 313 K) thereby signifying that the adsorption of RTN on the surface of ARSB was non-spontaneous in nature and required external energy (Ali et al., 2016; Hossain et al., 2012; Prado et al., 2004). The positive value of $\Delta H°$ signified that the adsorption of RTN on the surface of ARSB was endothermic in nature and the reaction went ahead by consuming energy from the concerned system (Banerjee et al., 2015b, 2016). The positive $\Delta S°$ meant that the ARSB and RTN both underwent active site interaction during the adsorption process (Balasubramani et al., 2020; Bhattacharya et al., 2021).

**Table 5.11**. Analysis of thermodynamic parameters and activation energy for RTN adsorption by ARSB.

| Temperature (K) | $\Delta G$ (kJ/mole) | $\Delta H$ (kJ/mole) | $\Delta S$ (joule/mole/kelvin) | $E_a$ ( kJ/mole) |
|---|---|---|---|---|
| 298 K | 2327.99 | 37.17 | 117.38 | 13.79 |
| 303 K | 1653.16 | | | |
| 308 K | 505.82 | | | |
| 313 K | 774.42 | | | |

### 5.4.5.4 Activation Energy and Adsorption Thermodynamics for the adsorption of BPA by ARSB

The result of the experiment is given in **Table 5.12**. The rate of the pseudo-second order kinetic model reaction was used as the rate constant. From there it was observed that the activation energy was 3.26 kJ/mole. As the activation energy value was less than 40 kJ/mole then it can be stated that the adsorption of BPA on the surface of ARSB was physical in nature (Kwon & Lee, 2015; Phatthanakittiphong & Seo, 2016; J. Xu et al., 2012).

From the thermodynamic study, it was observed that the Gibbs value was negative across the temperature range (-1301.66 kJ/mole – - 557.12 kJ/mole for 298 K to 313 K) thereby signifying that the adsorption of BPA on the surface of ARSB was spontaneous in nature under the given temperature range (Das et al., 2022). The negative value of $\Delta H°$ signified that the adsorption of BPA on the surface of ARSB was exothermic in nature (Kwon & Lee, 2015; Phatthanakittiphong & Seo, 2016; J. Xu et al., 2012). The negative $\Delta S°$ value meant that when the equilibrium was reached for the adsorption of BPA by ARSB, the randomness on the surface of ARSB decreased (Kwon & Lee, 2015; Phatthanakittiphong & Seo, 2016; J. Xu et al., 2012).

**Table 5.12**. Analysis of thermodynamic parameters and Activation energy for BPA adsorption by ARSB

| Temperature (K) | $\Delta G$ (kJ/mole) | $\Delta H$ (kJ/mole) | $\Delta S$ (joule/mole/kelvin) | $E_a$ ( kJ/mole) |
|---|---|---|---|---|
| 298 K | -1301.66 | -16.25 | -49.8 | 3.26 |
| 303 K | -1291.05 | | | |
| 308 K | -1006.09 | | | |
| 313 K | -557.12 | | | |

### 5.4.6 Process Optimization by RSM

*5.4.6.1 Optimization of the adsorption of CBZ by ARSB by RSM*

The RSM was performed with the aim of understanding the effect of inter parameter interaction on the experimental outcome. In **Table 5.13**, the outcome of the 20 experiments as proposed by the software for the CCD model of the RSM is given and in **Table 5.14** the result of the ANOVA of the RSM model is provided. From there it is observed that the $R^2$ value of the model was 0.98 and the adjusted $R^2$ value was 0.96 which propounded the fact that the polynomial model suggested by RSM much greater than unity) and the low value of P ($< 0.0001$) meant that the optimizing model was highly significant, with the experimental data points exhibiting a high degree of correlation with the predicted data points (Bhattacharya et al., 2021). **Fig. 5.6** shows the relation between the experimentally determined data points and the predicted data points and there also it can be noted that the experimental data points exhibits a high degree of correlation with the predicted data points. The real equation which was used to predict the effect of the input variables on the response output is presented as follows.

$Removal = -16.98564 + 3.19777 \times pH + 43.67209 \times Dose + 0.27140 \times Time - 0.27521 \times pH \times Dose - 0.018557 \times pH \times Time - 8.22829 \times 10^{-3} \times Dose \times Time - 0.067324 \times pH^2 - 7.40953 \times Dose^2 - 8.42521 \times 10^{-4} \times Time^2$ …………………………...........................(xxxv)

As per the RSM model the optimized conditions under which maximum removal of CBZ (66.64) was possible were: adsorbent dosage of 3 g/L, pH value of 4 and reaction time of 150 minutes. For this RSM model, the interaction between the experimental parameters (input variables) and their outcome on the percentage removal of CBZ (response variable) is illustrated by the contour plots shown in **Fig. 5.7-5.9**.

➢ **Effect of ARSB dosage and solution pH on CBZ removal by ARSB**

The interaction in between the pH of the experimental solution and the dosage of ARSB and its effect on the removal of EC's is conveyed in the contour plot of **Fig. 5.7**. From there it was observed that the removal of CBZ by ARSB increased with the increase in dosage of ARSB. The higher removal of CBZ at the higher dose of ARSB was due to the availability of greater surface area for the purpose of adsorption and the consequently the highest removal value was observed around the highest dosage of 3 g/L (Banerjee et al., 2016; Bhattacharya et al., 2021). In case of the variation of pH of the experimental solution, it was observed that the highest removal of CBZ by ARSB was obtained at the lower pH range and consequently the removal of CBZ by ARSB decreased at the higher pH range. This was similar to the result obtained from the batch study. With the pH$_{pzc}$ value of ARSB being 4.5 (Bhattacharya et al., 2021) at the lower pH range (pH 2 - pH 4) the surface of ARSB and the experimental solution both are positively charged resulting in the creation of a force of repulsion between the ARSB particles and the H$^+$ ions present in the experimental solution. When the pH is increased to pH 6, the surface of ARSB

attains a negative charge while the experimental solution is neutrally charged resulting in the higher adsorption of CBZ molecules onto the surface of ARSB. The rate of adsorption again decreases when the pH enters the basic range due to the force of repulsion existing between the surface of ARSB and the OH⁻ ions present in the experimental solution. Thus the highest removal of CBZ by ARSB takes place at highest adsorbent dosage and around neutral pH range.

➢ **Effect of solution pH and contact time on CBZ removal by ARSB**

The interaction in between the pH of the experimental solution and contact time and its effect on the removal of CBZ by ARSB is conveyed in the contour plot of **Fig. 5.8**. From there it was observed that the removal of CBZ by ARSB increased with increase in pH of the experimental solution from pH 2 to pH 6 due to the electrostatic force of attraction acting between the negatively charged surface of ARSB and the neutrally charged experimental solution. However, the rate of adsorption again decreased on increasing the pH beyond pH 6, due to the creation of a force of repulsion between the negatively charged surface of ARSB and the OH⁻ ions present in the experimental solution (Bhattacharya et al., 2021). The adsorption of CBZ on the surface of ARSB was found to be highest in the contact time range of 90-105 minutes. When the contact time increased beyond 105 minutes, the adsorption of CBZ molecules by ARSB decreased.

➢ **Effect of contact time and ARSB dosage on CBZ removal by ARSB**

The interaction in between the contact time and dosage of adsorbent and its effect on the removal of CBZ by ARSB is conveyed in the contour plot of **Fig. 5.9**. From there it was observed that removal of CBZ by ARSB increased with increase in dosage of ARSB which could be attributed to the greater availability of active sites for the uptake of CBZ molecules (Bhattacharya et al., 2021). The adsorption of CBZ by ARSB was found to be the highest in the contact time of 90-105 minutes, beyond which the adsorption of CBZ by ARSB decreased with the increase in contact time.

**Table 5.13** :- The table showing the 20 different set of parameters (runs) along with their corresponding outcome as proposed by CCD model of RSM for optimization of CBZ removal by ARSB

| Run | Block | Factor 1 | Factor 2 | Factor 3 | Response 1 |
|---|---|---|---|---|---|
| | | A:pH | B:Dose | C:Time | Percentage Removal |
| | | | g/L | min | |
| 1 | Block 1 | 6.5 | 2 | 120 | 59.10 |
| 2 | Block 1 | 6.5 | 0.32 | 120 | 20.57 |
| 3 | Block 1 | 4 | 3 | 150 | 66.64 |
| 4 | Block 1 | 9 | 3 | 90 | 65.15 |
| 5 | Block 1 | 6.5 | 2 | 69.55 | 61.43 |
| 6 | Block 1 | 6.5 | 2 | 170.45 | 51.51 |
| 7 | Block 1 | 9 | 3 | 150 | 55.76 |
| 8 | Block 1 | 4 | 1 | 150 | 38.36 |
| 9 | Block 1 | 6.5 | 2 | 120 | 59.10 |
| 10 | Block 1 | 6.5 | 3.68 | 120 | 54.75 |
| 11 | Block 1 | 6.5 | 2 | 120 | 59.10 |
| 12 | Block 1 | 4 | 1 | 90 | 41.20 |
| 13 | Block 1 | 4 | 3 | 90 | 63.80 |
| 14 | Block 1 | 9 | 1 | 90 | 38.63 |
| 15 | Block 1 | 9 | 1 | 150 | 36.89 |
| 16 | Block 1 | 10.7 | 2 | 120 | 56.85 |
| 17 | Block 1 | 6.5 | 2 | 120 | 59.10 |
| 18 | Block 1 | 6.5 | 2 | 120 | 59.10 |
| 19 | Block 1 | 2.3 | 2 | 120 | 58.00 |
| 20 | Block 1 | 6.5 | 2 | 120 | 59.10 |

**Table 5.14** :- ANOVA analysis for the RSM for the process operation of CBZ adsorption by ARSB

| $R^2$ Value | Adjusted $R^2$ Value | f- value | Probability Value P |
|---|---|---|---|
| 0.98 | 0.96 | 58.25 (>1) | 0.0001 (<0.001) Significant |
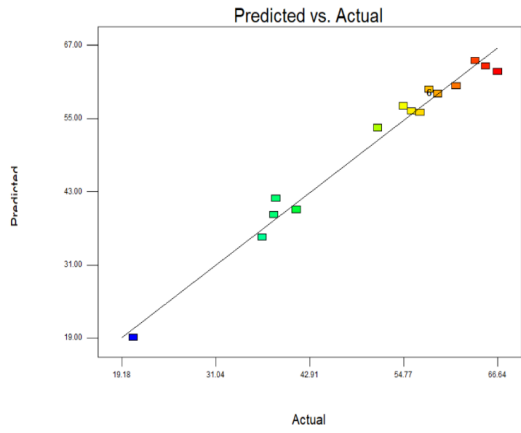
**Fig. 5.6**: Relation between the predicted data points and the experimental data points as per the RSM model.
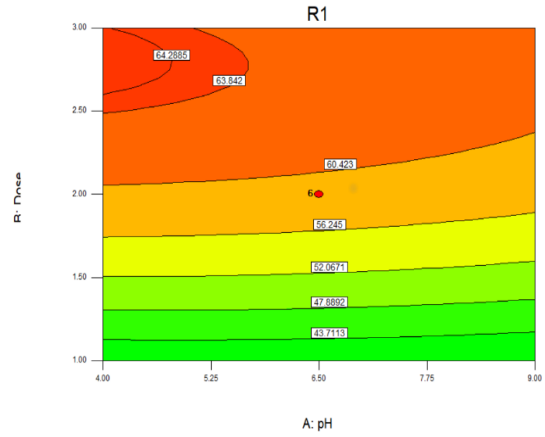


**Fig. 5.7**: Interaction between the pH of the experimental solution and the dose of the ARSB and their effect on the percentage removal of CBZ
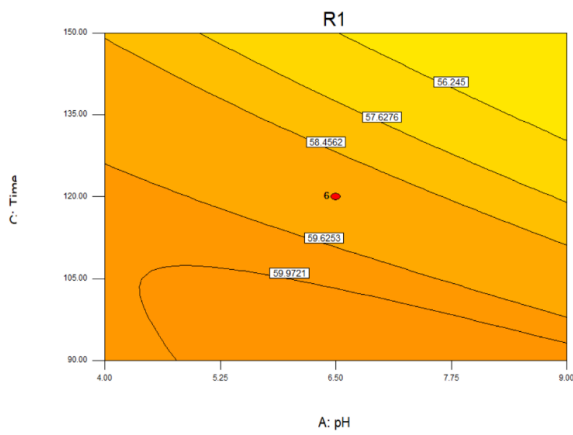


**Fig. 5.8**: The interaction between the pH of the experimental solution and the contact time (in minutes) and their effect on the percentage removal of CBZ by ARSB.
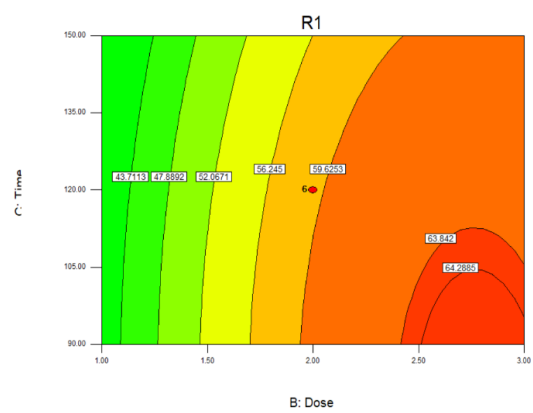


**Fig. 5.9**: The plot showing the interaction between the dose of the ARSB and the contact time (in minutes) as per the RSM model and their effect on the % removal of CBZ.

*5.4.6.2 Optimization of the adsorption of NPX by ARSB by RSM*

The RSM was performed with the aim of understanding the effect of inter parameter interaction on the experimental outcome. In **Table 5.15**, the outcome of the 20 experiments as proposed by the software for the CCD model of the RSM is given and in **Table 5.16** the result of the ANOVA of the RSM model is provided. From there it is observed that the $R^2$ value of the model was 0.93 and the adjusted $R^2$ value was 0.87 which propounded the fact that the polynomial model suggested by RSM was appropriate for predicting the outcome of this adsorption reaction. The high value of F (15.76, greater than unity) and the low value of P ($< 0.0001$) meant that the optimizing model was very much significant, with the experimental data points exhibiting a high degree of correlation with the predicted data points (Bhattacharya et al., 2021). **Fig. 5.10** shows the relation between the experimentally determined data points and the predicted data points and there also it can be noted that the experimental data points exhibits a high degree of correlation with the predicted data points. The real equation which was used to predict the effect of the input variables on the response output is presented as follows.

$Removal \% = 27.00958 + 2.50197 \times pH + 41.61311 \times Dose - 0.10844 \times Time - 4.11523 \times 10^{-3} \times pH \times Dose + 0.012483 \times pH \times Time - 3.31504 \times 10^{-3} \times Dose \times Time - 0.61537 \times pH^2 - 7.31920 \times Dose^2 + 4.73267 \times 10^{-4} * Time^2$……………(xxxvi)

As per the RSM model the optimized conditions under which maximum removal of NPX (83.35 %) was possible were: adsorbent dosage of 3 g/L, pH value of 4 and reaction time of 150 minutes. For this RSM model, the interaction between the experimental parameters (input variables) and their outcome on the percentage removal of NPX (response variable) is illustrated by the contour plots shown in **Fig. 5.11-5.13**.

> **Effect of ARSB dosage and solution pH on NPX removal by ARSB**

The interaction in between the pH of the experimental solution and the dosage of ARSB and its effect on the removal of NPX is conveyed in the contour plot of **Fig. 5.11**. From there it was observed that the removal of NPX by ARSB increased with the increase in dosage of ARSB. The higher removal of NPX at the higher dose of ARSB was due to the availability of greater surface area for the purpose of adsorption and the consequently the highest removal value was observed around the highest dosage of 3 g/L (Banerjee et al., 2016; Bhattacharya et al., 2021). In case of the variation of pH of the experimental solution, it was observed that the higher removal of NPX by ARSB was obtained at the lower pH range and consequently the removal of NPX by ARSB decreased at the higher pH range. This was similar to the result obtained from the batch study. With the pH$_{pzc}$ value of ARSB being 4.5 and the pKa value of NPX being 4.15 (Ciğeroğlu et al., 2020; Reynel-avila et al., 2015), at the lower pH range the positively charged surface of ARSB adsorbs the neutral molecules of NPX by hydrogen bonding and van deer Waals force (Iˑlbay et al., 2015). Subsequently, when the pH value is increased (beyond pH 4.15 for

NPX and pH 5 for ARSB) the surface of ARSB and the NPX molecules both acquire negative charge (I˙lbay et al., 2015; Mondal et al., 2020). As a consequence of which the removal of NPX by ARSB decreases with the increase in pH of the experimental solution. Thus highest removal was observed at the highest dose range and at the lowest pH range.

> **Effect of solution pH and contact time on NPX removal by ARSB**

The interaction in between the pH of the experimental solution and contact time and its effect on the removal of NPX by ARSB is conveyed in the contour plot of **Fig. 5.12**. From there it was observed that removal of NPX by ARSB increased with the increase in contact time due to higher number of interaction between the NPX molecules and the surface of ARSB resulting in greater adsorption of NPX molecules by ARSB (Bhattacharya et al., 2021). Similarly, in case of pH value it was observed that higher adsorption of NPX by ARSB took place in lower pH range which is attributed to the adsorption of NPX molecules by ARSB by van deer Waal's force and hydrogen bonding (I˙lbay et al., 2015). Thus the highest removal of NPX by ARSB took place at the higher contact time range and at the lower pH range.

> **Effect of contact time and ARSB dosage on NPX removal by ARSB**

The interaction in between the contact time and dosage of adsorbent and its effect on the removal of NPX by ARSB is conveyed in the contour plot of **Fig. 5.13**. From there it was observed that the removal of NPX by ARSB increased with the increase in contact time and also with the increase of adsorbent dosage. That is because, with the increase in contact time the interaction between the molecules of NPX and the particles of ARSB increases resulting in greater adsorption of the NPX molecules by the ARSB particles (Bhattacharya et al., 2021). On the other hand, the removal of NPX by ARSB increases with the increase in adsorbent dosage due to the greater availability of active sites for the uptake of the NPX molecules (Bhattacharya et al., 2021; I˙lbay et al., 2015). As a consequence of which the highest removal of NPX by ARSB was observed at the highest dose range of ARSB and at the highest contact time.

**Table 5.15** :- The table showing the 20 different set of parameters (runs) along with their corresponding outcome as proposed by CCD model of RSM for optimization of NPX removal by ARSB

| Run | Block | Factor 1 | Factor 2 | Factor 3 | Response R1 |
|-----|-------|----------|----------|----------|-------------|
|     |       | A: pH    | B: Dose (g/L) | C: Time (min) | Removal % |
| 1   | Block 1 | 6.50 | 2.00 | 120.00 | 73.85 |
| 2   | Block 1 | 6.50 | 0.32 | 120.00 | 25.27 |
| 3   | Block 1 | 4.00 | 3.00 | 150.00 | 83.35 |
| 4   | Block 1 | 9.00 | 3.00 | 90.00 | 55.86 |
| 5   | Block 1 | 6.50 | 2.00 | 69.55 | 72.95 |
| 6   | Block 1 | 6.50 | 2.00 | 170.45 | 79.29 |
| 7   | Block 1 | 9.00 | 3.00 | 150.00 | 63.21 |
| 8   | Block 1 | 4.00 | 1.00 | 150.00 | 67.38 |
| 9   | Block 1 | 6.50 | 2.00 | 120.00 | 73.85 |
| 10  | Block 1 | 6.50 | 3.68 | 120.00 | 83.16 |
| 11  | Block 1 | 6.50 | 2.00 | 120.00 | 73.85 |
| 12  | Block 1 | 4.00 | 1.00 | 90.00 | 63.37 |
| 13  | Block 1 | 4.00 | 3.00 | 90.00 | 80.11 |
| 14  | Block 1 | 9.00 | 1.00 | 90.00 | 39.53 |
| 15  | Block 1 | 9.00 | 1.00 | 150.00 | 46.91 |
| 16  | Block 1 | 10.70 | 2.00 | 120.00 | 49.77 |
| 17  | Block 1 | 6.50 | 2.00 | 120.00 | 73.85 |
| 18  | Block 1 | 6.50 | 2.00 | 120.00 | 73.85 |
| 19  | Block 1 | 2.30 | 2.00 | 120.00 | 78.35 |
| 20  | Block 1 | 6.50 | 2.00 | 120.00 | 73.85 |

**Table 5.16**:- ANOVA analysis for the RSM for the process operation of NPX adsorption by ARSB

| $R^2$ Value | Adjusted $R^2$ Value | f- value | Probability Value P |
|-------------|----------------------|----------|---------------------|
| 0.93 | 0.87 | 15.76 (>1) | <0.0001 Significant |
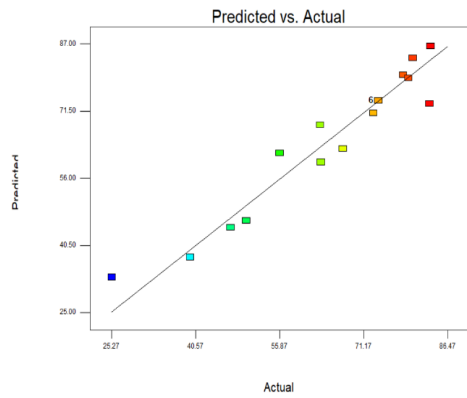
**Fig. 5.10**:- Relation between the predicted data points and the experimental data points as per the RSM model.
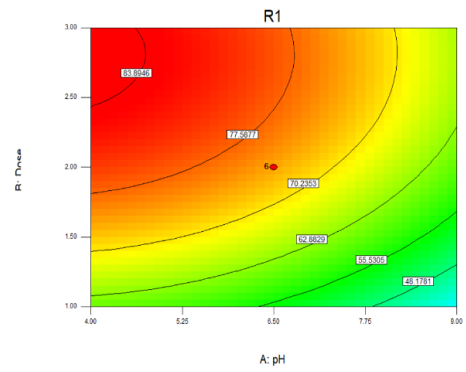


**Fig. 5.11**:- Interaction between the pH of the experimental solution and the dose of the ARSB and their effect on the percentage removal of NPX.



**Fig. 5.12**:- The interaction between the pH of the experimental solution and the contact time (in minutes) and their effect on the percentage removal of NPX by ARSB.



**Fig. 5.13**:- The plot showing the interaction between the dose of the ARSB and the contact time (in minutes) as per the RSM model and their effect on the percentage removal of NPX.

*5.4.6.3 Optimization of the adsorption of RTN by ARSB by RSM*

The RSM was performed with the aim of understanding the effect of inter parameter interaction on the experimental outcome. In **Table 5.17**, the outcome of the 20 experiments as proposed by the software for the CCD model of the RSM is given and in **Table 5.18** the result of the ANOVA of the RSM model is provided. From there it is observed that the $R^2$ value of the model was 0.9 and the adjusted $R^2$ value was 0.82 which propounded the fact that the polynomial model suggested by RSM was appropriate for predicting the outcome of this adsorption reaction. The high value of F (10.4, higher than unity) and the low value of P ($< 0.005$) meant that the optimizing model was very much significant, with the experimental data points exhibiting a high degree of correlation with the predicted data points (Bhattacharya et al., 2021). **Fig. 5.14** shows the relation between the experimentally determined data points and the predicted data points and there also it can be noted that the experimental data points exhibits a high degree of correlation with the predicted data points. The real equation which was used to predict the effect of the input variables on the response output is presented as follows.

$Removal = -124.39215 + 14.34984 \times pH + 8.3905 \times Dose + 1.68622 \times Time + 1.9925 \times pH \times Dose - 0.064335 \times pH \times Time + 0.18192 \times Dose \times Time - 0.75764 \times pH^2 - 6.63656 \times Dose^2 - 6.07746 \times 10^{-3} \times Time^2$ ……………………………………………………(xxxvii)

As per the RSM model the optimized conditions under which maximum removal of RTN (78.48 %) was possible were: adsorbent dosage of 3.68 g/L, pH value of 6.5 and reaction time of 120 minutes. For this RSM model, the interaction between the experimental parameters (input variables) and their outcome on the percentage removal of RTN (response variable) is illustrated by the contour plots shown in **Fig. 5.15-5.17**.

➢ **Effect of ARSB dosage and solution pH on RTN removal by ARSB**

The interaction in between the pH of the experimental solution and the dosage of ARSB and its effect on the removal of RTN is conveyed in the contour plot of **Fig. 5.15**. From there it was observed that the removal of RTN by ARSB increased with the increase in dosage of ARSB. This could be attributed to the higher availability of active sites for the uptake of RTN at the higher dosage of ARSB and consequently the highest removal value was observed around the highest dosage (Banerjee et al., 2016; Bhattacharya et al., 2021). In case of the variation of pH of the experimental solution, it was observed that the highest removal of RTN was observed at around pH 6.5. This could be attributed to the fact that around the neutral pH range, the molecules of RTN were neutral (Kortejarvi et al., 2005) and the surface of ARSB are negatively charged and as a result of which maximum adsorption of RTN molecules takes place on the surface of ARSB at this pH (Al-rub et al., 2020). At the lower pH range both RTN molecules and the surface of ARSB acquire positive charge whereas at the higher pH range both of these acquire negative charge (Al-rub et al., 2020). As a consequence of which at the higher and lower

pH range, the RTN molecules and ARSB surface experience repulsion from each other thereby decreasing the adsorption of RTN by ARSB at this pH. Thus highest removal of RTN is observed at the neutral pH range and at the high adsorbent dosage (Banerjee et al., 2016; Bhattacharyya et al., 2019).

➢ **Effect of solution pH and contact time on RTN removal by ARSB**

The interaction in between the pH of the experimental solution and contact time and its effect on the removal of RTN by ARSB is shown in the contour plot of **Fig. 5.16**. From there it was observed that removal of RTN by ARSB initially increased with the increase in contact time due to higher number of interaction between the RTN molecules and the surface of ARSB resulting in greater adsorption of RTN molecules by ARSB (Bhattacharya et al., 2021). However, beyond the optimum contact time, (around 135-150 minutes mark), a slight decrease in the removal of RTN by ARSB was observed in the contour plot, which could be attributed to desorption due to the physical nature of the adsorption reaction. In case of pH variation it was observed, that highest removal of RTN was around the neutral pH range, which could be attributed to the attraction between the neutral molecules of RTN and the negatively charged surface of ARSB (Al-rub et al., 2020).

➢ **Effect of contact time and ARSB dosage on RTN removal by ARSB**

The interaction in between the contact time and dosage of adsorbent and its effect on the removal of RTN by ARSB is shown in the contour plot of **Fig. 5.17**. From there it was observed that the removal of RTN by ARSB increased with the increase in dosage which could be attributed to the availability of greater surface area for the uptake of RTN molecules (Banerjee et al., 2016; Bhattacharya et al., 2021). On the other hand, the adsorption of RTN molecules by ARSB increased with the increase in contact time till the optimum time range, which in this contour plot was around 135-140 minutes, followed by which a slight decrease in the removal of RTN by ARSB was observed in the contour plot. This could be attributed to the desorption of RTN molecules from the surface of ARSB due to the physical nature of the adsorption. Thus highest removal of RTN was observed for the highest dosage and for the optimum contact time.

**Table 5.17**:- The table showing the 20 different set of parameters (runs) along with their corresponding outcome as proposed by CCD model of RSM for optimization of RTN removal by ARSB

| Run | Block | Factor 1 | Factor 2 | Factor 3 | Response 1 |
|-----|-------|----------|----------|----------|------------|
|     |       | A:pH     | B:Dose   | C:Time   | Percentage Removal |
|     |       |          | g/L      | min      |            |
| 1   | Block 1 | 6.5   | 2        | 120      | 61.04      |
| 2   | Block 1 | 9     | 1        | 90       | 23.60      |
| 3   | Block 1 | 9     | 3        | 150      | 68.57      |
| 4   | Block 1 | 4     | 1        | 150      | 27.92      |
| 5   | Block 1 | 10.7  | 2        | 120      | 50.06      |
| 6   | Block 1 | 6.5   | 2        | 120      | 61.04      |
| 7   | Block 1 | 4     | 1        | 90       | 24.82      |
| 8   | Block 1 | 6.5   | 2        | 120      | 61.04      |
| 9   | Block 1 | 6.5   | 2        | 120      | 61.04      |
| 10  | Block 1 | 6.5   | 3.6818   | 120      | 78.48      |
| 11  | Block 1 | 6.5   | 2        | 120      | 61.04      |
| 12  | Block 1 | 6.5   | 0.3182   | 120      | 16.22      |
| 13  | Block 1 | 9     | 3        | 90       | 62.95      |
| 14  | Block 1 | 9     | 1        | 150      | 26.86      |
| 15  | Block 1 | 2.3   | 2        | 120      | 55.48      |
| 16  | Block 1 | 4     | 3        | 150      | 69.17      |
| 17  | Block 1 | 6.5   | 2        | 69.55    | 46.28      |
| 18  | Block 1 | 6.5   | 2        | 120      | 61.04      |
| 19  | Block 1 | 6.5   | 2        | 170.45   | 55.03      |
| 20  | Block 1 | 4     | 3        | 90       | 24.82      |

**Table 5.18** :- ANOVA analysis for the RSM for the process operation of RTN adsorption by ARSB

| $R^2$ Value | Adjusted $R^2$ Value | f- value | Probability Value P |
|-------------|----------------------|----------|---------------------|
| 0.9         | 0.82                 | 10.4 (>1) | 0.0005 (<0.001) Significant |
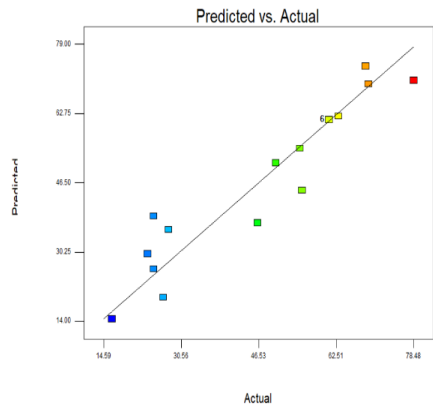
**Fig. 5.14**: Relation between the predicted data points and the experimental data points as per the RSM model.



**Fig. 5.15**: Interaction between the pH of the experimental solution and the dose of the ARSB and their effect on the percentage removal of RTN.
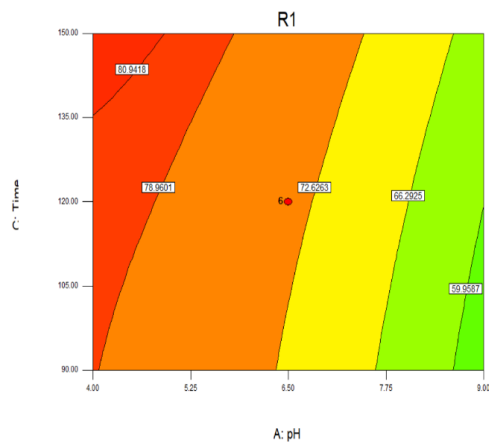


**Fig. 5.16**: The interaction between the pH of the experimental solution and the contact time (in minutes) and their effect on the percentage removal of RTN by ARSB.
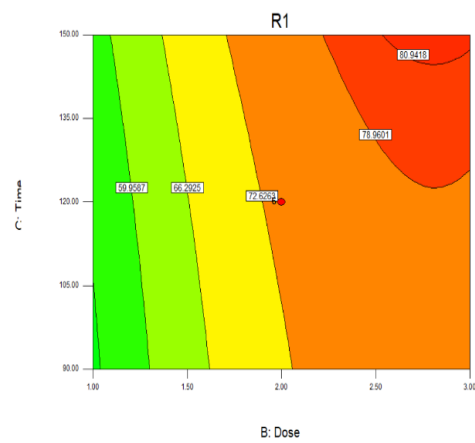


**Fig. 5.17**: The plot showing the interaction between the dose of the ARSB and the contact time (in minutes) as per the RSM model and their effect on the percentage removal of RTN by ARSB.

*5.4.6.4 Process Optimization of the adsorption of BPA by ARSB by RSM*

The Response Surface Methodology was performed with the aim of understanding the effect of inter parameter interaction on the experimental outcome. In **Table 5.19**, the outcome of the 20 experiments as proposed by the software for the CCD model of the RSM is given and in **Table 5.20** the result of the ANOVA of the RSM model is provided. From there it is observed that the $R^2$ value of the model was 0.86 and the adjusted $R^2$ value was 0.73 which propounded the fact that the polynomial model suggested by RSM was appropriate for predicting the outcome of this adsorption reaction. The value of F is 6.66, which is higher than unity and the value of P is 0.0033 (<0.05) meaning the that the optimizing model was significant and there is only a 0.33 % chance of a model F-value this large being a work of noise (Bhattacharya et al., 2021). **Fig. 5.18** shows the relation between the experimentally determined data points and the predicted data points and there also it can be noted that the experimental data points exhibits a high degree of correlation with the predicted data points. The real equation which was used to predict the effect of the input variables on the response output is presented as follows.

$$Removal \% = -114.65736 + 16.20997 \times pH + 32.58413 \times Dose + 1.7646 \times Time - 1.06306 \times pH \times Dose - 0.057676 \times pH \times Time - 0.027708 \times Dose \times Time - 0.78517 \times pH^2 - 4.84218 \times Dose^2 - 5.11753 \times 10^{-3} \times Time^2 \quad \ldots\ldots\ldots\ldots\ldots\ldots\ldots\ldots\ldots\ldots\text{(xxxviii)}$$

As per the RSM model the optimized conditions under which maximum removal of BPA (84.08 %) was possible were: adsorbent dosage of 2 g/L, pH value of 2.3 and reaction time of 120 minutes. For this RSM model, the interaction between the experimental parameters (input variables) and their outcome on the percentage removal of BPA (response variable) is illustrated by the contour plots shown in **Fig. 5.19-5.21**.

> ➤ **Effect of ARSB dosage and solution pH on BPA removal by ARSB**

The interaction in between the pH of the experimental solution and the dosage of ARSB and its effect on the removal of BPA is conveyed in the contour plot of **Fig. 5.19**. From there it was observed that the removal of BPA by ARSB increased with the increase in dosage of ARSB. This could be attributed to the higher availability of active sites for the uptake of BPA at the higher dosage of ARSB and as a result of which the highest percentage removal value was obtained around the highest dosage of 3 g/L (Banerjee et al., 2016; Bhattacharya et al., 2021). In case of the variation of pH of the experimental solution, it was observed that the highest removal of BPA was observed at the lower pH range of the experimental solution and the removal percentage decreased with the increase in pH of the experimental solution. This could be attributed to the fact that the $pK_a$ value of BPA is 9.6 (Xu et al., 2018), and at around pH 8 the deprotonation of BPA starts by virtue of which it acquires a negative charge and is dissociated to form negatively charged bis-phenolate monoanions (Chang et al., 2012). On the other hand, the $pH_{pzc}$ of ARSB is 4.5 (Bhattacharya et al., 2021), as a consequence of which at pH higher than

4.5, the surface of ARSB also acquires a negative charge (Banerjee et al., 2016; Bhattacharya et al., 2020). Thus as a result of which, at the higher pH range the adsorption of BPA by ARSB is obstructed by the electrostatic force of repulsion acting between the negatively charged BPA molecules and the negative surface of ARSB (Chang et al., 2012; Kwon & Lee, 2015; Phatthanakittiphong & Seo, 2016; Xu et al., 2012). Therefore, the highest removal percentage was observed for the higher dosage of ARSB and for the lower pH range of the experimental solution.

➢ **Effect of solution pH and contact time on BPA removal by ARSB**

The interaction in between the pH of the experimental solution and contact time and its effect on the removal of BPA by ARSB is shown in the contour plot of **Fig. 5.20**. From the result of the experiment it was observed that the removal of BPA by ARSB increased with the increase in contact time which could be attributed to the higher number of interaction between the BPA molecules and the surface of ARSB resulting in greater adsorption of BPA molecules by ARSB (Bhattacharya et al., 2021). In case of pH variation it was observed, that highest removal of BPA was achieved in the acidic pH range, as because at higher pH value in the basic range both the surface of ARSB and the molecules of BPA acquire a negative charge (Banerjee et al., 2016; Chang et al., 2012; Xu et al., 2012). The $pK_a$ value of BPA is 9.6, and at around pH 8, the BPA molecules dissociate to form bis-phenolate monoanion (Chang et al., 2012). On the other hand, the $pH_{pzc}$ of ARSB is 4.5 (Bhattacharya et al., 2021), therefore at the higher pH range the surface of ARSB also acquires a negative charge. As a result of which at the higher pH range, the adsorption of BPA by ARSB is obstructed due to the electrostatic force of repulsion acting between the molecules of BPA and the surface of ARSB (Chang et al., 2012; Kwon & Lee, 2015; Phatthanakittiphong & Seo, 2016; Xu et al., 2012). The highest removal of BPA by ARSB was therefore observed at the highest contact time and at the lowest pH range.

➢ **Effect of contact time and ARSB dosage on BPA removal by ARSB**

The interaction in between the contact time and dosage of adsorbent and its effect on the removal of BPA by ARSB is shown in the contour plot of **Fig. 5.21**. From there it was observed that the removal of BPA by ARSB increased with the increase in dosage which could be ascribed to the availability of greater surface area for the uptake of BPA molecules (Banerjee et al., 2016; Bhattacharya et al., 2021). On the other hand, the adsorption of BPA molecules by ARSB increased with the increase in contact time which could be attributed to the greater interaction between the BPA molecules and the surface of ARSB leading to the greater uptake of BPA by ARSB. From the analysis of the activation energy it was found that the adsorption of BPA on the surface of ARSB was physical in nature ($E_a = 3.26$ kJ/mole < 40 kJ/mole), and as physical adsorption increases with contact time therefore the adsorption of BPA by ARSB also increased with increase in contact time (Bhattacharya et al., 2021). Therefore, adsorption of BPA by ARSB was found to be highest at the highest dosage of ARSB and at the highest contact time.

**Table 5.19** :- The table showing the 20 different set of parameters (runs) along with their corresponding outcome as proposed by CCD model of RSM for optimization of BPA removal by ARSB

| Run | Block | Factor 1 A:pH | Factor 2 B:Dose g/L | Factor 3 C:Time min | Response 1 Percentage Removal |
|---|---|---|---|---|---|
| 1 | Block 1 | 6.50 | 0.32 | 120.00 | 53.08 |
| 2 | Block 1 | 6.50 | 2.00 | 120.00 | 75.87 |
| 3 | Block 1 | 4.00 | 1.00 | 150.00 | 70.28 |
| 4 | Block 1 | 4.00 | 3.00 | 90.00 | 60.36 |
| 5 | Block 1 | 6.50 | 2.00 | 170.45 | 67.29 |
| 6 | Block 1 | 6.50 | 2.00 | 69.55 | 60.72 |
| 7 | Block 1 | 6.50 | 2.00 | 120.00 | 75.87 |
| 8 | Block 1 | 9.00 | 1.00 | 150.00 | 59.56 |
| 9 | Block 1 | 9.00 | 3.00 | 90.00 | 56.32 |
| 10 | Block 1 | 6.50 | 3.68 | 120.00 | 73.64 |
| 11 | Block 1 | 6.50 | 2.00 | 120.00 | 75.87 |
| 12 | Block 1 | 6.50 | 2.00 | 120.00 | 75.87 |
| 13 | Block 1 | 10.70 | 2.00 | 120.00 | 42.28 |
| 14 | Block 1 | 4.00 | 1.00 | 90.00 | 52.89 |
| 15 | Block 1 | 9.00 | 1.00 | 90.00 | 57.42 |
| 16 | Block 1 | 9.00 | 3.00 | 150.00 | 53.08 |
| 17 | Block 1 | 6.50 | 2.00 | 120.00 | 75.87 |
| 18 | Block 1 | 4.00 | 3.00 | 150.00 | 76.48 |
| 19 | Block 1 | 6.50 | 2.00 | 120.00 | 75.87 |
| 20 | Block 1 | 2.30 | 2.00 | 120.00 | 84.08 |

**Table 5.20**:- ANOVA analysis for the RSM for the process operation of BPA adsorption by ARSB

| $R^2$ Value | Adjusted $R^2$ Value | f- value | Probability Value P |
|---|---|---|---|
| 0.86 | 0.72 | 6.66 (>1) | 0.0033          (<0.05) Significant |
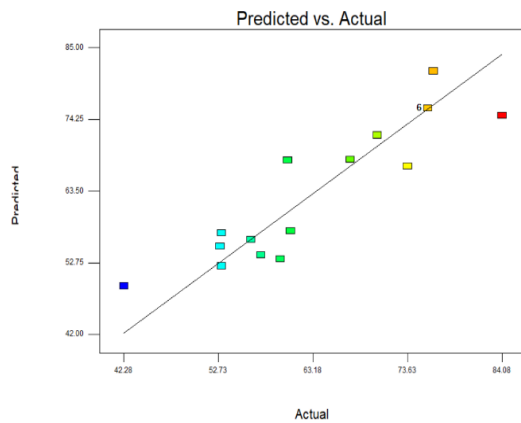
**Fig. 5.18**:- Relation between the predicted data points and the experimental data points as per the RSM model.
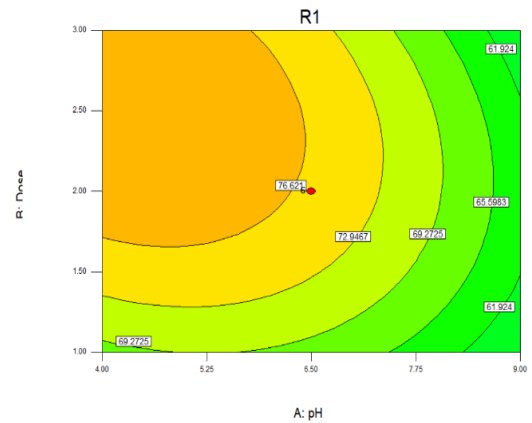


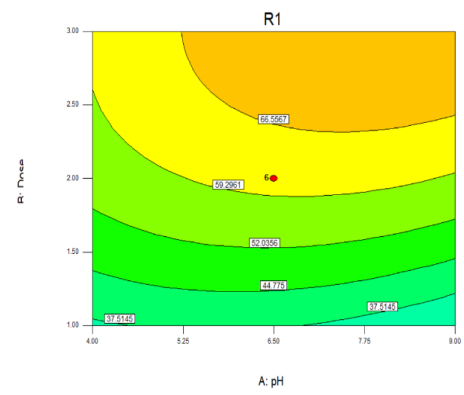**Fig. 5.19**:- Interaction between the pH of the experimental solution and the dose of the ARSB and their effect on the percentage removal of BPA by ARSB
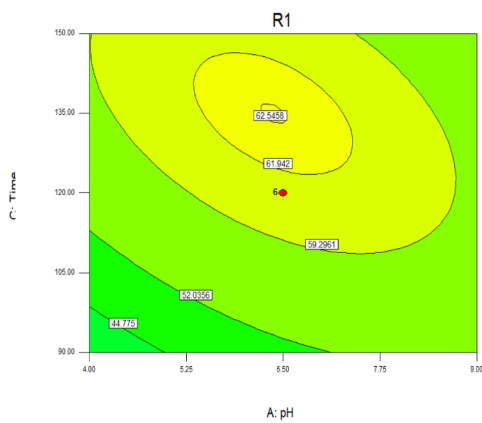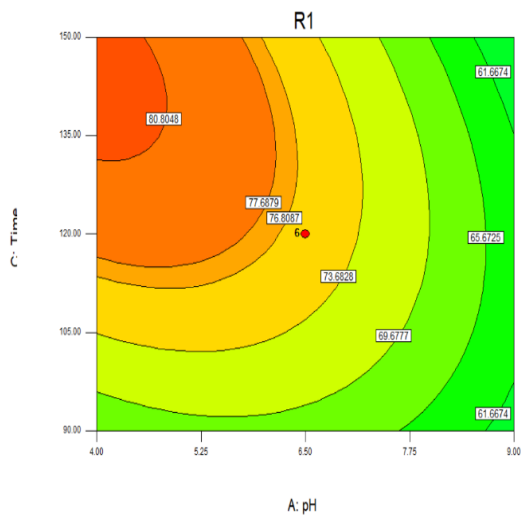


**Fig. 5.20**:- The interaction between the pH of the experimental solution and the contact time (in minutes) and their effect on the percentage removal of BPA by ARSB.
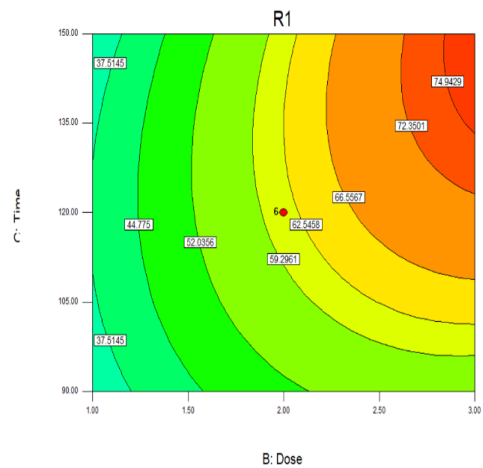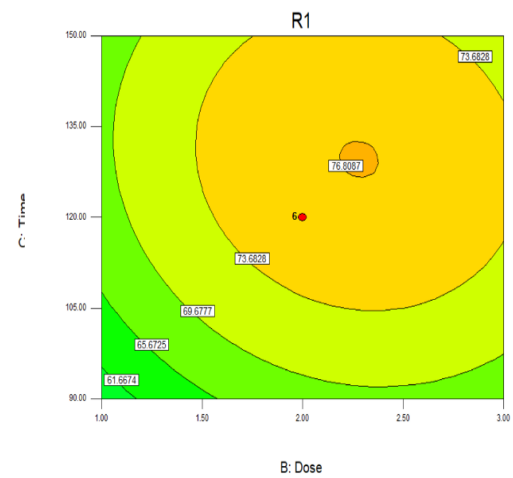


**Fig. 5.21**:- The plot showing the interaction between the dose of the GO and the contact time (in minutes) as per the RSM model and their effect on the percentage removal of BPA by ARSB.

## 5.4.7 Removal of the EC's by ARSB in an RPB

An experiment was conducted with the RPB in order to intensify the adsorption process. The concentration of the EC's were kept constant at 10 mg/L and the dosage of ARSB was kept fixed at 2 g/L. The agitation speed of the RPB was kept at 100 R.P.M. From the result of the experiment shown in **Fig. 5.22** it was observed that the removal of RTN was highest (92.88 %), followed by BPA (83.5 %), followed by NPX (75.37 %), followed by CBZ (71.46 %). In case of each of these EC's, the removal achieved in the RPB was higher than that obtained in case of the batch studies under same conditions (i.e., concentration of EC = 10 mg/L, dosage = 2 g/L, pH = Neutral, temperature = 303 K) thereby signifying that the RPB was able to intensify the process of adsorption. This could be attributed to the dispersion of the liquid from the distributor, leading to the formation of thin liquid films and tiny droplets which reduces the mass transfer resistance resulting in enhanced adsorption of the EC's by the ARSB (Das et al., 2008; Hashim et al., 2019; Kundu et al., 2015). Thus, using the RPB enhanced the adsorption capacity of the adsorbent ARSB.
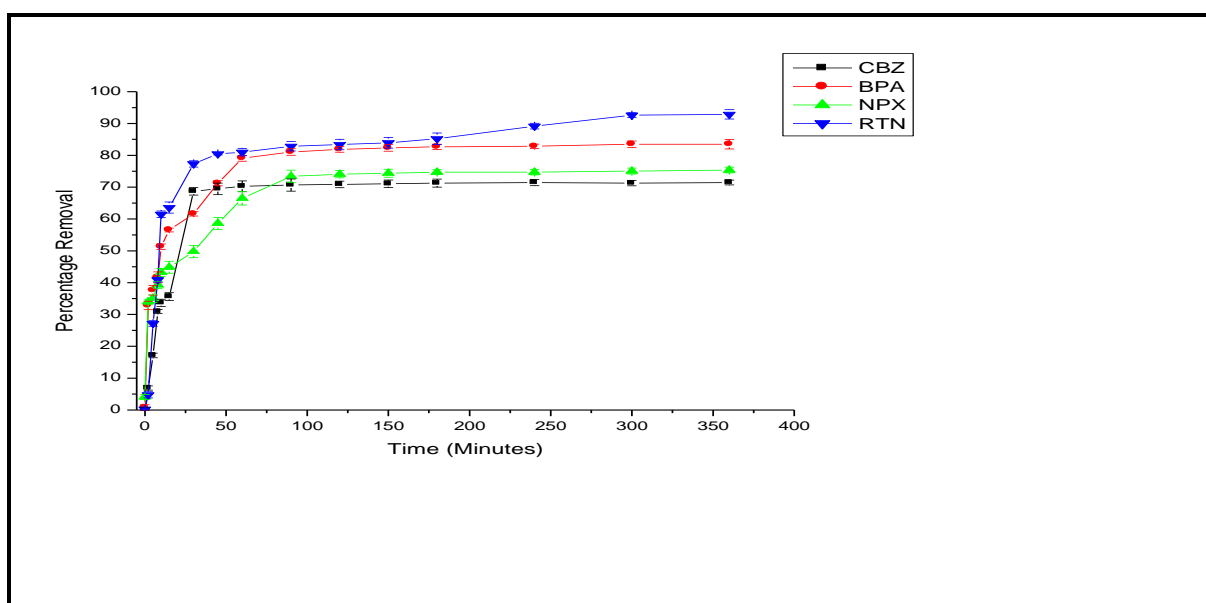


**Fig. 5.22**:- Removal of CBZ, NPX, RTN and BPA by ARSB in a RPB by ARSB.

## 5.4.8 Reusability Study

### 5.4.8.1 Reusability of ARSB after treating CBZ

Out of the six solutions that were used for the regeneration of used ARSB after treating CBZ, the greatest effectivity was exhibited by the 10% NaOH solution. By washing the ARSB with the 10 % NaOH solution it was observed that in the first cycle, the ARSB was able to remove 53.34 % of the CBZ from the aqueous solution. In the next cycle the removal of CBZ was 48.63 % and in the third cycle the removal was 43.97 %. However for the last two cycles the removal decreased to 36.64 % and 15.23 % respectively. Thus from the experimental study it can be stated that on regenerating the ARSB with 10 % NaOH solution it can be reused for upto three times for removing CBZ with a removal percentage of over 40 % (Bhattacharya et al., 2021). The result of the experiment is shown in **Fig. 5.23**.
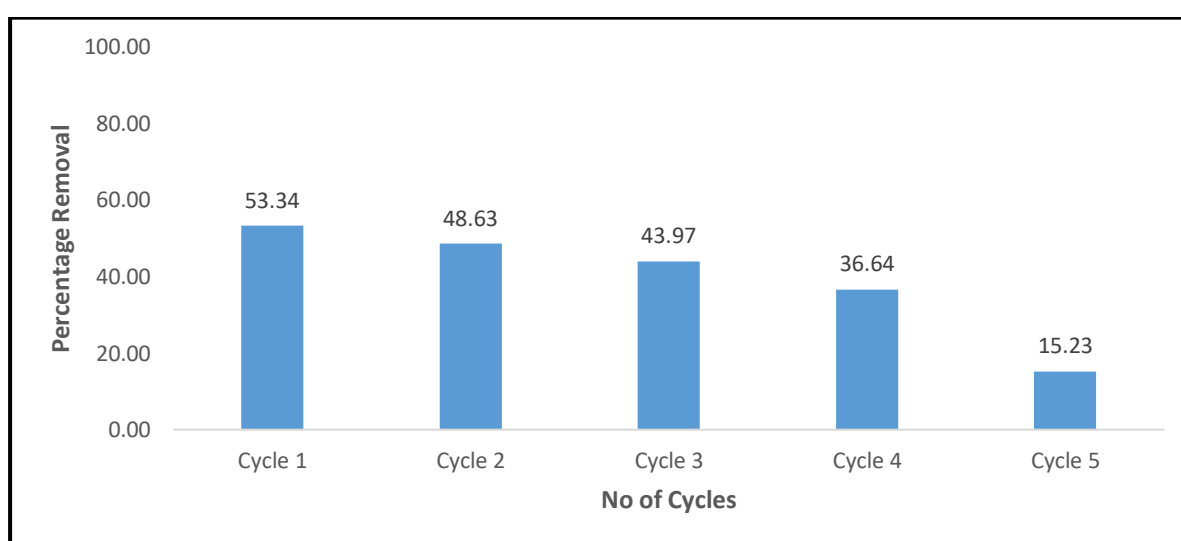


**Fig. 5.23**:- Removal of CBZ by ARSB in different steps of the reusability cycle.

### 5.4.8.2 Reusability of ARSB after treating NPX

Out of the six solutions that were used for the regeneration of used ARSB after treating NPX, the greatest effectivity was exhibited by the 10% HCl solution, therefore further reusability study was performed by this solution only. By treating the ARSB with the 10 % HCl solution after each adsorption cycle, it was observed that the removal capacity of ARSB for the purpose of treating NPX remained over 65 % for the first two cycles followed by which it decreased to 60.38 % in the third cycle. Followed by this it further decreased to 42.17 % and 23.48 % with the subsequent regeneration studies. Thus from the reusability study it was inferred that by washing ARSB with 10 % HCl solution, it could be used for 2-3 times with significant adsorption efficacy for the purpose of removing NPX from its aqueous solution (Bhattacharya et al., 2020). The result of the experiment is shown in **Fig. 5.24**.
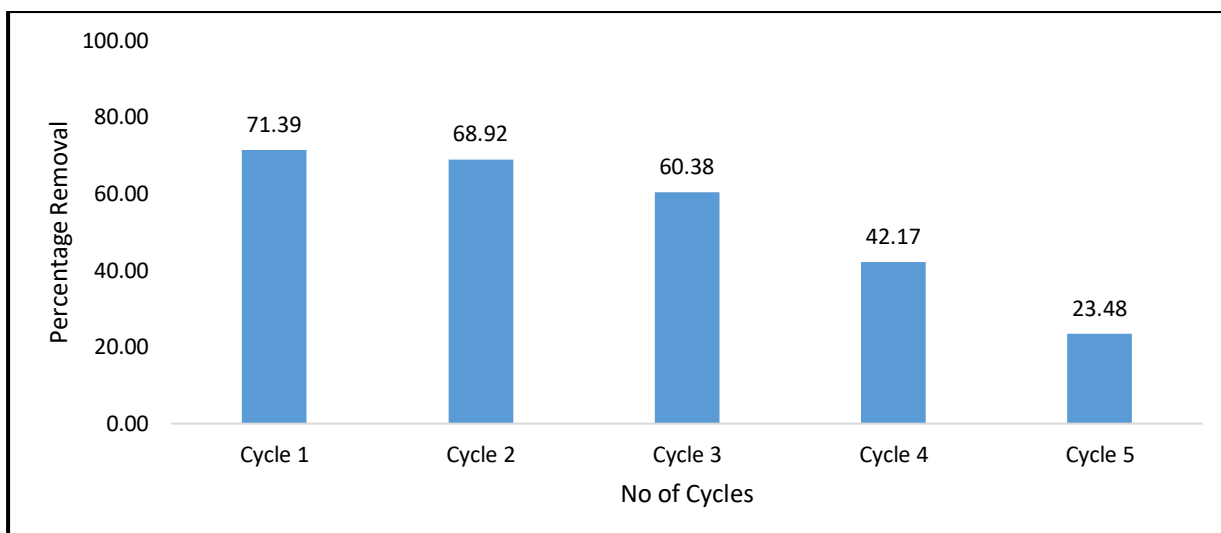
**Fig. 5.24**:- Removal of NPX by ARSB in different steps of the reusability cycle.

### 5.4.8.3 Reusability of ARSB after treating RTN

Out of the six solutions that were used for the regeneration of used ARSB after treating RTN, the greatest effectivity was exhibited by the 10 % ethanol solution, therefore further reusability study was performed by this solution only. This could be attributed to the high hydrophilicity of RTN molecules (Siew et al., 2012). By treating the ARSB with the 10 % ethanol solution after each adsorption cycle, it was observed that the removal capacity of ARSB for the purpose of treating RTN remained over 50 % for the first two cycles followed by a gradual decrease in further cases. Thus it can be stated that on washing a particular mass of ARSB by 10 % ethanol, it could be effectively reused for the purpose of removing RTN from the aqueous solution for at least two cycles. The result of the experiment is shown in **Fig. 5.25**.
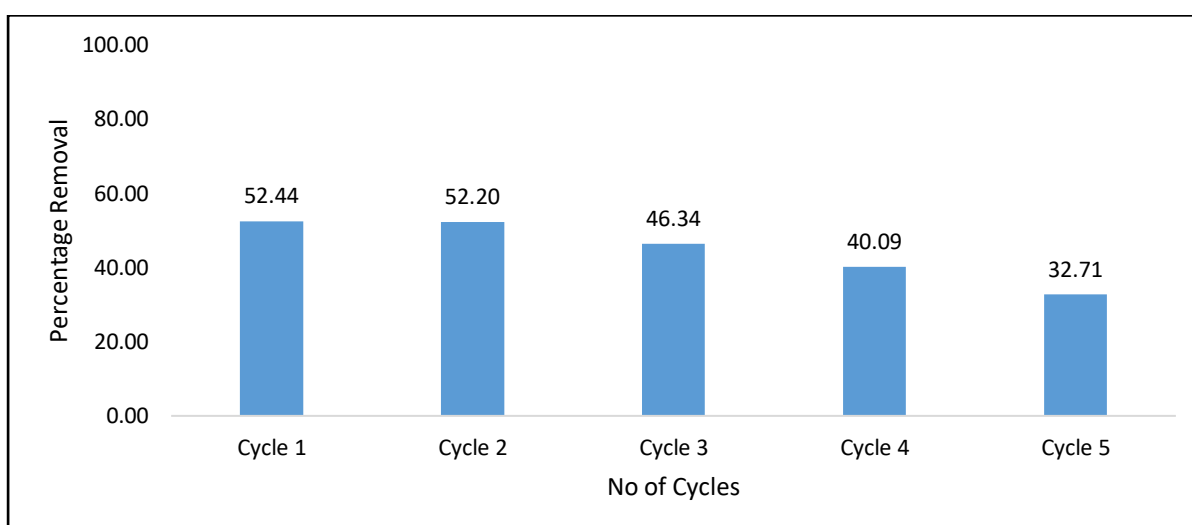


**Fig. 5.25:**- Removal of RTN by ARSB in different steps of the reusability cycle

### 5.4.8.4 Reusability of ARSB after treating BPA

Out of the six solutions that were used for the regeneration of used ARSB after treating BPA, the greatest effectivity was exhibited by the 10% HCl solution, therefore further reusability study was performed by this solution only. By treating the ARSB with the 10 % HCl solution after each adsorption cycle, it was observed that the removal capacity of ARSB for the purpose of treating BPA was 68.51 % for the first cycle. For the second cycle of treatment the adsorption efficiency of ARSB decreased a bit, and the removal percentage decreased to 65.04 %, and for the third cycle it decreased to 57.57 %. The removal of BPA by ARSB in the last two cycles were 50.58 % and 36.44 % respectively. Thus from the result of the regeneration study it can be inferred that, on washing with 10 % HCl solution, the same mass of ARSB can be used for two to three times for the purpose of removing BPA from its aqueous solution. The result of the experiment is shown in **Fig. 5.26**.
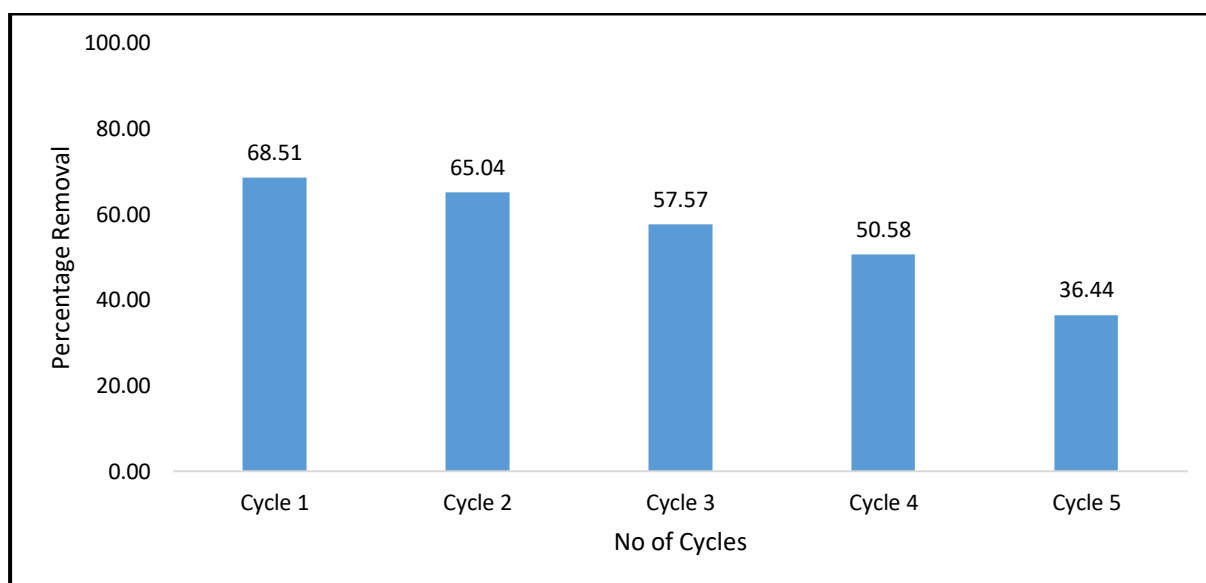


**Fig. 5.26**:- Removal of BPA by ARSB in different steps of the reusability cycle.

## 5.5 CONCLUSION :-

In the above study, ARSB was utilized for the adsorption of four trace pollutants viz., the three pharmaceuticals CBZ, RTN, NPX and the plasticizer BPN from there aqueous solution. For the purpose of synthesizing the ARSB, rice straw was selected as the starting material. The rice straw was collected from a local vendor followed by which it was washed and cut into small pieces. Then it was heated at 450°C under anaerobic conditions converting the rice straw into biochar. Followed by which, the biochar was activated by treating it with a modified Hummer's method. The finished product was named Activated Rice Straw Biochar (ARSB). The synthesized ARSB was characterized by SEM, XRD, FTIR and Raman analysis. From there it was observed that the synthesized ARSB contained various functional groups on its surface. It was used for removing the EC's from there aqueous solution. Two types of studies were involved namely, the batch adsorption studies and the fixed bed column studies. The parameters that were evaluated in the batch studies were the concentration of the EC's, dosage of ARSB, pH of the experimental solution and temperature. From the results of the batch study the highest removal for CBZ were recorded to be 61.51 % which was attained at CBZ concentration of 10 mg/L, adsorbent dosage of 2 g/L, pH 7 of experimental solution, temperature of 313 K and reaction time of 120 minutes. For NPX it was recorded to be 83.19 % which was attained at NPX concentration of 5 mg/L, adsorbent dosage of 2 g/L, pH 7 of experimental solution, temperature of 303 K and reaction time of 120 minutes. The highest percentage removal of RTN was 74.69 % which was attained at RTN concentration of 5 mg/L, adsorbent dosage of 2 g/L, pH 7 of experimental solution, temperature of 303 K and reaction time of 120 minutes. The highest percentage removal for BPA was 82.23 % obtained at BPA concentration of 10 mg/L, adsorbent dosage of 2 g/L, pH 2 of experimental solution, temperature of 303 K and reaction time of 120 minutes. Further optimization was done with RSM studies, from there the highest removal of CBZ was 66.64 which were possible at the ARSB dosage of 3 g/L, pH value of 4 and reaction time of 150 minutes. The highest removal of NPX was 83.35 % which was possible at ARSB dosage of 3 g/L, pH value of 4 and reaction time of 150 minutes. The highest removal of RTN was 78.48 % which were possible at adsorbent dosage of 3.68 g/L, pH value of 6.5 and reaction time of 120 minutes. The highest removal of BPA was 84.08 % which were possible at ARSB dosage of 2 g/L, pH value of 2.3 and reaction time of 120 minutes. And lastly, the removal of the EC's by ARSB was evaluated inside an RPB in order to intensify the adsorption process. The concentration of the EC's were kept constant at 10 mg/L, the dosage of ARSB was kept constant at 2 g/L, the pH of the experimental solution was kept constant at 7 and the rotation speed was kept constant at 150 R.P.M. From there it was observed that the removal of the EC's under the same conditions were higher in RPB than in the batch study. The removal of RTN was highest (92.88 %), followed by BPA (83.5 %), followed by NPX (75.37 %), followed by CBZ (71.46 %). This could be attributed to the effect of decreased mass transfer resistance due to formation of tiny droplets. Thus it can be stated that ARSB was able to remove EC's from there aqueous solution in both batch scale as well as under a dynamic

condition. However, on comparing the efficiency of ARSB with that GO it can be stated that GO was more efficient for the purpose of adsorption than ARSB. Therefore, further research can be directed towards increasing the adsorption efficiency of the ARSB so that this laboratory made adsorbent can attain the same level of efficiency as that of other commercially available adsorbents.

# CHAPTER 6

# SYNTHESIS OF A GO-TIO₂ COMPOSITE AND ITS UTILIZATION FOR REMOVING EC'S FROM THE AQUATIC SOLUTION

## 6.1 INTRODUCTION

Addressing the effect of pollution on the environment and finding the necessary solutions should be a global objective of topmost priority (Schneider et al., 2014). In the recent times, mostly due to intense anthropogenic activities, more and more pollutants are being introduced into the environment mostly in the water bodies which have negative consequences for human health and environment (Wu et al., 2020). Rate of consumption of PHA's has rapidly gone up in the last few decades. These PHA products, if not disposed properly make their way back in the environment as persistent pollutants in the aquatic system. The level of the PHA's compounds in the water remains in the range of µg/L to ng/L, but still, the continuous influx of these materials has a deleterious effect on the environment (Nawaz et al., 2017). Along with PHA's, E.D.C's are also an important group of trace organic pollutants which mimics the activity of the hormone estrogen and can alter and harm the hormonal system of the body (Chouhan et al., 2014; Gogoi et al., 2018). Therefore, exploring environmentally friendly and efficient techniques to remove this type of trace organic pollutants from the environment should be a priority concern.

Different techniques have been studied to remove these contaminants that include filtration, evaporation, coagulation, chemical precipitation, ion exchange, electrodeposition, solvent extraction, membrane system, adsorption and reverse osmosis (Zhang et al., 2019). The most commonly used technology to eliminate the pollutants from wastewater is adsorption due to operational simplicity and economic feasibility (Zhang et al., 2019). Adsorption is a cost-effective technique to remove pollutants, but it does not result in the complete mineralization of contaminants (Shen, Zhu, Chen, Fang, et al., 2020). The total destruction of the contaminants can only be attained by oxidation, either photo-chemically or chemically. $TiO_2$ is widely used as a photo-catalyst for treatment of dyes (Xu et al., 2013), phenol (Alim et al., 2016), and toxic aromatic vapours removal (Jo & Kang, 2013) because of its non-toxic and photo-stable nature (Singh & Mehata, 2019). However, $TiO_2$ has a very wide bandgap (Singh & Mehata, 2019) and the rapid recombination rate between electron–hole pairs makes it inefficient for

practical applications (Yang et al., 2013). To overcome these problems, $TiO_2$ are often attached to supporting structures to enhance its operability and functionality (Zhu et al., 2020b). GO is one such component which has high surface area, ample pores and changeable properties (Zhu et al., 2020a). Structurally, GO is two-dimensional (2-D) which facilitates its operability as a channel for electron transport (Wu et al., 2020). Therefore, GO is able to promote the catalytic activity of photo-catalyst materials like $TiO_2$ (Wu et al., 2020). GO also has a prominent capacity for the adsorption of benzene ring containing compounds (Shen, et al., 2020). Therefore, the doping of $TiO_2$ with GO has various advantages to oxidize the pollutants (Yang et al., 2013). The mechanism of photoelectron generation and the subsequent photo-catalysis by $TiO_2$ can be elaborated as :- The first step of photoreaction activity is photo-reduction that entails the excitement of electrons from GO-$TiO_2$ nano-sheet valence band (VB) to the conduction band (CB) after absorbing light energy (photon) and resulting in the formation of holes ($h^+$). The generated holes cannot oxidize ($H_2O$) into ($OH^\bullet$) radical directly. However, these photo-generated electrons reduce $O_2$ to super-oxide radicals ($O_2^{\bullet-}$), and then generate ($OH^\bullet$) radical through ($O_2^{\bullet-}$)- $H_2O_2$-($OH^\bullet$) pathway (Shen et al., 2019; Shen et al., 2020). The generated radicals in the above process are highly responsive and represents as one of the important intermediates in the process of oxidation of different contaminants. These generated radicals successively degenerate the pollutants to innocuous end-products (Chowdhury & Balasubramanian, 2014). In this particular study three PHA compounds (CBZ, NPX and RTN) and one EDC compound (BPA) was used as the target pollutant. The synthesis of GO-$TiO_2$ composite was done by a solvo-thermal method following the method of (Xiang et al., 2012). The characterization was done with SEM, XRD, FTIR and Raman spectroscopy analysis. The band gap of the GO-$TiO_2$ composite was evaluated by the Kubelka-Munk equation from its UV-visible spectroscopy by plotting a Tauc plot (Fazal et al., 2020; L. Xu et al., 2018). Firstly, a screening study was done with UVA, UVB, UVC and visible light for finding the most suitable radiation for activating the GO-$TiO_2$ composite. Then a series of batch studies were performed with different experimental parameters like concentration of the pollutant, dosage of photo-catalyst, pH of the experimental solution and agitation speed of the reactor in order to find the conditions under which the highest removal of the EC's by the GO-$TiO_2$ was possible. The process was further optimized with RSM. The adsorption efficiency of the GO-$TiO_2$ composite was evaluated in an RPB method, followed by photo-catalysis. The reusability of GO-$TiO_2$ after treating the pollutant was also evaluated.

## 6.2 MATERIALS AND METHODS :-

### 6.2.1 Materials required

The $TiO_2$ powders were acquired from Platonic. The rest of the materials was collected in the same manner as mentioned in the previous chapter, **Chapter 4, Section 4.2.1.**

### 6.2.2 Synthesis of GO

GO was synthesized using the same procedure as mentioned in **Chapter 4, Section 4.2.2.**

### 6.2.3 Synthesis of GO-TiO$_2$

The GO-$TiO_2$ composite was synthesized with 9 parts by weight of GO and 1 part by weight of $TiO_2$ (a 3:1 physical mixture of Anatase phase and Rutile phase) by following a solvothermal process. First, 190 mg of GO was added to a solution of 40% ethanol solution. Followed by which the sample was ultra-sonicated for 30 minutes with a frequency of 40 kHz and power of 100 W. Followed by this, 10 mg of $TiO_2$ (3:1 weight of Anatase and Rutile) was added to this solution and then it was stirred for 30 minutes with a magnetic stirrer. Then the whole solution was transferred to a Teflon lined autoclave which was heated at 120°C for 12 hours. After the completion of the solvothermal reaction, the supernatant was drained off and the composite was obtained as the precipitate. It was then washed three times with alcohol and three times with demineralized water. The product was then dried by freeze drying and stored in a cool dry place for further use (Bhattacharya et al., 2022; Xiang et al., 2012).

### 6.2.4 Characterization

Characterization of the synthesized GO-$TiO_2$ particles were done by SEM, XRD, FTIR and Raman Spectroscopy.

The particulars are the same as mentioned in **Chapter 4, Section 4.2.3.**

The absorbance spectra was measured in a UV-Vis spectrophotometer (Perkin Elmer, Lambda-360) in the spectral range of 200-1100 nm.

### 6.2.5 Preparation of the Experimental Solution.

Using the same process as mentioned **Chapter 4, Section 4.2.4.**

### 6.2.6 Screening Study

The screening for the most appropriate wavelength for the activation of the GO-TiO2 composite was done with three types of UV radiations UVA, UVB and UVC and visible light. The UV lights were placed inside a UV reactor. The visible lights were placed inside a BOD reactor. The UV lights were the tube light (Phillips) with each of them having a wattage of 6 W. The visible lights were LED bulbs also having a wattage of 6 W. For the screening test, the concentration of the solution of the EC's were

taken as 10 mg/L. The dosage of GO-TiO2 were taken as 2 g/L. The pH of the experimental solution was kept neutral, the temperature was kept at room temperature (in case of the BOD incubator the temperature was kept at 303 K, the UV reactor had no provision for temperature control). Samples were taken at pre-determined time intervals. After taking samples, they were filtered, centrifuged and measured spectrophotometrically by following the same techniques as mentioned in **Chapter 4, Section 4.2.5.**
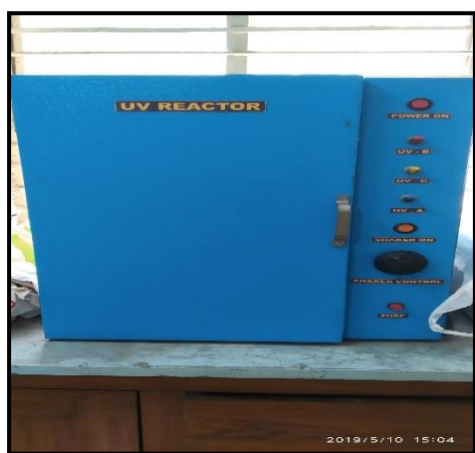


**Fig. 6.1 :-** UV reactor



**Fig. 6.2:-** Incubator for visible light Reaction.

## 6.2.7 Batch study

A batch study was performed in order to find the experimental conditions under which the highest removal of the EC's by the GO-TiO$_2$ was possible. Four experimental parameters were investigated namely concentration of the EC's (5 mg/L-20 mg/L), dosage of the photo-catalyst (0.5 g/L- 2 g/L), pH of the experimental solution (pH 2 – pH 10) and agitation speed of the reactor (80 RPM – 120 RPM). Before turning on the incident light, the EC's were stirred with the GO-TiO$_2$ in the dark for 30 minutes in order for the adsorption equilibrium to take place. Followed by which the incident light was turned on.

The sample collection, filtration, centrifugation and the analysis of EC's in sample before and after treatment were done by following the same method as mentioned in **Chapter 4, Section 4.2.5**.

## 6.2.8 Process optimization with RSM

In case of the RSM study, the Box Behnken Model (BBM) was used for optimizing the removal of the EC's by GO-TiO$_2$. The input parameters were the pH of the experimental solution, the dosage of GO-TiO$_2$ and the agitation speed of the UV reactor in RPM. The concentration of the EC's were kept fixed at 10 mg/L and each experimental run was conducted for a fixed time of 1 hour. The number of experimental runs suggested by BBM model is 17. The output was recorded as the percentage removal.

### 6.2.9 Process Intensification with the RPB study

A RPB study was conducted in order to evaluate the adsorption efficiency of the GO-TiO$_2$ composite. Firstly, a 10 mg/L solution of each of the EC's were taken and to it the GO-TiO$_2$ composite was added at a dosage of 2 g/L. Then the experimental solution consisting of the EC and the GO-TiO$_2$ composite were irradiated with activating radiation for 1 hour. Then the whole experimental solution was transferred to the reservoir used for holding the experimental solution in the RPB. The rest of the process was similar to what has been described in **Chapter 4, Section 4.2.8**.

### 6.2.10 Reusability study of the GO-TiO$_2$

Following the same procedure as mentioned in **Chapter 4, Section 4.2.8**.

## 6.3 CALCULATIONS :-

### 6.3.1. Percentage removal

Same as mentioned in **Chapter 4, Section 4.3.1**.

### 6.3.2. Optimization using RSM

Same as mentioned in **Chapter 4, Section 4.3.5.**

## 6.4 RESULTS :-

### 6.4.1 Characterization

#### 6.4.1.1 SEM analysis of GO-TiO$_2$

**Fig. 6.3(a)** shows the SEM image of GO-TiO$_2$ nanocomposite. By comparing the SEM images of the GO (**Chapter 4, Section 4.4, Fig. 4.3(a)**) with that of the GO- TiO$_2$ nanocomposites, it can be inferred that the surface of GO-TiO$_2$ had the same rough, lamellar structure of GO as reported in previous literatures (Banerjee et al., 2015b; P. Das & Das, 2016). Moreover the surface of GO were interspersed with tiny particles which could be attributed to be TiO$_2$ particles. In accordance with the previous literature (Nawaz et al., 2017; Williams et al., 2008), it can be stated that TiO$_2$ attaches itself to the surface by physical sorption, electrostatic binding, or charge transfer (Al-shamali, 2013; M. J. Li et al., 2014; Nawaz et al., 2017). This morphology of the GO-TiO$_2$ composite, enhances its adsorption capacity, which in turn helps to promote the photo-catalysis by TiO$_2$.
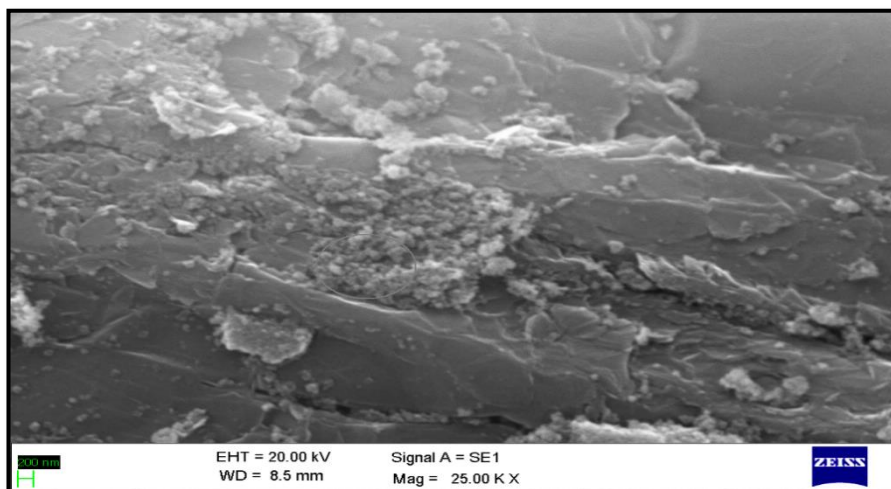
**Fig. 6.3 (a)**:- SEM image of GO-TiO$_2$

### *6.4.1.2 FTIR analysis of GO-TiO$_2$*

The FT-IR spectrum of the GO-TiO$_2$ composite is represented in **Fig. 6.3 (b)**, which shows distinctive peaks at 3430 cm$^{-1}$, 1620 cm$^{-1}$, 1050 cm$^{-1}$ and 550 cm$^{-1}$ which could be assigned to the O–H hydroxyl bond vibration, C = C bond vibration and C-O bond vibration, respectively. The simultaneous presence of the O–H bond, and C = C on the surface of GO marks the presence of the -COOH carboxyl functional group which could be considered as the site of attachment of TiO$_2$ on the surface of GO (Ganguly et al., 2020). The peak at 550 cm$^{-1}$ can be assigned to the stretching vibration of Ti–O-C which further confirms the presence of TiO$_2$ in the nanocomposite (Ye et al., 2020). Moreover, reduction in the number of functional groups of GO-TiO$_2$ nanocomposite compared to that of synthesized GO (**Chapter 4, Section 4.4, Fig. 4.3(b)**)), can be attributed due to the reduction of GO by TiO$_2$ under high temperature and pressure. Therefore, from the FT-IR analysis of the GO- TiO$_2$ nano-composite, it can be implied that the TiO$_2$ was combined with GO during the synthesis of the nanocomposite by the hydro-thermal treatment.
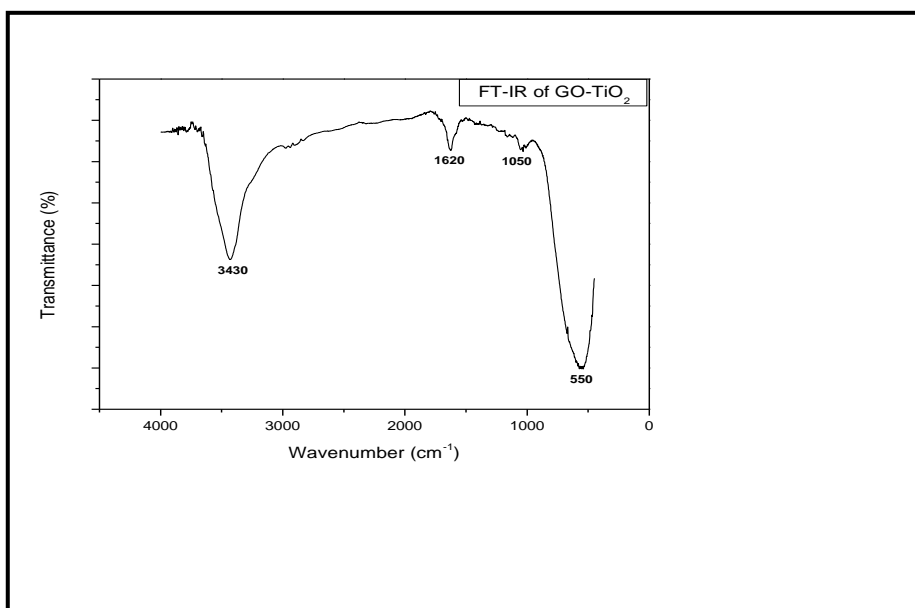
**Fig. 6.3 (b)**:- FT-IR spectra image of GO-TiO$_2$

### 6.4.1.3  XRD analysis of GO-TiO$_2$

The XRD peaks (**Fig. 6.3 (c)**) of GO-TiO$_2$ were observed at 25.48°, 37.99°, 48.07°, 54.97°, 62.63°, 70.25° and 75.25° denotes the characteristic peak assigned to (101), (004), (200), (211), (204), (116), and (215) planes of TiO$_2$ (Li et al., 2016; Ye et al., 2020a). From **Fig. 6.3 (c)**, anatase phase of TiO$_2$ (peak at 25.4°, 37.7°, 48.10°, 62.7°, 70.4°, 75.4°) and a small peak of rutile phase (peak at 54.97°) of TiO$_2$ was observed (Li et al., 2016; Ye et al., 2020a). The absence of distinctive peak of rutile (except 54.97°) can be attributed to its low concentration present in the mixture composite. No characteristic peak of GO ($2\theta = 10-12°$) (Banerjee et al., 2015b) was observed in the XRD spectrum, thereby implying that the GO was reduced to reduced GO or rGO during the synthesis of the nanocomposite by the solvothermal treatment (Li et al., 2016).
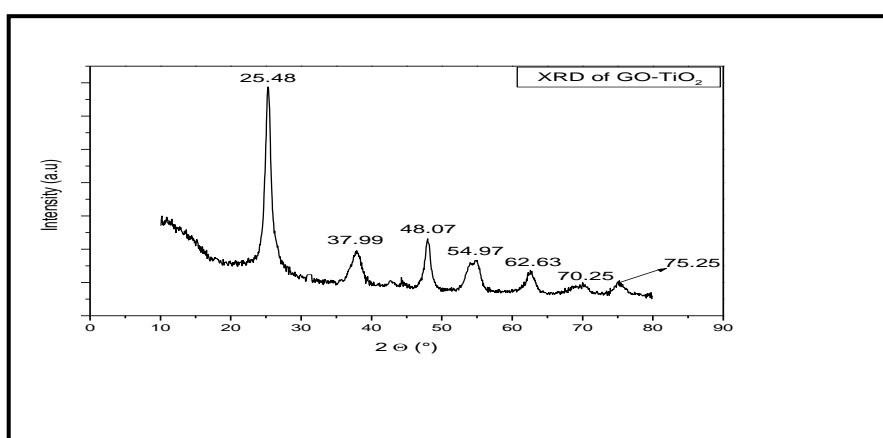


**Fig. 6.3 (c)**:- XRD image of GO-TiO$_2$

*6.4.1.4 Raman Spectroscopy of GO-TiO₂*

From the Raman Spectra of GO-TiO₂ is show in **Fig. 6.3 (d)**, the D-band and the G-band were observed at 1331 cm$^{-1}$ and 1572.41 cm$^{-1}$ respectively. The D-band denotes the sp$^2$ carbon atom with structural defect proportional to the extent of oxidation and the G-band denoted the in-plane vibration of sp$^2$ bonded graphitic structure (Zhang et al., 2018). The ratio of $I_D/I_G$ serves as the parameter for observing the defects and disorders in graphitic structures (Nawaz et al., 2017). In the case of the GO-TiO₂ the ratio of $I_D/I_G \sim 1.1$, thereby signifying that the structure of sp$^3$ hybridized carbon molecules were disordered, which could be attributed to the decreased size of the sp$^2$ hybridized molecules, thereby marking that the TiO₂ was able to reduce the GO molecules (Nawaz et al., 2017).
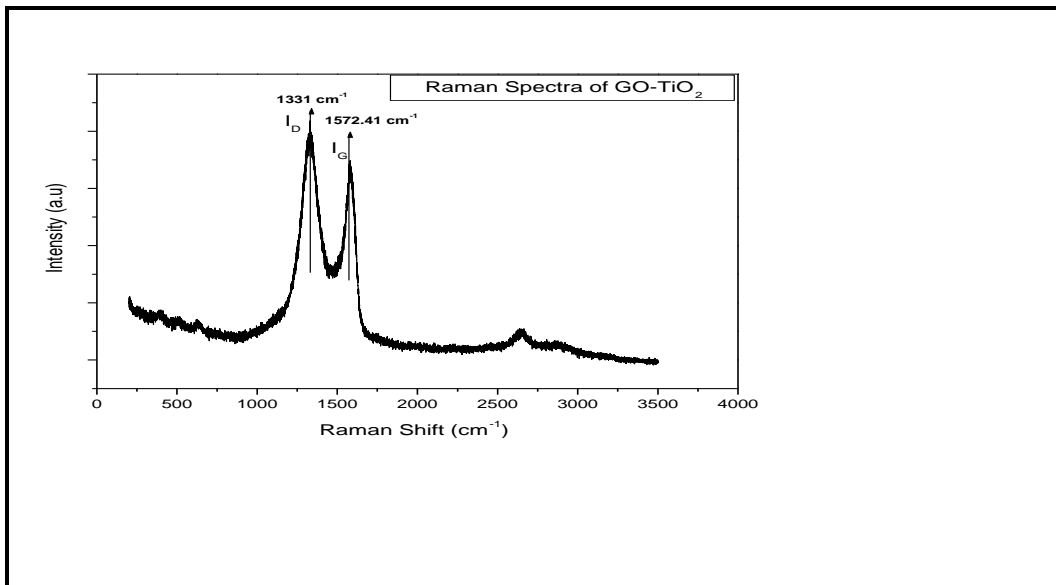


**Fig. 6.3 (d)** :- Raman Spectra of GO-TiO₂

*6.4.1.5 UV adsorption spectra and Band gap of GO-TiO₂*

From the UV absorbance spectra of GO, TiO₂ and GO-TiO₂ spectra (**Fig. 6.3 (e)**) it was observed that the peak absorbance of GO-TiO₂ shifted to the right side as compared to GO and TiO₂, thereby signifying that the composite material was more well suited for adsorbing light at a higher wavelength. This could be attributed to the combination of GO with TiO₂ during the solvothermal reaction which in turn can lower the band gap of the TiO₂ molecule (Fazal et al., 2020; Nawaz et al., 2017; L. Xu et al., 2018).

The energy of the incoming wavelength was calculated by the equation

$E_g$ = hv …………………………………………………………………………………...(xxxix)

Where, $E_g$ is the band gap energy (eV) and 'h' is the Plank's constant and 'v' is the frequency of the incoming radiation.

$E_g$ can also be represented as :-

$E_g = 1240/ \lambda$…………………………………………………………………………(xxxx)

Where $\lambda$ is the wavelength of the incoming radiation.

The band gap of the GO, $TiO_2$ and the GO-$TiO_2$ composite was evaluated by virtue a Tauc plot by plotting $E_g$ vs the Kubelka Munk function $\alpha h v^2$, where '$\alpha$' is the adsorption coefficient. From the plot of $E_g$ vs $\alpha h v^2$ (**Fig. 6.3 (f)**), a slope was obtained. A tangent was drawn against the linear part of the slope and the point where the tangent dissected the x-axis denoted the band gap of that material (Fazal et al., 2020; Xu et al., 2018). From the corresponding analysis, the band gap of GO, $TiO_2$ and GO-$TiO_2$ were obtained as 3.4 eV, 3.44 eV and 3.24 eV respectively. The lowering of the band gap for GO-$TiO_2$ can be attributed to the formation of Ti-O-C bond which results in a formation of a new energy layer, thereby decreasing the energy required by the electron to move from the valance band to the conduction band (Wang et al., 2016).
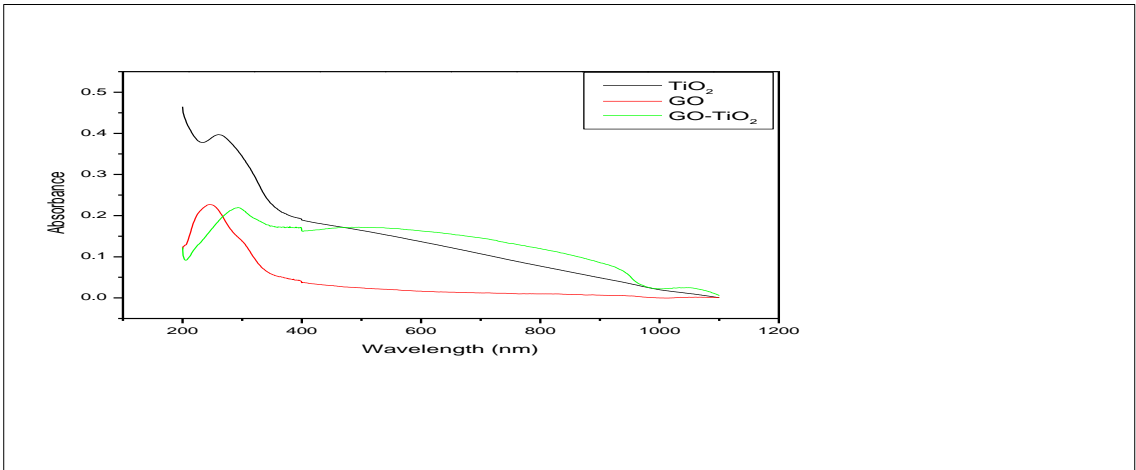


**Fig. 6.3 (e) :-** UV-Vis spectra of $TiO_2$, GO and GO-$TiO_2$
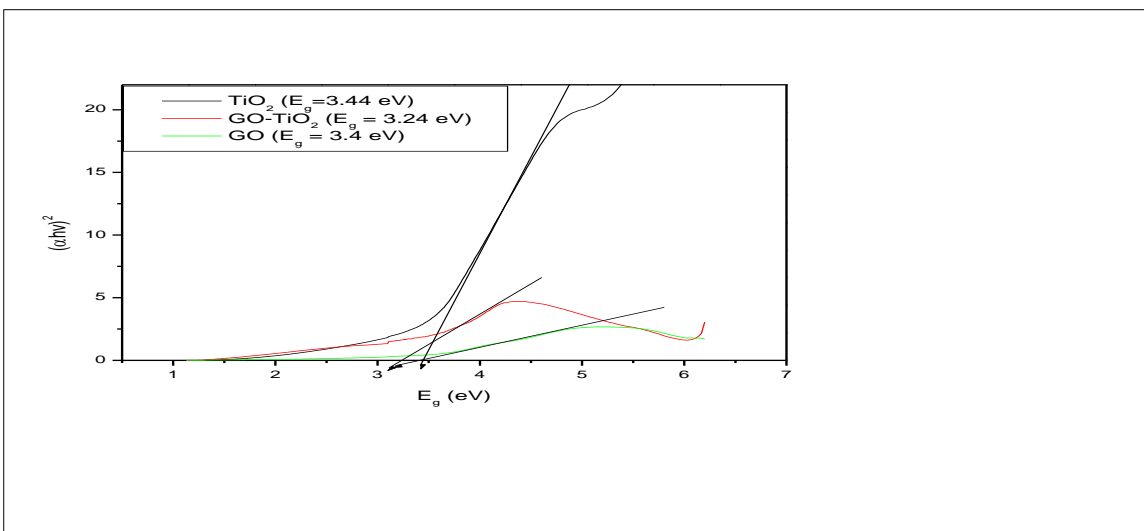


**Fig. 6.3 (f) :-** Energy band gap of $TiO_2$, GO and GO-$TiO_2$

## 6.4.2 Comparative Removal Study

At first a comparative study was performed in order to find which wavelength can most suitably excite the GO-TiO$_2$ composite. As mentioned before, the concentration of the four EC's (CBZ, NPX, RTN and BPA) were kept constant at 10 mg/L. The dose of the GO-TiO$_2$ was taken as 2 g/L. All the other parameters were also kept constant. The radiations used for activating the GO-TiO$_2$ composite were UVA, UVB, UVC and visible light. From the result of the experiment as shown in **Fig. 6.4** it was observed that in each case the radiation UVA exhibited the highest efficiency for the purpose of removing the materials. This can be ascribed to two facts, firstly, the band gap of GO-TiO$_2$ was 3.24 eV thereby denoting they could be only be activated by UV light (3.1-3.94 eV for UVA light, 3.94-4.43 eV for UVB light and 4.43 eV- 12.4 eV for UVC light) (Bhattacharya et al., 2022) and the photon energy of visible light (2-2.74 eV) (Diwald et al., 2004) is not sufficient to activate the GO-TiO$_2$. Therefore, the removal by GO-TiO$_2$ in case of visible light is almost exclusively due to adsorption. In case of the UV lights, the highest removal was observed in case of UVA light as because, as all the lights were operating at the same wattage, then the source of light with lowest photon energy would emit the highest number of photons. Thus UVA tube lights emitted the highest number of photons. And as the energy of the UVA radiation was enough to excite the GO-TiO$_2$ composite therefore highest efficiency was exhibited by UVA radiation in case of each of the EC's. And due to their stable chemical structure, none of the molecules of EC's were degraded by UVA light or visible light on their own. Thus highest efficiency was exhibited by the UVA light and thus it was used in further studies.
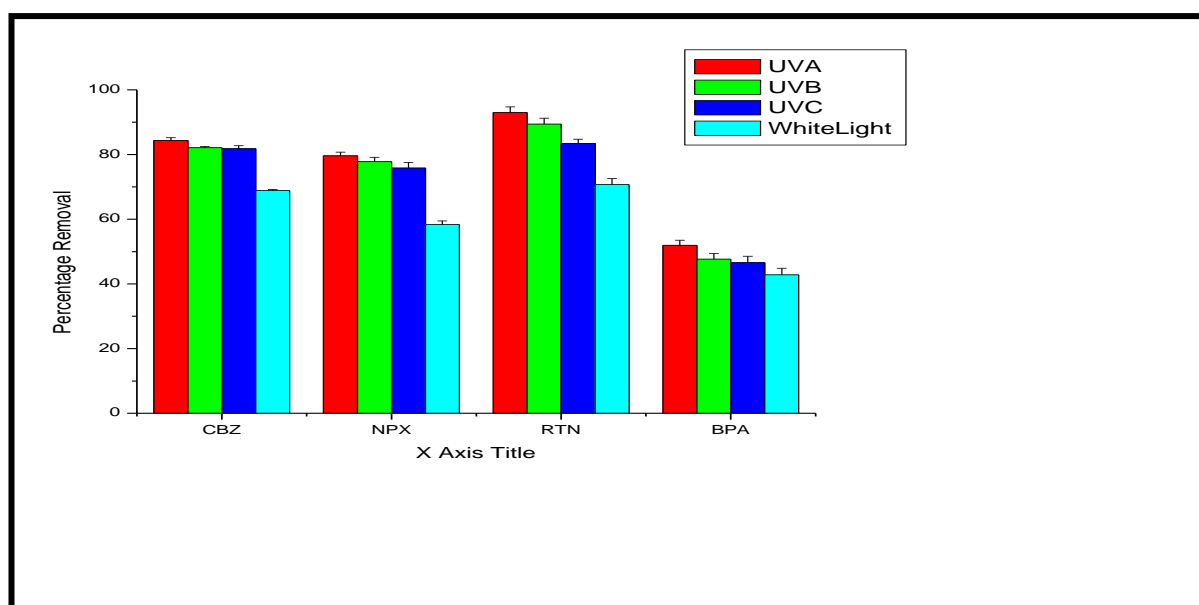


**Fig. 6.4**:- Effect of incident radiation on the removal of the EC's by GO-TiO$_2$

### 6.4.3 Batch Study Results

*6.4.3.1 Effect of concentration of the EC's on the removal efficacy of GO-TiO$_2$*

In order to investigate the effect of concentration of EC's on the removal efficiency of GO-TiO$_2$ a batch study was conducted with four concentration of the EC's namely 5 mg/L, 10 mg/L, 15 mg/L and 20 mg/L. The dose of GO-TiO$_2$ was kept constant at 2 g/L, the pH of the experimental solution was kept neutral and the agitation speed kept at 120 RPM. The result of the experiment is shown in **Fig. 6.5((a)-(d))**. A similar trend was observed in case of each of the EC's that is the removal of the EC's was higher for the lower concentration range and correspondingly decreased with the increase in concentration of the EC's. This could be attributed to the fact that with increase in concentration, the surface area available for the adsorption of the EC's molecules got saturated. And as the rate of photocatalysis is dependent on the rate of adsorption of the EC molecules on the surface of GO-TiO$_2$ (Nawaz et al., 2017; L. Xu et al., 2018; Yu Zhang et al., 2018) therefore the removal of the EC's by GO-TiO$_2$ also decreased with increase in concentration of the EC's . For CBZ, (**Fig. 6.5 (a)**) the highest removal was observed in case of 5 mg/L (95.94%), followed by 10 mg/L (91.65 %), followed by 15 mg/L (79.92 %), followed by 20 mg/L (74.08 %). For NPX (**Fig. 6.5 (b)**), the highest removal was observed in case of 5 mg/L (89.56 %), followed by 10 mg/L (80.71 %), followed by 15 mg/L (74.07 %), followed by 20 mg/L (72.38 %). In case of RTN (**Fig. 6.5(c)**) the highest removal was observed in case of 5 mg/L (94.11 %), followed by 10 mg/L (93.84 %), followed by 15 mg/L (88.14 %), followed by 20 mg/L (83.3 %). In case of BPA (**Fig. 6.5(d)**) the highest removal was observed in case of 5 mg/L (99.65 %), followed by 10 mg/L (72.5 %), followed by 15 mg/L (70.46 %), followed by 20 mg/L (64.8 %). For further experiments, the 10 mg/L concentration of the EC's were used.
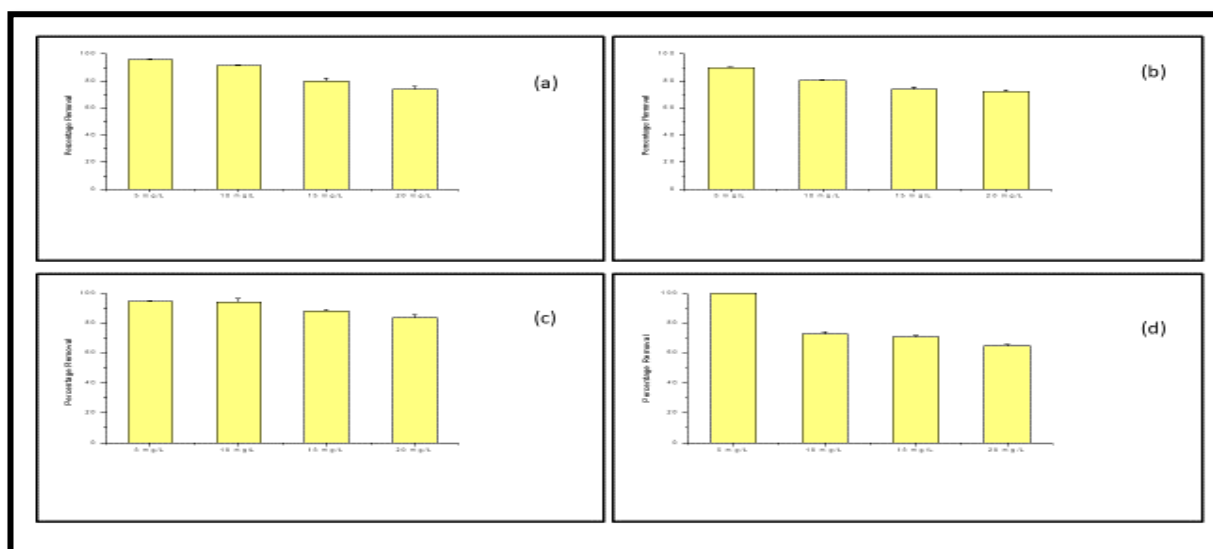


**Fig. 6.5:-** Effect of concentration on removal of **(a)** CBZ **(b)** NPX **(c)** RTN **(d)** BPA by GO-TiO$_2$

### 6.4.3.2 *Effect of dosage of photo-catalyst GO-TiO₂ on the removal of the EC's by GO-TiO₂*

The effect of the dosage of the photo-catalyst on its removal efficacy was investigated over four different dosage of GO-TiO$_2$ i.e., 0.5 g/L, 1 g/L, 1.5 g/L and 2 g/L. The concentration of EC's were kept constant at 10 mg/L, the pH of the experimental solution was kept neutral and the agitation speed was kept 120 RPM. From the result of the experiment as shown in **Fig. 6.6 ((a)-(d))** it was observed that the removal of EC's by GO-TiO$_2$ increased with increase in dosage of GO-TiO$_2$. This outcome could be attributed to the greater availability of active sites at higher dosage of GO-TiO$_2$ which facilitates the higher adsorption and subsequent greater photo-catalysis of the EC's (Bhattacharya et al., 2022; Dong et al., 2015; L. Xu et al., 2018). In case of the removal of CBZ by GO-TiO$_2$ (**Fig. 6.6(a)**), the removal at the 0.5 g/L dose of GO-TiO$_2$ was observed to be 77.71 %, the removal at 1 g/L dosage was found to be 85.23 %, at 1.5 g/L dosage was found to be 91.73 % and at the 2 g/L dosage was 92.91 % respectively. Also the higher dosage of GO may have facilitated the greater adsorption of CBZ molecules on its surface by virtue of π-π bonds (Ziegmann & Frimmel, 2010). In case of NPX (**Fig. 6.6 (b)**), the removal at the 0.5 g/L dose of GO-TiO$_2$ was observed to be 65.22 %, the removal at 1 g/L dosage was found to be 79.59 %, at 1.5 g/L dosage was found to be 81.1 % and at the 2 g/L dosage was 85.96 % respectively. In case of the removal of RTN (**Fig. 6.6 (c)**), the removal at the 0.5 g/L dose of GO-TiO$_2$ was observed to be 86.54 %, the removal at 1 g/L dosage was found to be 91.27 %, at 1.5 g/L dosage was found to be 92.51 % and at the 2 g/L dosage was 94.95 % respectively. In case of BPA (**Fig. 6.6 (d)**) the removal at the 0.5 g/L dose of GO-TiO$_2$ was observed to be 41.16 %, the removal at 1 g/L dosage was found to be 53.77 %, at 1.5 g/L dosage was found to be 69 % and at the 2 g/L dosage was 76.71 % respectively. In case of all the EC's the highest removal was achieved for the 2 g/L dosage of GO-TiO$_2$ therefore this dosage of GO-TiO$_2$ was utilized for further studies.
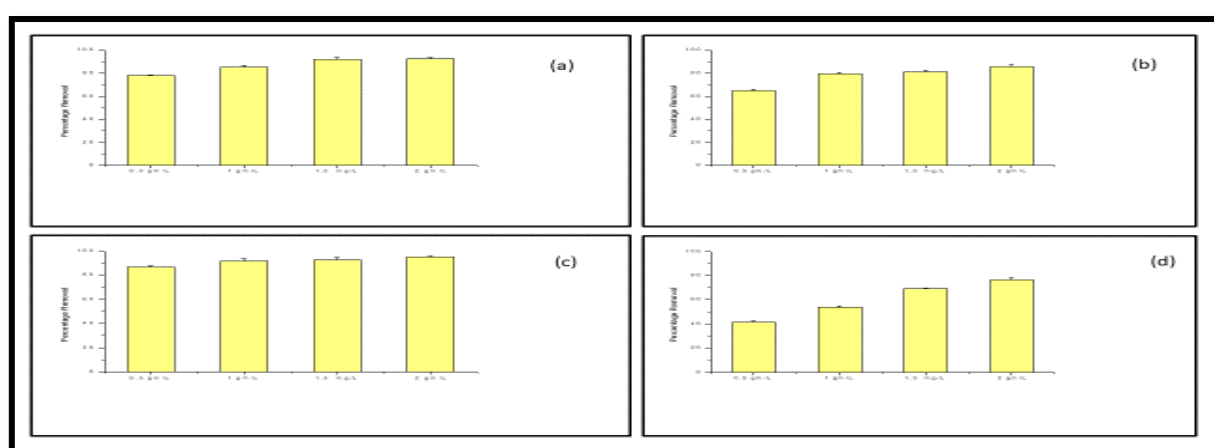


**Fig. 6.6:-** Effect of GO-TiO$_2$ dosage on the removal of **(a)** CBZ **(b)** NPX **(c)** RTN **(d)** BPA by GO-TiO$_2$

### 6.4.3.3 Effect of pH of the experimental solution on the removal efficacy of GO-TiO$_2$

The effect of pH on the removal of EC's by GO-TiO$_2$ was investigated under five different pH of the experimental solution, viz., pH 2, pH 4, pH 6, pH 8 and pH 10. The concentration of EC's were kept constant at 10 mg/L and the dosage of GO-TiO$_2$ was kept fixed at 2 g/L. The result of the experiment is given in **Fig. (6.7 (a)-(d))**. From the result of the experimental study as shown in **Fig. 6.7(a)** it was observed that the removal of CBZ by GO-TiO$_2$ was highest at the lower pH range, with the removal percentage being 93.58 % at pH 2 and 91.87 % at pH 4. On increasing the pH further from pH 6 to pH 10, the removal percentage decreased to 90.04 % (pH 6), 85.49 % (pH 8) and pH 10 (81.53 %). The pH$_{pzc}$ of GO-TiO$_2$ was obtained to be 4.5 and the pK$_a$ value of CBZ is around 13.9 (Al-hamadani et al., 2018). The logic behind this result can be given as, the presence of high amount of GO in the GO-TiO$_2$ composite imparts a negative charge to the surface of the GO-TiO$_2$. As a consequence of which at the lower pH range, the attachment of the CBZ molecules on the surface of GO is enhanced leading to the greater adsorption and subsequent greater photo-degradation of CBZ at the lower pH range (Bhattacharya et al., 2022). When the pH of the experimental solution was further increased, the removal of CBZ by GO-TiO$_2$ decreased which could be attributed to the force of repulsion between the negative charge on the surface of GO-TiO$_2$ and the OH$^-$ ions present in the experimental solution.

In case of NPX **Fig. 6.7(b)** it was observed that the removal of NPX by GO-TiO$_2$ was highest at the lower pH range, with the highest removal percentage being recorded at pH 2 (91 %), followed by pH 4 (88.57 %), pH 6 (85.55 %), pH 8 (84.81 %) and pH 10 (77.53 %). The reason behind this phenomenon can be attributed to the fact that, the pH$_{pzc}$ of GO-TiO$_2$ was 4.5 and the pKa value of NPX was 4.15 (Mondal et al., 2020). Therefore at pH less than pH 4, the molecules of NPX remains neutrally charged and the surface of GO-TiO$_2$ remains positively charged. And at pH greater than pH 5, both the molecules of NPX and the surface of GO-TiO$_2$ acquires a negative charge. As a consequence of which at the lower pH range, more adsorption of NPX molecules takes place on the surface of GO-TiO$_2$ by virtue of H-H bonding and van der Waals force between the GO particles and the NPX molecules (Bhattacharya et al., 2021). However, with the eventual increase in the pH of the experimental solution, a force of repulsion takes place between the negatively charged surfaces of GO particles and the negatively charged NPX molecules. As a consequence of which the uptake of the NPX molecules by the surface of the GO-TiO$_2$ composite decreases at higher pH range, resulting in reduced adsorption and subsequently reduced photo-degradation at the higher pH range.

In case of the removal of RTN by GO-TiO$_2$ (**Fig. 6.7 (c)**) it was observed that the removal increased with the increase in pH from pH 2 to pH 8, followed by which a decrease in the removal of RTN by GO-TiO$_2$ was observed. The removal of RTN by GO-TiO$_2$ at pH 2 was 91.65 %, at pH 4 was 94.92 %, at pH 6 was 95.05 %, at pH 8 was 95.27 % and at pH 10 was 91.11 %. The result of the experiment can

be explained as follows, the drug RTN has two $pK_a$ values at 2.6 and 8.2 (Kortejarvi et al., 2005). As a consequence of which the molecules of RTN are positively charged at pH below 2.6 and negatively charged at pH above 8.2 (Al-rub et al., 2020). In the pH between 2.6 and 8.2 the molecules of RTN remains neutrally charged. On the other hand, the $pH_{pzc}$ of GO-TiO$_2$ has been found to be 4.5, as a consequence of which at a pH less than pH 4.5 the surface of GO-TiO$_2$ remains positively charged and at a pH greater than pH 4.5, the surface of GO-TiO$_2$ remains negatively charged. Therefore in the pH range of 4 to 8, the molecules of RTN remain neutrally charged and the surface of GO-TiO$_2$ remains positively or negatively charged. As a consequence of which, the molecules of RTN are more actively adsorbed on the surface of GO-TiO$_2$ at this pH range. At the lower pH range, both the molecules of RTN and the surface of GO-TiO$_2$ retain a positive charge, as a result of which the adsorption is inhibited due to electrostatic force of repulsion. In the same way, at the higher pH range the adsorption of RTN molecules on the surface of GO-TiO$_2$ is inhibited due to the accumulation of similar negative charge on the surface of GO-TiO$_2$ and the molecules of RTN (Al-rub et al., 2020). And as in the case photo-degradation, photo-catalysis mainly happens to the molecules which are adsorbed on the surface (Zhang et al., 2018) therefore the removal of RTN increases with the increase in adsorption rate. As a consequence of which the highest removal was observed at the pH range of pH 4-8, with the highest removal being observed at pH 8 (95.27 %).

In case of the removal of BPA by GO-TiO$_2$ (**Fig. 6.7 (d)**) it was observed that the highest removal was at the lower pH range, with the removal percentage being 95.27 % at pH 2 and 98.42 % at pH 4. On increasing the pH further from pH 6 to pH 10, the removal percentage decreased to 84.06 % (pH 6), 76.01 % (pH 8) and 74.08 % (pH 10). The logic behind this result can be given as, the $pH_{pzc}$ of GO-TiO$_2$ was around pH 4.5. Therefore at pH less than pH 4.5, the surface of GO-TiO$_2$ remains positively charged and at pH greater than 4.5, the surface of GO-TiO$_2$ remains negatively charged. On the other hand, the $pK_a$ value of BPA is 9.6 (Phatthanakittiphong & Seo, 2016), and at pH equal to or near pH 9, the molecules of BPA dissociate to form bis-phenolate anions, thereby obtaining a negative charge. At pH less than 9.6, the molecules of BPA remain positively charged (Xu et al., 2012). Therefore at the lower pH range, the adsorption of BPA by GO-TiO$_2$ was facilitated due to the negative surface charge of GO-TiO$_2$ and the positive charge of BPA molecules. When the pH of the experimental solution becomes closer to pH 8, the BPA molecules dissociates to form bis-phenolate anions (Xu et al., 2012). As a consequence of which, the adsorption of BPA molecules by GO-TiO$_2$ is hindered at this higher pH range due to electrostatic force of repulsion between the like charges. And as the photo-catalysis is preceded by adsorption, therefore the photo-degradation of the BPA molecules are higher at the lower pH range and the removal of BPA by GO-TiO$_2$ decreases with increase in pH of the experimental solution (Dong et al., 2015).
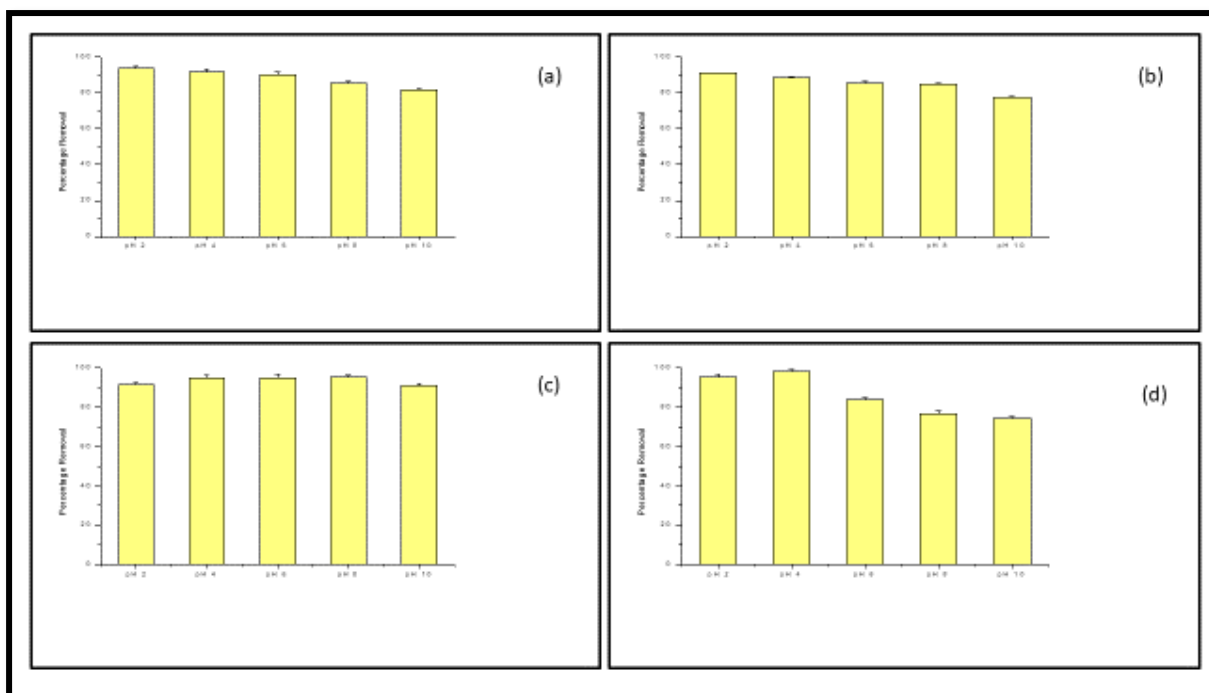
**Fig. 6.7 :-** Effect of pH on the removal of **(a)** CBZ **(b)** NPX **(c)** RTN **(d)** BPA by GO-TiO$_2$

*6.4.3.4 Effect of agitation speed on the removal of EC's by GO-TiO$_2$*

The effect of agitation speed on the removal of EC's by GO-TiO$_2$ was investigated for three sets of RPM namely 80, 100 and 120. In case of each of these experiment, the dosage of GO-TiO$_2$ was kept constant at 2 g/L, the pH of experimental solution was kept at neutral and the concentration of EC's was kept fixed at 10 mg/L. The result of the experiment is given in (**Fig. 6.8 (a)-(d)**). From there a similar trend was observed in case of each experiment, i.e., the removal of the EC's increased with the increase in agitation speed of the photo-reactor. This could be attributed to the greater interaction between the molecules of EC and the surface of GO-TiO$_2$ due to the higher agitation speed. As a consequence of which, when the agitation speed increases the adsorption of the EC's by GO-TiO$_2$ increases and as a consequence of which the rate of photo-catalysis also increases (Bhattacharya et al., 2022; Dong et al., 2015; Xu et al., 2018). Similar result was observed in case of the study of (Bhattacharya et al., 2022). However, when the agitation speed was increased beyond 120 RPM, no further increase in the removal of EC's by GO-TiO$_2$ was observed which could be attributed to the dislodging of the EC molecules from the surface of GO-TiO$_2$. In case of the removal of CBZ by GO-TiO$_2$ (**Fig. 6.8 (a)**), the removal percentage at 80 RPM was observed to be 75.47 %, the removal at 100 RPM was observed to be 91.51 % and the removal at 120 RPM was observed to be 92.93 %. In case of NPX (**Fig. 6.8 (b)**) the removal at 80 RPM was observed to be 75.25 %, the removal at 100 RPM was observed to be 80.82 % and the removal at 120 RPM was observed to be 85.08 %. In case of RTN (**Fig. 6.8 (c)**) the removal at 80 RPM was observed to be 86.3 %, the removal at 100 RPM was observed to be 91.97 % and the removal at 120 RPM was observed to be 95.35 %. In case of BPA (**Fig. 6.8 (d)**) the

167

removal at 80 RPM was observed to be 67.25 %, the removal at 100 RPM was observed to be 75.83 % and the removal at 120 RPM was observed to be 77.41 %.

As because the highest removal was observed at 120 RPM therefore this agitation speed was used for the batch studies.
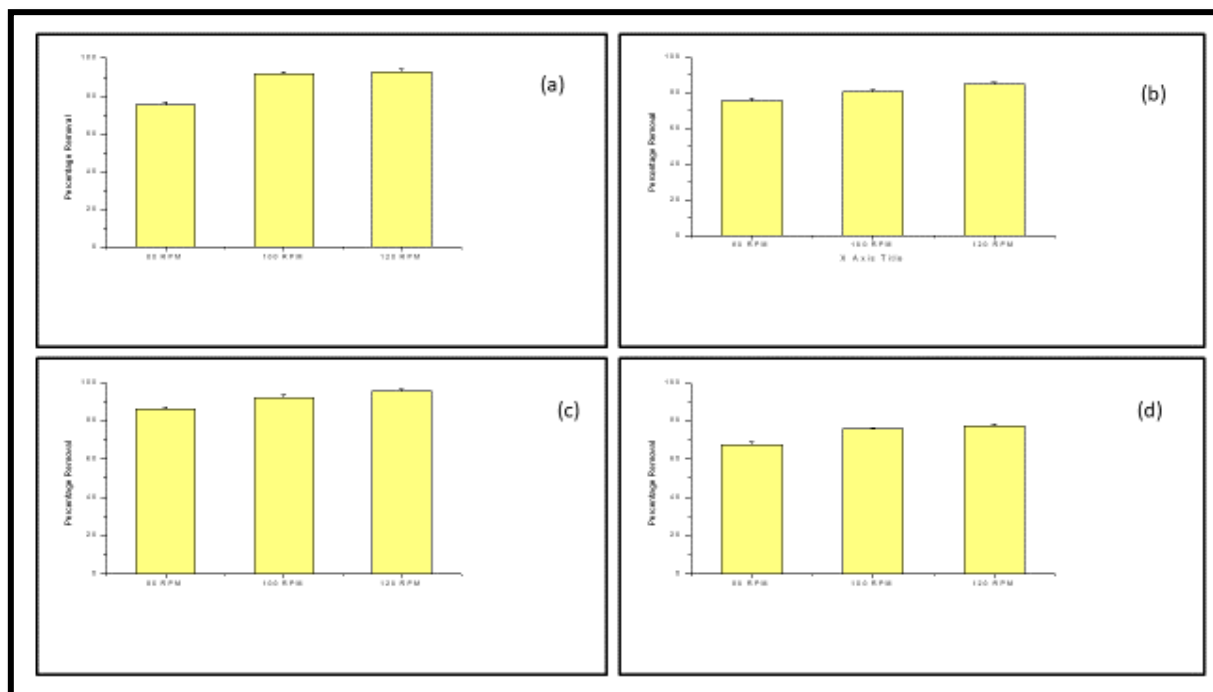


**Fig. 6.8:-** Effect of agitation speed on removal of **(a)** CBZ **(b)** NPX **(c)** RTN **(d)** BPA by GO-TiO$_2$

### 6.4.4 Process Optimization by RSM

#### 6.4.4.1 Optimization of the removal of CBZ by GO-TiO₂ by RSM

The Response Surface Methodology was performed with the aim of understanding the effect of inter parameter interaction on the experimental outcome. In **Table 6.1**, the outcome of the 17 experiments as proposed by the software for the BB model of the RSM is given and in **Table 6.2** the result of the ANOVA of the RSM model is provided. From there it is observed that the $R^2$ value of the model was 0.98 and the adjusted $R^2$ value was 0.95 which propounded the fact that the polynomial model suggested by RSM was appropriate for predicting the outcome of this adsorption reaction. The high value of F (34.37, much greater than unity) and the low value of P ($<0.0001$) meant that the optimizing model was highly significant, with the experimental data points exhibiting a high degree of correlation with the predicted data points (Bhattacharya et al., 2021). **Fig. 6.9** shows the relation between the experimentally determined data points and the predicted data points and there also it can be noted that the experimental data points exhibits a high degree of correlation with the predicted data points. The real equation which was used to predict the effect of the input variables on the response output is presented as follows.

$$Removal\% = +101.4336 + 4.11636 \times pH - 48.2562 \times Dose + 0.5441 \times Agitation\ Speed + 0.067069 \times pH \times Dose - 1.67673 \times 10^{-3} \times pH \times Agitation\ Speed + 1.167 \times Dose \times Agitation\ Speed - 0.59524 \times pH^2 - 21.32797 \times Dose^2 - 1.69769 \times 10^{-3} \times Agitation\ Speed^2 \ldots\ldots\ldots\ldots\ldots\ldots\ldots\ldots\ldots\ldots\ldots\ldots\ldots\ldots\ldots\ldots\ldots\ldots\ldots\ldots\ldots\ldots\ldots\ldots\text{(xxxxi)}$$

As per the RSM model the optimized conditions under which maximum removal of CBZ (82.29 %) was possible were: GO-TiO₂ dosage of 1 g/L, pH value of 4 and agitation speed of 100 RPM. For this RSM model, the interaction between the experimental parameters (input variables) and their outcome on the percentage removal of CBZ (response variable) is illustrated by the contour plots shown in **Fig. 6.10-6.12**.

➤ **Effect of GO-TiO₂ dosage and solution pH on CBZ removal by GO-TiO₂**

The interaction in between the pH of the experimental solution and the dosage of GO-TiO₂ and its effect on the removal of CBZ is conveyed in the contour plot of **Fig. 6.10**. From the result of the experiment it was observed that the removal of CBZ was highest at the lower pH range and decreased with the increase in pH of the experimental solution. This could be attributed to the fact that the surface of GO-TiO₂ has a negative charge due to the presence of high quantity of GO. Therefore at the lower pH range, due to the availability of $H^+$ ions present in the experimental solution, greater adsorption of CBZ takes place on the surface of GO-TiO₂ (Bhattacharya et al., 2022; Carabin et al., 2015). In case of the dose variation study, it was observed that the removal of CBZ by GO-TiO₂ was higher at the higher dose range and subsequently decreased with the decrease in dosage of GO-TiO₂. This could be attributed to

the fact that with increase in dosage of GO-TiO$_2$, the surface area available for the uptake of CBZ increased leading to the greater adsorption and simultaneously greater degradation of CBZ molecules (Bhattacharya et al., 2022; Xu et al., 2018).

> **Effect of solution pH and agitation speed on CBZ removal by GO-TiO$_2$**

The interaction in between the pH of the experimental solution and agitation speed and its effect on the removal of CBZ by GO-TiO$_2$ is conveyed in the contour plot of **Fig. 6.11**. From there it was observed that the removal of CBZ by GO-TiO$_2$ was highest at the lower pH range and subsequently decreased with the increase in pH of the experimental solution. This could be attributed to the negative surface charge of GO-TiO$_2$, which enhances the adsorption of CBZ at the lower pH range due to the presence of H$^+$ ions in the experimental solution (Bhattacharya et al., 2022). On the other hand, the interaction between CBZ molecules and the surface of GO-TiO$_2$ most probably increases with the increase in agitation speed leading to increased removal of CBZ by adsorption followed by photo-catalysis (Fazal et al., 2020; L. Xu et al., 2018).

> **Effect of agitation speed and dosage of GO-TiO$_2$ dosage on CBZ removal by GO-TiO$_2$**

The interaction in between the agitation speed and dosage of GO-TiO$_2$ and its effect on the removal of CBZ by GO-TiO$_2$ is conveyed in the contour plot of **Fig. 6.12**. From there it was observed that removal of CBZ by GO-TiO$_2$ increased with increase in dosage of GO-TiO$_2$ which could be attributed to the greater availability of active sites for the uptake of CBZ molecules which is followed by their photo-catalysis (Bhattacharya et al., 2022). The adsorption of CBZ molecules on the surface of GO-TiO$_2$ mostly takes place by π-π bonds (Ziegmann & Frimmel, 2010). On the other hand, the removal of CBZ by GO-TiO$_2$ increases with the increase in agitation speed which could be attributed to the enhanced interaction between the surface of GO-TiO$_2$ and the CBZ molecules at the greater agitation speed, leading to their higher adsorption followed by photo-catalysis (Bhattacharya et al., 2022).

**Table 6.1** :- The table showing the 17 different set of parameters (runs) along with their corresponding outcome as proposed by Box Behnken model of RSM for optimization of CBZ removal by GO-TiO$_2$

| Run | Block | Factor 1 | Factor 2 | Factor 3 | Response 1 |
|---|---|---|---|---|---|
| | | A:pH | B:Dose | C: Agitation Speed | Percentage Removal |
| | | | g/L | RPM | |
| 1 | Block 1 | 7.00 | 0.75 | 100.00 | 68.21 |
| 2 | Block 1 | 4.00 | 0.50 | 100.00 | 68.00 |
| 3 | Block 1 | 10.00 | 0.75 | 80.00 | 48.89 |
| 4 | Block 1 | 10.00 | 1.00 | 100.00 | 55.13 |
| 5 | Block 1 | 7.00 | 1.00 | 80.00 | 73.44 |
| 6 | Block 1 | 7.00 | 0.75 | 100.00 | 68.21 |
| 7 | Block 1 | 4.00 | 0.75 | 120.00 | 75.65 |
| 8 | Block 1 | 7.00 | 0.75 | 100.00 | 68.21 |
| 9 | Block 1 | 7.00 | 0.75 | 100.00 | 68.21 |
| 10 | Block 1 | 10.00 | 0.50 | 100.00 | 40.64 |
| 11 | Block 1 | 7.00 | 0.50 | 80.00 | 62.58 |
| 12 | Block 1 | 4.00 | 0.75 | 80.00 | 73.44 |
| 13 | Block 1 | 7.00 | 0.50 | 120.00 | 47.28 |
| 14 | Block 1 | 4.00 | 1.00 | 100.00 | 82.29 |
| 15 | Block 1 | 10.00 | 0.75 | 120.00 | 50.70 |
| 16 | Block 1 | 7.00 | 0.75 | 100.00 | 68.21 |
| 17 | Block 1 | 7.00 | 1.00 | 120.00 | 81.49 |

**Table 6.2** :- ANOVA analysis for the RSM for the photocatalytic removal of CBZ by GO-TiO$_2$

| R$^2$ Value | Adjusted R$^2$ Value | f- value | Probability Value P |
|---|---|---|---|
| 0.98 | 0.95 | 34.37 (>1) | <0.0001 Significant |
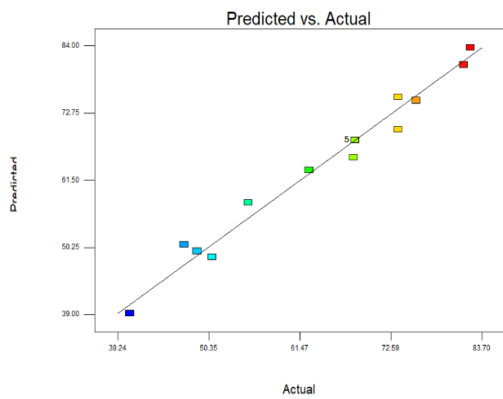
**Fig. 6.9** :- Relation between the predicted data points and the experimental data points as per the RSM model.



**Fig. 6.10** :- Interaction between the pH of the experimental solution and the dose of the GO-TiO$_2$ and their effect on the percentage removal of CBZ.



**Fig. 6.11** :- The interaction between the pH of the experimental solution and agitation speed and their effect on the percentage removal of CBZ byGO-TiO$_2$.



**Fig. 6.12**:- The plot showing the interaction between the dose of the GO-TiO$_2$ and the agitation speed as per the RSM model and their effect on the percentage removal of CBZ.

*6.4.4.2 Process Optimization of the removal of NPX by GO-TiO₂ by RSM*

The Response Surface Methodology was performed with the aim of understanding the effect of inter parameter interaction on the experimental outcome. In **Table 6.3**, the outcome of the 17 experiments as proposed by the software for the BB of the RSM is given and in **Table 6.4** the result of the ANOVA of the RSM model is provided. From there it is observed that the $R^2$ value of the model was 0.96 and the adjusted $R^2$ value was 0.92 which propounded the fact that the polynomial model suggested by RSM was appropriate for predicting the outcome of this adsorption reaction. The high value of F (22.37, much greater than unity) and the low value of P (0.0002 <0.005) meant that the optimizing model was highly significant, with the experimental data points exhibiting a high degree of correlation with the predicted data points (Bhattacharya et al., 2021). **Fig. 6.13** shows the relation between the experimentally determined data points and the predicted data points and there also it can be noted that the experimental data points exhibits a high degree of correlation with the predicted data points. The real equation which was used to predict the effect of the input variables on the response output is presented as follows.

$$Removal\ \% = -174.73291 - 14.79701 \times pH + 70.74176 \times Dose + 5.27072 \times$$
$$Agitation\ Speed - 4.12088 \times pH \times Dose + 0.088141 \times pH \times Agitation\ Speed + 1.42857 \times$$
$$Dose \times Agiotation\ Speed + 0.2442 \times pH^2 - 89.01099 \times Dose^2 - 0.034169 \times$$
$$Agitation\ Speed^2 \dots\dots\dots\dots\dots\dots\dots\dots\dots\dots\dots\dots\dots\dots\dots\dots\dots\dots\dots..(xxxxii)$$

As per the RSM model the optimized conditions under which maximum removal of NPX (96.98 %) was possible were: GO-TiO₂ dosage of 1 g/L, pH value of 4 and agitation speed of 100 RPM. For this RSM model, the interaction between the experimental parameters (input variables) and their outcome on the percentage removal of NPX (response variable) is illustrated by the contour plots shown in **Fig. 6.14-6.16**.

> **Effect of GO-TiO₂ dosage and solution pH on NPX removal by GO-TiO₂**

The interaction in between the pH of the experimental solution and the dosage of GO-TiO₂ and its effect on the removal of NPX by GO-TiO₂ is conveyed in the contour plot of **Fig. 6.14**. From the result of the experiment it was observed that the removal of NPX was highest at the lower pH range and decreased with the increase in pH of the experimental solution. This could be attributed to the fact that at the lower pH range the surface of GO-TiO₂ acquires a positive charge and the NPX molecules acquire neutral charge ($pH_{pzc}$ of GO-TiO₂ is 4.5 and the $pK_a$ of NPX is 4.15) (Bhattacharya et al., 2021; Mondal et al., 2020). The neutrally charged NPX molecules are adsorbed on the surface of GO-TiO₂, followed by which the molecules are photodegraded. However, when the pH of the experimental solution reaches the higher pH range, the molecules of NPX undergoes a resonance change and becomes more negatively charged (Bhattacharya et al., 2021; Mondal et al., 2020). On the other hand, the surface charge of GO-

TiO$_2$ also becomes negative when the pH of the experimental solution goes to the higher range. Due to the electrostatic force of repulsion formed due to the presence of like charges, the adsorption of NPX molecules on the surface of GO-TiO$_2$ is disrupted at this higher pH. As a result of which the photo-degradation of the NPX molecules by GO-TiO$_2$ is also less at the higher pH range (Dong et al., 2015). In case of the dose variation, it was observed that the removal of NPX by GO-TiO$_2$ was higher at the higher dose range and subsequently decreased with the decrease in dosage of GO-TiO$_2$. This could be attributed to the fact that with increase in dosage of GO-TiO$_2$, the surface area available for the uptake of NPX increased leading to the greater adsorption and simultaneously greater degradation of NPX molecules (Bhattacharya et al., 2022; L. Xu et al., 2018).

➢ **Effect of solution pH and agitation speed on NPX removal by GO-TiO$_2$**

The interaction in between the pH of the experimental solution and agitation speed and its effect on the removal of NPX by GO-TiO$_2$ is conveyed in the contour plot of **Fig. 6.15**. From there it was observed that the removal of NPX by GO-TiO$_2$ was highest at the lower pH range and subsequently decreased with the increase in pH of the experimental solution. This could be attributed to the neutral charge of NPX molecules and positive charge on the surface of GO-TiO$_2$ at the lower pH which accelerates the adsorption of NPX on the surface of GO-TiO$_2$ , followed by which the molecules of NPX are degraded (Bhattacharya et al., 2021; Xu et al., 2018). On the other hand, at the higher pH range, both the NPX molecules and the surface of GO-TiO$_2$ acquire a negative charge, leading to the formation of an electrostatic force of repulsion which inhibits the adsorption of NPX molecules onto the surface of GO-TiO$_2$. As a consequence of which, the removal of NPX by GO-TiO$_2$ decreases at the higher pH range. On the other hand, the interaction between NPX molecules and the surface of GO-TiO$_2$ most probably increases with the increase in agitation speed leading to increased removal of NPX by adsorption followed by photo-catalysis (Fazal et al., 2020; Xu et al., 2018).

➢ **Effect of agitation speed and dosage of GO-TiO$_2$ dosage on NPX removal by GO-TiO$_2$**

The interaction in between the agitation speed and dosage of GO-TiO$_2$ and its effect on the removal of NPX by GO-TiO$_2$ is conveyed in the contour plot of **Fig. 6.16**. From there it was observed that removal of NPX by GO-TiO$_2$ increased with increase in dosage of GO-TiO$_2$ which could be attributed to the greater availability of more active sites for the uptake of NPX molecules which is followed by their photo-catalysis (Bhattacharya et al., 2022). The adsorption of NPX molecules on the surface of GO-TiO$_2$ mostly takes place by hydrogen bonding and van deer Waals force (Bhattacharya et al., 2021). On the other hand, the removal of NPX by GO-TiO$_2$ increases with the increase in agitation speed which could be attributed to the enhanced interaction between the surface of GO-TiO$_2$ and the NPX molecules at the greater agitation speed, leading to their higher adsorption followed by photo-catalysis (Bhattacharya et al., 2022).

**Table 6.3**:- The table showing the 17 different set of parameters (runs) along with their corresponding outcome as proposed by Box Behnken model of RSM for optimization of NPX removal by GO-TiO$_2$

| Run | Block | Factor 1 | Factor 2 | Factor 3 | Response 1 |
|-----|-------|----------|----------|----------|------------|
| | | A:pH | B:Dose | C: Agitation Speed | Percentage Removal |
| | | | g/L | RPM | |
| 1 | Block 1 | 7.00 | 0.75 | 100.00 | 69.23 |
| 2 | Block 1 | 7.00 | 1.00 | 80.00 | 53.85 |
| 3 | Block 1 | 7.00 | 1.00 | 120.00 | 78.57 |
| 4 | Block 1 | 7.00 | 0.75 | 100.00 | 69.23 |
| 5 | Block 1 | 4.00 | 0.50 | 100.00 | 71.98 |
| 6 | Block 1 | 7.00 | 0.75 | 100.00 | 69.23 |
| 7 | Block 1 | 10.00 | 1.00 | 100.00 | 53.57 |
| 8 | Block 1 | 7.00 | 0.50 | 80.00 | 35.71 |
| 9 | Block 1 | 4.00 | 0.75 | 120.00 | 67.58 |
| 10 | Block 1 | 10.00 | 0.50 | 100.00 | 40.93 |
| 11 | Block 1 | 4.00 | 0.75 | 80.00 | 78.57 |
| 12 | Block 1 | 7.00 | 0.50 | 120.00 | 31.87 |
| 13 | Block 1 | 7.00 | 0.75 | 100.00 | 69.23 |
| 14 | Block 1 | 10.00 | 0.75 | 80.00 | 37.36 |
| 15 | Block 1 | 7.00 | 0.75 | 100.00 | 69.23 |
| 16 | Block 1 | 4.00 | 1.00 | 100.00 | 96.98 |
| 17 | Block 1 | 10.00 | 0.75 | 120.00 | 47.53 |

**Table 6.4** :- ANOVA analysis for the RSM for the photocatalytic removal of NPX by GO-TiO$_2$

| $R^2$ Value | Adjusted $R^2$ Value | f- value | Probability Value P |
|-------------|----------------------|----------|---------------------|
| 0.96 | 0.92 | 22.37 (>1) | 0.0002 (<0.05) Significant |
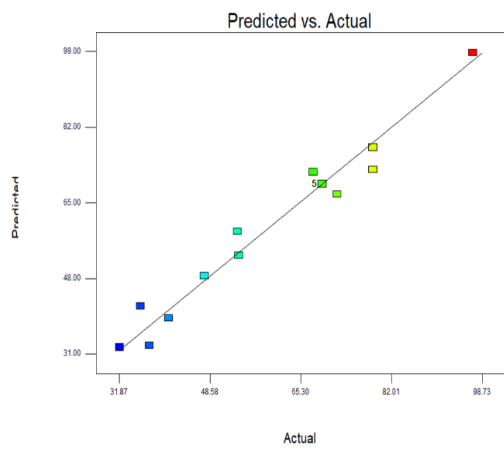
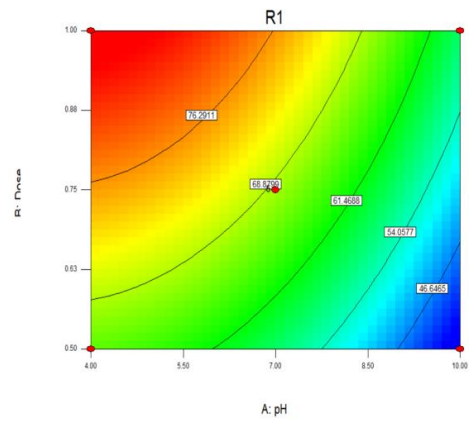**Fig. 6.13**: Relation between the predicted data points and the experimental data points as per the RSM model.



**Fig. 6.14**: Interaction between the pH of the experimental solution and the dose of the GO-$TiO_2$ and their effect on the percentage removal of NPX.
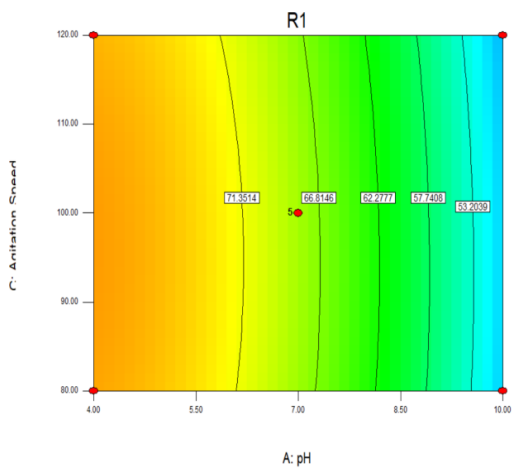


**Fig. 6.15**: The interaction between the pH of the experimental solution and agitation speed and their effect on the percentage removal of NPX by GO-$TiO_2$.
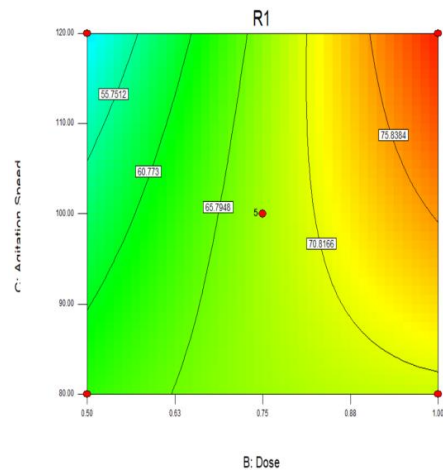


**Fig. 6.16**: The plot showing the interaction between the dose of the GO-$TiO_2$ and the agitation speed as per the RSM model and their effect on the percentage removal of NPX.

### 6.4.4.3 Process Optimization of the removal of RTN by GO-TiO₂ by RSM

The Response Surface Methodology was performed with the aim of understanding the effect of inter parameter interaction on the experimental outcome. In **Table 6.5** the outcome of the 17 experiments as proposed by the software for the BB model of the RSM is given and in **Table 6.6** the result of the ANOVA of the RSM model is provided. From there it is observed that the $R^2$ value of the model was 0.96 and the adjusted $R^2$ value was 0.91 which propounded the fact that the polynomial model suggested by RSM was appropriate for predicting the outcome of this adsorption reaction. The high value of F (19.59, much greater than unity) and the low value of P (0.0004) meant that the optimization model was highly significant, with the experimental data points exhibiting a high degree of correlation with the predicted data points (Bhattacharya et al., 2021). **Fig. 6.17** shows the relation between the experimentally determined data points and the predicted data points and there also it can be noted that the experimental data points exhibits a high degree of correlation with the predicted data points. The real equation which was used to predict the effect of the input variables on the response output is presented as follows.

$$Removal = -33.91408 + 1.66527 \times pH + 72.75399 \times Dose + 1.4216 \times Agitation\ Speed +$$
$$0.41982 \times pH \times Dose - 0.047229 \times pH \times Agitation\ Speed + 0.15113 \times Dose \times$$
$$Agitation\ Speed + 0.25889 \times pH^2 - 44.33249 \times Dose^2 - 5.35264 \times 10^{-3} \times$$
$$Agitation\ Speed^2 \dots\dots\dots\dots\dots\dots\dots\dots\dots\dots\dots\dots\dots\dots\dots\dots\dots\dots\text{(xxxxiii)}$$

As per the RSM model the optimized conditions under which maximum removal of RTN (96.73 %) was possible were: GO-TiO₂ dosage of 0.75 g/L, pH value of 10 and agitation speed of 100 RPM. For this RSM model, the interaction between the experimental parameters (input variables) and their outcome on the percentage removal of RTN (response variable) is illustrated by the contour plots shown in **Fig. 6.18-6.20**.

➢ **Effect of GO-TiO₂ dosage and solution pH on RTN removal by GO-TiO₂**

The interaction in between the pH of the experimental solution and the dosage of GO-TiO₂ and its effect on the removal of RTN is conveyed in the contour plot of **Fig. 6.18**. From there it was observed that the removal of RTN by GO-TiO₂ was higher at the higher pH range. This could be attributed to the fact that the RTN molecules remains neutrally charged between its two $pK_a$ values of pH 2.6 and 8.2. On the other hand, GO-TiO₂ whose $pH_{pzc}$ value is 4.5, remains both positively and negatively charged with in this pH range. Thus, in the pH range of 4 to 10, the adsorption of RTN is facilitated onto the surface of GO-TiO₂. At the lower pH range, both the GO-TiO₂ surface and the RTN molecules retain a positive charge and adsorption is disrupted due to electrostatic force of repulsion. (Al-rub et al., 2020) whereas, at the higher pH range, the deprotonation of the RTN molecules helps in its adsorption by the surface

of GO-TiO$_2$ (Das & Goud, 2020). And as in case of photo-degradation with a semiconductor, photo-catalysis generally follows adsorption ( Zhang et al., 2018), therefore highest removal is observed at the medium pH range. On the other hand, it was observed that the removal of RTN increased with the increase of dosage of GO-TiO$_2$ which could be attributed to the availability of greater surface area for uptake of RTN molecules (Bhattacharya et al., 2022; Ziegmann & Frimmel, 2010).

> **Effect of solution pH and agitation speed on RTN removal by GO-TiO$_2$**

The interaction in between the pH of the experimental solution and agitation speed and its effect on the removal of RTN by GO-TiO$_2$ is conveyed in the contour plot of **Fig. 6.19**. From there it was observed that the removal of RTN by GO-TiO$_2$ was higher at the higher pH range and decreased with lowering of pH. At the lower pH range, due to the force of repulsion acting between the surface of GO-TiO$_2$ and the RTN molecules, the adsorption and subsequent photo-catalysis of RTN molecules by GO-TiO$_2$ is inhibited at this pH range (Al-rub et al., 2020). However, at the higher pH range, the molecules of RTN deprotonates, thereby enhancing their adsorption by GO-TiO$_2$ followed by their greater photo-degradation (Das & Goud, 2020; Dong et al., 2015). On the other hand, with the increase in rotation speed, the interaction between the RTN molecules and the surface of GO-TiO$_2$ increased leading to greater adsorption and consequently greater degradation of RTN molecules by GO-TiO$_2$ (Bhattacharya et al., 2022).

> **Effect of agitation speed and dosage of GO-TiO$_2$ dosage on RTN removal by GO-TiO$_2$**

The interaction in between the agitation speed and dosage of GO-TiO$_2$ and its effect on the removal of RTN by GO-TiO$_2$ is conveyed in the contour plot of **Fig. 6.20**. From there it was observed that removal of RTN by GO-TiO$_2$ increased with increase in dosage of GO-TiO$_2$ which could be attributed to the greater availability of active sites for the uptake of RTN molecules which is followed by their photo-catalysis (Bhattacharya et al., 2022). The adsorption of RTN molecules on the surface of GO-TiO$_2$ might be due to H bonding and dipole-dipole interaction (Al-rub et al., 2020). On the other hand, the removal of RTN by GO-TiO$_2$ increases with the increase in agitation speed which could be attributed to the enhanced interaction between the surface of GO-TiO$_2$ and the RTN molecules at the greater agitation speed, leading to their higher adsorption followed by photo-catalysis (Bhattacharya et al., 2022).

**Table 6.5** :- The table showing the 17 different set of parameters (runs) along with their corresponding outcome as proposed by Box Behnken model of RSM for optimization of RTN removal by GO-TiO$_2$

| Run | Block | Factor 1 | Factor 2 | Factor 3 | Response 1 |
|---|---|---|---|---|---|
| | | A:pH | B:Dose | C: Agitation Speed | Percentage Removal |
| | | | g/L | RPM | |
| 1 | Block 1 | 7.00 | 0.75 | 100.00 | 89.17 |
| 2 | Block 1 | 4.00 | 0.50 | 100.00 | 81.36 |
| 3 | Block 1 | 10.00 | 0.75 | 80.00 | 91.18 |
| 4 | Block 1 | 10.00 | 1.00 | 100.00 | 96.73 |
| 5 | Block 1 | 7.00 | 1.00 | 80.00 | 88.92 |
| 6 | Block 1 | 7.00 | 0.75 | 100.00 | 89.17 |
| 7 | Block 1 | 4.00 | 0.75 | 120.00 | 93.20 |
| 8 | Block 1 | 7.00 | 0.75 | 100.00 | 89.17 |
| 9 | Block 1 | 7.00 | 0.75 | 100.00 | 89.17 |
| 10 | Block 1 | 10.00 | 0.50 | 100.00 | 85.14 |
| 11 | Block 1 | 7.00 | 0.50 | 80.00 | 77.08 |
| 12 | Block 1 | 4.00 | 0.75 | 80.00 | 79.35 |
| 13 | Block 1 | 7.00 | 0.50 | 120.00 | 78.09 |
| 14 | Block 1 | 4.00 | 1.00 | 100.00 | 91.68 |
| 15 | Block 1 | 10.00 | 0.75 | 120.00 | 93.70 |
| 16 | Block 1 | 7.00 | 0.75 | 100.00 | 89.17 |
| 17 | Block 1 | 7.00 | 1.00 | 120.00 | 92.95 |

**Table 6.6** :- ANOVA analysis for the RSM for the photocatalytic removal of RTN by GO-TiO$_2$

| $R^2$ Value | Adjusted $R^2$ Value | f- value | Probability Value P |
|---|---|---|---|
| 0.96 | 0.91 | 19.59 (>1) | 0.0004 (<0.005)  Significant |
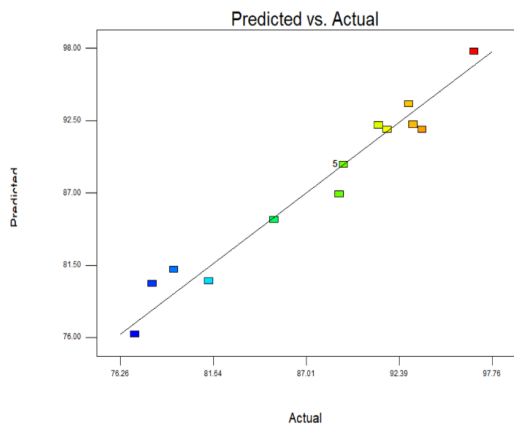
**Fig. 6.17**: Relation between the predicted data points and the experimental data points as per the RSM model.
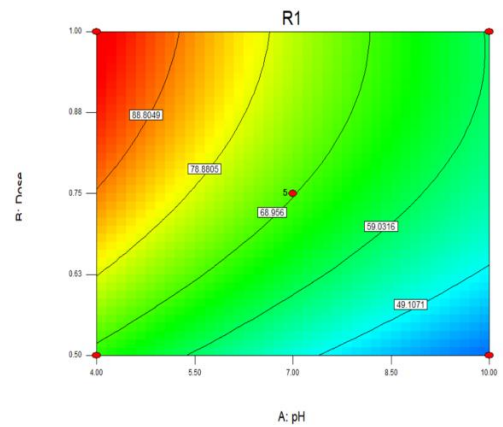


**Fig. 6.18**: Interaction between the pH of the experimental solution and the dose of the GO-TiO$_2$ and their effect on the percentage removal of RTN.
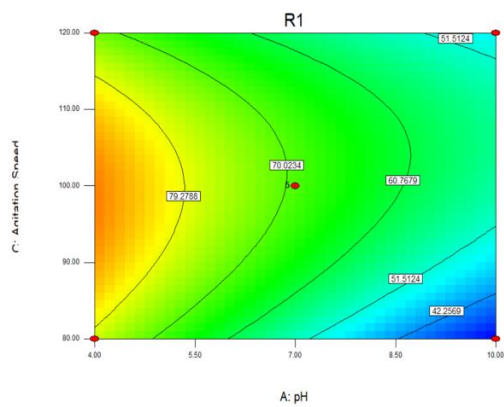


**Fig. 6.19**: The interaction between the pH of the experimental solution and agitation speed and their effect on the percentage removal of RTN by GO-TiO$_2$.
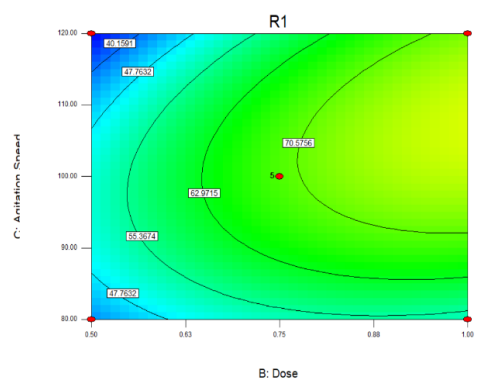


**Fig. 6.20**: The plot showing the interaction between the dose of the GO-TiO$_2$ and the agitation speed as per the RSM model and their effect on the percentage removal of RTN.

### 6.4.4.4 Process Optimization of the removal of BPA by GO-TiO₂ by RSM

The Response Surface Methodology was performed with the aim of understanding the effect of inter parameter interaction on the experimental outcome. In **Table 6.7**, the outcome of the 17 experiments as proposed by the software for the BBM model of the RSM is given and in **Table 6.8** the result of the ANOVA of the RSM model is provided. From there it is observed that the $R^2$ value of the model was 0.97 and the adjusted $R^2$ value was 0.94 which propounded the fact that the polynomial model suggested by RSM was appropriate for predicting the outcome of this adsorption reaction. The high value of F (28.71, much greater than unity) and the low value of P ($< 0.0001$) meant that the optimizing model was highly significant, with the experimental data points exhibiting a high degree of correlation with the predicted data points (Bhattacharya et al., 2021). **Fig. 6.21** shows the relation between the experimentally determined data points and the predicted data points and there also it can be noted that the experimental data points exhibits a high degree of correlation with the predicted data points. The real equation which was used to predict the effect of the input variables on the response output is presented as follows.

$$Removal = -11.85785 - 8.58873 \times pH - 192.87799 \times Dose + 3.32202 \times Agitation\ Speed + 4.0864 \times pH \times Dose - 0.12916 \times pH \times Agitation\ Speed - 0.24518 \times Dose \times Agitation\ Speed + 1.20403 \times pH^2 + 140.45534 \times Dose^2 - 0.010563 \times Agitation\ Speed^2 \dots\dots\dots\dots\text{(xxxxiv)}$$

As per the RSM model the optimized conditions under which maximum removal of BPA (66.64 %) was possible were: GO-TiO₂ dosage of 1 g/L, pH value of 4 and reaction time of 100 minutes. For this RSM model, the interaction between the experimental parameters (input variables) and their outcome on the percentage removal of BPA (response variable) is illustrated by the contour plots shown in **Fig. 6.22-6.24**.

> ➤ **Effect of GO-TiO₂ dosage and solution pH on BPA removal by GO-TiO₂**

The interaction in between the pH of the experimental solution and the dosage of GO-TiO₂ and its effect on the removal of BPA is conveyed in the contour plot of **Fig. 6.22**. From the result of the experiment it was observed that the removal of BPA was highest at the lower pH range and decreased with the increase in pH of the experimental solution. This could be attributed to the fact at higher pH range (around pH >= 8), the BPA molecules dissociate to form bis-phenolate anion. On the other hand, the pH$_{pzc}$ of GO-TiO₂ particles were found to be pH 4.5. As a result of which at the higher pH range, both surface of GO-TiO₂ and the molecules of BPA both attain a negative charge, due to which the adsorption of BPA molecules on to the surface of GO-TiO₂ was disrupted due to electrostatic force of repulsion (Xu et al., 2012; Xu et al., 2018). And as the photo-degradation of the BPA molecules is preceded by the adsorption of the molecules on the surface of GO-TiO₂ (Nawaz et al., 2017), therefore the removal

of BPA was also found to be less in the higher pH range and was found to be high at the lower pH range (Xu et al., 2018).  In case of the dose variation study, it was observed that the removal of BPA by GO-TiO$_2$ was higher at the higher dose range and subsequently decreased with the decrease in dosage of GO-TiO$_2$. This could be attributed to the fact that with increase in dosage of GO-TiO$_2$, the surface area available for the uptake of BPA increased leading to the greater adsorption and simultaneously greater degradation of BPA molecules  (Bhattacharya et al., 2022; Xu et al., 2018).

> **Effect of solution pH and agitation speed on BPA removal by GO-TiO$_2$**

The interaction in between the pH of the experimental solution and agitation speed and its effect on the removal of BPA by GO-TIO2 is conveyed in the contour plot of **Fig. 6.23**. From there it was observed that the removal of BPA by GO-TiO$_2$ was highest at the lower pH range and subsequently decreased with the increase in pH of the experimental solution. This could be attributed to the similar surface charge of GO-TiO$_2$ and BPA molecules at the higher pH range (pH >= 8) (Xu et al., 2018). On the other hand, the interaction between BPA molecules and the surface of GO-TiO$_2$ increased with increase in agitation speed, which could be attributed to the higher interaction between the surface of GO-TiO$_2$ and the molecules of BPA at this higher agitation speed (Fazal et al., 2020; Xu et al., 2018).

> **Effect of agitation speed and of GO-TiO$_2$ dosage on the removal of BPA by GO-TiO$_2$**

The interaction in between the agitation speed and dosage of GO-TiO$_2$ and its effect on the removal of BPA by GO-TiO$_2$ is conveyed in the contour plot of **Fig. 6.24**. From there it was observed that removal of BPA by GO-TiO$_2$ increased with increase in dosage of GO-TiO$_2$ which could be attributed to the greater availability of active sites for the uptake of BPA molecules which is followed by their photo-catalysis (Bhattacharya et al., 2022). On the other hand, the removal of BPA by GO-TiO$_2$ increases with the increase in agitation speed which could be attributed to the enhanced interaction between the surface of GO-TiO$_2$ and the BPA molecules at the greater agitation speed, leading to their higher adsorption followed by photo-catalysis (Bhattacharya et al., 2022).

**Table 6.7** :- The table showing the 17 different set of parameters (runs) along with their corresponding outcome as proposed by Box Behnken model of RSM for optimization of BPA removal by GO-TiO$_2$

| Run | Block | Factor 1 | Factor 2 | Factor 3 | Response 1 |
|---|---|---|---|---|---|
| | | A:pH | B:Dose | C: Agitation Speed | Percentage Removal |
| | | | g/L | RPM | |
| 1 | Block 1 | 7.00 | 0.75 | 100.00 | 60.60 |
| 2 | Block 1 | 7.00 | 1.00 | 80.00 | 70.40 |
| 3 | Block 1 | 7.00 | 1.00 | 120.00 | 73.56 |
| 4 | Block 1 | 7.00 | 0.75 | 100.00 | 60.60 |
| 5 | Block 1 | 4.00 | 0.50 | 100.00 | 85.81 |
| 6 | Block 1 | 7.00 | 0.75 | 100.00 | 60.60 |
| 7 | Block 1 | 10.00 | 1.00 | 100.00 | 80.74 |
| 8 | Block 1 | 7.00 | 0.50 | 80.00 | 54.29 |
| 9 | Block 1 | 4.00 | 0.75 | 120.00 | 79.86 |
| 10 | Block 1 | 10.00 | 0.50 | 100.00 | 66.37 |
| 11 | Block 1 | 4.00 | 0.75 | 80.00 | 60.25 |
| 12 | Block 1 | 7.00 | 0.50 | 120.00 | 62.35 |
| 13 | Block 1 | 7.00 | 0.75 | 100.00 | 60.60 |
| 14 | Block 1 | 10.00 | 0.75 | 80.00 | 70.05 |
| 15 | Block 1 | 7.00 | 0.75 | 100.00 | 60.60 |
| 16 | Block 1 | 4.00 | 1.00 | 100.00 | 87.92 |
| 17 | Block 1 | 10.00 | 0.75 | 120.00 | 58.67 |

**Table 6.8** :- ANOVA analysis for the RSM for the photocatalytic removal of BPA by GO-TiO$_2$

| $R^2$ Value | Adjusted $R^2$ Value | f- value | Probability Value P |
|---|---|---|---|
| 0.97 | 0.94 | 28.71 (>1) | 0.0001 (<0.05) |
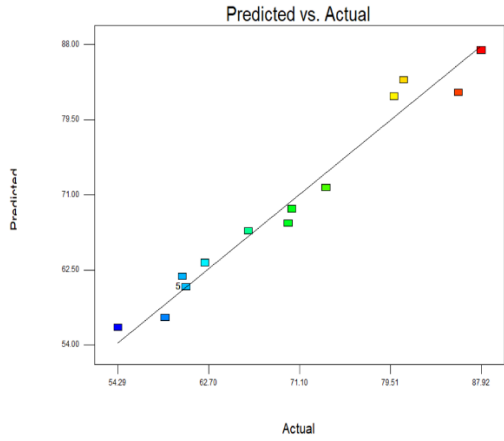
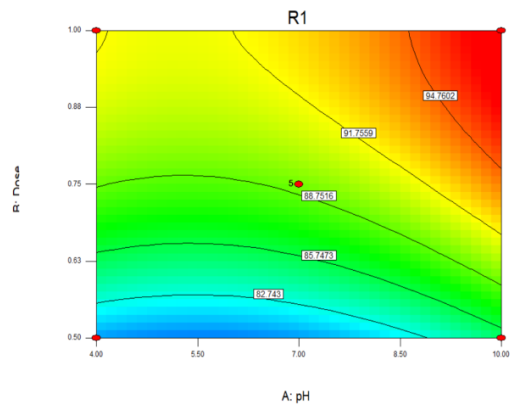**Fig. 6.21**: Relation between the predicted data points and the experimental data points as per the RSM model.
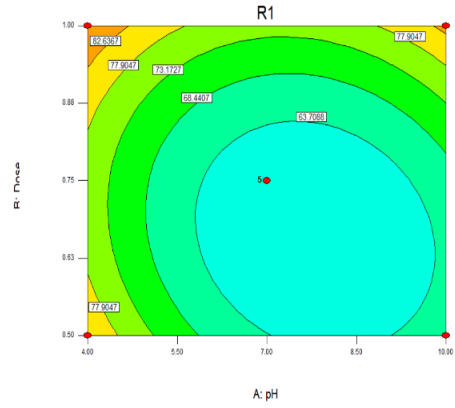


**Fig. 6.22**: Interaction between the pH of the experimental solution and the dose of the GO-$TiO_2$ and their effect on the percentage removal of BPA.
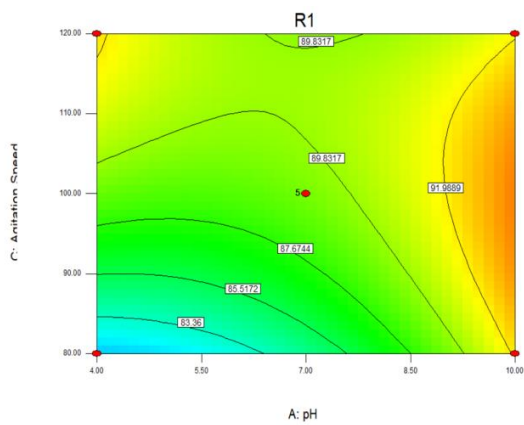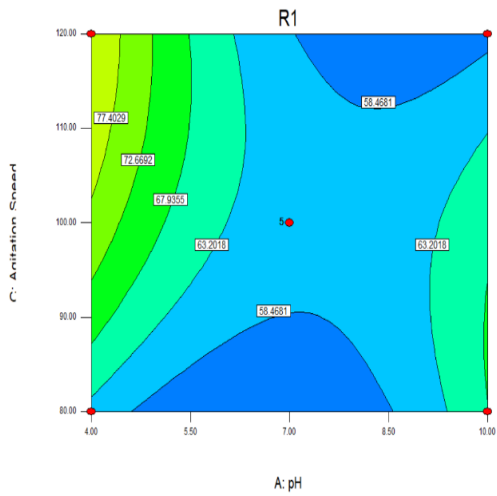


**Fig. 6.23**: The interaction between the pH of the experimental solution and agitation speed and their effect on the percentage removal of BPA by GO-$TiO_2$.
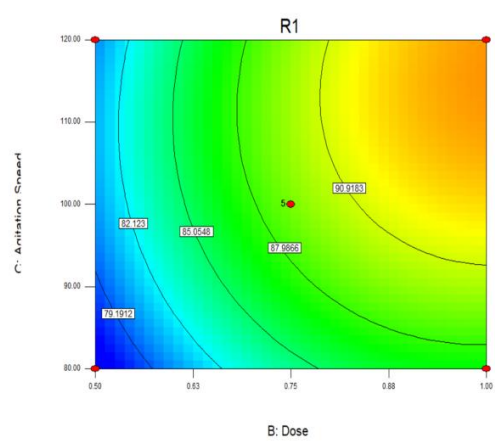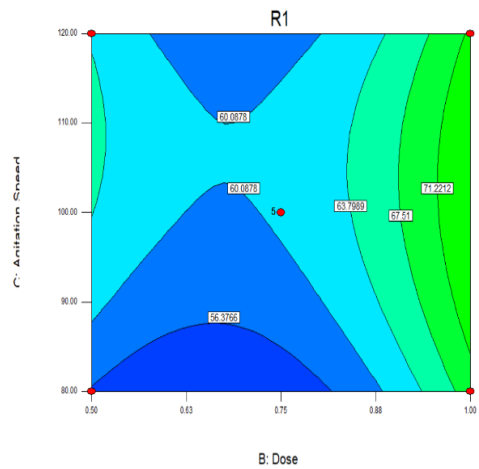


**Fig. 6.24**: The plot showing the interaction between the dose of the GO-$TiO_2$ and the agitation speed as per the RSM model and their effect on the percentage removal of BPA.

## 6.4.5 Removal of the EC's by GO-TiO$_2$ in an RPB

As mentioned before, an experiment was conducted with the RPB in order to intensify the adsorption ability of the GO-TiO$_2$ composite. As mentioned before, before the start of the reaction the EC's were treated by GO-TiO$_2$ inside the UV reactor for 1 hour under UVA irradiation. After 1 hour the solutions were taken out and the level of the EC's were determined spectrophotometrically. From there it was observed that 67.52 % of CBZ, 83.25 % of NPX, 93.93 % of RTN and 51.8 % of BPA were removed after the photocatalytic reaction. The adsorption reaction in the RPB was continued for 6 hours and at the end of the reaction 89.37 % of CBZ, 98.36 % of NPX, 99.47 % of RTN and 82.68 % of BPA were removed by the GO-TiO$_2$ composite during the RPB reaction. As in case of RTN and NPX, both of these EC's were removed in high percentage by photo-catalysis by GO-TiO$_2$ therefore in their case, the scope of GO-TiO$_2$ to operate as an adsorbent was very less. However, in case of CBZ and BPA, the GO-TiO$_2$ has operated as an effective adsorbent, thereby implying that the GO-TiO$_2$ composite can also act as an efficient adsorbent (Bhattacharya et al., 2022). The result of the experiment is shown in **Fig. 6.25**.
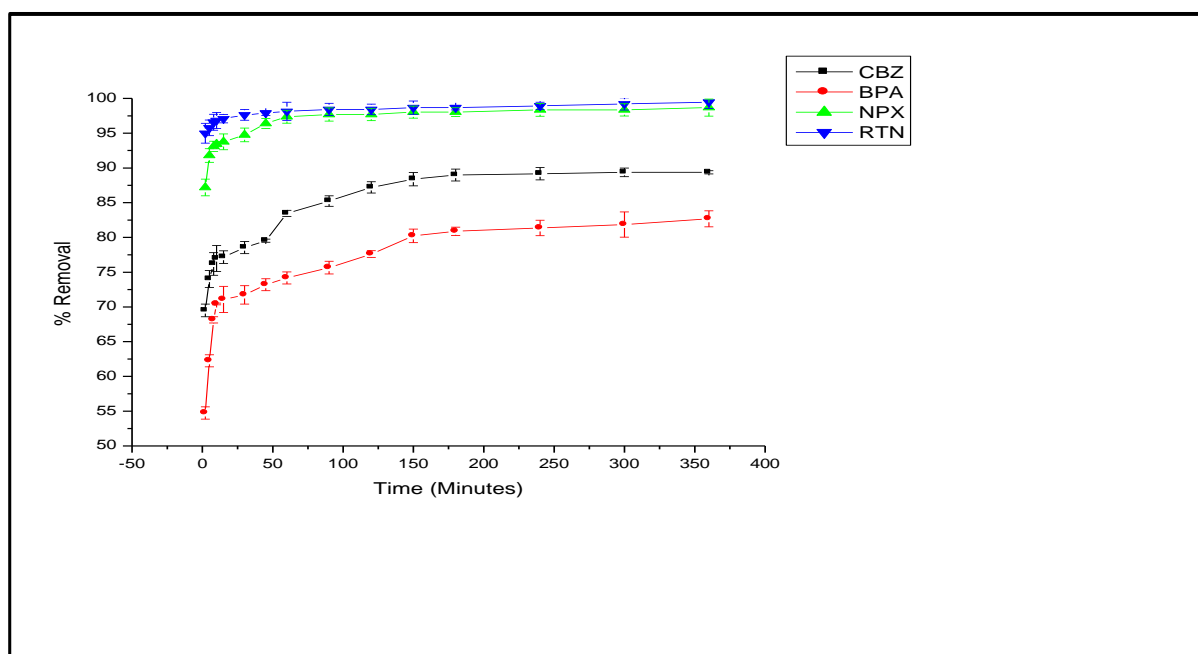


**Fig. 6.25**:- Removal of CBZ, NPX, RTN and BPA by GO-TiO$_2$ in a RPB

## 6.4.6 Reusability Study

### 6.4.6.1 Reusability of GO-TiO$_2$ after treating CBZ

Evaluation of the reusability of GO-TiO$_2$ was important for determining the economic feasibility of the composite. Out of the six solutions that were used for the regeneration of used GO-TiO$_2$ after treating CBZ, the greatest effectivity was exhibited by the 10% NaOH solution. By washing the GO-TiO$_2$ with the 10 % NaOH solution it was observed that in the first cycle, the GO-TiO$_2$ was able to remove 88.31 % of the CBZ from the aqueous solution, a value which was close to the effectivity exhibited by pristine GO-TiO$_2$. In the next cycle the removal of CBZ was 87.22 % and in the third cycle the removal was 80.06 %. For the fourth and the fifth cycle, the removal of CBZ by GO-TiO$_2$ was 79.4 % and 75.31 % respectively. Therefore it can be stated that the GO-TiO$_2$ regenerated by 10 % NaOH solution, can remove 75 % of CBZ from its aqueous solution for up-to five cycles. Thus, the synthesized GO-TiO$_2$ can be recycled up-to five times with a significant level of effectivity. The result of the experimental study is shown in **Fig. 6.26**.
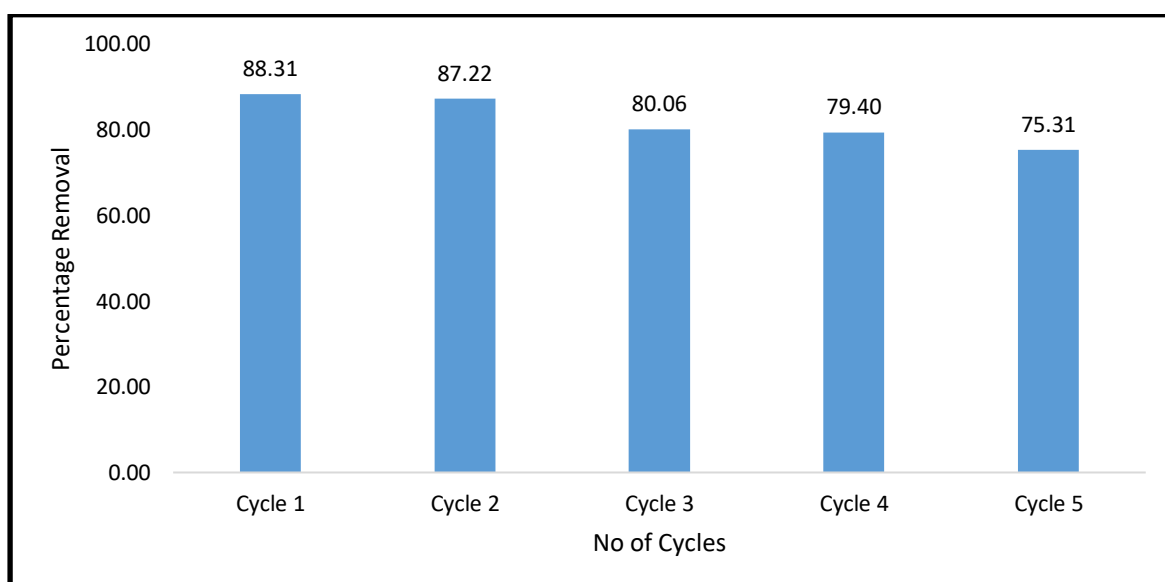


**Fig. 6.26**:- Removal of CBZ by GO-TiO$_2$ in different steps of the reusability cycle.

### 6.4.6.2 Reusability Study of GO-TiO$_2$ after treating NPX

Evaluation of the reusability of GO-TiO$_2$ was important for determining the economic feasibility of the composite. Out of the six solutions that were used for the regeneration of used GO-TiO$_2$ after treating NPX, the greatest effectivity was exhibited by the 10 % HCl solution. By regenerating the GO-TiO$_2$ composite with the 10 % HCl solution it was observed that in the first cycle, the GO-TiO$_2$ was able to remove 70.41 %, in the second cycle it was able to remove 69.18 % and in the third cycle it was able to remove 60.69 % of the NPX from the aqueous solution. In the third and fourth cycle the GO-TiO$_2$ was able to remove 57.12 % and 53.63 % of NPX respectively. The percentage of NPX removed by GO-TiO$_2$ after regeneration with 10 % HCl in the first and second cycle, was quite close to the original effectivity of GO-TiO$_2$. In the third cycle also the effectivity of GO-TiO$_2$ remained over 60 %. The effectivity of GO-TiO$_2$ only decreased in the last two cycles. Therefore it can be stated that, GO-TiO$_2$ can be reused for up-to three times with reasonably high effectivity by regenerating the composite by washing it with 10 % HCl solution. The result of the experimental study is shown in **Fig. 6.27**.
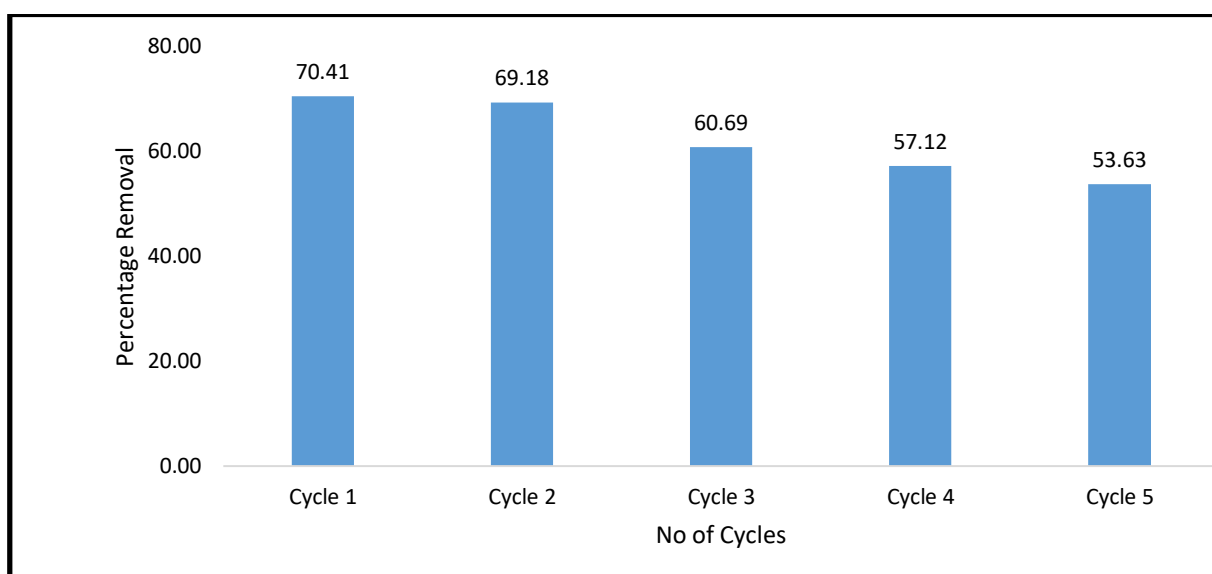


**Fig. 6.27:**- Removal of NPX by GO-TiO$_2$ in different steps of the reusability cycle.

### 6.4.6.3 Reusability Study of GO-TiO$_2$ after treating RTN

Evaluation of the reusability of GO-TiO$_2$ was important for determining the economic feasibility of the composite. Out of the six solutions that were used for the regeneration of used GO-TiO$_2$, the greatest effectivity was exhibited by the 10% ethanol solution. By regenerating the GO-TiO$_2$ composite with the 10 % ethanol solution it was observed that in the first cycle, the GO-TiO$_2$ was able to remove 93.39 % of RTN, in the second cycle it was able to remove 92.13 % of RTN and in the third cycle it was able to remove 90.89 % of the RTN from the aqueous solution. In the fourth and fifth cycle the GO-TiO$_2$ was able to remove 81.61 % and 74.13 % of RTN respectively. Thus from the result of the experiment it was observed that by washing the GO-TiO$_2$ with 10 % ethanol, it was able to remove more than 90 % of ranitidine for up-to three cycles, thereby signifying that the GO-TiO$_2$ composite can be reused multiple times through proper regeneration. The result of the experimental study is shown in **Fig. 6.28**.
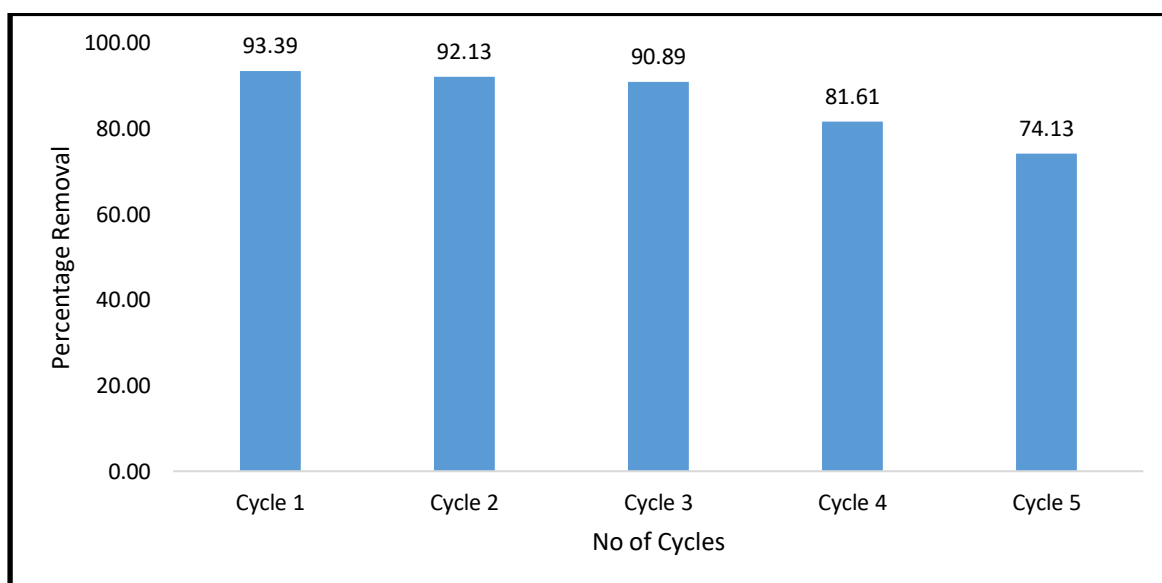


**Fig. 6.28**:- Removal of RTN by GO-TiO$_2$ in different steps of the reusability cycle.

### 6.4.6.4 Reusability Study of GO-TiO$_2$ after treating BPA

Evaluation of the reusability of GO-TiO$_2$ was important for determining the economic feasibility of the composite. Out of the six solutions that were used for the regeneration of used GO-TiO$_2$ after treating BPA, the greatest effectivity was exhibited by the 10% HCl solution. By regenerating the GO-TiO$_2$ composite with the 10 % HCl solution it was observed that in the first cycle, the GO-TiO$_2$ was able to remove 71.75 % of BPA, in the second cycle it was able to remove 67.11 % of BPA and in the third cycle it was able to remove 55.9 % of the BPA from the aqueous solution. In the fourth and fifth cycle the GO-TiO$_2$ was able to remove 43.89 % and 36.18 % of BPA respectively. Therefore, from the result of the experimental study as shown in **Fig. 6.29**, it was observed that GO-TiO$_2$ was able to remove more than 50 % of BPA from its aqueous solution for up-to three cycles on being regenerated by washing with 10 % HCl solution.
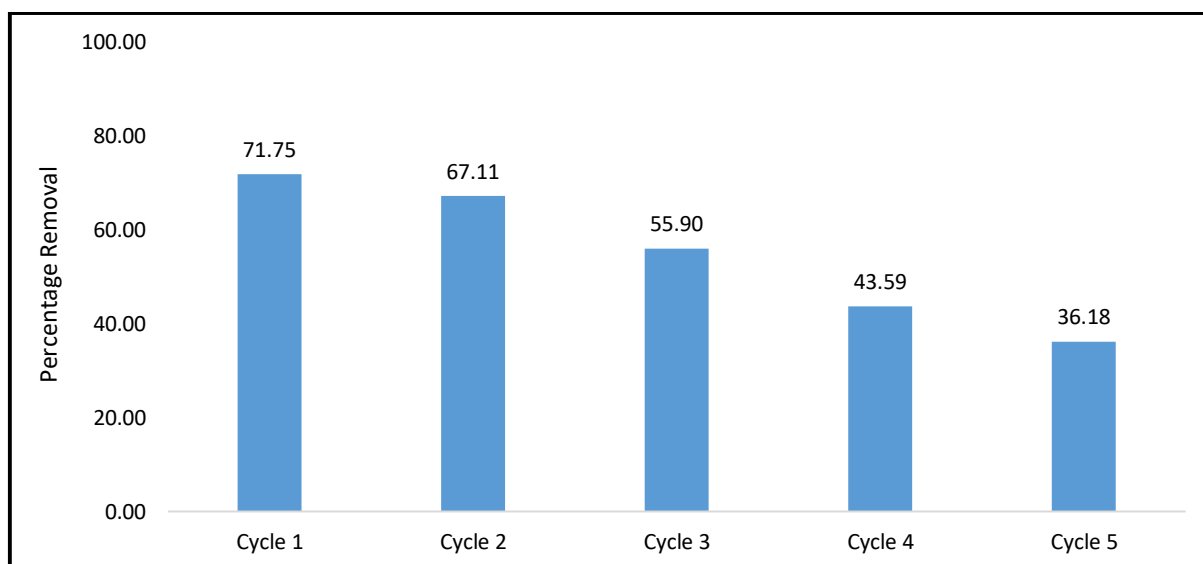


**Fig. 6.29**:- Removal of BPA by GO-TiO$_2$ in different steps of the reusability cycle.

## 6.5 CONCLUSION :-

In the above experiment, a composite was synthesized by combining GO with $TiO_2$ by a solvothermal method. The composite was utilized for removing the EC's from there aquatic solution by means of photo-degradation. The $TiO_2$ was chosen as the semiconductor material for photo-catalysis by virtue of its inert nature, chemical and physical stability and ease of availability. However, the drawbacks of utilizing $TiO_2$ were its high band gap (3.2 eV for anatase and 3 eV for rutile) and it's hydrophobicity, by virtue of which the $TiO_2$ attains a tendency to clump together. In order to alleviate this problems, the $TiO_2$ was combined with GO. Combining GO with $TiO_2$ is supposed to increase the surface area, thereby providing more active sites for the uptake of adsorbate molecules. Also the combination of GO with $TiO_2$ is supposed to bring down the band gap of $TiO_2$. The GO and $TiO_2$ composite consisted of 9 parts by weight of GO and 1 part by weight of $TiO_2$ (which is a combination of 3 parts by weight of anatase and 1 part by weight of rutile $TiO_2$). The GO-$TiO_2$ composite was synthesized by a solvormal method in a Teflon lined autoclave at a temperature of 120°C for 12 hours. The synthesized material was characterized by SEM, XRD, FTIR and Raman Spectroscopy. From the SEM analysis it was observed, that the surface of GO-$TiO_2$ was interspersed with $TiO_2$ particles and the surface morphology of GO-$TiO_2$ made it suitable for the purpose of adsorption of pollutants. From the XRD analysis of GO-$TiO_2$ it was found that GO was reduced during the solvothermal reaction, leading to the absence of the characteristic peak of GO. The characteristic peaks of $TiO_2$ were also observed in the XRD analysis of GO-$TiO_2$. From the FTIR analysis of GO-$TiO_2$ it was observed that the GO was reduced, leading to the formation of fewer peaks (denoting fewer functional groups) as compared to GO. Furthermore, the peak at 524 $cm^{-1}$ denotes the Ti-O-Ti bond, thereby stating that the surface of GO had combined with that of $TiO_2$. From the Raman analysis it was observed, that the $sp^2$ hybridized structure of carbon had many defects on its surface. The band gap of the synthesized GO-$TiO_2$ was calculated by virtue of a Tauc plot using the Kubelka Munk expression from its UV-Vis spectra. From there it was observed that, the band gap of $TiO_2$ (found to be 3.44 eV) decreased (to 3.24 eV) on being combined with GO. This could be attributed to the formation of a new energy band on being combined with GO. Then a screening study was performed in order to find which incident radiation was most capable of activating the GO-$TiO_2$ composite. Out of the four radiation calculated, i.e., UVA, UVB, UVC and visible light, it was observed that UVA radiation exhibited the highest efficiency. So UVA radiation was used as the activating radiation in the further studies. From the result of the experiment it was observed that the GO-$TiO_2$ composite was able to remove significant amount of the EC's from there aqueous solution, with the highest removal for CBZ being 95.94 % at CBZ concentration of 5 mg/L, GO-$TiO_2$ dosage of 2 g/L, pH 7 of experimental solution, agitation speed of 120 RPM. For NPX the highest removal was 90.99 % which was obtained at pH 2 of experimental solution, GO-$TiO_2$ dosage of 2 g/L, NPX concentration of 10 mg/L and agitation speed of 120 RPM. For RTN the highest removal was 95.27 % which was obtained at pH 8, GO-$TiO_2$ dosage of 2 g/L, RTN concentration of 10 mg/L and agitation speed of 120

RPM. For BPA the highest removal was 99.65 % which was obtained at pH 7 of the experimental solution, GO-TiO$_2$ dosage of 2 g/L, BPA concentration of 5 mg/L and agitation speed of 120 RPM. The batch studies were further optimized with RSM there the maximum removal of CBZ was 82.29 % was possible under the GO-TiO$_2$ dosage of 1 g/L, pH value of 4 and agitation speed of 100 RPM. For NPX the maximum removal was 96.98 % which were possible under the experimental conditions of GO-TiO$_2$ dosage of 1 g/L, pH value of 4 and agitation speed of 100 RPM. For RTN the maximum removal was 96.73 % which was possible at GO-TiO$_2$ dosage of 1 g/L, pH value of 10 and agitation speed of 100 RPM. For BPA the maximum removal was 87.92 % which was possible were under the experimental conditions of GO-TiO$_2$ dosage of 1 g/L, pH value of 4 and agitation speed of 100 RPM. And lastly, the adsorption ability of GO-TiO$_2$ was evaluated by virtue of a RPB study. The adsorption reaction in the RPB was continued for 6 hours and at the end of the reaction 89.37 % of CBZ, 98.36 % of NPX, 99.47 % of RTN and 82.68 % of BPA were removed by the GO-TiO$_2$ composite during the RPB reaction. The GO-TiO$_2$ composite also exhibited the capacity to be reused for at least 2-3 times with efficiency comparable to that of the original material on being treated with regenerating solutions. Thus, from the result of the experimental studies, it was inferred that GO-TiO$_2$ was very effective in removing the EC's from their aquatic solution. Further research can be done to make process more effective and emphasis can also be laid on the separation of the composite materials from water.

# CHAPTER 7

# SYNTHESIS OF A ARSB-TIO₂ COMPOSITE AND ITS UTILIZATION FOR REMOVING EC'S FROM THE AQUATIC SYSTEM

## 7.1 INTRODUCTION

In the recent times, mostly due to anthropogenic activities, large quantities of trace organic pollutants are being released into the aquatic ecosystem (Bhattacharya et al., 2022). PHA's compounds form a major part of these trace pollutants (Khan et al., 2017). Huge amounts of PHA's are consumed by humans and is used for treating their pets and cattle's. A high proportion of these PHA's are excreted in a non-metabolised state, in the form of an active compound into the aquatic ecosystem (Khan et al., 2017). PHA compounds are also released into the freshwater ecosystem in the form of industrial effluents and hospital wastes (Khan et al., 2017). The PHA's being chemically active compounds, can cause undesirable effects if they are consumed by non-target organisms. The untreated traces of PHA's in the aquatic ecosystem can result in the formation of resistant strains of microorganisms which can be detrimental for the human well-being (Gogoi et al., 2018). Along with PHA's, E.D.C's are also an important group of trace organic pollutants which mimics the activity of the hormone estrogen and can alter and harm the hormonal system of the body (Chouhan et al., 2014; Gogoi et al., 2018). For this particular chapter, three PHA's namely CBZ, NPX and RTN and one E.D.C, namely BPA were used to represent the pollutant compounds.

Various techniques have been utilized in order to remove these trace pollutants from water like filtration, evaporation, coagulation, chemical precipitation, ion exchange, electrodeposition solvent extraction, membrane system, adsorption and reverse osmosis (Zhang et al., 2019). Among these different methods, photo-catalysis is considered to be one of the most effective techniques for removing these types of trace organic pollutants from water. In the process of photo-catalysis, the trace organic pollutants are adsorbed on the surface of the photo-catalyst followed by which they are degraded by into smaller compounds (preferably into benign end products like $CO_2$ and $H_2O$) (Dong et al., 2015). Among the different semiconductors that are utilized in the process of photo-catalysis, $TiO_2$ was

selected for this particular experiment by virtue of its physical and chemical stability, non-toxic nature and relatively low cost and easy availability (Silva et al., 2021). However, using $TiO_2$ as the semiconducting material has its drawbacks, such as tendency to agglomerate in aquatic solution, lesser ability to adsorb organic pollutants (especially hydrophobic ones) and high band gap (3.2 eV for anatase and 3 eV for rutile) that can only be activated by UV radiation (Dong et al., 2015). In order to alleviate this problems, $TiO_2$ is generally combined with some other material like metals, non-metals and dyes etc. In **Chapter 6**, the mixing of $TiO_2$ with GO and the efficacy of the GO-$TiO_2$ composite for the purpose of removing the EC's like CBZ, NPX, RTN and BPA were evaluated. In the present chapter, $TiO_2$ was combined with the previously denoted ARSB, by a solvo-thermal method and then this material was used for removing the above mentioned EC's from there aquatic solution.

The characterization of the synthesized ARSB-$TiO_2$ was done with SEM, XRD, FTIR and Raman spectroscopy analysis. The band gap of the ARSB-$TiO_2$ composite was evaluated by the Kubelka-Munk equation from its UV-visible spectroscopy by plotting a Tauc plot (Fazal et al., 2020; Xu et al., 2018). Firstly, a screening study was done with UVA, UVB, UVC and visible light for finding the most suitable radiation for activating the ARSB-$TiO_2$ composite. Then a series of batch studies were performed with different experimental parameters like concentration of the pollutant, dosage of photo-catalyst, pH of the experimental solution and temperature in order to find the conditions under which the highest removal of the EC's by the ARSB-$TiO_2$ was possible. The process was further optimized with RSM. In the end, the adsorption efficiency of the ARSB-$TiO_2$ composite was evaluated in an RPB method, followed by photo-catalysis. The regeneration of the ARSB-$TiO_2$ after treating the EC's were also evaluated.

## 7.2 MATERIALS AND METHODS :-

### 7.2.1 Materials required

The $TiO_2$ powders were acquired from Platonic. The rest of the materials was collected in the same manner as mentioned in the previous chapter, **Chapter 5, Section 5.2.1.**

### 7.2.2 Synthesis of ARSB

ARSB was synthesized using the same procedure as mentioned in **Chapter 5, Section 5.2.2.**

### 7.2.3 Synthesis of ARSB-$TiO_2$

Using the same solvo-thermal process as utilized for the synthesis of GO-$TiO_2$ as described in **Chapter 6, Section 5.2.3.**

### 7.2.4 Characterization

Same as mentioned in **Chapter 6, Section 6.2.4**.

### 7.2.5 Preparation of the Experimental Solution.

Using the same process as mentioned **Chapter 4, Section 4.2.4.**

### 7.2.6 Screening Study

Using the same process as mentioned in **Chapter 6, Section 7.2.6.**

### 7.2.7 Batch study

A batch study was performed in order to find the experimental conditions under which the highest removal of the EC's by the ARSB-TiO$_2$ was possible. Four experimental parameters were investigated namely concentration of the EC's (5 mg/L-20 mg/L), dosage of the photo-catalyst (0.5 g/L- 2 g/L), pH of the experimental solution (pH 2-pH 10) and temperature. Before turning on the incident light, the ARSB-TiO$_2$ and the EC's were stirred in the dark for 30 minutes in order for the adsorption equilibrium to take place. Followed by which the incident light was turned on.

The sample collection, filtration, centrifugation and the analysis of EC's in sample before and after treatment were done by following the same method as mentioned in **Chapter 4, Section 4.2.5**.

### 7.2.8 Process optimization with RSM

In case of the RSM study, the CCD model of RSM was used for optimizing the removal of the EC's by ARSB-TiO$_2$. The input parameters were the pH of the experimental solution, the dosage of ARSB-TiO$_2$ and the contact time. Rest of the experiment is same as mentioned in **Chapter 4, Section 4.2.6**.

### 7.2.9 Process Intensification with Rotating Packed Bed (RPB) study

A RPB study was conducted in order to evaluate the adsorption efficiency of the ARSB-TiO$_2$ composite. Firstly, a 10 mg/L solution of each of the EC's were taken and to it the ARSB-TiO$_2$ composite was added at a dosage of 2 g/L. Then the experimental solution consisting of the EC and the ARSB-TiO$_2$ composite were irradiated with activating radiation for 1 hour. Then the whole experimental solution was transferred to the reservoir used for holding the experimental solution in the RPB. The rest of the process was similar to what has been described in **Chapter 4, Section 4.2.8**.

### 7.2.10 Reusability study of the ARSB-TiO$_2$

Following the same procedure as mentioned in **Chapter 4, Section 4.2.8**.

## 7.3 CALCULATIONS :-

### 7.3.1. Percentage removal

Same as mentioned in **Chapter 4, Section 4.3.1**.

### 7.3.2. Optimization using RSM

Same as mentioned in **Chapter 4, Section 4.3.5.**

## 7.4 RESULTS :-

### 7.4.1 Characterization

#### 7.4.1.1 SEM analysis of ARSB-TiO$_2$

**Fig. 7.1 (a)** shows the SEM image of ARSB-TiO$_2$ nanocomposite. From there it was observed that the surface of ARSB consisted of folded lamellar sheets of carbon, which is characteristic of the morphology of ARSB as reported in (Bhattacharya et al., 2021). The layers and wrinkles that are observed on the surface of ARSB might have been formed by the interconnection of the oxygen containing functional groups among themselves. The granular structures observed on the surface of ARSB might be attributed to that of TiO$_2$. Thus from the SEM image of ARSB-TiO$_2$ it can be observed that the particles of TiO$_2$ were evenly dispersed on the surface of ARSB. The TiO$_2$ particles may have attached to the surface of ARSB by electrostatic binding, physi-sorption or charge transfer (Al-Shamali, 2013; Li et al., 2014). The pollutants are adsorbed on the surface of ARSB followed by which they are photo-catalytically degraded by the TiO$_2$ molecules.
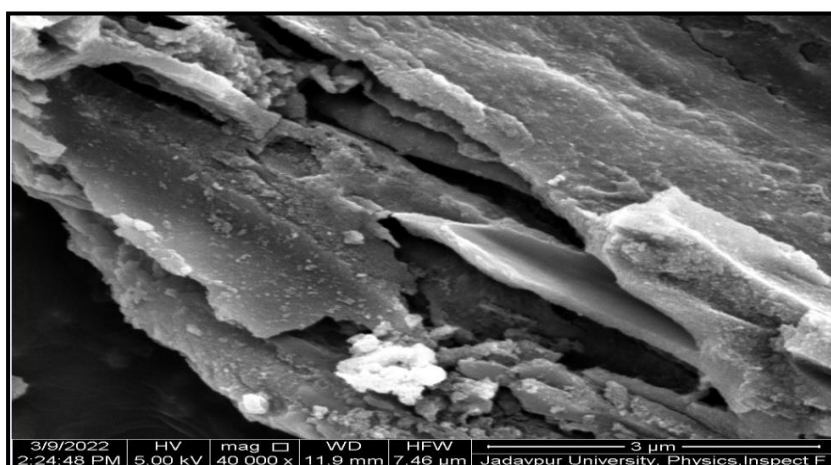


**Fig. 7.1 (a)**:- SEM image of ARSB-TiO$_2$

### 7.4.1.2 FTIR analysis of ARSB-TiO$_2$

The FT-IR spectrum of the ARSB-TiO$_2$ composite is represented in **Fig. 7.1 (b)**, which shows distinctive peaks at 3436 cm$^{-1}$, 2914 cm$^{-1}$, 2848 cm$^{-1}$, 1619 cm$^{-1}$ and 1380 cm$^{-1}$ which could be assigned to the O–H hydroxyl bond vibration, C-H bond vibration, C = C bond and O-C vibration, respectively. The simultaneous presence of the O–H bond, and C = C on the surface of ARSB marks the presence of the -COOH carboxyl functional group which could be considered as the site of attachment of TiO$_2$ on the surface of ARSB (Ganguly et al., 2020). The set of peaks observed after the 1000 cm$^{-1}$ mark can be assigned to the Ti-O-Ti or Ti-O-C bonds (Cai et al., 2018; Ye et al., 2020). Thus, from the FTIR analysis of ARSB-TiO$_2$ composite, it was observed that the TiO$_2$ materials were attached on the surface of the ARSB.
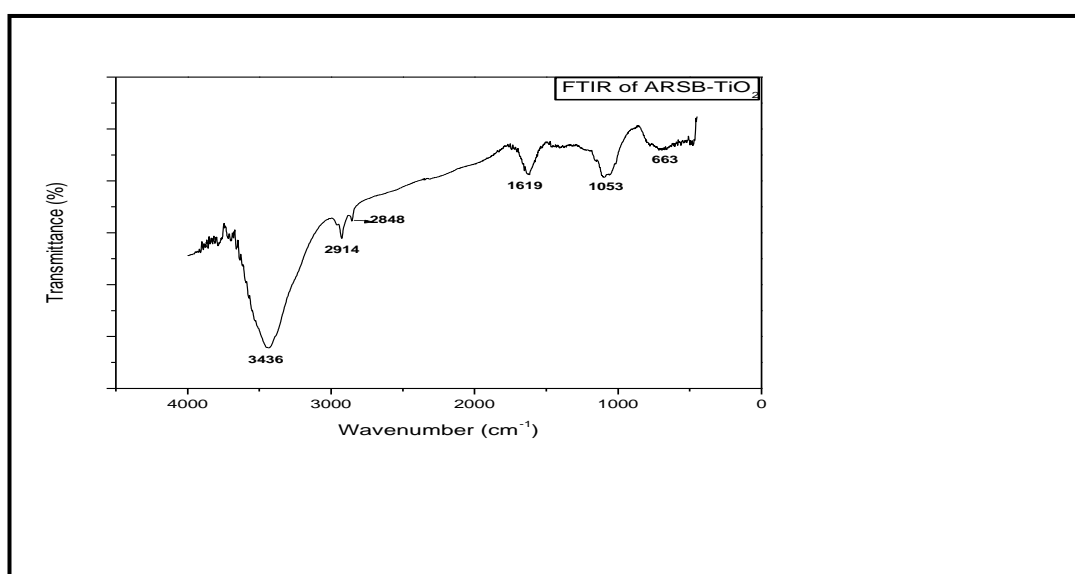


**Fig. 7.1 (b):-** FT-IR spectra image of ARSB-TiO$_2$

### 7.4.1.3 XRD analysis of ARSB-TiO$_2$

The XRD peaks (**Fig. 7.1 (c)**) of ARSB-TiO$_2$ were observed at 25.48°, 38.18°, 48.26°, 54.81° and 62.82 °, denotes the characteristic peak assigned to (101), (004), (200), (211), (204), (116), and (215) planes of TiO$_2$ (Li et al., 2016; Ye et al., 2020). From **Fig. 7.1 (c)**, anatase phase of TiO$_2$ (peak at 25.48°, 38.18°, 48.26° and 62.82°) and a small peak of rutile phase (peak at 54.81°) of TiO$_2$ were observed (Li et al., 2016; Ye et al., 2020). The absence of distinctive peak of rutile (except 54.81°) can be attributed to its low concentration present in the mixture composite. The peak at around 10-13° θ denoting the oxidation of the graphitic structure was not observed thereby denoting that the activated ARSB was reduced during the hydrothermal treatment (Fazal et al., 2020; Nawaz et al., 2017). The sharp peak observed at 26.78° can be attributed to the crystalline structure of the ARSB lattice. Thus from the XRD analysis of ARSB-TiO$_2$ it was inferred that the TiO$_2$ crystals were combined with the ARSB during the

solvo-thermal method and the ARSB particles were themselves reduced during the hydrothermal reaction.
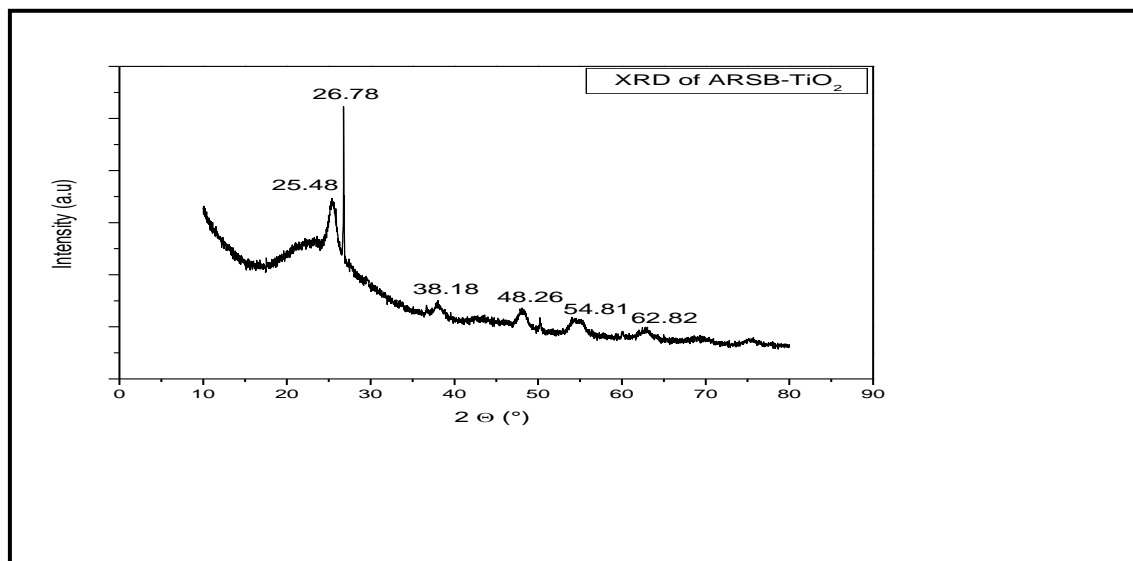


**Fig. 7.1 (c)**:- XRD image of ARSB-TiO$_2$

### 7.4.1.4 Raman Spectroscopy of ARSB-TiO$_2$

From the Raman Spectra of ARSB as shown in **Fig. 7.1 (d)**, the D-band and the G-band were observed at 1331 cm$^{-1}$ and 1586 cm$^{-1}$ respectively. The D-band denotes the sp$^2$ carbon atom with structural defect proportional to the extent of oxidation and the G-band denoted the in-plane vibration of the sp$^2$ bonded graphitic structure (Zhang et al., 2018). The ratio of I$_D$/I$_G$ serves as the parameter for observing the defects and disorders in graphitic structures (Nawaz et al., 2017). In the case of the ARSB-TiO$_2$ the ratio of I$_D$/I$_G$ >1, thereby signifying that the structure of sp$^3$ hybridized carbon molecules were disordered, which could be attributed to the decreased size of the sp$^2$ hybridized molecules, thereby marking that the TiO$_2$ was able to reduce the ARSB molecules (Nawaz et al., 2017).
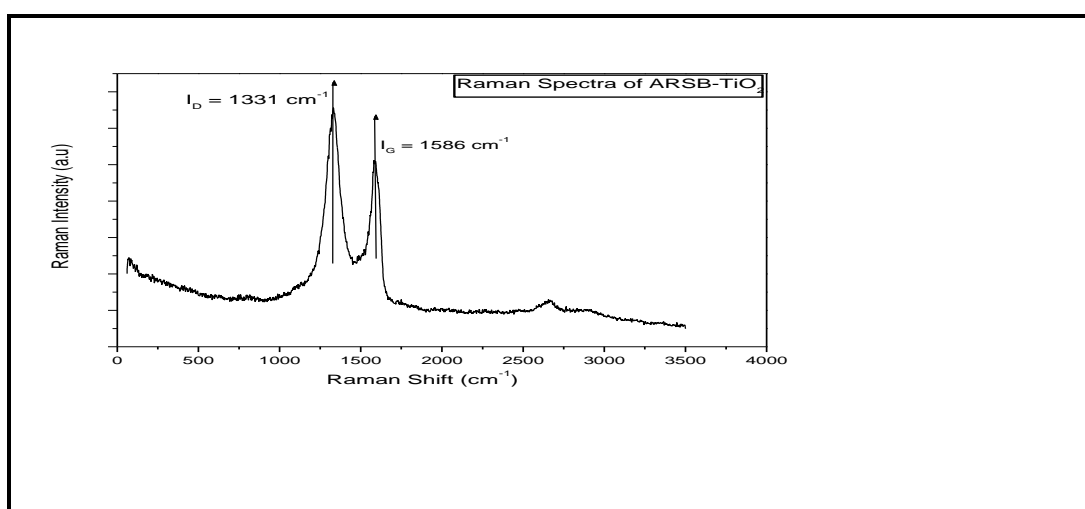


**Fig. 7.1 (d)** :- Raman Spectra of ARSB-TiO$_2$

### 7.4.1.5 UV adsorption spectra and band gap of ARSB-TiO$_2$

The UV adsorption spectra of ARSB-TiO$_2$ is shown in **Fig. 7.1 (e)**. From there it was observed that the peak of the adsorption spectra of ARSB-TiO$_2$ was observed more towards longer wavelength as compared to TiO$_2$ and ARSB. This could be attributed to the combination between TiO$_2$ and ARSB as has been observed from the FTIR and XRD analysis (Fazal et al., 2020; Xu et al., 2018). The combination of ARSB with TiO$_2$ by the Ti-O-C or Ti-O-Ti bond results in the formation of a new energy band which eventually results in the shifting of the adsorption spectra into the visible wavelength.

The band gap of ARSB-TiO$_2$ was evaluated using the Kubelka Munk function from the Tauc plot using the same method as used in **Chapter 6, Section 6.4.1** and is shown in **Fig. 7.1 (f)**. From there it was observed that the band gap ($E_g$) of TiO$_2$ was 3.36 eV, for ARSB was 3.31 eV and for ARSB-TiO$_2$ it was 2.4 eV. The lowering of the band gap of ARSB-TiO$_2$ can be attributed to the combination of TiO$_2$ with ARSB. The Ti-O-C bond formed due to the combination of TiO$_2$ with ARSB results in the formation of a new energy band thereby decreasing the band gap energy of ARSB-TiO$_2$ (Wang et al., 2016).
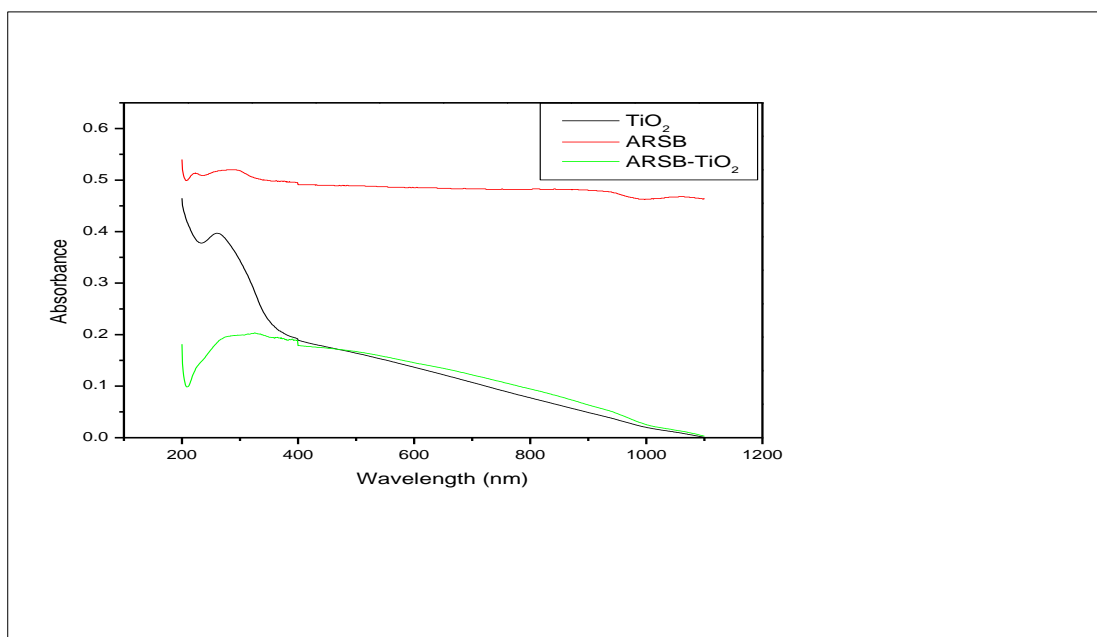


**Fig. 7.1 (e) :-** UV-Vis spectra of TiO$_2$, ARSB and ARSB-TiO$_2$
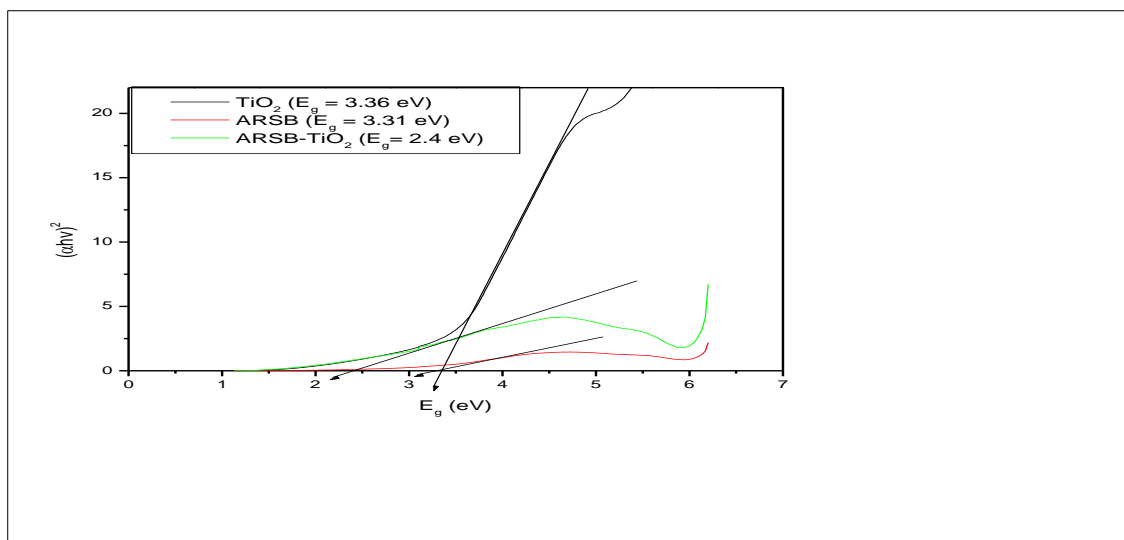
**Fig. 7.1 (f) :-** Energy band gap of $TiO_2$, ARSB and $ARSB-TiO_2$

## 7.4.2 Comparative Removal Study

At first a comparative study was performed in order to find which wavelength can most suitably excite the $ARSB-TiO_2$ composite. As mentioned before, the concentration of the four EC's (CBZ, NPX, RTN and BPA) were kept constant at 10 mg/L. The dose of the $ARSB-TiO_2$ was taken as 2 g/L. All the other parameters were also kept constant. The radiations used for activating the $ARSB-TiO_2$ composite were UVA, UVB, UVC and visible light. From the result of the experiment as shown in **Fig. 7.2** it was observed that in each case the visible light exhibited the highest efficiency for the purpose of removing the materials. The reason can be given as follows, as all the incident radiations were operating at the same wattage, therefore the incident radiations with the lowest photon energy will be generated at the highest quantity. As a consequence of which, the photons of visible light or visible light will be highest in number. As the particles of $ARSB-TiO_2$ (band gap energy = 2.4 eV) can be activated even by visible light (photon energy = 2.2- 2.7 eV) (Diwald et al., 2004), therefore the highest photocatalytic efficiency was exhibited under visible light. Thus, visible light was used in further experiment for the activation of $ARSB-TiO_2$ particles. Also, a set of experiments were conducted where only the visible light was utilized for degrading the EC molecules (figure not shown). There it was observed that only visible light was unable to degrade any of the EC's on its own.
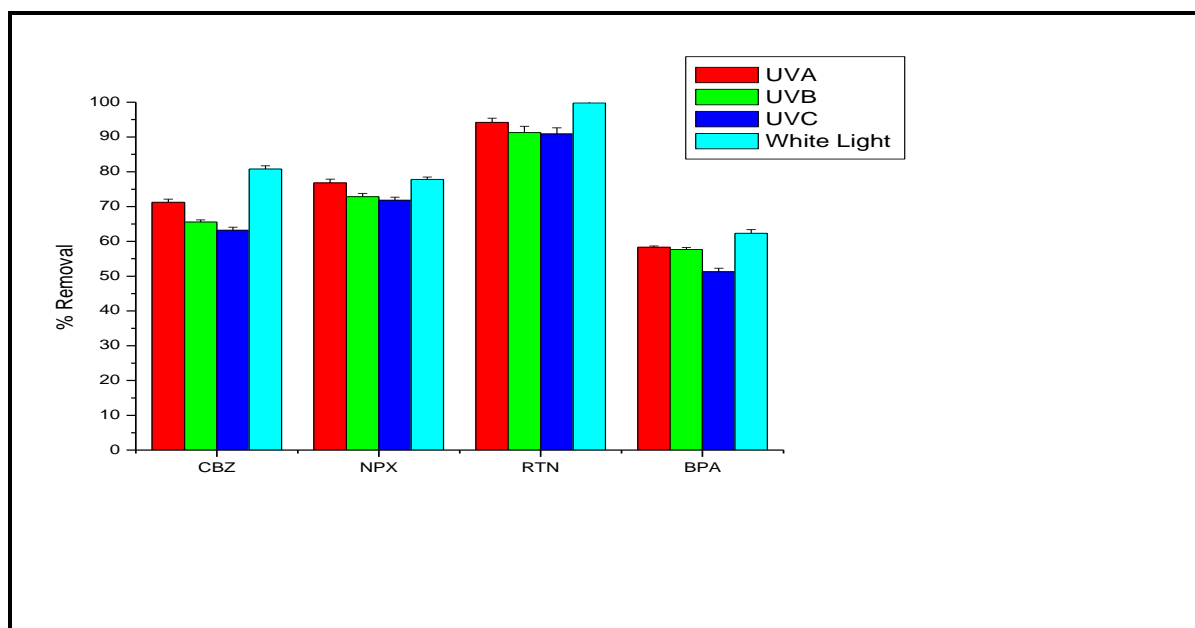
**Fig. 7.2**:- Effect of incident radiation on the removal of the EC's by ARSB-TiO$_2$

## 7.4.3 Batch Study

### 7.4.3.1 Effect of concentration of EC's on the removal of the EC's by ARSB-TiO$_2$

In order to investigate the effect of concentration of EC's on the removal efficiency of ARSB-TiO$_2$ a batch study was conducted with four concentration of EC's namely 5 mg/L, 10 mg/L, 15 mg/L and 20 mg/L. The dose of ARSB-TiO$_2$ was kept constant at 2 g/L, the pH of the experimental solution was kept at neutral and the temperature was kept at 303 K. The result of the experiment is shown in **Fig. 7.3(a)-(d)**. From the result of the experiment it was observed that the removal of CBZ, RTN and BPA by ARSB-TiO$_2$ increased with increase in concentration from 5 mg/L to 10 mg/L. This phenomenon could be attributed to the fact that, with increase in concentration of EC's, the gradient based transfer of the molecules of EC from the experimental solution to the surface of ARSB-TiO$_2$ took place. As a consequence of which the adsorption of EC molecules on the surface of ARSB-TiO$_2$ increased leading to the subsequent greater photo-degradation of CBZ molecules (Banerjee et al., 2016; Dong et al., 2015; Xu et al., 2018). However, when the concentration increased beyond 10 mg/L, the surface of ARSB-TiO$_2$ got saturated by the EC molecules, as a consequence of which the rate of adsorption and subsequent photo-degradation decreased leading to lesser removal of the EC's by ARSB-TiO$_2$ at this higher concentration. In case of NPX, however the removal of the EC's by ARSB-TiO$_2$ decreased with the increase in concentration which could be attributed to the saturation of the surface of ARSB-TiO$_2$ with NPX molecules, leading to decreased adsorption and subsequent photo-degradation at increasing concentration (Nawaz et al., 2017; Xu et al., 2018; Zhang et al., 2018). The removal of CBZ by ARSB-TiO$_2$ (**Fig. 7.3 (a)**) was 72.43 % at 5 mg/L, 78.6 % at 10 mg/L, 64.2 % at 15 mg/L and 56.07 % at 20

mg/L. The removal of NPX by ARSB-TiO$_2$ (**Fig. 7.3(b)**) was 83.46 % at 5 mg/L, 78.2 % at 10 mg/L, 71.68 % at 15 mg/L and 66.12 % at 20 mg/L. The removal of RTN by ARSB-TiO$_2$ (**Fig. 7.3(c)**) was 97.19 % at 5 mg/L, 99.73 % at 10 mg/L, 96.92 % at 15 mg/L and 89.66 % at 20 mg/L. The removal of BPA by ARSB-TiO$_2$ (**Fig. 7.3(d)**) at 5 mg/L, 10 mg/L, 15 mg/L and 20 mg/L were observed to be 71.13 %, 75.23 %, 70.57 % and 67.73 % respectively. For further experiment, the 10 mg/L concentration of the EC's were used.
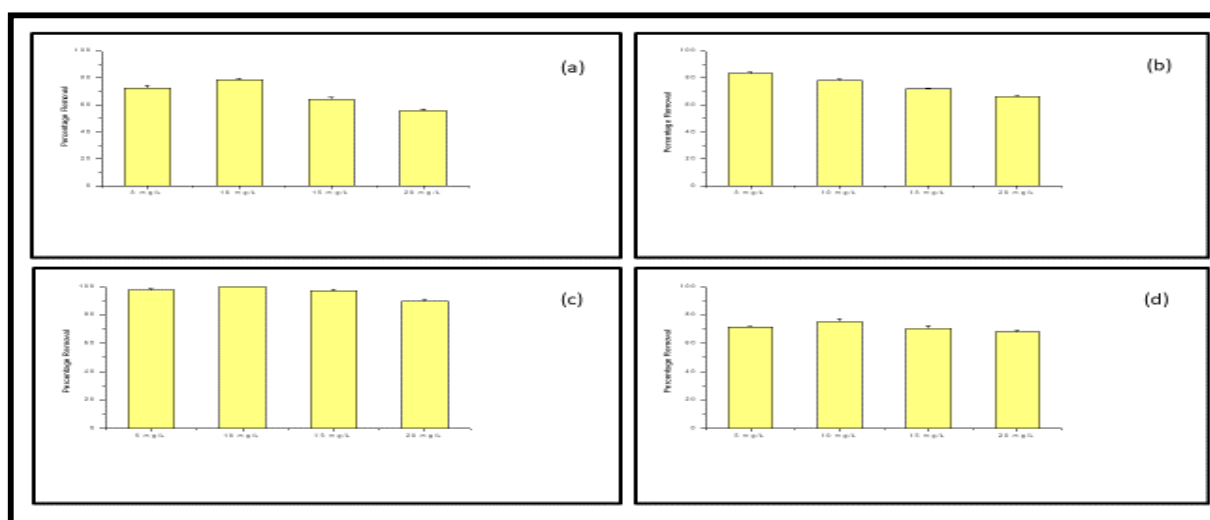


**Fig. 7.3:-** Effect of concentration on removal of  **(a)** CBZ **(b)** NPX **(c)** RTN **(d)** BPA by ARSB-TiO$_2$

### 7.4.3.2 Effect of dosage of photo-catalyst ARSB-TiO$_2$ on the removal CBZ by ARSB-TiO$_2$

The effect of the dosage of the adsorbent on its removal efficacy was investigated over four different dosage of ARSB-TiO$_2$ i.e., 0.5 g/L, 1 g/L, 1.5 g/L and 2 g/L. The concentration of the EC's were kept constant at 10 mg/L. The pH of the solution was kept at neutral and the temperature was kept at 303 K. From the result of the experiment as shown in **Fig. 7.4 ((a)-(d))** it was observed that the removal of EC's by ARSB-TiO$_2$ increased with increase in dose of ARSB-TiO$_2$. This outcome could be attributed to the greater availability of active sites at higher dosage of ARSB-TiO$_2$ which facilitates the higher adsorption and subsequent greater photo-catalysis of the EC's (Bhattacharya et al., 2022; Dong et al., 2015; Xu et al., 2018). In case of the removal of CBZ by ARSB-TiO$_2$ (**Fig. 7.4 (a)**) the removal at the 0.5 g/L dose of ARSB-TiO$_2$ was observed to be 49.79 %, the removal at 1 g/L dosage was found to be 61.73 %, at 1.5 g/L dosage was found to be 71.6 % and at the 2 g/L dosage was 80.04 % respectively. The removal of NPX by ARSB-TiO$_2$ (**Fig. 7.4 (b)**) at the 0.5 g/L dose of ARSB-TiO$_2$ was observed to be 56.62 %, the removal at 1 g/L dosage was found to be 64.89 %, at 1.5 g/L dosage was found to be 70.62 % and at the 2 g/L dosage was 78.35 % respectively. The removal of RTN by ARSB-TiO$_2$ (**Fig. 7.4 (c)**) at 0.5 g/L dose of ARSB-TiO$_2$ was observed to be 46.58 %, the removal at 1 g/L dosage was found to be 84.73 %, at 1.5 g/L dosage was found to be 86.43 % and at the 2 g/L dosage was 98.96 %

respectively. The removal of BPA by ARSB-TiO$_2$ (**Fig. 7.4 (d)**) at the 0.5 g/L dose of ARSB-TiO$_2$ was observed to be 39.75 %, the removal at 1 g/L dosage was found to be 60.22 %, at 1.5 g/L dosage was found to be 71.06 % and at the 2 g/L dosage was 74.27 % respectively. In case of each of these EC's, the highest removal was achieved for the 2 g/L dosage of ARSB-TiO$_2$ therefore this dosage of ARSB-TiO$_2$ was utilized for further studies.
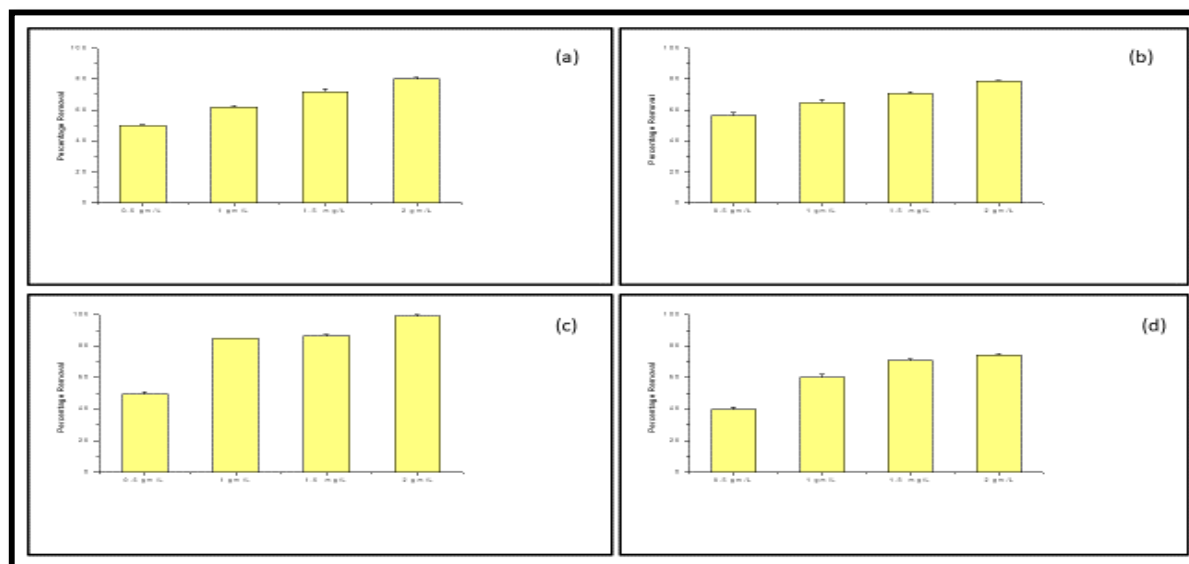


**Fig. 7.4 :-** Effect of dosage of ARSB-TiO$_2$ on the removal of **(a)** CBZ **(b)** NPX **(c)** RTN **(d)** BPA by ARSB-TiO$_2$

### 7.4.3.3 Effect of pH of the experimental solution on the removal efficacy of ARSB-TiO$_2$

The effect of pH on the removal of EC's by ARSB-TiO$_2$ was investigated under five different pH of the experimental solution, viz., pH 2, pH 4, pH 6, pH 8 and pH 10. The concentration of the EC's were kept constant at 10 mg/L and the dosage of ARSB-TiO$_2$ was kept fixed at 2 g/L. From the result of the experimental study as shown in **Fig. 7.5 ((a)-(d)).** The removal of CBZ by ARSB-TiO$_2$ (**Fig. 7.5 (a)**) was highest at the lower pH range. The pH$_{pzc}$ of ARSB-TiO$_2$ was obtained to be 7.5 and the pK$_a$ value of CBZ is around 13.9 (Al-hamadani et al., 2018). Therefore during the whole pH range, the molecules of CBZ remain neutral whereas the surface of ARSB-TiO$_2$ remains positive below pH 7.5 and becomes negative above pH 7.5. At the lower pH range, the adsorption of the CBZ molecules on the positive surface of ARSB is facilitated. Similar results were observed in the works of (Delhiraja et al., 2019) and (Khalil et al., 2020), where higher amount of CBZ were adsorbed on the surface of GO and graphene respectively at the lower pH range. Therefore, due to the higher adsorption of CBZ on ARSB-TiO$_2$ at the lower pH range higher photo-degradation was also observed at the lower pH range, leading to higher removal. Similarly, when the pH of the experimental solution was increased, the adsorption of CBZ on

the surface of ARSB-TiO$_2$ decreased leading to the lower adsorption, and thereby simultaneously resulting into lower photo-degradation of CBZ molecules (Chen et al., 2017; Lima et al., 2021; Naghdi et al., 2019). As a consequence of which, the highest removal of CBZ was observed at pH 2 (88.27 %) followed by pH 4 (80.04 %), followed by pH 6 (73.66 %) followed by pH 8 (71.6 %) followed by pH 10 (53.09 %).

The removal of NPX by ARSB-TiO$_2$ (**Fig. 7.5 (b)**) was highest at the lower pH range, with the highest removal percentage being recorded at pH 2 (85.4 %), followed by pH 4 (82.93 %), pH 6 (78.27 %), pH 8 (71.44 %) and pH 10 (65.35 %). The reason behind this phenomenon can be attributed to the fact that, the pH$_{pzc}$ of ARSB-TiO$_2$ was 7.51 and the pK$_a$ value of NPX was 4.15 (Mondal et al., 2020). Therefore at pH less than pH 4, the molecules of NPX remains neutrally charged and the surface of ARSB-TiO$_2$ remains positively charged. As a consequence of which at the lower pH range, more adsorption of NPX molecules takes place on the surface of ARSB-TiO$_2$ by virtue of H-H bonding and van der Waals force between the ARSB particles and the NPX molecules (Bhattacharya et al., 2021). However, with the increase in pH of the experimental solution (greater than pH 4.15 for NPX and greater than 7.5 for ARSB-TiO$_2$) both the NPX molecules and the surface of ARSB-TiO$_2$ acquire a net negative charge. Thus at the higher pH range (> pH 8) a force of repulsion takes place between the negatively charged surfaces of ARSB particles and the negatively charged NPX molecules. As a consequence of which the uptake of the NPX molecules by the surface of the ARSB-TiO$_2$ composite decreases at higher pH range, resulting in reduced adsorption and subsequently reduced photo-degradation at the higher pH range.

The removal of RTN by ARSB-TiO$_2$ (**Fig. 7.5 (c)**) decreased with the increase in pH of the experimental solution with the highest removal being observed at pH 2 (96.37 %) followed by pH 4 (96.11 %), followed by pH 6 (91.7 %), followed by pH 8 (86.46 %) followed by pH 10 (82.14 %). In order to find the reason behind this phenomenon, the pH$_{pzc}$ of ARSB-TiO$_2$ (pH = 7.5) and the pK$_a$ value of RTN has to be considered (pH 2.6 and pH 8.2) (Al-rub et al., 2020). At the lower pH range (pH 2-4), the surface charge of ARSB-TiO$_2$ remains positive whereas the RTN molecules remains highly protonated leading to enhanced adsorption of RTN by ARSB-TiO$_2$ followed by its photo-catalysis (Dong et al., 2015; Mondal et al., 2020). On the other hand, at the higher pH range (pH 8-10), the surface of ARSB-TiO$_2$ remains negative and the RTN molecules remains weakly protonated, leading to decreased adsorption of RTN molecules by ARSB-TiO$_2$, thereby leading to decreased photo-catalysis (Dong et al., 2015; Mondal et al., 2020). As a consequence of which, the highest removal of RTN by ARSB-TiO$_2$ was observed at pH 2.

The removal of BPA by ARSB-TiO$_2$ (**Fig. 7.5 (d)**) was highest at the lowest pH and subsequently decreased with the increase in pH of the experimental solution. The removal of BPA at pH 2, pH 4, pH 6, pH 8 and pH 10 were observed to be 95.73 %, 87.76 %, 75.53 %, 71.03 % and 60.29 % respectively. This could be attributed to the fact that the pK$_a$ value of BPA was 9.6 (Phatthanakittiphong & Seo, 2016) and the pH$_{pzc}$ of ARSB-TiO$_2$ was 7.5. Therefore at pH less than 7.5 the surface of ARSB-TiO$_2$ remains positive and below pH 8, the molecules of BPA also remains neutrally charged (Garikoé et al., 2020). Therefore at this pH range the adsorption of BPA by ARSB-TiO$_2$ was facilitated. As a consequence of which the removal of BPA by ARSB-TiO$_2$ was also facilitated at the lower pH range (Dong et al., 2015). However, when the pH increased to around pH 8, then the BPA molecules dissociated to form mono valent anions (Garikoé et al., 2020) and the surface of ARSB-TiO$_2$ also attains a negative charge. As a consequence of which, the removal of BPA by ARSB-TiO$_2$ at this higher pH range is inhibited by the electrostatic force of repulsion acting between the surface of ARSB-TiO$_2$ and the molecules of BPA, which reduces the rate of adsorption and hence photo-catalysis (Dong et al., 2015; L. Xu et al., 2018).
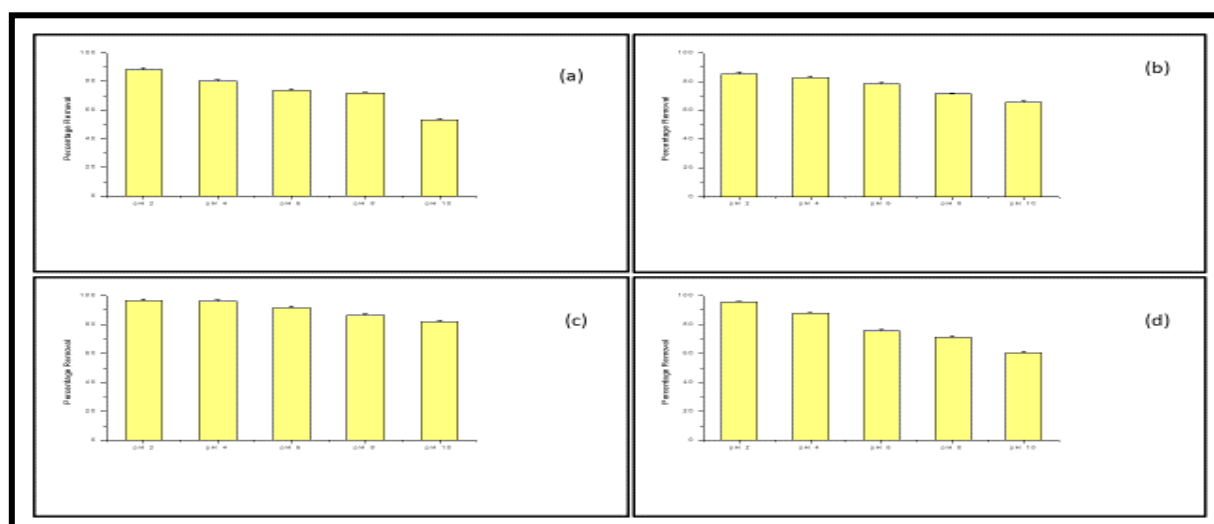


**Fig. 7.5:-** Effect of pH on the removal of **(a)** CBZ **(b)** NPX **(c)** RTN **(d)** BPA by ARSB-TiO$_2$

### 7.4.3.4 Effect of temperature on the removal of EC's by ARSB-TiO$_2$

The effect of temperature on the removal of EC's by ARSB-TiO$_2$ was investigated for four temperatures namely 298 K, 303 K, 308 K and 313 K. The dosage of ARSB-TiO$_2$ was kept constant at 2 g/L, the pH of experimental solution was kept constant at pH 7 and the concentration of EC's was kept fixed at 10 mg/L. The result of the experiment is shown in **Fig. 7.6 (a)-(d)**. From the result of the experiment as shown in **Fig. 7.6 (a)** it was observed that the removal of CBZ increased with the increase in temperature up-to 308 K. Thereafter, when the temperature was increased to 313 K, the removal of CBZ by ARSB-

TiO$_2$ exhibited a slight decrease. The logic behind this result can be attributed to the fact that, with the increase in temperature, the pore space of ARSB increased leading to greater adsorption of CBZ molecules on its surface (Bhattacharya et al., 2021). With the increase in temperature, the interaction between the CBZ molecules and the surface of ARSB might also have increased, leading to greater adsorption of CBZ molecules on the surface of ARSB-TiO$_2$. And as photo-catalysis by a semiconducting material has to be preceded by adsorption of the pollutant on the surface of the semiconductor, therefore the rate of removal by photo-catalysis also increased with the increase in adsorption (Dong et al., 2015). However, when the temperature was increased beyond the optimum point of 308 K and increased to 313 K, then the rate of adsorption decreased. As a consequence of which the removal by photo-catalysis also decreased. The highest removal was observed at 308 K (80.04 %), followed by 303 K (76.34 %), followed by 313 K (74.69 %) and lastly by 298 K (73.05 %).

In case of the removal of NPX (**Fig. 7.6 (b)**) it was observed that the removal of NPX increased with the increase in temperature. The removal at 298 K was found to be 76.45 %, at 303 K was found to be 77.59 %, at 308 K was found to be 78.7 % and at 313 K was found to be 81.35 %. The increase in removal of NPX by ARSB-TiO$_2$ with subsequent increase in temperature can be attributed to the increase in the pore space of ARSB-TiO$_2$ and the increased interaction between the surface of ARSB-TiO$_2$ and NPX molecules leading to the increased adsorption and subsequently increased photo-degradation of the NPX molecules (Bhattacharya et al., 2021; Dong et al., 2015).

The removal of RTN by ARSB-TiO$_2$ (**Fig. 7.6 (c)**) showed a similarity to the removal of CBZ by ARSB-TiO$_2$. In this case also the removal increased with the increase in temperature till 308 K. This could be attributed to the increase in pore size and increased interaction between the surface of ARSB-TiO$_2$ and the RTN molecules leading to higher adsorption and subsequently greater photo-degradation of RTN molecules by ARSB-TiO$_2$ (Banerjee et al., 2016; Bhattacharya et al., 2021; Dong et al., 2015). However, when the temperature increased beyond 308 K, a decrease in the percentage removal of RTN by ARSB-TiO$_2$ was observed, which could be attributed to reduced adsorption due to higher kinetic energy of adsorbate molecules (Banerjee et al., 2016; Bhattacharya et al., 2021). As a consequence of which, the percentage removal by photo-degradation also decreased at 313 K. The percentage removal of RTN at the four temperature points were 89.76 % at 298 K, 94.08 % at 303 K, 99.38 % at 308 K and 90.45 % at 313 K.

The removal of BPA by ARSB-TiO$_2$ (**Fig. 7.6 (d)**) decreased with the increase in temperature with the removal for 298 K, 303 K, 308 K and 313 K being 81.74 %, 78.11 %, 75.83 % and 73.61 % respectively. This could be attributed to the fact that with the increase in temperature, the kinetic energy of the BPA molecules increases. As a consequence of which the adsorption of BPA onto the surface of ARSB is decreased with the increase in temperature. And as the process of photo-catalysis is preceded by adsorption therefore the rate of photo-degradation also decreases with the increase in temperature (Dong et al., 2015). Thus, it can be inferred that the degradation of BPA by ARSB-TiO$_2$ was exothermic in nature.
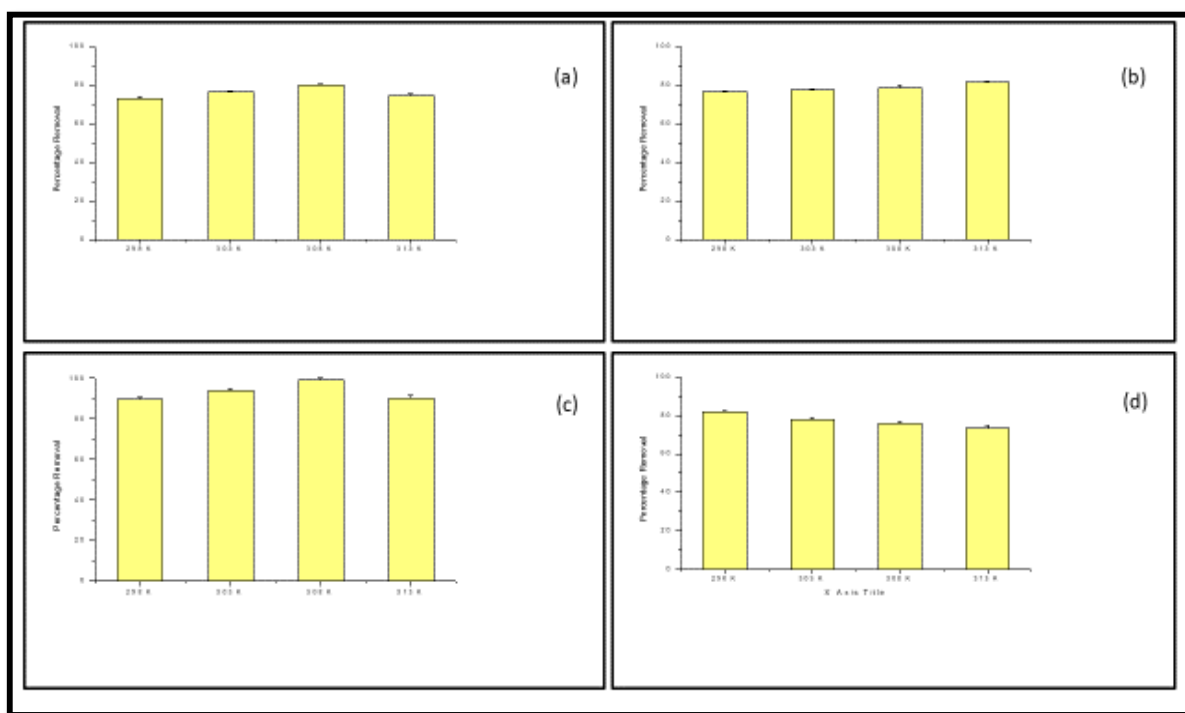


**Fig. 7.6 :-** Effect of temperature on the removal of **(a)** CBZ **(b)** NPX **(c)** RTN **(d)** BPA by ARSB-TiO$_2$

### 7.4.4  Process Optimization by RSM

#### 7.4.4.1 Optimization of the removal of CBZ by ARSB-TiO₂ by RSM

The RSM was performed with the aim of understanding the effect of inter parameter interaction on the experimental outcome. In **Table 7.1**, the outcome of the 20 experiments as proposed by the software for the CCD model of the RSM is given and in **Table 7.2** the result of the ANOVA of the RSM model is provided. From there it is observed that the $R^2$ value of the model was 0.94 and the adjusted $R^2$ value was 0.89 which propounded the fact that the polynomial model suggested by RSM was appropriate for predicting the outcome of this adsorption reaction. The high value of F (18.32, much greater than unity) and the low value of P ($< 0.0001$) meant that the optimizing model was highly significant, with the experimental data points exhibiting a high degree of correlation with the predicted data points (Bhattacharya et al., 2021). **Fig. 7.7** shows the relation between the experimentally determined data points and the predicted data points and there also it can be noted that the experimental data points exhibits a high degree of correlation with the predicted data points. The real equation which was used to predict the effect of the input variables on the response output is presented as follows :-

$$Removal = -86.1272 + 1.74409 \times pH + 70.50974 \times Dose + 1.19032 \times Time + 0.1595 \times pH \times Dose + 0.081283 \times pH \times Time - 0.11487 \times Dose \times Time - 0.96817 \times pH^2 - 12.06413 \times Dose^2 - 5.30914 \times 10^{-3} \times Time^2 \dots\dots\dots\dots\dots\dots\dots\dots\dots................. \text{(xxxxv)}$$

As per the RSM model the optimized conditions under which maximum removal of CBZ (81.34 %) was possible were: ARSB-TiO₂ dosage of 2 g/L, pH value of 6.5 and reaction time of 120 minutes. For this RSM model, the interaction between the experimental parameters (input variables) and their outcome on the percentage removal of CBZ (response variable) is illustrated by the contour plots shown in **Fig. 7.8-7.10**.

➢ **Effect of ARSB-TiO₂ dosage and solution pH on CBZ removal by ARSB-TiO₂**

The interaction in between the pH of the experimental solution and the dosage of ARSB-TiO₂ and its effect on the removal of CBZ is conveyed in the contour plot of **Fig. 7.8**. From the result of the experiment it was observed that the removal of CBZ was highest at the lower pH range. This could be attributed to the higher adsorption of CBZ molecules on the surface of ARSB-TiO₂ at the lower pH range (Delhiraja et al., 2019; A. M. E. Khalil et al., 2020). The rate of adsorption of CBZ on the surface of ARSB-TiO₂ decreased with the increase in pH of the experimental solution (D. Chen et al., 2017; Lima et al., 2021; Naghdi et al., 2019), therefore the rate of photo-catalysis also decreased with the increase in pH of the experimental solution. In case of the dose variation study, it was observed that the removal of CBZ by ARSB-TiO₂ was higher at the higher dose range and subsequently decreased with the decrease in dosage of ARSB-TiO₂. This could be attributed to the fact that with increase in dosage

of ARSB-TiO$_2$, the surface area available for the uptake of CBZ increased leading to the greater adsorption and simultaneously greater degradation of CBZ molecules (Bhattacharya et al., 2022; L. Xu et al., 2018).

➢ **Effect of solution pH and contact time on CBZ removal by ARSB-TiO$_2$**

The interaction in between the pH of the experimental solution and agitation speed and its effect on the removal of CBZ by ARSB-TiO$_2$ is conveyed in the contour plot of **Fig. 7.9**. From there it was observed that the removal of CBZ by ARSB-TiO$_2$ was highest at the lower pH range and subsequently decreased with the increase in pH of the experimental solution. This could be attributed to the enhanced adsorption of CBZ molecules on the surface of ARSB-TiO$_2$ at the lower pH range (Delhiraja et al., 2019; A. M. E. Khalil et al., 2020) and the reduced adsorption of CBZ on the surface of ARSB-TiO$_2$ at the higher pH range (D. Chen et al., 2017; Dong et al., 2015; Lima et al., 2021; Naghdi et al., 2019). In case of the effect of contact time on the removal of CBZ by ARSB-TiO$_2$ it was observed that higher removal of CBZ was achieved at the higher contact time, which could be attributed to greater interaction between CBZ molecules and the surface of ARSB-TiO$_2$ leading to higher adsorption and subsequently greater photo-degradation of CBZ molecules by ARSB-TiO$_2$ (Bhattacharya et al., 2021; Dong et al., 2015).

➢ **Effect of contact time and dosage of ARSB-TiO$_2$ dosage on CBZ removal by ARSB-TiO$_2$**

The interaction in between the contact time and dosage of ARSB-TiO$_2$ and its effect on the removal of CBZ by ARSB-TiO$_2$ is conveyed in the contour plot of **Fig. 7.10**. From there it was observed that removal of CBZ by ARSB-TiO$_2$ increased with increase in dosage of ARSB-TiO$_2$ which could be attributed to the greater availability of active sites for the uptake of CBZ molecules which is followed by their photo-catalysis (Bhattacharya et al., 2022; Dong et al., 2015). On the other hand, the removal of CBZ by ARSB-TiO$_2$ increases with the increase in contact time which could be attributed to the enhanced interaction between the surface of ARSB-TiO$_2$ and the CBZ molecules at the greater contact time, leading to their higher adsorption followed by photo-catalysis (Bhattacharya et al., 2021).

**Table 7.1**:- The table showing the 20 different set of parameters (runs) along with their corresponding outcome as proposed by CCD model of RSM for optimization of CBZ removal by ARSB-TiO$_2$

| | | | Factor 1 | Factor 2 | Factor 3 | Response 1 |
|---|---|---|---|---|---|---|
| Std | Run | Block | A:pH | B:Dose | C:Time | R1 |
| | | | | mg/10 ml | min | |
| 20 | 1 | Block 1 | 6.50 | 2 | 120.00 | 81.34 |
| 19 | 2 | Block 1 | 9.00 | 1 | 90.00 | 27.76 |
| 1 | 3 | Block 1 | 9.00 | 3 | 150.00 | 77.88 |
| 3 | 4 | Block 1 | 4.00 | 1 | 150.00 | 51.19 |
| 9 | 5 | Block 1 | 10.70 | 2 | 120.00 | 55.02 |
| 16 | 6 | Block 1 | 6.50 | 2 | 120.00 | 81.34 |
| 12 | 7 | Block 1 | 4.00 | 1 | 90.00 | 44.69 |
| 4 | 8 | Block 1 | 6.50 | 2 | 120.00 | 81.34 |
| 2 | 9 | Block 1 | 6.50 | 2 | 120.00 | 81.34 |
| 6 | 10 | Block 1 | 6.50 | 3.68 | 120.00 | 62.49 |
| 13 | 11 | Block 1 | 6.50 | 2 | 120.00 | 81.34 |
| 8 | 12 | Block 1 | 6.50 | 0.32 | 120.00 | 32.63 |
| 15 | 13 | Block 1 | 9.00 | 3 | 90.00 | 60.78 |
| 18 | 14 | Block 1 | 9.00 | 1 | 150.00 | 69.51 |
| 5 | 15 | Block 1 | 2.30 | 2 | 120.00 | 74.19 |
| 17 | 16 | Block 1 | 4.00 | 3 | 150.00 | 68.83 |
| 7 | 17 | Block 1 | 6.50 | 2 | 69.55 | 62.51 |
| 10 | 18 | Block 1 | 6.50 | 2 | 120.00 | 81.34 |
| 11 | 19 | Block 1 | 6.50 | 2 | 170.45 | 73.83 |
| 14 | 20 | Block 1 | 4.00 | 3 | 90.00 | 65.25 |

**Table 7.2** :- ANOVA analysis for the RSM for the photocatalytic removal of CBZ by ARSB-TiO$_2$

| R$^2$ Value | Adjusted R$^2$ Value | F-value | Probability Value P |
|---|---|---|---|
| 0.94 | 0.89 | 18.32 | <0.0001 Significant |
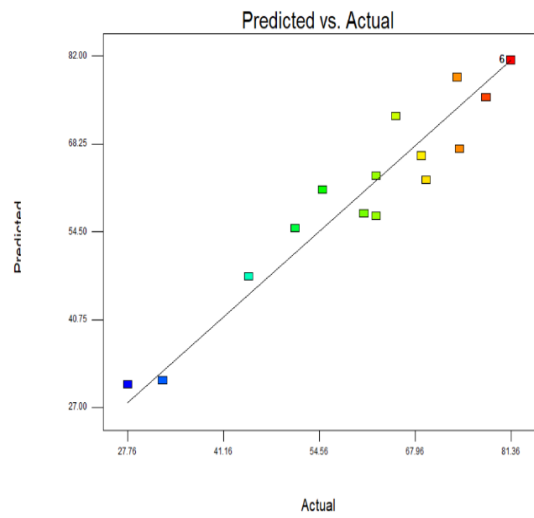
**Fig. 7.7**: Relation between the predicted data points and the experimental data points as per the RSM model.
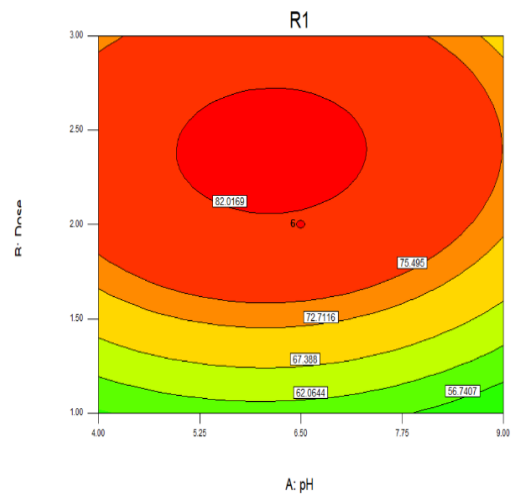


**Fig. 7.8**: Interaction between the pH of the experimental solution and the dose of the ARSB-TiO$_2$ and their effect on the percentage removal of
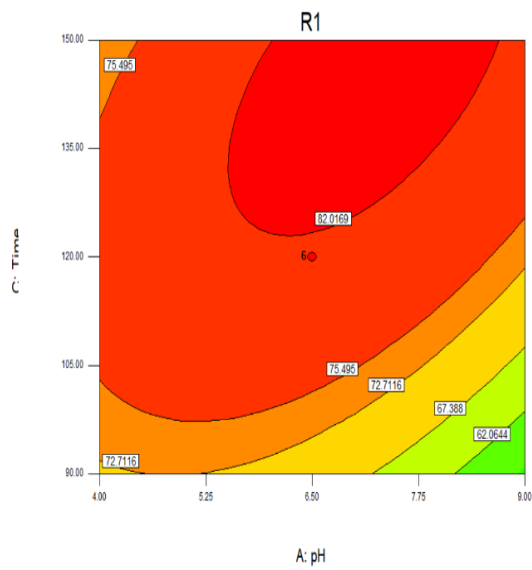


**Fig. 7.9**: The interaction between the pH of the experimental solution and contact time and their effect on the percentage removal of CBZ by ARSB-TiO$_2$.
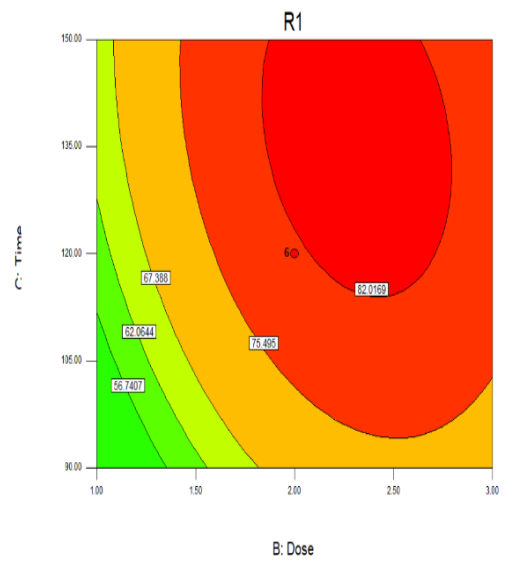


**Fig. 7.10**: The plot showing the interaction between the dose of the ARSB-TiO$_2$ and the contact time as per the RSM model and their effect on the percentage removal of CBZ.

### 7.4.4.2 Process Optimization of the removal of NPX by ARSB-TiO₂ by RSM

The Response Surface Methodology was performed with the aim of understanding the effect of inter parameter interaction on the experimental outcome. In **Table 7.3**, the outcome of the 20 experiments as proposed by the software for the CCD model of the RSM is given and in **Table 7.4** the result of the ANOVA of the RSM model is provided. From there it is observed that the $R^2$ value of the model was 0.92 and the adjusted $R^2$ value was 0.84 which propounded the fact that the polynomial model suggested by RSM was appropriate for predicting the outcome of this adsorption reaction. The high value of F (12.23, much greater than unity) and the low value of P (0.0003 <0.0005) meant that the optimizing model was highly significant, with the experimental data points exhibiting a high degree of correlation with the predicted data points(Bhattacharya et al., 2021). **Fig. 7.11** shows the relation between the experimentally determined data points and the predicted data points and there also it can be noted that the experimental data points exhibited a high degree of correlation with the predicted data points. The real equation which was used to predict the effect of the input variables on the response output is presented as follows.

$Removal\% = -7.38128 + 7.57467 \times pH + 29.55393 \times Dose + 0.6581 \times Time + 1.43164 \times pH \times Dose + 0.042949 \times pH \times Time + 0.077547 \times Dose \times Time - 1.55469 \times pH^2 - 8.82912 \times Dose^2 - 4.72541 \times 10^{-3} \times Time^2 \dots\dots\dots\dots\dots\dots\dots\dots\dots\dots\dots$(xxxxvi)

As per the RSM model the optimized conditions under which maximum removal of NPX (89.62 %) was possible were: ARSB-TiO₂ dosage of 3.68 g/L, pH value of 6.5 and reaction time of 120 minutes. For this RSM model, the interaction between the experimental parameters (input variables) and their outcome on the percentage removal of NPX (response variable) is illustrated by the contour plots shown in **Fig. 7.12-7.14**.

> **Effect of ARSB-TiO₂ dosage and solution pH on NPX removal by ARSB-TiO₂**

The interaction in between the pH of the experimental solution and the dosage of ARSB-TiO₂ and its effect on the removal of NPX by ARSB-TiO₂ is conveyed in the contour plot of **Fig. 7.12**. From the result of the experiment it was observed that the removal of NPX was highest at the lower pH range and decreased with the increase in pH of the experimental solution. This could be attributed to the fact that at the lower pH range the surface of ARSB-TiO₂ acquires a positive charge and the NPX molecules acquire neutral charge (pH$_{pzc}$ of ARSB-TiO₂ is 7.5 and the pK$_a$ of NPX is 4.15) (Mondal et al., 2020). The neutrally charged NPX molecules are adsorbed on the surface of ARSB-TiO₂, followed by which the molecules are photodegraded. However, when the pH of the experimental solution reaches the higher pH range (greater than pH 4.15), the molecules of NPX undergoes a resonance change and becomes more negatively charged (Bhattacharya et al., 2021; Mondal et al., 2020)**.** On the other hand, the surface charge of ARSB-TiO₂ also becomes negative when the pH of the experimental solution goes

over pH 7.5. Due to the electrostatic force of repulsion formed due to the presence of like charges, the adsorption of NPX molecules on the surface of ARSB-TiO$_2$ is disrupted at this high pH. As a result of which, the photo-degradation of NPX molecules is also less at the higher pH range (Dong et al., 2015). In case of the dose variation study, it was observed that the removal of NPX by ARSB-TiO$_2$ was higher at the higher dose range and subsequently decreased with the decrease in dosage of ARSB-TiO$_2$. This could be attributed to the fact that with increase in dosage of ARSB-TiO$_2$, the surface area available for the uptake of NPX increased leading to the greater adsorption and simultaneously greater photo-degradation of NPX molecules (Bhattacharya et al., 2022; Dong et al., 2015; L. Xu et al., 2018).

➢ **Effect of solution pH and contact time on NPX removal by ARSB-TiO$_2$**

The interaction in between the pH of the experimental solution and contact time and its effect on the removal of NPX by ARSB-TiO$_2$ is conveyed in the contour plot of **Fig. 7.13**. From there it was observed that the removal of NPX by ARSB-TiO$_2$ was highest at the lower pH range and subsequently decreased with the increase in pH of the experimental solution. This could be attributed to the neutral charge of NPX molecules and positive charge on the surface of ARSB-TiO$_2$ at the lower pH which accelerates the adsorption of NPX on the surface of ARSB-TiO$_2$, followed by which the molecules of NPX are degraded (Bhattacharya et al., 2021; Dong et al., 2015; L. Xu et al., 2018). On the other hand, at the higher pH range (pH >8), both the NPX molecules and the surface of ARSB-TiO$_2$ acquire a negative charge, resulting in the formation of an electrostatic force of repulsion which inhibits the adsorption of NPX molecules onto the surface of ARSB-TiO$_2$. As a consequence of which, the adsorption, and subsequent photo-degradation of NPX molecules by ARSB-TiO$_2$ decreases at the higher pH range (Bhattacharya et al., 2021; Dong et al., 2015; L. Xu et al., 2018). On the other hand, the interaction between NPX molecules and the surface of ARSB-TiO$_2$ most probably increases with the increase in contact time up-to to an optimum point (around the 120 minute mark). Till that point the adsorption of NPX molecules on the surface of ARSB-TiO$_2$ increases with the increase in contact time, simultaneously leading to the greater photo-degradation of the NPX molecules (Bhattacharya et al., 2021; Dong et al., 2015; L. Xu et al., 2018). However, beyond that point, the adsorption of NPX molecules on the surface of ARSB-TiO$_2$ -is decreased, probably due to desorption leading to decreased adsorption and thus, reduced photo-degradation at the high contact time.

➢ **Effect of contact time and dosage of ARSB-TiO$_2$ dosage on NPX removal by ARSB-TiO$_2$**

The interaction in between the contact time and dosage of ARSB-TiO$_2$ and its effect on the removal of NPX by ARSB-TiO$_2$ is conveyed in the contour plot of **Fig. 7.14**. From there it was observed that removal of NPX by ARSB-TiO$_2$ increased with increase in dosage of ARSB-TiO$_2$ which could be attributed to the greater availability of more active sites for the uptake of NPX molecules which is followed by their photo-catalysis (Bhattacharya et al., 2022; Dong et al., 2015; L. Xu et al., 2018). The

adsorption of NPX molecules on the surface of ARSB-TiO$_2$ mostly takes place by hydrogen bonding and van deer Waals force (Bhattacharya et al., 2021). On the other hand, the removal of NPX by ARSB-TiO$_2$ increases with the increase in contact time up-to an optimum point (120 minutes), which could be attributed to increase in adsorption, hence photo-degradation with increase in contact time (Bhattacharya et al., 2021). However, beyond this optimum point, a decrease in percentage removal of NPX by ARSB-TiO$_2$ was observed with increase in contact time, which could be attributed to the decrease in adsorption due to desorption beyond the optimum point (Bhattacharya et al., 2021).

**Table 7.3** :- The table showing the 20 different set of parameters (runs) along with their corresponding outcome as proposed by the CCD model of RSM for optimization of NPX removal by ARSB-TiO$_2$

| | | | Factor 1 | Factor 2 | Factor 3 | Response 1 |
|---|---|---|---|---|---|---|
| Std | Run | Block | A:pH | B:Dose | C:Time | R1 |
| | | | | g/L | min | |
| 20 | 1 | Block 1 | 6.50 | 2.00 | 120.00 | 81.39 |
| 19 | 2 | Block 1 | 9.00 | 1.00 | 90.00 | 38.8 |
| 1 | 3 | Block 1 | 9.00 | 3.00 | 150.00 | 68.5 |
| 3 | 4 | Block 1 | 4.00 | 1.00 | 150.00 | 55.98 |
| 9 | 5 | Block 1 | 10.70 | 2.00 | 120.00 | 32.36 |
| 16 | 6 | Block 1 | 6.50 | 2.00 | 120.00 | 81.39 |
| 12 | 7 | Block 1 | 4.00 | 1.00 | 90.00 | 62.06 |
| 4 | 8 | Block 1 | 6.50 | 2.00 | 120.00 | 81.39 |
| 2 | 9 | Block 1 | 6.50 | 2.00 | 120.00 | 81.39 |
| 6 | 10 | Block 1 | 6.50 | 3.68 | 120.00 | 89.62 |
| 13 | 11 | Block 1 | 6.50 | 2.00 | 120.00 | 81.39 |
| 8 | 12 | Block 1 | 6.50 | 0.32 | 120.00 | 31.28 |
| 15 | 13 | Block 1 | 9.00 | 3.00 | 90.00 | 52.4 |
| 18 | 14 | Block 1 | 9.00 | 1.00 | 150.00 | 29.13 |
| 5 | 15 | Block 1 | 2.30 | 2.00 | 120.00 | 83.54 |
| 17 | 16 | Block 1 | 4.00 | 3.00 | 150.00 | 64.57 |
| 7 | 17 | Block 1 | 6.50 | 2.00 | 69.55 | 74.59 |
| 10 | 18 | Block 1 | 6.50 | 2.00 | 120.00 | 81.39 |
| 11 | 19 | Block 1 | 6.50 | 2.00 | 170.45 | 72.1 |
| 14 | 20 | Block 1 | 4.00 | 3.00 | 90.00 | 77.81 |

**Table 7.4** :- ANOVA analysis for the RSM for the photocatalytic removal of NPX by ARSB-TiO$_2$

| $R^2$ Value | Adjusted $R^2$ Value | f- value | Probability Value P |
|---|---|---|---|
| 0.92 | 0.84 | 12.23 (>1) | 0.0003 (<0.0005)  Significant |
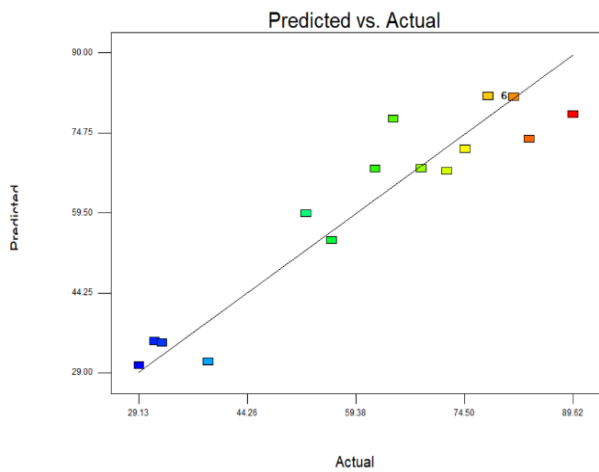
**Fig. 7.11**: Relation between the predicted data points and the experimental data points as per the RSM model.
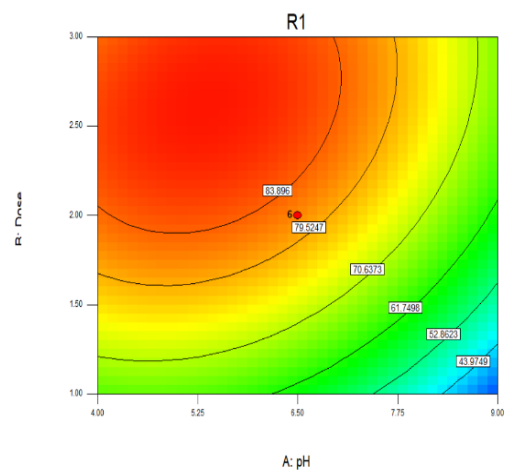


**Fig. 7.12**: Interaction between the pH of the experimental solution and the dose of the ARSB-$TiO_2$ and their effect on the percentage removal of NPX.
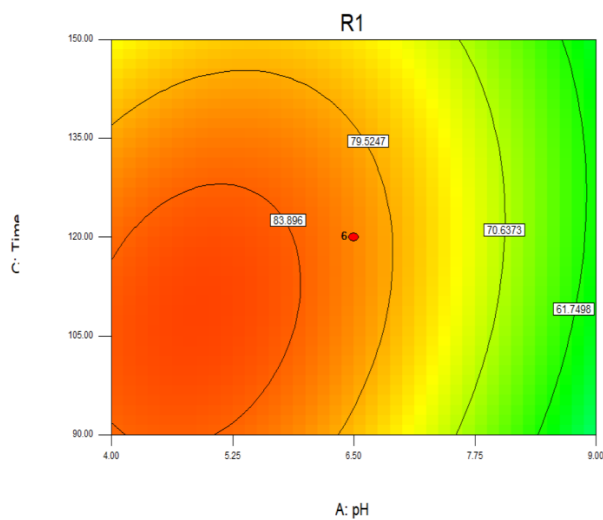


**Fig. 7.13**: The interaction between the pH of the experimental solution and agitation speed and their effect on the percentage removal of NPX by ARSB-$TiO_2$.
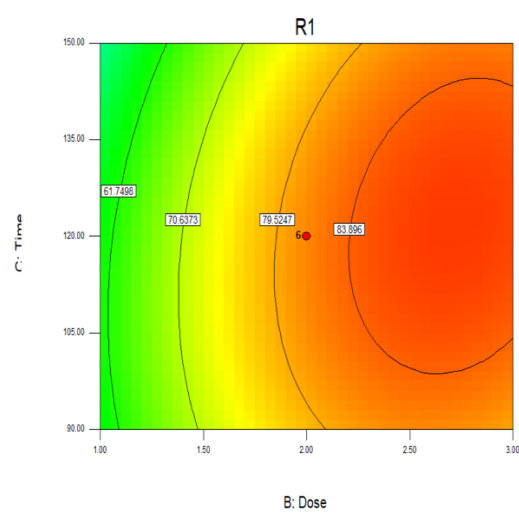


**Fig. 7.14**: The plot showing the interaction between the dose of the ARSB-$TiO_2$ and the agitation speed as per the RSM model and their effect on the percentage removal of NPX.

### 7.4.4.3 Process Optimization of the removal of RTN by ARSB-TiO$_2$ by RSM

The Response Surface Methodology was performed with the aim of understanding the effect of inter parameter interaction on the experimental outcome. In **Table 7.5** the outcome of the 20 experiments as proposed by the software for the CCD model of the RSM is given and in **Table 7.6** the result of the ANOVA of the RSM model is provided. From there it is observed that the $R^2$ value of the model was 0.82 and the adjusted $R^2$ value was 0.66 which propounded the fact that the polynomial model suggested by RSM was appropriate for predicting the outcome of this adsorption reaction. The high value of F (5.14, greater than unity) and the low value of P ( $0.0087 < 0.01$) meant that the optimizing model was highly significant, with the experimental data points exhibiting a high degree of correlation with the predicted data points (Bhattacharya et al., 2021). **Fig.7.15** shows the relation between the experimentally determined data points and the predicted data points and there also it can be noted that the experimental data points exhibits a high degree of correlation with the predicted data points. The real equation which was used to predict the effect of the input variables on the response output is presented as follows.

$$Removal = 32.08801 - 1.01019 \times pH + 0.63777 \times Dose - 0.20753 \times Time - 0.018512 \times pH \times Dose + 0.015575 \times pH \times Time + 2.57937 \times 10^{-4} \times Dose \times Time + 0.18745 \times pH^2 - 1.10428 \times 10^{-3} \times Dose^2 + 4.15637 \times 10^{-4} \times Time^2 \dots\dots\dots\dots\dots\dots(xxxxvii)$$

As per the RSM model the optimized conditions under which maximum removal of RTN (96.19 %) was possible were: ARSB-TiO$_2$ dosage of 3 g/L, pH value of 4 and reaction time of 90 minutes. For this RSM model, the interaction between the experimental parameters (input variables) and their outcome on the percentage removal of RTN (response variable) is illustrated by the contour plots shown in **Fig. 7.16-7.18**.

> **Effect of ARSB-TiO$_2$ dosage and solution pH on RTN removal by ARSB-TiO$_2$**

The interaction in between the pH of the experimental solution and the dosage of ARSB-TiO$_2$ and its effect on the removal of RTN is conveyed in the contour plot of **Fig. 7.16**. From there it was observed that the removal of RTN by ARSB-TiO$_2$ was higher at the lower pH range. This could be attributed to the pH$_{pzc}$ of ARSB-TiO$_2$ (pH = 7.5) and the two pK$_a$ values of RTN (2.6 and 8.2) (Al-rub et al., 2020). At the lower pH range (pH 2-4), the molecules of RTN are highly protonated whereas the surface of ARSB-TiO$_2$ is positively charged, leading to enhanced adsorption at this lower pH range (Mondal et al., 2020) and as photo-degradation have to be preceded by adsorption, therefore higher removal was also observed at this lower pH range (Dong et al., 2015). On the other hand, at the higher pH range (pH 8-10) the surface of ARSB-TiO$_2$ becomes negatively charged whereas the molecules of RTN remains

weakly protonated resulting in reduced adsorption by electrostatic forces of attraction (Mondal et al., 2020). As a consequence of which, removal of RTN by ARSB-TiO$_2$ is reduced at the higher pH range by photo-catalysis (Dong et al., 2015). In case of the dose variation study it was observed that the removal of RTN increased with the increase of dosage of ARSB-TiO$_2$ which could be attributed to the availability of greater surface area for uptake of RTN molecules (Bhattacharya et al., 2022; Ziegmann & Frimmel, 2010). Inversely, the removal of RTN by ARSB-TiO$_2$ reduced with the decrease in dosage of ARSB-TiO$_2$.

➢ **Effect of solution pH and contact time on RTN removal by ARSB-TiO$_2$**

The interaction in between the pH of the experimental solution and contact time and its effect on the removal of RTN by ARSB-TiO$_2$ is shown in the contour plot of **Fig. 7.17**. From there it was observed that the removal of RTN by ARSB-TiO$_2$ was higher at the lower pH range and decreased with the increase in pH of the experimental solution. The logic behind this observation is that, at the lower pH range the molecules of RTN (with pK$_a$ values 2.6 and 8.2) are highly protonated whereas the surface of ARSB-TiO$_2$ is positively charged (pH$_{pzc}$ = 7.5) leading to enhanced adsorption of RTN molecules by the surface of ARSB-TiO$_2$ followed by their photo-degradation (Dong et al., 2015; Mondal et al., 2017). At the higher pH range, the surface of ARSB-TiO$_2$ is negatively charged whereas the molecules of RTN are weakly protonated leading to reduced adsorption of RTN molecules by the surface of ARSB-TiO$_2$ due to electrostatic forces of attraction (Mondal et al., 2017). As a consequence of which the photo-degradation of RTN molecules by ARSB-TiO$_2$ is reduced at this higher pH range (Dong et al., 2015). On the other hand, with the increase in contact time the interaction in between the RTN molecules and the surface of ARSB-TiO$_2$ increases leading to greater adsorption and subsequently greater photo-degradation of the RTN molecules (Bhattacharya et al., 2021; Dong et al., 2015). The increase in rate of adsorption, with the increase in contact time denotes that the adsorption of RTN molecules on the surface of ARSB-TiO$_2$ is physical in nature (Bhattacharya et al., 2021).

➢ **Effect of contact time and dosage of ARSB-TiO$_2$ dosage on RTN removal by ARSB-TiO$_2$**

The interaction in between the agitation speed and dosage of ARSB-TiO$_2$ and its effect on the removal of RTN by ARSB-TiO$_2$ is conveyed in the contour plot of **Fig. 7.18**. From there it was observed that removal of RTN by ARSB-TiO$_2$ increased with increase in dosage of ARSB-TiO$_2$ which could be attributed to the greater availability of active sites for the uptake of RTN molecules which is followed by their photo-catalysis (Bhattacharya et al., 2022; Dong et al., 2015). On the other hand, the removal of RTN by ARSB-TiO$_2$ increases with the increase in contact time which could be attributed to the enhanced interaction between the surface of ARSB-TiO$_2$ and the RTN molecules at the higher contact time, leading to higher adsorption and subsequently greater photo-degradation of RTN molecules (Bhattacharya et al., 2021; Dong et al., 2015). The increase in the adsorption of RTN molecules with

increase in contact time could be attributed to the proposition that the adsorption of RTN molecules on the surface of ARSB-TiO$_2$ is physical in nature (Bhattacharya et al., 2021).

**Table 7.5 :-** The table showing the 20 different set of parameters (runs) along with their corresponding outcome as proposed by the CCD model of RSM for optimization of RTN removal by ARSB-TiO$_2$

| | | | Factor 1 | Factor 2 | Factor 3 | Response 1 |
|---|---|---|---|---|---|---|
| Std | Run | Block | A:pH | B:Dose | C:Time | R1 |
| | | | | g/L | min | |
| 15 | 1 | Block 1 | 6.50 | 2.00 | 120.00 | 92.23 |
| 2 | 2 | Block 1 | 9.00 | 1.00 | 90.00 | 81.25 |
| 8 | 3 | Block 1 | 9.00 | 3.00 | 150.00 | 89.17 |
| 5 | 4 | Block 1 | 4.00 | 1.00 | 150.00 | 79.79 |
| 10 | 5 | Block 1 | 10.70 | 2.00 | 120.00 | 95.63 |
| 19 | 6 | Block 1 | 6.50 | 2.00 | 120.00 | 92.23 |
| 1 | 7 | Block 1 | 4.00 | 1.00 | 90.00 | 72.08 |
| 17 | 8 | Block 1 | 6.50 | 2.00 | 120.00 | 92.23 |
| 20 | 9 | Block 1 | 6.50 | 2.00 | 120.00 | 92.23 |
| 12 | 10 | Block 1 | 6.50 | 3.68 | 120.00 | 91.7 |
| 18 | 11 | Block 1 | 6.50 | 2.00 | 120.00 | 92.23 |
| 11 | 12 | Block 1 | 6.50 | 0.32 | 120.00 | 28.42 |
| 4 | 13 | Block 1 | 9.00 | 3.00 | 90.00 | 73.69 |
| 6 | 14 | Block 1 | 9.00 | 1.00 | 150.00 | 80.48 |
| 9 | 15 | Block 1 | 2.30 | 2.00 | 120.00 | 93.57 |
| 7 | 16 | Block 1 | 4.00 | 3.00 | 150.00 | 93.84 |
| 13 | 17 | Block 1 | 6.50 | 2.00 | 69.55 | 92.82 |
| 16 | 18 | Block 1 | 6.50 | 2.00 | 120.00 | 92.23 |
| 14 | 19 | Block 1 | 6.50 | 2.00 | 170.45 | 91.88 |
| 3 | 20 | Block 1 | 4.00 | 3.00 | 90.00 | 96.19 |

**Table 7.6** :- ANOVA analysis for the RSM for the photocatalytic removal of RTN by ARSB-TiO$_2$

| $R^2$ Value | Adjusted $R^2$ Value | f- value | Probability Value P |
|---|---|---|---|
| 0.82 | 0.66 | 5.14 | $(0.0087) < 0.05$ <br> Significant |
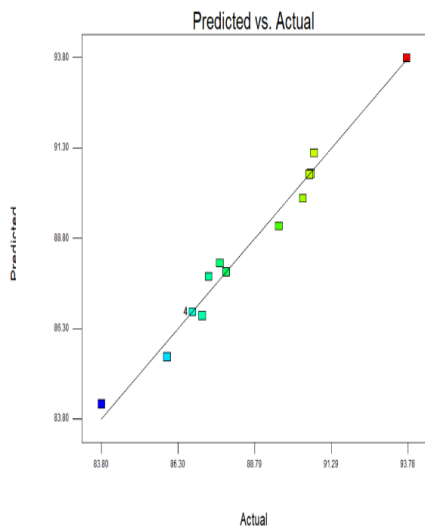
**Fig.7.15**: Relation between the predicted data points and the experimental data points as per the RSM model.
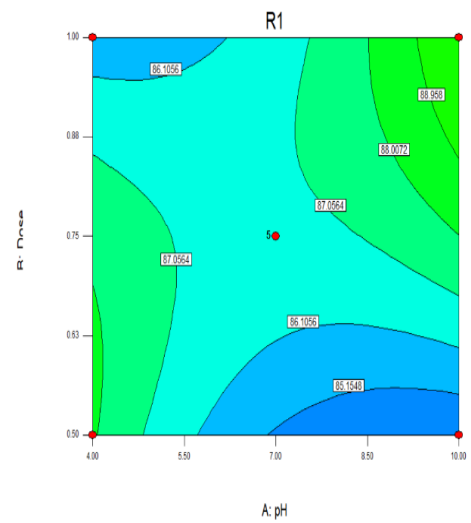


**Fig. 7.16**: Interaction between the pH of the experimental solution and the dose of the ARSB-$TiO_2$ and their effect on the percentage removal of RTN.
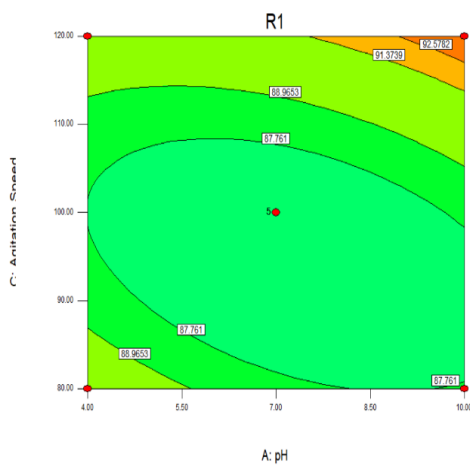


**Fig. 7.17**: The interaction between the pH of the experimental solution and contact time and their effect on the percentage removal of RTN by ARSB-$TiO_2$.
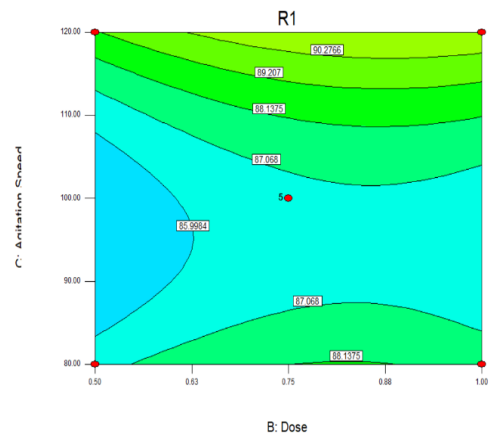


**Fig. 7.18**: The plot showing the interaction between the dose of the ARSB-$TiO_2$ and the contact time as per the RSM model and their effect on the percentage removal of RTN by ARSB-$TiO_2$.

### 7.4.4.4 Process Optimization for the removal of BPA by ARSB-TiO₂ by RSM

The RSM was performed with the aim of understanding the effect of inter parameter interaction on the experimental outcome. In **Table 7.7**, the outcome of the 20 experiments as proposed by the software for the CCD model of the RSM is given and in **Table 7.8** the result of the ANOVA of the RSM model is provided. From there it is observed that the $R^2$ value of the model was 0.94 and the adjusted $R^2$ value was 0.89 which propounded the fact that the polynomial model suggested by RSM was appropriate for predicting the outcome of this adsorption reaction. The high value of F (17.99, much greater than unity) and the low value of P ($< 0.0001$) meant that the optimizing model was highly significant, with the experimental data points exhibiting a high degree of correlation with the predicted data points (Bhattacharya et al., 2021). **Fig. 7.19** shows the relation between the experimentally determined data points and the predicted data points and there also it can be noted that the experimental data points exhibits a high degree of correlation with the predicted data points. The real equation which was used to predict the effect of the input variables on the response output is presented as follows.

$$Removal = -6.08185 - 5.55237 \times pH + 44.55273 \times Dose + 0.82925 \times Time - 1.39123 \times pH \times Dose + 0.073356 \times pH \times Time - 0.020377 \times Dose \times Time - 0.17439 \times pH^2 - 6.91543 \times Dose^2 - 5.28385 \times 10^{-3} \times Time^2 \dots\dots\dots\dots\dots\dots\dots\dots\dots\dots(xxxxviii)$$

As per the RSM model the optimized conditions under which maximum removal of BPA (83.11 %) was possible were: ARSB-TiO₂ dosage of 2 g/L, pH value of 2.3 and reaction time of 120 minutes. For this RSM model, the interaction between the experimental parameters (input variables) and their outcome on the percentage removal of BPA (response variable) is illustrated by the contour plots shown in **Fig. 7.20-7.22**.

> ➢ **Effect of ARSB-TiO₂ dosage and solution pH on BPA removal by ARSB-TiO₂**

The interaction in between the pH of the experimental solution and the dosage of ARSB-TiO₂ and its effect on the removal of BPA is conveyed in the contour plot of **Fig. 7.20**. From the result of the experiment it was observed that the removal of BPA was highest at the lower pH range and decreased with the increase in pH of the experimental solution. This could be attributed to the fact at higher pH range (around pH >= 8), the BPA molecules dissociate to form bis-phenolate anion. On the other hand, the pH$_{pzc}$ of ARSB-TiO₂ was found to be at pH 7.5. As a result of which at the higher pH range, both surface of ARSB-TiO₂ and the molecules of BPA both attain a negative charge, due to which the adsorption of BPA molecules on to the surface of ARSB-TiO₂ was inhibited due to the electrostatic force of repulsion (J. Xu et al., 2012; L. Xu et al., 2018). And as the photo-degradation of the BPA

molecules is preceded by the adsorption of the molecules on the surface of ARSB-TiO$_2$ (Dong et al., 2015; Nawaz et al., 2017), therefore the removal of BPA was also found to be less in the higher pH range and was found to be high at the lower pH range (L. Xu et al., 2018). In case of the dose variation study, it was observed that the removal of BPA by ARSB-TiO$_2$ increased with increase in dosage of ARSB-TiO$_2$ and subsequently decreased with the decrease in dosage of ARSB-TiO$_2$. This could be attributed to the fact that with increase in dosage of ARSB-TiO$_2$, the surface area available for the uptake of BPA increased leading to the greater adsorption and simultaneously greater degradation of BPA molecules (Bhattacharya et al., 2022; L. Xu et al., 2018).

> **Effect of solution pH and contact time on BPA removal by ARSB-TiO$_2$**

The interaction in between the pH of the experimental solution and agitation speed and its effect on the removal of BPA by ARSB-TIO$_2$ is conveyed in the contour plot of **Fig. 7.21**. From there it was observed that the removal of BPA by ARSB-TiO$_2$ was highest at the lower pH range and subsequently decreased with the increase in pH of the experimental solution. This could be attributed to the fact that ARSB-TiO$_2$ and the BPA molecules attain similar surface charges at the higher pH range (pH $>=$ 8) (L. Xu et al., 2018). As a consequence of which, at the higher pH range a force of repulsion acts between the BPA molecules and the surface of ARSB-TiO$_2$, leading to decreased rate of adsorption at the higher pH range. And as the process of photo-degradation has to be preceded by adsorption therefore at the higher pH range, the removal of BPA by ARSB-TiO$_2$ also decreased (Dong et al., 2015; L. Xu et al., 2018). On the effect of contact time, from the experimental result it was observed that the removal of BPA by ARSB-TiO$_2$ increased with increase in contact time up-to a particular point (around the 105 min-120 min time range). Beyond this particular time range, the removal of BPA by ARSB-TiO$_2$ decreased slightly. This phenomenon could be attributed to the fact that adsorption equilibrium was reached around the time range of 105 min-120 min. When the contact time increased beyond this particular point, desorption of the BPA particles from the surface of ARSB-TiO$_2$ might have taken place. Similar observation have been observed in the works of (Roy et al., 2018). As a consequence of which, the removal of BPA by photo-degradation was also found to have been decreased at this higher pH range (Dong et al., 2015; Xu et al., 2018).

> **Effect of contact time and dosage of ARSB-TiO$_2$ on the removal of BPA by ARSB-TiO$_2$**

The interaction in between the dosage and contact time of ARSB-TiO$_2$ and its effect on the removal of BPA by ARSB-TiO$_2$ is conveyed in the contour plot of **Fig. 7.22**. From there it was observed that removal of BPA by ARSB-TiO$_2$ increased with increase in dosage of ARSB-TiO$_2$ which could be attributed to the greater availability of active sites for the uptake of BPA molecules which is followed by their photo-catalysis (Dong et al., 2015; L. Xu et al., 2018). On the other hand, the removal of BPA by ARSB-TiO$_2$ increased with the increase in contact time up-to an optimum point beyond which a

decrease in removal was observed. This could be attributed to the desorption of BPA molecules from the surface of ARSB-TiO$_2$ beyond the optimum point leading to decreased adsorption and hence decreased photo-degradation of BPA molecules. Similar results were obtained from the work of (Roy et al., 2018).

**Table 7.7** :- The table showing the 20 different set of parameters (runs) along with their corresponding outcome as proposed by CCD model of RSM for optimization of BPA removal by ARSB-TiO$_2$

| | | | Factor 1 | Factor 2 | Factor 3 | Response 1 |
|---|---|---|---|---|---|---|
| Std | Run | Block | A:pH | B:Dose | C:Time | R1 |
| | | | | g/L | min | |
| 17 | 1 | Block 1 | 6.50 | 2.00 | 120.00 | 77.23 |
| 16 | 2 | Block 1 | 9.00 | 1.00 | 90.00 | 55.14 |
| 14 | 3 | Block 1 | 9.00 | 3.00 | 150.00 | 72.51 |
| 8 | 4 | Block 1 | 4.00 | 1.00 | 150.00 | 60.71 |
| 4 | 5 | Block 1 | 10.70 | 2.00 | 120.00 | 63.24 |
| 7 | 6 | Block 1 | 6.50 | 2.00 | 120.00 | 77.23 |
| 1 | 7 | Block 1 | 4.00 | 1.00 | 90.00 | 60.03 |
| 19 | 8 | Block 1 | 6.50 | 2.00 | 120.00 | 77.23 |
| 20 | 9 | Block 1 | 6.50 | 2.00 | 120.00 | 77.23 |
| 9 | 10 | Block 1 | 6.50 | 3.68 | 120.00 | 68.63 |
| 2 | 11 | Block 1 | 6.50 | 2.00 | 120.00 | 77.23 |
| 12 | 12 | Block 1 | 6.50 | 0.32 | 120.00 | 45.53 |
| 6 | 13 | Block 1 | 9.00 | 3.00 | 90.00 | 52.28 |
| 10 | 14 | Block 1 | 9.00 | 1.00 | 150.00 | 66.1 |
| 13 | 15 | Block 1 | 2.30 | 2.00 | 120.00 | 83.81 |
| 18 | 16 | Block 1 | 4.00 | 3.00 | 150.00 | 69.31 |
| 5 | 17 | Block 1 | 6.50 | 2.00 | 69.55 | 61.21 |
| 15 | 18 | Block 1 | 6.50 | 2.00 | 120.00 | 77.23 |
| 11 | 19 | Block 1 | 6.50 | 2.00 | 170.45 | 65.09 |
| 3 | 20 | Block 1 | 4.00 | 3.00 | 90.00 | 82.8 |

**Table 7.8** :- ANOVA analysis for the RSM for the photocatalytic removal of BPA by ARSB-TiO$_2$

| R$^2$ Value | Adjusted R$^2$ Value | f- value | Probability Value P |
|---|---|---|---|
| 0.94 | 0.89 | 17.99 | <0.0001<br><br>Significant |
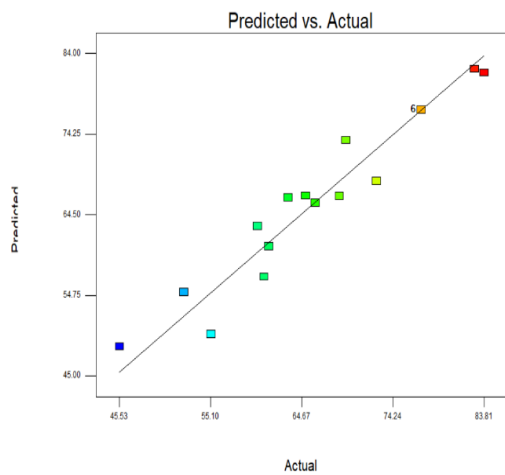
**Fig. 7.19**: Relation between the predicted data points and the experimental data points as per the RSM model.
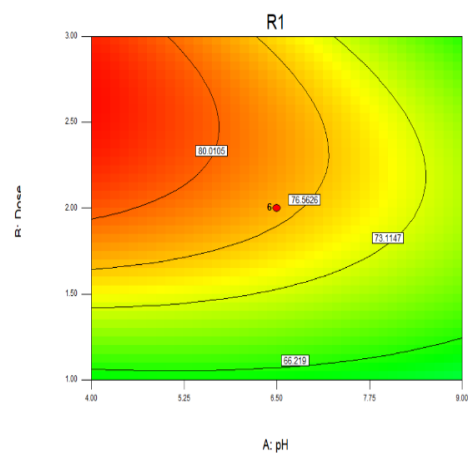


**Fig. 7.20**: Interaction between the pH of the experimental solution and the dose of the ARSB-TiO$_2$ and their effect on the percentage removal of BPA.
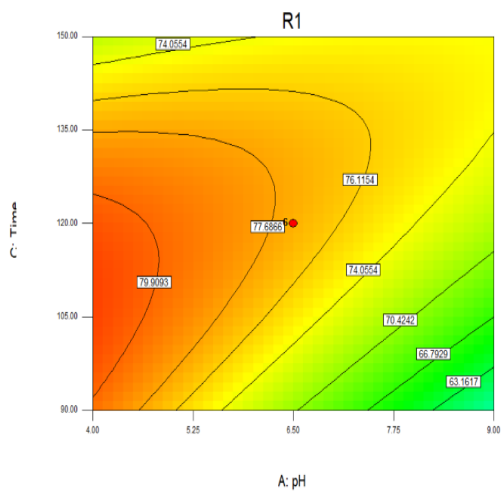


**Fig. 7.21**: The interaction between the pH of the experimental solution and agitation speed and their effect on the percentage removal of BPA by ARSB-TiO$_2$.
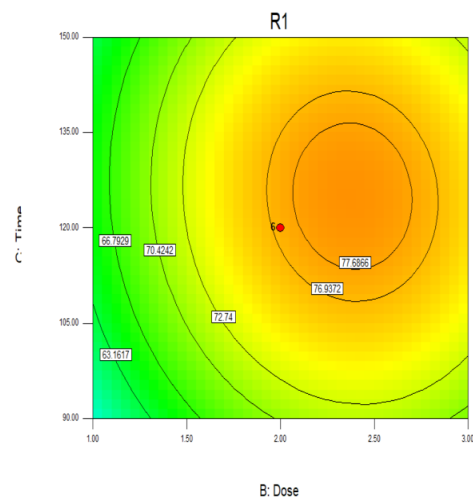


**Fig. 7.22**: The plot showing the interaction between the dose of the ARSB-TiO$_2$ and the agitation speed as per the RSM model and their effect on the percentage removal of BPA.

224

## 7.4.5 Removal of the EC's by ARSB-TiO₂ in an RPB

As mentioned before, an experiment was conducted with the RPB in order to intensify the adsorption efficacy of the ARSB-TiO₂ composite. As mentioned before, before the start of the reaction the EC's were treated by ARSB-TiO₂ under visible light radiation for 1 hour. After 1 hour the solutions were taken out and the level of the EC's were determined spectrophotometrically. From there it was observed that 14.96 % of CBZ, 27.42 % of NPX, 19.26 % of RTN and 37.25 % of RTN were removed after the photocatalytic reaction. As was observed, that the photo-catalysis reaction which was performed for 1 hour, was unable to significantly degrade the four EC's. Therefore, ARSB-TiO₂ had significant scope to operate as an adsorbent. The adsorption reaction in the RPB was done for 6 hours. From the result of the experiment as shown in **Fig. 7.23**, it was observed that ARSB-TiO₂ was able to remove 69.09 % of CBZ, 72.41 % of NPX, 89.18 % of RTN and 75.33 % of BPA during the RPB reaction. Thus, it can be inferred that ARSB-TiO₂ was also an efficient adsorbent that could be used to remove the trace organic pollutants. This property could be attributed to the presence of 9 parts by weight of ARSB in the ARSB-TiO₂ composite.
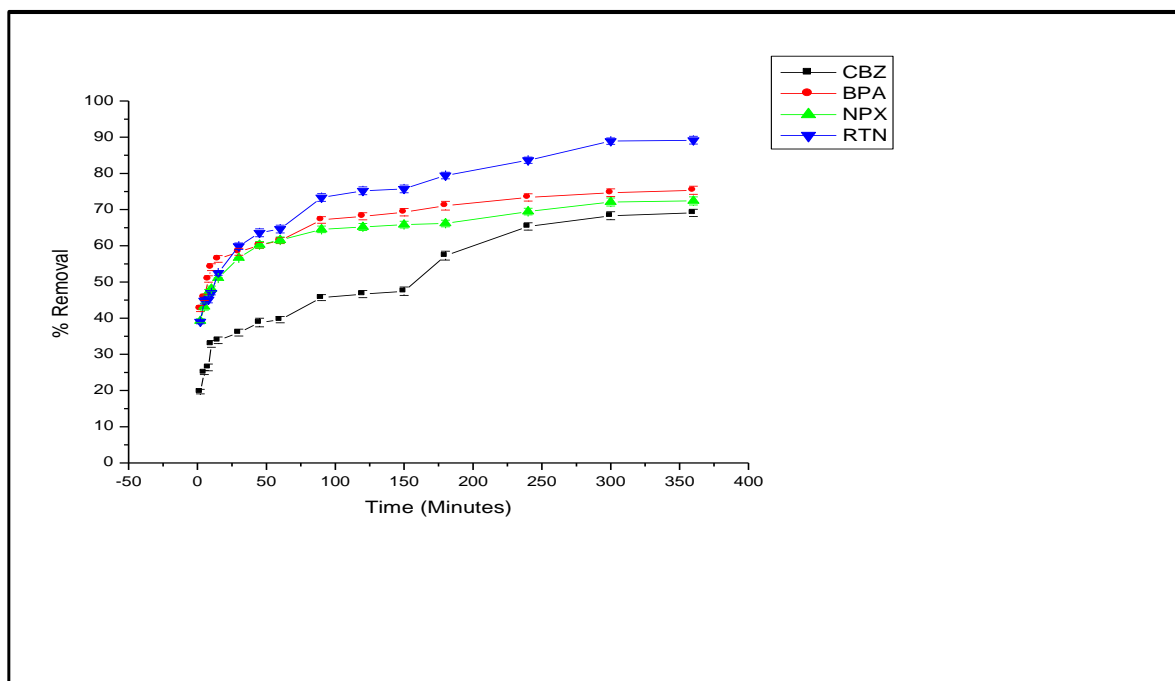


**Fig. 7.23**:- Removal of CBZ, NPX, RTN and BPA by ARSB-TiO₂ in a RPB

## 7.4.6 Reusability Study

### 7.4.6.1 Reusability of ARSB-TiO$_2$ after treating CBZ

Out of the six solutions that were used for the regeneration of used ARSB-TiO$_2$ after treating CBZ, the greatest effectivity was exhibited by the 10% ethanol solution. By washing the ARSB-TiO$_2$ with the 10 % ethanol solution it was observed that in the first cycle, the ARSB-TiO$_2$ was able to remove 78.57 % of the CBZ from the aqueous solution, a value which was close to the effectivity exhibited by pristine ARSB-TiO$_2$. In the next cycle the removal of CBZ was 77.89 % and in the third cycle the removal was 77.81 %. For the fourth and the fifth cycle, the removal of CBZ by ARSB-TiO$_2$ was 76.44 % and 73.82 % respectively. Therefore it can be stated that the ARSB-TiO$_2$ regenerated by 10 % ethanol solution, can remove more than 73 % of CBZ from its aqueous solution for up-to five cycles. Thus, the synthesized ARSB-TiO$_2$ can be recycled up-to five times with a significant level of effectivity. The result of the experimental study is shown in **Fig. 7.24**.
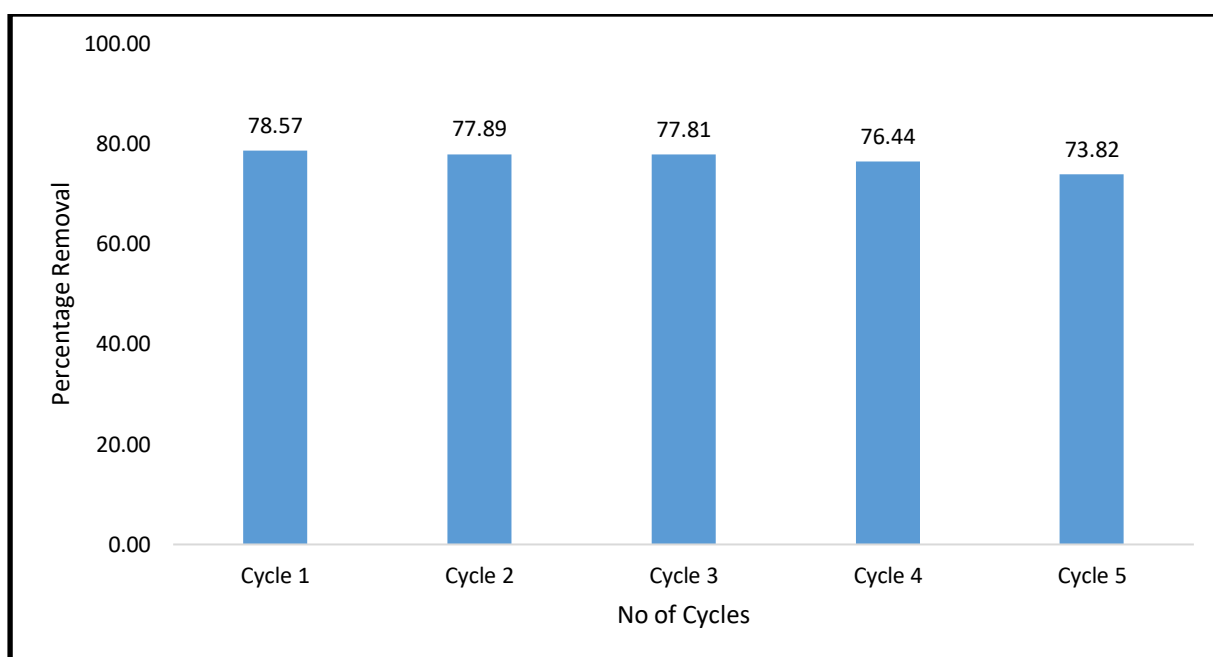


**Fig. 7.24**:- Removal of CBZ by ARSB-TiO$_2$ in different steps of the reusability cycle.

### 7.4.6.2 Reusability of ARSB-TiO$_2$ after treating NPX

Out of the six solutions that were used for the regeneration of used ARSB-TiO$_2$, the greatest effectivity was exhibited by the 10% HCl solution. By regenerating the ARSB-TiO$_2$ composite with the 10 % HCl solution it was observed that in the first cycle, the ARSB-TiO$_2$ was able to remove 74.98 %, in the second cycle it was able to remove 66.54 % and in the third cycle it was able to remove 56.94 % of the NPX from the aqueous solution. In the third and fourth cycle the ARSB-TiO$_2$ was able to remove 48.32 % and 35.36 % of the NPX respectively. Thus from the regeneration study it was observed that ARSB-TiO$_2$ could be used for three times with effectivity greater than 50 % on being washed with 10 % HCl solution. The result of the experimental study is shown in **Fig. 7.25**.
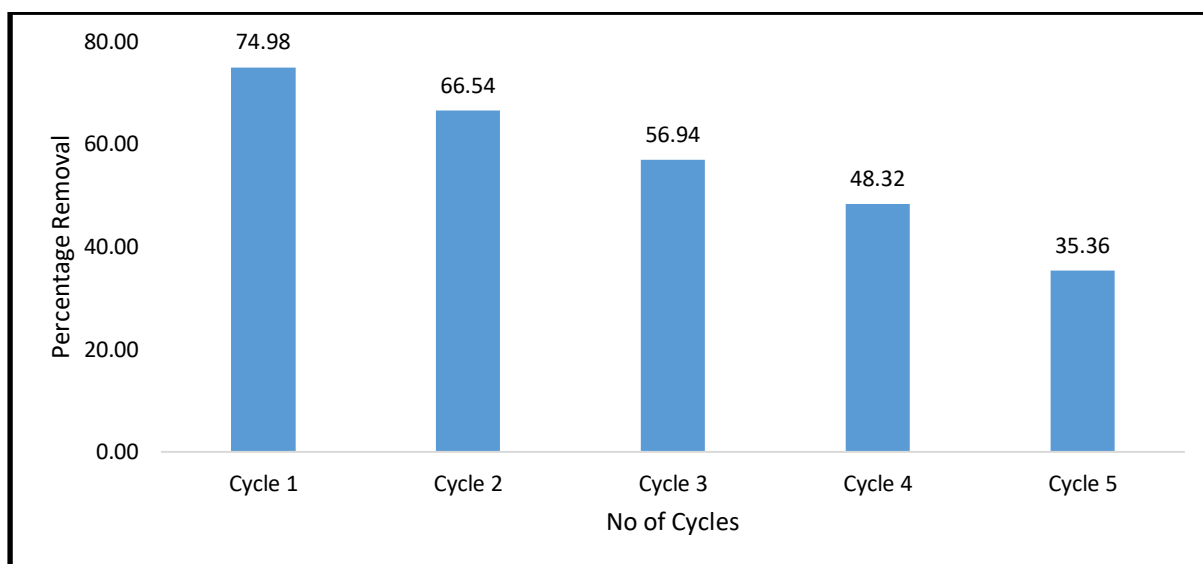


**Fig. 7.25**:- Removal of NPX by ARSB-TiO$_2$ in different steps of the reusability cycle.

### 7.4.6.3 Reusability of ARSB-TiO$_2$ after treating RTN

Out of the six solutions that were used for the regeneration of used ARSB-TiO$_2$ after treating RTN, the greatest effectivity was exhibited by the 10% ethanol solution. By regenerating the ARSB-TiO$_2$ composite with the 10 % ethanol solution it was observed that the ARSB-TiO$_2$ was able to remove 86.82 %, 82.2 %, 77.29 %, 76.07 % and 72.83 % of RTN from aqueous solution after the first, second, third, fourth and fifth cycle of regeneration respectively. Thus from the result of the experiment it could be inferred that ARSB-TiO$_2$ can be used for several times, with sufficient adsorption efficiency for the purpose of removing RTN from its aqueous solution on being washed with 10 % ethanol solution. The result of the experimental study is shown in **Fig. 7.26**.
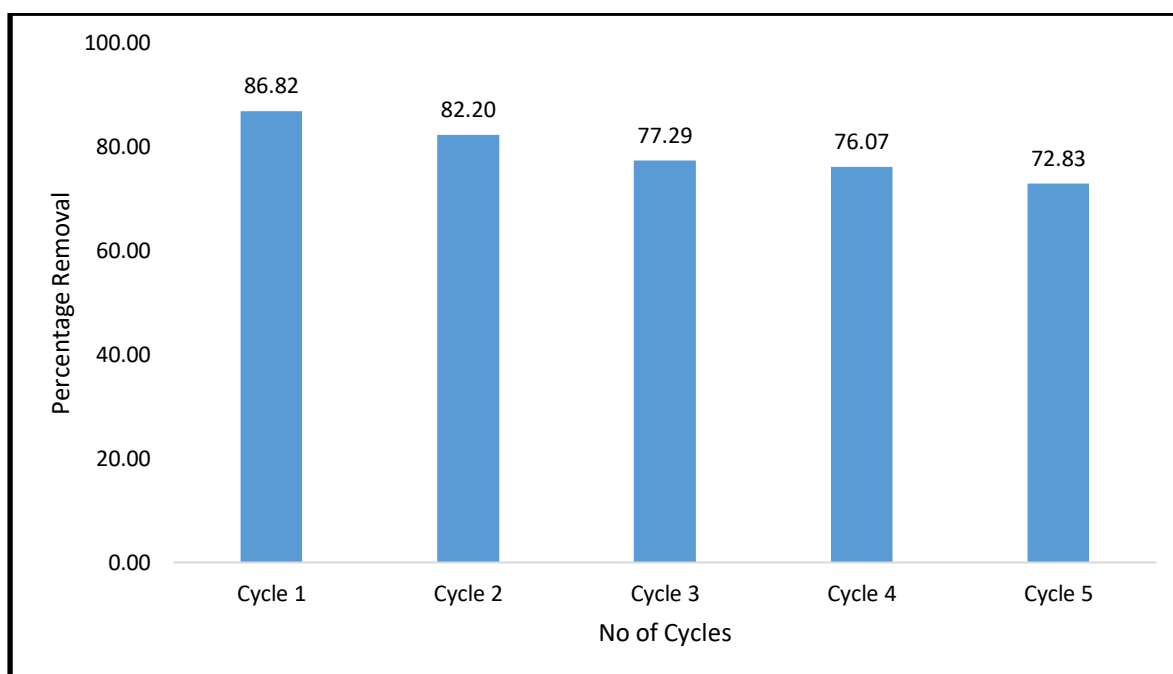


**Fig. 7.26**:- Removal of RTN by ARSB-TiO$_2$ in different steps of the reusability cycle.

### 7.4.6.4 Reusability Study of ARSB-TiO$_2$ after treating BPA

Out of the six solutions that were used for the regeneration of used ARSB-TiO$_2$ after treating BPA, the greatest effectivity was exhibited by the 10% NaOH solution. By regenerating the ARSB-TiO$_2$ composite with the 10 % NaOH solution it was observed that in the first cycle, the ARSB-TiO$_2$ was able to remove 75.6 % of BPA, in the second cycle it was able to remove 74.65 % of BPA and in the third cycle it was able to remove 71.55 % of the BPA from the aqueous solution. In the fourth and fifth cycle the ARSB-TiO$_2$ was able to remove 43.89 % and 36.18 % of BPA respectively. Therefore from the result of the regeneration study it was inferred that on being regenerated with 10 % NaOH solution, the ARSB-TiO$_2$ was able to remove more than 70 % BPA for three cycles. The efficacy of ARSB-TiO$_2$ remained over 55 % even for the fifth, thereby signifying that ARSB-TiO$_2$ can be reused for several times after regeneration. The result of the experimental study is shown in **Fig. 7.27**.
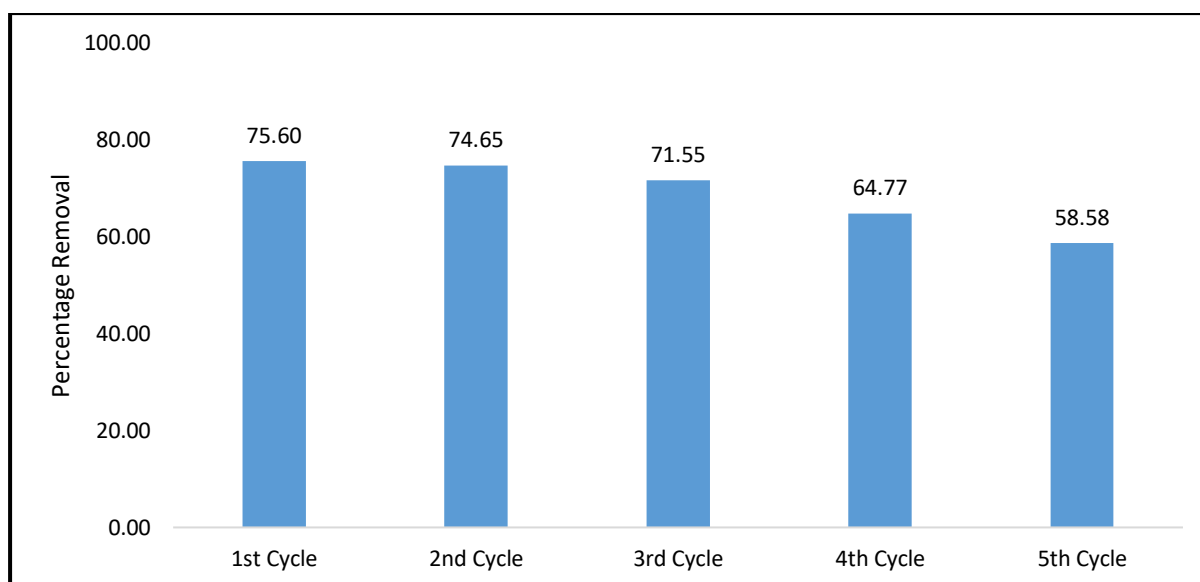


**Fig. 7.27**:- Removal of BPA by ARSB-TiO$_2$ in different steps of the reusability cycle.

## 7.5 CONCLUSION :-

In the above experiment, a composite was synthesized by combining ARSB with $TiO_2$ by a hydrothermal method. The reason for combining ARSB with $TiO_2$ was to increase the surface area in order to enhance the transfer of organic pollutants on the surface of the photo-catalyst, to inhibit electron hole recombination and to decrease the band gap of $TiO_2$. From the SEM analysis of ARSB-$TiO_2$ it was observed that the surface of ARSB consisted of thin lamellar sheets of carbon which enhances adsorption and particles of $TiO_2$ were also distributed on the surface of ARSB. From the XRD analysis it was observed that the oxidized peaks of graphite (found at around 10-13 2θ) were absent in ARSB-$TiO_2$ thereby denoting ARSB was reduced during the hydrothermal process. From the FTIR analysis it was observed that ARSB-$TiO_2$ consisted of both O-H bond and C=C bond thereby denoting the site of attraction of $TiO_2$ molecules. Similarly, the peaks between 600 $cm^{-1}$ and 800 $cm^{-1}$ denote the presence of Ti-O-C and Ti-O-Ti bond. From the Raman analysis it was observed that the lattice of ARSB-$TiO_2$ consisted of many defects in its $sp^2$ hybridization structure. The band gap of the synthesized ARSB-$TiO_2$ was calculated by virtue of a Tauc plot using the Kubelka Munk expression from its UV-Vis spectrum. From there it was observed that, the band gap of $TiO_2$ (found to be 3.36 eV) decreased (to 2.4 eV) on being combined with ARSB. This could be attributed to the formation of a new energy band on being combined with ARSB. Then a screening study was performed in order to find which incident radiation was most capable of activating the ARSB-$TiO_2$ composite. Out of the four radiation calculated, i.e., UVA, UVB, UVC and visible light, it was observed that Visible light radiation exhibited the highest efficiency. This could be attributed to the highest number of photon liberated from visible light due to all the lights operating at the same voltage. Therefore further studies were carried out only with visible light. From the result of the experiment it was observed that the ARSB-$TiO_2$ composite was able to remove significant amount of the EC's from there aqueous solution, with the highest removal for CBZ being 88.27 % at CBZ concentration of 10 mg/L, ARSB-$TiO_2$ dosage of 2 g/L, pH 2 of experimental solution and temperature of 303 K. For NPX the highest removal was 85.4 % which was obtained at pH 2 of experimental solution, ARSB-$TiO_2$ dosage of 2 g/L, NPX concentration of 10 mg/L and temperature of 303 K. For RTN the highest removal was 99.73 % which was obtained at pH 7, ARSB-$TiO_2$ dosage of 2 g/L, RTN concentration of 10 mg/L and temperature of 303 K. For BPA the highest removal was 95.73 % which was obtained at pH 2 of the experimental solution, ARSB-$TiO_2$ dosage of 2 g/L, BPA concentration of 10 mg/L and temperature of 303 K. The batch studies were further optimized with RSM. From there the highest removal by CBZ was 81.34 % were possible at ARSB-$TiO_2$ dosage of 2 g/L, pH value of 6.5 and reaction time of 120 minutes. For NPX the highest removal was 89.62 % which were obtained at ARSB-$TiO_2$ dosage of 3.68 g/L, pH value of 6.5 and reaction time of 120 minutes. For RTN the maximum removal was 96.19 % which were possible at

adsorbent dosage of 3 g/L, pH value of 4 and reaction time of 90 minutes. For BPA the maximum removal was 83.11 % which were possible at the experimental conditions of ARSB-TiO2 dosage of 2 g/L, pH value of 2.3 and reaction time of 120 minutes. And lastly, the adsorption ability of ARSB-TiO$_2$ was evaluated by virtue of a RPB study. From there it was observed that ARSB-TiO$_2$ can also operate as an effective adsorbent, which could be attributed to the presence of 9 parts by weight of ARSB in the composite. The ARSB-TiO$_2$ composite also exhibited the capacity to be reused for at least 2-3 times with efficiency comparable to that of the original material on being treated with accurate regenerating solutions. Thus, from the result of the experimental studies, it was inferred that ARSB-TiO$_2$ was very effective in removing the EC's from there aquatic solution. Also, although ARSB-TiO$_2$ was slightly less effective than GO-TiO$_2$ for removing the EC's but still it exhibited much higher efficiency than only ARSB. Thus, from the result of the experiment it can be clearly concluded that by adding TiO$_2$, the removal efficacy of ARSB was highly increased. Further research can be done to make process more effective and emphasis can also be laid on the separation of the composite materials from water.

# CHAPTER 8

# REMOVAL OF EC'S FROM THE AQUATIC SYSTEM BY FENTON OXIDATION REACTION

## 8.1 INTRODUCTION

Among the different methods that have been utilized for the treatment of trace organic pollutants in water, advanced oxidation by Fenton's reagent method is one of the most effective process (Kanakaraju et al., 2018; Neyens & Baeyens, 2003). Fenton reagent composed of $H_2O_2$ and a source of $Fe^{2+}$ ions, mainly $FeSO_4.7H_2O$. $H_2O_2$ in itself is a strong oxidizing agent, utilized in various reactions like bleaching of pulp, and reaction with $SO_2$ and $NO_2$ to form their respective acids etc. (Neyens & Baeyens, 2003). However $H_2O_2$ alone is not effective for the treatment of trace organic pollutants in water. In order to expedite the degradation of trace organic pollutants by $H_2O_2$, $Fe^{2+}$ ions are added to the solution mixture in the form of $FeSO_4.7H_2O$ salts. The presence of $Fe^{2+}$ ions helps in the catalysis and decomposition of $H_2O_2$ molecules resulting in the formation of $OH^{\bullet}$ radicals which can decompose the organic pollutants in water. As the Fenton oxidation reaction is an AOP, therefore after the completion of the reaction, there is a high probability that reaction intermediates will be present in the experimental solution (Poerschmann et al., 2010; M. Zhang et al., 2019). In order to remove those intermediates from the experimental solution, an adsorption reaction was performed with GO. GO was added to the experimental solution and the adsorption reaction was continued for 2 hours with the aim being the removal of the traces of the pharmaceuticals and the intermediates from the experimental solution. Similar works have been reported by (Dwivedi et al., 2018) and (Della-flora et al., 2021).

For this particular study, Fenton oxidation was utilized for degrading the four EC's (viz., CBZ, NPX, RTN and BPA). Three concentration of the EC's were taken at 20 mg/L, 10 mg/L and 5 mg/L respectively. After the degradation of the EC's by Fenton reagent, the solutions were treated by a 2 g/L dosage of GO in order to remove the degraded EC's from the water by adsorption. The level of EC's were evaluated by UV-Vis spectrophotometry. The aim of this experiment were to degrade this EC's by Fenton oxidation reaction followed by their efficient removal by adsorption by GO.

## 8.2 MATERIALS AND METHODS

### 8.2.1 Materials required

The FeSO$_4$.7H$_2$O was brought from Merck. The rest of the materials were brought from the same sources as mentioned in the previous chapters.

### 8.2.2 Fenton reaction followed by adsorption with GO

The Fenton reagent was synthesized with 25 mg/L ($1 \times 10^{-4}$ M) of FeSO$_4$.7H$_2$O and $3.26 \times 10^{-5}$ M of H$_2$O$_2$. Firstly, 2.5 mg of FeSO$_4$.7H$_2$O was dissolved in 100 mL of the pharmaceutical solution and then 0.2 µL of H$_2$O$_2$ was added to the experimental solution. Then the solution was allowed to sit overnight for the Fenton reaction to take place. After that the solution was filtered to remove any precipitate (if formed). After that, 2 g/L dosage of GO was added to each of this experimental solution and the solution was treated for 2 hours. Samples were taken two times, first after the completion of the Fenton reaction and then after the addition of GO. Samples were firstly filtered by a syringe filter (0.22 µm pore size) followed by which they were centrifuged for 15 minutes at 150000 RPM. After that the level of EC's present in the sample were determined spectrophotometrically. A blank was prepared with only FeSO$_4$.7H$_2$O and H$_2$O$_2$ for the purpose of the spectrophotometric analysis of the solution. Each of the experiment were performed three times and the result was represented as the average value of the three results along with the respective standard deviation.

## 8.3 CALCULATIONS

### 8.3.1 Percentage Removal of the EC's

The percentage removal of the EC's were done by using the same equation as mentioned in **Chapter 4, Section 4.3.1.**

## 8.4 RESULTS

The removal of the EC's by Fenton oxidation followed by its adsorption by GO is shown in the figures shown in **Fig. 8.1 (a)-(d)**. **Fig. 8.1 (a)** shows the removal of CBZ, **Fig. 8.1 (b)** shows the removal of NPX, **Fig. 8.1 (c)** shows the removal of RTN and **Fig. 8.1 (d)** shows the removal of BPA. From the result of the experiment it was observed that the removal of the pharmaceuticals by Fenton reagent decreased with the increase in concentration of the pollutant. This could be attributed to the fact, that with increase in concentration the organic load of the experimental solution increased and as a consequence of which, the concentration of the OH• radicals along with other oxidizing radicals generated during the Fenton reaction becomes less sufficient for the removal of the pollutants

(Kanakaraju et al., 2018; Neyens & Baeyens, 2003; Trovo et al., 2016). In case of CBZ the removal at 5 mg/L, 10 mg/L and 20 mg/L were observed to be 90 %, 85.68 % and 56.12 % respectively. In case of NPX the removal at 5 mg/L, 10 mg/L and 20 mg/L were observed to be 87.97 %, 84.42 % and 77.2 % respectively. In case of RTN the removal at 5 mg/L, 10 mg/L and 20 mg/L were observed to be 88.65 %, 87.57 % and 81.08 % respectively. In case of BPA the removal at 5 mg/L, 10 mg/L and 20 mg/L were observed to be 63.25 %, 61.29 % and 52.08 % respectively. After the completion of the Fenton reaction, the experimental solutions were treated by GO. After the treatment by GO, the removal of the EC's from the experimental solution further increased. In case of CBZ, the removal of the experimental solutions with concentrations of 5 mg/L, 10 mg/L and 20 mg/L after GO treatment were observed to be 95.87 %, 98.95 % and 89.35 % respectively. In case of NPX the removal of the experimental solutions with concentration of 5 mg/L, 10 mg/L and 20 mg/L after GO treatment were observed to be 99.18 %, 98.08 % and 96.84 % respectively. In case of RTN the removal of 5 mg/L, 10 mg/L and 20 mg/L after GO treatment were observed to be 94.05 %, 95.14 % and 96.49 % respectively. In case of BPA the removal of 5 mg/L, 10 mg/L and 20 mg/L after GO treatment were observed to be 81.21 %, 82.35 % and 76.08 % respectively. From the results of the experiment it was observed that the Fenton reaction was able to effectively remove high concentration of the EC's from the experimental solution up-to 20 mg/L. The Fenton reaction followed by adsorption with GO resulted in effective removal of the EC's from the experimental solution.
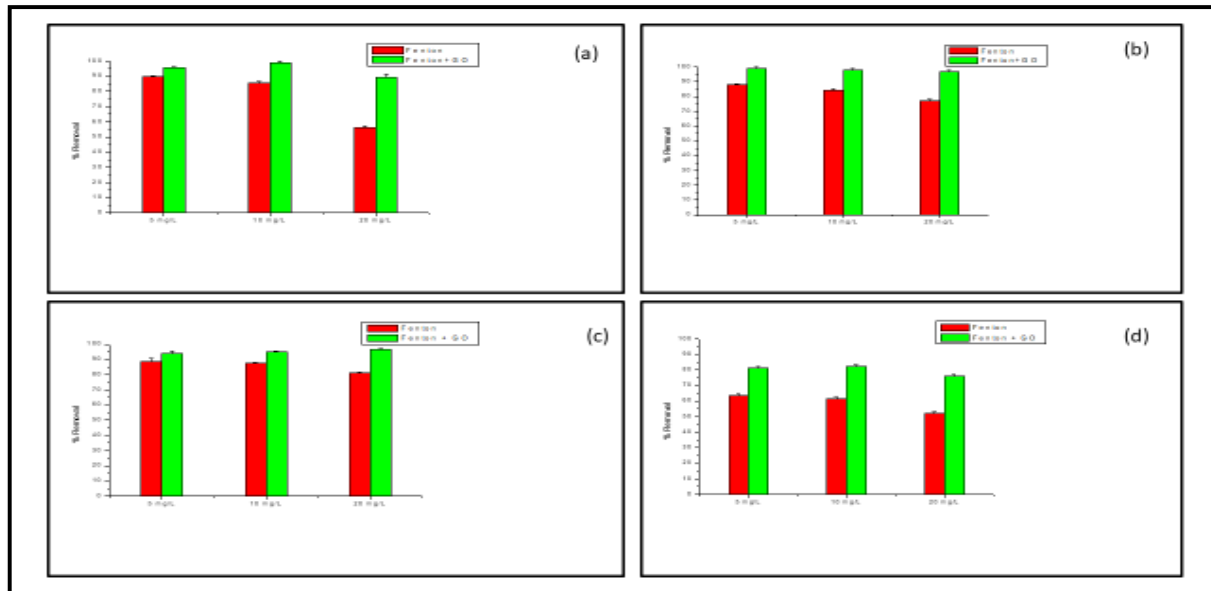


**Fig. 8.1:-** Removal by Fenton oxidation followed by adsorption by GO **(a)** CBZ **(b)** NPX **(c)** RTN **(d)** BPA

## 8.5 CONCLUSION

In order to degrade the EC's in the experimental solution, oxidation with Fenton reagent, i.e., the Fenton oxidation reaction was employed. Three concentration of each of the EC's were considered, that being 5 mg/l, 10 mg/L and 20 mg/L respectively. The removal percentage generally decreased with the increase in concentration of the pharmaceuticals, due to increase in organic load of the experimental solution. But still from the experimental results it was observed that barring the case of BPA, all the other three compounds were significantly degraded by the Fenton oxidation reaction. The application of GO further helped to decrease the level of the pharmaceuticals in the aquatic solution. Thus in conclusion it can be stated that the combination of Fenton oxidation and adsorption by GO was very effective for removing the pharmaceuticals from their aqueous solution.

# CHAPTER 9

# APPLICATION OF THE INVESTIGATED WATER TREATMENTS METHODS FOR THE TREATMENT OF WASTEWATER SAMPLE

## 9.1 INTRODUCTION

In order to explore the commercial prospect of the wastewater treatment techniques that have been investigated in this research work, their efficacy would have to be tested against real wastewater. Till now, the efficacy of the treatment techniques have been tested against simulated wastewater solutions with distilled water as the primary solvent. These synthesized solutions did not contain the complex matrix of real time wastewater for obvious reasons. Real time wastewater generally consists of a high organic load along with various other pollutants (Park et al., 2013; Saryel-deen et al., 2017; Tebeje et al., 2020). In order to examine the ability of the investigated water treatment systems for the purpose of purifying polluted water, a study was devised. First water sample was collected from two sites, one site being a lake with water having high pollutant load and the other being the effluent collected from an industry situated in South Kolkata, West Bengal, India. Then the different waste water treatment techniques i.e., adsorption with GO and ARSB, photo-degradation with GO-TiO$_2$ and ARSB-TiO$_2$ and Fenton oxidation followed by adsorption with GO were used to treat the real time waste-water collected from two sites. Chemical oxygen demand (COD) was chosen to be the parameter for evaluating the effectivity of wastewater treatment techniques. The reason for choosing COD is because it is one of the most important water quality parameters (Bansode et al., 2004; Kayaalp et al., 2010; Saryel-deen et al., 2017). As per the Environmental Standards in India, the acceptable level of COD in treated waste water should be less than 250 mg/L (COD). From this study, a comparison can be done about the efficacy of different waste water treatment techniques for the purpose of treating real waste water.

## 9.2 MATERIALS AND METHODS:-

### 9.2.1 Materials Required

All the chemicals required for this experiment i.e., Potassium Dichromate ($K_2Cr_2O_7$), Silver Sulphate ($AgSO_4$), Mercuric Sulphate ($HgSO_4$), Sulfuric Acid ($H_2SO_4$), Ferrous Ammonium Sulphate (FAS) ($Fe(NH_4)_2(SO_4)_2.6 H_2O$), Ferroin indicator were brought from Merck and were used as received.

### 9.2.2 Collection of Samples

The water were collected from two sites, one being a lake with polluted water and the other being the industrial effluent from an industry in south Kolkata. Proper procedures were followed for collecting and storing the sample till it arrived at the laboratory. For the sake of anonymity, the exact name of the places or their co-ordinates have not being disclosed. The physical parameters such as the pH, salinity, conductivity and Total Dissolved Solid (TDS) of the sample were measured by a PCSTester 35 multipurpose tester on the day of the arrival of the samples. The Total Suspended Solid (TSS) were measured by a gravimetric method.

### 9.2.3 Synthesis of Reagents

1. Standard Potassium Dichromate standard solution (0.04167 M) :- 12.26 g of $K_2Cr_2O_7$, previously dried were added to 500 mL water. 167 mL of concentrated $H_2SO_4$ was also added. Then the whole solution were diluted to 1 L. 33.3 g of $HgSO_4$ were added to inhibit the interference of chloride ions.

2. Sulfuric Acid Reagent:- Sulfuric acid (concentrated) plus $AgSO_4$ (10.12 g/L) for halide ion interference.

3. Standard FAS (O.1 M) :- 39.2 g of $Fe(NH_4)_2(SO_4)_2.6 H_2O$ in 500 mL water plus 20 ml of $H_2SO_4$. Diluted to 1L.

### 9.2.4 Treatment of the samples

After the collection of the sample, they were treated by the different methods. For the process of adsorption with GO and ARSB, the experimental conditions were :- adsorbent dosage of 2 g/L, temperature of 303 K and agitation speed of 150 RPM. In case of photo-degradation with ARSB-$TiO_2$ the experimental conditions were same as that of adsorption, with the addition of visible light as the incident radiation for the activation of ARSB-$TiO_2$. In case of photo-degradation with GO-$TiO_2$ the dosage of GO-$TiO_2$ was 2 g/L and the rotation speed was 120 RPM, along with the irradiation of UVA for the activation of GO-$TiO_2$. In case of the treatment of the waste water by Fenton oxidation followed by adsorption with GO, the quantities of the reactants and the experimental methodology were the same as mentioned in **Chapter 8, Section 8.2**.

After the completion of treatment, the samples were carefully filtered out, first by a Whatman filter paper followed by syringe filtration. This was done with proper care to ensure that no adsorbent or photo-catalyst particle remain in the experimental solution. After that the COD of the treated solutions were evaluated by a titrimetric method. Each experiment were conducted three times and the average result was displayed along with the standard deviation.

### 9.2.5 Process for measuring COD :-

1. All the apparatus for testing have to be washed and clean beforehand so that no contamination or error in test takes place.

2. Then 2.5 mL of sample have to be taken.

3. To that 1.5 mL of (0.04167 M) $K_2Cr_2O_7$ solution have to be added.

4. Then 3.5 mL of $H_2SO_4$ reagent have to be added to the experimental apparatus carefully.

5. Then the experimental apparatus have to closed and the solution have to digested at 150°C for 2 hours inside a heater with a lid.

6. After the digestion has taken place the samples have to be taken out of the heater.

7. The level of $K_2Cr_2O_7$ present in the solution have to be determined by titration with FAS solution. Before the start of titration, few drops of Ferroin indicator is added to the solution. The end point is a sharp colour change from blue green to reddish brown.

8. The COD of the sample have to be checked against a blank.

## 9.3 CALCULATIONS:-

### 9.3.1 Percentage removal of COD

The percentage removal of COD of the treated was checked against the waste water by using the formula :-

$$Removal\ of\ COD\ (\%) = \frac{COD_{Sample} - COD_{Treated\ Water}}{COD_{Sample}} \times 100 \quad \ldots\ldots\ldots\ldots\ldots\ldots\ldots\ldots\ldots(xxxxix)$$

## 9.4 RESULTS

### 9.4.1 Physical parameters of the sampled waste water

The pH, conductivity, salinity and TDS of the waste waters are given as follows in the following **Table 9.1**.

**Table 9.1**:- Water quality parameters as measured for the two water samples

| Water Quality Parameters | Waste water collected from lake | Waste water collected from industry |
|---|---|---|
| Ph | 6.12 | 9.38 |
| Conductivity (µS) | 78 | 1320 |
| Salinity (mg/L) | 36.7 | 570 |
| TDS (mg/L) | 554 | 947 |
| TSS (mg/L) | 2300 | 1290 |

### 9.4.2 COD level of the water samples after treatment

The original COD of the lake water was observed to be 1466.78 mg/L thereby indicating very high organic load. From the result of the experiment as shown in **Fig. 9.1**, it was observed that the highest removal of COD from lake water was exhibited by the treatment method of Fenton oxidation followed by adsorption with GO, which was able to decrease the COD of the lake water by 90.91 %. This could be attributed to the fact that Fenton oxidation was able to effectively degrade the organic pollutants in lake water, as has been reported in previous literatures (Babuponnusami & Muthukumar, 2014; Kavitha & Palanivelu, 2005). Further adsorption by GO was able to further reduce the COD of the water. Adsorption by GO was also effective and was able to decrease the COD of the lake water by 72.73 % which could be attributed to its very high surface area and the presence of various functional groups on its surface (Banerjee et al., 2015b, 2016; Bhattacharya et al., 2020). GO-TiO$_2$ was able to decrease the COD of the lake by 54.55 %. The comparatively lower effectivity of GO-TiO$_2$ could be attributed to the presence of high organic contaminants in the water, which could adsorb some of the incident radiation thereby decreasing the effectivity of GO-TiO$_2$ (Carabin et al., 2015). Treatment by ARSB and ARSB-TiO$_2$ was able to decrease the COD of the lake water by 45.62 % and 22.97 % respectively. This was the reversal of the trend that was observed in case of the batch studies. As in the case of GO-TiO$_2$, the relatively lower effectivity of ARSB-TiO$_2$ could also be attributed to the high pollution load of the lake water which might have obstructed the incident radiation from reaching the water sample.

The COD of the industrial effluent was found to be 253.35 mg/L. From the result of the experiment as given in **Fig. 9.1** it was observed that the highest reduction in the COD was observed after treatment

with GO (84.21 %). After treatment with GO-TiO$_2$ the reduction in COD was observed to be 78.63 %. After treatment with Fenton oxidation followed by adsorption with GO, the COD came down to 57.89 %. The lesser effectivity of Fenton oxidation followed by adsorption with GO in case of the industrial effluent as compared in case of the lake water can be attributed to the fact that the lower organic load of the industrial effluent might have resulted in some of the H$_2$O$_2$ to be remained unused. As a consequence of which this remaining traces of H$_2$O$_2$ might have reacted with the K$_2$Cr$_2$O$_7$ thereby recording a higher COD value and subsequently recording a lower decrease of COD. The percentage reduction in COD after treatment with ARSB and ARSB-TiO$_2$ were observed to be 26.32 % and 18.41 % respectively. In this case also, ARSB showed higher effectivity, although by a small margin as compared to the lake water.
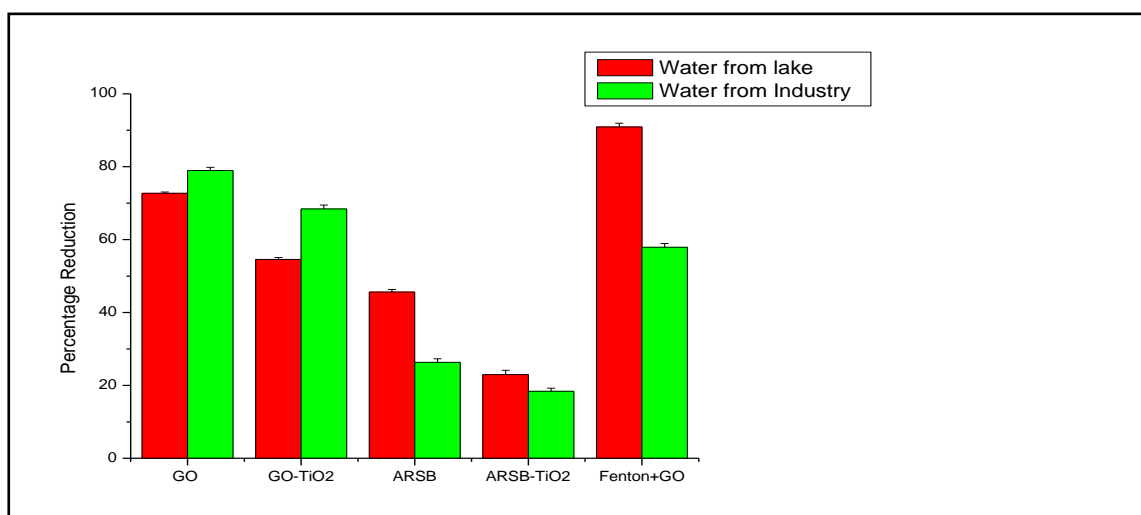


**Fig. 9.1**:- Percentage reduction of COD after treatment with different methods

## 9.5 CONCLUSION

The experiment was conducted to assess the efficacy of the water treatment techniques for treating real waste water. The water sample collected from the lake water was highly polluted with a COD value of 1466.78 mg/L. However, the process of Fenton oxidation followed by adsorption with GO was able to reduce the COD level by 90.91 %. The COD of the same waste water after treatment with GO came down by 72.73 %. In case of the industrial effluent, the original COD level of the water was 253.35 mg/L and after treatment with GO it came down by 84.21 % and after treatment with GO-TiO$_2$ it came down by 73.68 %. In case of both the polluted lake water and the industrial effluent, the best performing

treatment techniques were able to decrease the COD level by more than 80 %. In case of both the water samples, the photo-catalysts GO-TiO$_2$ and ARSB-TiO$_2$ exhibited less COD removal as compared to the adsorbents GO and ARSB . This could be attributed to the high organic load of the polluted water which might have obstructed the incident light from activating the photo-catalysts. While in case of the batch studies, GO generally exhibited higher efficiency than GO-TiO$_2$, but in case of ARSB and ARSB-TiO$_2$ a reversal in trend was observed in case of the treatment of waste water. The process of Fenton oxidation followed by adsorption by GO exhibited lower efficiency in case of the industrial effluent, which could be attributed to the lower organic load of the effluent which might have left some traces of H$_2$O$_2$ to be remained unused which in turn might have increased the COD level of the water after treatment.

# CHAPTER 10

# GENERAL DISCUSSION AND SCOPE FOR FUTURE WORK

Water is one of the essential resources for the sustenance of all forms of life. However, water is getting polluted by different forms of pollutants on a daily basis. Pollution of water can be considered to be a threat to the existence of life itself. As a consequence, utmost importance must be taken for the purification of water. In recent times various types of organic chemical, mainly anthropogenic in nature are emerging as a potent group of pollutants named trace organic pollutants. These pollutants comprise of drugs and medicine, cosmetics and other personal care products, like plasticizers etc. Collectively they can be termed as emerging pollutants or emerging contaminants (EC's). These chemicals generally are not degraded easily and the common wastewater treatment facilities are unable to properly remove them. Therefore they have a tendency to remain in the aquatic system and can have various unintended effects on organisms that consumes this water or comes in contact with it.

As conventional methods of waste water treatment are not sufficient to remove the EC's from water therefore various different methods have been investigated for the purpose of removing these EC's from water. For this particular thesis, four chemicals were selected as the target pollutants, three pharmaceuticals CBZ, NPX and RTN and one plasticizer BPA. The methods that were investigated for treating these EC's were adsorption and advanced oxidation.

GO was selected as one of the adsorbents due to it having a very high surface area and presence of various functional groups on its surface. The GO was synthesized from graphite by a modified Hummer's method. The synthesized GO were characterised by SEM analysis, FTIR spectroscopy, XRD spectroscopy and Raman spectroscopy. From the characterization of GO it was observed that GO consisted of thin lamellar sheets of carbon imposed on one another. From the FT-IR analysis it was also confirmed that the synthesized GO consisted of various functional groups on its surface. In order to evaluate the removal efficacy of GO for the purpose of removing the designated pollutants, a series of batch studies were conducted. From there it was observed that GO was very effective in removing the designated pollutants from there aquatic solution. From the batch study data, the adsorption isotherm, adsorption kinetics and adsorption thermodynamics were calculated which gave an idea about the mechanism and chemical nature of the adsorption reaction. The process was further optimized with the CCD model of RSM. And lastly, the ability of GO to remove the EC's under a dynamic condition was

checked by the RPB method. There also it was observed that GO was very effective in removing the pollutants.

In spite of the high effectivity of GO, one problem associated with its wide scale application is its relative high cost of manufacturing. Therefore, an adsorbent was needed to be synthesized whose cost of manufacturing would be less than that of GO but it would still exhibit high level of efficiency. In order to suffice the above mentioned criteria's, firstly a biochar was synthesized from rice straw, which is an abundantly available, cheap agricultural by-product. Then this synthesized biochar was activated by a modified Hummer's method. The resultant product was named Activated Rice Straw Biochar (**ARSB**). ARSB was characterized in the same way as in the case of GO. From there it was observed that ARSB had some morphological and structural similarities to GO. From the batch study data and optimization data it was observed that ARSB was able to remove significant quantities of the targeted pollutants from its aquatic system. ARSB also exhibited relatively high effectivity in the RPB system. This signified that ARSB was an efficient adsorbent. However, the removal efficacy of ARSB was less than that of GO.

Although adsorption is an effective method for treating trace organic pollutants in water, it does not result in the degradation of pollutants. In adsorption, the pollutants move from the aqueous phase to the solid phase and are not degraded or transformed to other products. Thus in order to degrade the pollutants, preferably to benign end products like $CO_2$ and $H_2O$ the process of advanced oxidation (AOP) was adopted. First, the process of photo-catalysis was investigated. For the purpose of photo-catalysis, $TiO_2$ was chosen as the semiconductor due to its chemical and physical stability, non-toxic nature and relative ease of availability. Then it was combined with the previously synthesized adsorbents GO and ARSB in order to increase its adsorption ability, to delay the recombination of the ejected electron on its surface and to decrease the band gap of $TiO_2$. The photo-catalysts were synthesized by combining the GO and ARSB with $TiO_2$ (3 part by weight of anatase and 1 part by weight of rutile) by a solvo-thermal method. The synthesized photo-catalysts were named GO-$TiO_2$ and ARSB-$TiO_2$ and it consisted of 9 parts by weight of GO/ARSB and 1 part by weight of $TiO_2$. The photo-catalysts were characterized by the same methods as used in case of adsorbents. From there it was observed that both GO and ARSB were reduced by $TiO_2$ during the solvo-thermal method. This signifies that the $TiO_2$ was irreversibly bounded with the adsorbents during the process of synthesis. The band gap of the synthesized photo-catalysts were calculated by a Tauc plot. From there it was observed that the band gap of GO-$TiO_2$ (3.24 eV) and ARSB-$TiO_2$ (2.4 eV) were less than $TiO_2$ thereby signifying that the band gap of $TiO_2$ was decreased on combining with GO and ARSB. In case of the photo-catalysts, before starting the batch study a screening study was conducted with different incident radiations (UVA,UVB, UVC and visible light) in order to find which radiation best activates the photo-catalysts. From there it was observed GO-$TiO_2$ was best activated by UVA radiation and ARSB-$TiO_2$ was best activated by visible light. From the result of the batch study it was observed that GO-$TiO_2$ was

highly effective in removing the EC's from water. ARSB-TiO$_2$ also exhibited removal efficiency which was comparable to that of GO-TiO$_2$. From the result of the experiment of ARSB-TiO$_2$ it can be stated that on addition of TiO$_2$, the removal efficiency of ARSB had increased very highly.

Other than photo-catalysis, Fenton oxidation was also employed for removing the EC's. Fenton oxidation also exhibited very high efficiency for the purpose removing the EC's from water, and that also at a very low dosage of FeSO$_4$.7H$_2$O and H$_2$O$_2$. After treatment with Fenton oxidation, the water was treated with GO, with the intention of removing all the reaction intermediates and residual EC's. The combined effect of Fenton oxidation and GO treatment were able to significantly remove the EC's from their aquatic solution.

The ability of the different treatment methods to treat real waste water was also evaluated. Water samples was collected from two sites, one being a polluted lake and the other being the effluent from an industry. The COD of the water before and after treatment were evaluated. From there it was observed that the water of the lake had very high COD (1466.78 mg/L) and the highest reduction in the COD was observed after treatment with Fenton oxidation followed by adsorption with GO which was 90.91 % of the original value. The second highest reduction in the COD was observed after treatment with GO which was 72.73 %. In case of the industrial effluent, the level of COD was 253.35 mg/L and in this case the highest reduction in COD was observed after treatment with GO which was 84.21 % and the second highest reduction was observed after treatment with GO-TiO$_2$ which was 73.68 %. Thus, from the result it was observed that water treatment techniques investigated in this research was able to treat real waste water. Overall, GO exhibited higher efficiency than the other methods.

From this thesis it was observed that, carbonaceous materials like GO and ARSB are able to effectively remove trace organic pollutants from water. As adsorbents, GO and ARSB can adsorb large amounts of EC's by virtue of their high surface area and functional groups. On being combined with TiO$_2$ they can enhance the performance of TiO$_2$ by adsorbing the pollutants and decreasing the band gap of TiO$_2$. The GO and GO-TiO$_2$ were also able to effectively reduce the COD load of polluted water samples. All the synthesized materials also exhibited reusability to some degree, thereby signifying that they are economically viable for use. At the end, a set of viable, robust options were provided which were able to effectively remove the trace organic pollutants from water.

After the completion of the study, some topics which can warrant future investigation can be listed as:-

1.> ARSB exhibited the lowest efficiency among all the different treatment methods investigated, therefore effort can be taken to increase the efficiency of ARSB.

2.> A toxicological study can also be done in order to evaluate the quality of the treated water, especially after the treatment by advanced oxidation methods.

3.> Effective techniques for separating the GO, ARSB, GO-$TiO_2$ and ARSB-$TiO_2$ from water after treatment could also be investigated so that these materials can be efficiently removed from the water.

4.> The synthesized materials could be utilized for the treatment of different types of real time waste water and the commercial potential of the synthesized materials can also be investigated.

# CHAPTER 11

# REFERENCE

Ács, A., Liang, X., Bock, I., Griffitts, J., Ivánovics, B., Vásárhelyi, E., Ferincz, Á., Pirger, Z., Urbányi, B., Csenki, Z., & 1. (2022). Chronic Effects of Carbamazepine , Progesterone and Their Mixtures at Environmentally Relevant Concentrations on Biochemical Markers of Zebrafish ( Danio rerio ). *Antioxidants*, *11*(1776).

Ahmed, S. N., & Haider, W. (2018). Heterogeneous photocatalysis and its potential applications in water and wastewater treatment : a review. *Nanotechnology*, *29*(34), 342001. https://doi.org/https://doi.org/10.1088/1361-6528/aac6ea

Al-ghouti, M. A., & Da, D. A. (2020). Guidelines for the use and interpretation of adsorption isotherm models: A review. *Journal of Hazardous Materials*, 122383. https://doi.org/10.1016/j.jhazmat.2020.122383

Al-hamadani, Y. A. J., Lee, G., Kim, S., Park, C. M., & Jang, M. (2018). Sonocatalytic degradation of carbamazepine and diclofenac in the presence of graphene oxides in aqueous solution. In *Chemosphere*. Elsevier Ltd. https://doi.org/10.1016/j.chemosphere.2018.04.129

Al-rub, F. A. A., Fares, M. M., & R.Mohammad, A. (2020). *Use of nanohybrid nanomaterials in water treatment : highly e ffi cient removal of ranitidine †*. *10*, 37050–37063. https://doi.org/10.1039/d0ra05530a

Al-shamali, S. S. (2013). Photocatalytic Degradation of Methylene Blue in the Presence of TiO2 Catalyst Assisted Solar Radiation. *Australian Journal of Basic and Applied Sciences*, *7*(4), 172–176.

Al-Shamali, S. S. (2013). Photocatalytic Degradation of Methylene Blue in the Presence of TiO 2 Catalyst Assisted Solar Radiation. *Australian Journal of Basic and Applied Sciences*, *7*(4), 172–176.

Ali, R. M., Hamad, H. A., Hussein, M. M., & Malash, G. F. (2016). Potential of using green adsorbent of heavy metal removal from aqueous solutions : Adsorption kinetics , isotherm , thermodynamic , mechanism and economic analysis. *Ecological Engineering*, *91*, 317–332.

https://doi.org/10.1016/j.ecoleng.2016.03.015

Alim, N. S., Lintang, H. O., & Yuliati, L. (2016). Photocatalytic removal of phenol over titanium dioxide- reduced graphene oxide photocatalyst. *IOP Conference Series: Materials Science and Engineering*, *107*(1). https://doi.org/10.1088/1757-899X/107/1/012001

Amalraj Appavoo, I., Hu, J., Huang, Y., Li, S. F. Y., & Ong, S. L. (2014). Response surface modeling of Carbamazepine (CBZ) removal by Graphene-P25 nanocomposites/UVA process using central composite design. *Water Research*, *57*, 270–279. https://doi.org/10.1016/j.watres.2014.03.007

Ameta, R., Solanki, M. S., Benjamin, S., & Ameta, S. C. (2018). *6.1 introduction*. https://doi.org/10.1016/B978-0-12-810499-6.00006-1

Babuponnusami, A., & Muthukumar, K. (2014). A review on Fenton and improvements to the Fenton process for wastewater treatment. *Journal of Environmental Chemical Engineering*, *2*(1), 557–572. https://doi.org/10.1016/j.jece.2013.10.011

Balasubramani, K., Sivarajasekar, N., Muthusaravanan, S., Ram, K., Naushad, M., Ahamad, T., & Sharma, G. (2020). Efficient removal of antidepressant Flupentixol using graphene oxide/cellulose nanogel composite: Particle swarm algorithm based artificial neural network modelling and optimization. *Journal of Molecular Liquids*, *319*, 114371. https://doi.org/10.1016/j.molliq.2020.114371

Balasubramani, K., Sivarajasekar, N., & Naushad, M. (2020). Effective adsorption of antidiabetic pharmaceutical ( metformin ) from aqueous medium using graphene oxide nanoparticles : Equilibrium and statistical modelling. *Journal of Molecular Liquids*, *301*, 112426. https://doi.org/10.1016/j.molliq.2019.112426

Banerjee, P., Das, P., Zaman, A., & Das, P. (2016). Application of graphene oxide nanoplatelets for adsorption of Ibuprofen from aqueous solutions : Evaluation of process kinetics and. *Process Safety and Environmental Protection*, *101*, 45–53. https://doi.org/10.1016/j.psep.2016.01.021

Banerjee, P., Mukhopadhyay, A., & Das, P. (2017). Graphene oxide – nanobentonite composite sieves for enhanced desalination and dye removal. *Desalination*, *June*, 0–1. https://doi.org/10.1016/j.desal.2017.06.010

Banerjee, P., Roy Barman, S., Mukhopadhayay, A., & Das, P. (2017). Ultrasound assisted mixed azo dye adsorption by chitosan–graphene oxide nanocomposite. *Chemical Engineering Research and Design*, *117*, 43–56. https://doi.org/10.1016/j.cherd.2016.10.009

Banerjee, P., Sau, S., Das, P., & Mukhopadhayay, A. (2015a). Ecotoxicology and Environmental Safety Optimization and modelling of synthetic azo dye wastewater treat- ment using Graphene

oxide nanoplatelets : Characterization toxicity evaluation and optimization using Arti fi cial Neural Network. *Ecotoxicology and Environmental Safety*, *119*, 47–57. https://doi.org/10.1016/j.ecoenv.2015.04.022

Banerjee, P., Sau, S., Das, P., & Mukhopadhayay, A. (2015b). Optimization and modelling of synthetic azo dye wastewater treatment using Graphene oxide nanoplatelets: Characterization toxicity evaluation and optimization usingArtificial Neural Network. *Ecotoxicology and Environmental Safety*, *119*, 47–57. https://doi.org/10.1016/j.ecoenv.2015.04.022

Bansode, R. R., Losso, J. N., Marshall, W. E., Rao, R. M., & Portier, R. J. (2004). *Pecan shell-based granular activated carbon for treatment of chemical oxygen demand ( COD ) in municipal wastewater*. *94*, 129–135. https://doi.org/10.1016/j.biortech.2003.12.009

Barman, S. R., Banerjee, P., Das, · Papita, & Mukhopadhayay, A. (2018). Urban wood waste as precursor of activated carbon and its subsequent application for adsorption of polyaromatic hydrocarbons. *International Journal of Energy and Water Resources*, *0123456789*. https://doi.org/10.1007/s42108-018-0001-4

Batucan, P., Tremblay, L. A., Northcott, G. L., & Matthaei, C. D. (2022). *Medicating the environment ? A critical review on the risks of carbamazepine , diclofenac and ibuprofen to aquatic organisms*. *7*. https://doi.org/10.1016/j.envadv.2021.100164

Berger, K., Eskenazi, B., Balmes, J., Kogut, K., Holland, N., Calafat, A. M., & Harley, K. G. (2019). *Prenatal high molecular weight phthalates and bisphenol A , and childhood respiratory and allergic outcomes*. *October 2018*, 36–46. https://doi.org/10.1111/pai.12992

Bergheim, M., Gieré, R., & Kümmerer, K. (2012). *Biodegradability and ecotoxicitiy of tramadol , ranitidine , and their photoderivatives in the aquatic environment*. 72–85. https://doi.org/10.1007/s11356-011-0536-y

Bhatnagar, A., & Anastopoulos, I. (2017). Adsorptive removal of bisphenol A (BPA) from aqueous solution: A review. In *Chemosphere* (Vol. 168, pp. 885–902). Elsevier Ltd. https://doi.org/10.1016/j.chemosphere.2016.10.121

Bhattacharya, S., Banerjee, P., Das, P., Bhowal, A., Majumder, S. K., & Ghosh, P. (2020). Removal of aqueous carbamazepine using graphene oxide nanoplatelets: process modelling and optimization. *Sustainable Environment Research*, *30*(1). https://doi.org/10.1186/s42834-020-00062-8

Bhattacharya, S., Das, P., Bhowal, A., & Majumder, S. K. (2022). Metal-oxide coated Graphene oxide nano-composite for the treatment of pharmaceutical compound in photocatalytic reactor: Batch, Kinetics and Mathematical Modeling using Response Surface Methodology and Artificial

Neural Network. *Environmental Science and Pollution Research*, *0123456789.* https://doi.org/10.1007/s11356-021-18227-2

Bhattacharya, S., Das, P., Bhowal, A., & Saha, A. (2021). Thermal, Chemical and ultrasonic assisted synthesis of carbonized Biochar and its application for reducing Naproxen: Batch and Fixed bed study and subsequent optimization with response surface methodology (RSM) and artificial neural network. *Surfaces and Interfaces*, *26*(August), 101416. https://doi.org/10.1016/j.surfin.2021.101416

Bhattacharyya, S., Banerjee, P., Bhattacharya, S., Rathour, R. K. S., Majumder, S. K., Das, P., & Datta, S. (2018). Comparative assessment on the removal of ranitidine and prednisolone present in solution using graphene oxide (GO) nanoplatelets. *Desalination and Water Treatment*, *132*, 287–296. https://doi.org/10.5004/dwt.2018.23170

Bhattacharyya, S., Das, P., & Datta, S. (2019). *Removal of Ranitidine from Pharmaceutical Waste Water Using Activated Carbon ( AC ) Prepared from Waste Lemon Peel*. Springer Singapore. https://doi.org/10.1007/978-981-13-2619-6

Bhattacharyyaa, S., Banerjeeb, P., Bhattacharyaa, S., Rishi Karan Singh Rathour Subrata Kumar Majumderd Papita Das, & Siddhartha, D. (2018). *Comparative Assessment on the Removal of Ranitidine and Prednisolone Present In Solution Using Graphene Oxide ( GO ) Nanoplatelets Comparative assessment on the removal of ranitidine and prednisolone present in solution using graphene oxide ( GO ) nanopla. November*. https://doi.org/10.5004/dwt.2018.23170

Brugnera, M. F., Rajeshwar, K., Cardoso, J. C., & Zanoni, M. V. B. (2010). Bisphenol A removal from wastewater using self-organized TIO2 nanotubular array electrodes. *Chemosphere*, *78*(5), 569–575. https://doi.org/10.1016/j.chemosphere.2009.10.058

Burkhardt-Holm, P. (2010). *Endocrine Disruptors and Water Quality : A State-of-the-Art Review. January 2015*, 37–41. https://doi.org/10.1080/07900627.2010.489298

Cai, X., Li, J., Liu, Y., Yan, Z., Tan, X., Liu, S., Zeng, G., Gu, Y., Hu, X., & Jiang, L. (2018). Titanium dioxide-coated biochar composites as adsorptive and photocatalytic degradation materials for the removal of aqueous organic pollutants. *Journal of Chemical Technology and Biotechnology*, *93*(3), 783–791. https://doi.org/10.1002/jctb.5428

Carabin, A., Drogui, P., & Robert, D. (2015). Photo-degradation of carbamazepine using TiO2 suspended photocatalysts. *Journal of the Taiwan Institute of Chemical Engineers*, *54*, 109–117. https://doi.org/10.1016/j.jtice.2015.03.006

Chakraborty, V., & Das, P. (2021). *Synthesis and application of various metal oxide – / biomaterial – coated carbonaceous nanomaterials derived from waste biomass for removal of Cr + 6 present*

*in solution*.

Chang, C., & Lee, S. (2012). Adsorption behavior of pesticide methomyl on activated carbon in a high gravity rotating packed bed reactor. *Water Research*, *46*(9), 2869–2880. https://doi.org/10.1016/j.watres.2012.02.041

Chang, H., Choo, K., Lee, B., & Choi, S. (2009). *The methods of identification , analysis , and removal of endocrine disrupting compounds ( EDCs ) in water*. *172*, 1–12. https://doi.org/10.1016/j.jhazmat.2009.06.135

Chang, K., Hsieh, J., Ou, B., Chang, M., Hseih, W., Chang, K., Hsieh, J., Ou, B., & Chang, M. (2012). Separation Science and Technology Adsorption Studies on the Removal of an Endocrine- Disrupting Compound ( Bisphenol A ) using Activated Carbon from Rice Straw Agricultural Waste Adsorption Studies on the Removal of an Endocrine-Disrupting Compound ( Bisp. *Separation Science and Technology*, *March 2013*, 37–41. https://doi.org/10.1080/01496395.2011.647212

Chen, D., Xie, S., Chen, C., Quan, H., & Hua, L. (2017). RSC Advances Activated biochar derived from pomelo peel as a high-capacity sorbent for removal of carbamazepine from aqueous solution †. *RSC Advances*, *7*, 54969–54979. https://doi.org/10.1039/C7RA10805B

Chen, F., Ying, G., Kong, L., Wang, L., Zhao, J., Zhou, L., & Zhang, L. (2011). *Distribution and accumulation of endocrine-disrupting chemicals and pharmaceuticals in wastewater irrigated soils in Hebei , China*. *159*, 1490–1498. https://doi.org/10.1016/j.envpol.2011.03.016

Chen, Z., Liu, Z., Hu, J., Cai, Q., Li, X., & Wang, W. (2020). β -Cyclodextrin-modified graphene oxide membranes with large adsorption capacity and high flux for efficient removal of bisphenol A from water β -Cyclodextrin-modified graphene oxide membranes with large adsorption capacity and high flux for efficient rem. *Journal of Membrane Science*, *595*(September), 117510. https://doi.org/10.1016/j.memsci.2019.117510

Cheng, N., Wang, B., Wu, P., Lee, X., Xing, Y., Chen, M., & Gao, B. (2021). Adsorption of emerging contaminants from water and wastewater by modi fi ed biochar : A review *. *Environmental Pollution*, *273*, 116448. https://doi.org/10.1016/j.envpol.2021.116448

Chouhan, S., Yadav, S. K., Prakash, J., Swati, & Singh, S. P. (2014). Effect of Bisphenol A on human health and its degradation by microorganisms: A review. In *Annals of Microbiology* (Vol. 64, Issue 1, pp. 13–21). https://doi.org/10.1007/s13213-013-0649-2

Chowdhury, S., & Balasubramanian, R. (2014). Applied Catalysis B : Environmental Graphene / semiconductor nanocomposites ( GSNs ) for heterogeneous photocatalytic decolorization of wastewaters contaminated with synthetic dyes : A review. *"Applied Catalysis B,*

Environmental," 160–161, 307–324. https://doi.org/10.1016/j.apcatb.2014.05.035

Ciğeroğlu, Z., Özdemir, O. K., Şahin, S., & Haşimoğlu, A. (2020). Naproxen Adsorption onto Graphene Oxide Nanopowders : Equilibrium , Kinetic , and Thermodynamic Studies. *Water Air Soil Pollut*, *231*(101).

Dai, J., Meng, X., Zhang, Y., & Huang, Y. (2020). Bioresource Technology E ff ects of modi fi cation and magnetization of rice straw derived biochar on adsorption of tetracycline from water. *Bioresource Technology*, *311*(December 2019), 123455. https://doi.org/10.1016/j.biortech.2020.123455

Das, A., Bhowal, A., & Datta, S. (2008). *Continuous Biosorption in Rotating Packed-Bed Contactor*. 4230–4235.

Das, L., Saha, N., Ganguli, A., Das, P., Bhowal, A., & Bhattacharjee, C. (2021). Calcium alginate–bentonite/activated biochar composite beads for removal of dye and Biodegradation of dye-loaded composite after use: Synthesis, removal, mathematical modeling and biodegradation kinetics. *Environmental Technology and Innovation*, *24*, 101955. https://doi.org/10.1016/j.eti.2021.101955

Das, P., Banerjee, P., Rathour, R., & Misra, R. (2015). Assessment on linear and non-linear analysis for the estimation of pseudo-second-order kinetic parameters for removal of dye using graphene nanosheet. *Desalination and Water Treatment*, *56*(2), 502–508. https://doi.org/10.1080/19443994.2014.937759

Das, P., & Das, P. (2016). Graphene oxide for the treatment of ranitidine containing solution: Optimum sorption kinetics by linear and non linear methods and simulation using artificial neural network. *Process Safety and Environmental Protection*, *102*, 589–595. https://doi.org/10.1016/j.psep.2016.05.018

Das, Sagnik, Bhattacharya, S., & Das, P. (2022). Titanium oxide–coated coconut husk–derived biochar composite and its application for removal of crystal violet dye. *Biomass Conversion and Biorefinery*. https://doi.org/10.1007/s13399-022-02956-6

Das, Sutapa, & Goud, V. V. (2020). Characterization of a low-cost adsorbent derived from agro-waste for ranitidine removal. *Materials Science for Energy Technologies*, *3*, 879–888. https://doi.org/10.1016/j.mset.2020.10.009

Davididou, K., Nelson, R., Monteagudo, J. M., Durán, A., Expósito, A. J., & Chatzisymeon, E. (2018). Photocatalytic degradation of bisphenol-A under UV-LED, blacklight and solar irradiation. *Journal of Cleaner Production*, *203*, 13–21. https://doi.org/10.1016/j.jclepro.2018.08.247

Delhiraja, K., Vellingiri, K., Boukhvalov, D. W., & Philip, L. (2019). Development of Highly Water Stable Graphene Oxide-Based Composites for the Removal of Pharmaceuticals and Personal Care Products [Research-article]. *Industrial & Engineering Chemistry Research*, *58*, 2899–2913. https://doi.org/10.1021/acs.iecr.8b02668

Della-flora, A., Wilde, M. L., Lima, D., Lima, E. C., & Sirtori, C. (2021). Journal of Environmental Chemical Engineering Combination of tertiary solar photo-Fenton and adsorption processes in the treatment of hospital wastewater : The removal of pharmaceuticals and their transformation products. *Journal of Environmental Chemical Engineering*, *9*(4), 105666. https://doi.org/10.1016/j.jece.2021.105666

Ding, T., Lin, K., Yang, B., Yang, M., Li, J., & Li, W. (2017). Biodegradation of Naproxen by freshwater algae Cymbella sp. and Scenedesmus quadricauda and the comparative toxicity. *Bioresource Technology*. https://doi.org/10.1016/j.biortech.2017.04.018

Diwald, O., Thompson, T. L., Zubkov, T., Goralski, E. G., Walck, S. D., & Yates, J. T. (2004). Photochemical Activity of Nitrogen-Doped Rutile TiO 2 ( 110 ) in Visible Light. *The Journal of Physical Chemistry B*, *2*(110), 6004–6008.

Dong, H., Zeng, G., Tang, L., & Fan, C. (2015). ScienceDirect An overview on limitations of TiO 2 - based particles for photocatalytic degradation of organic pollutants and the corresponding countermeasures. *Water Research*, *79*, 128–146. https://doi.org/10.1016/j.watres.2015.04.038

Drillia, P., Dokianakis, S. N., Fountoulakis, M. S., Kornaros, M., Stamatelatou, K., & Lyberatos, G. (2005). *On the occasional biodegradation of pharmaceuticals in the activated sludge process : The example of the antibiotic sulfamethoxazole*. *122*, 259–265. https://doi.org/10.1016/j.jhazmat.2005.03.009

Dwivedi, K., Morone, A., Chakrabarti, T., & Pandey, R. A. (2018). Evaluation and optimization of Fenton pretreatment integrated with granulated activated carbon (GAC) filtration for carbamazepine removal from complex wastewater of pharmaceutical industry. *Journal of Environmental Chemical Engineering*, *6*(3), 3681–3689. https://doi.org/10.1016/j.jece.2016.12.054

Ebele, J. A., Abdallah, M. A., & Harrad, S. (2017). Pharmaceuticals and personal care products ( PPCPs ) in the freshwater aquatic environment. *Emerging Contaminants*, *3*(1), 1–16. https://doi.org/10.1016/j.emcon.2016.12.004

Fazal, T., Razzaq, A., Javed, F., Hafeez, A., Rashid, N., Amjad, U. S., Ur Rehman, M. S., Faisal, A., & Rehman, F. (2020). Integrating adsorption and photocatalysis: A cost effective strategy for textile wastewater treatment using hybrid biochar-TiO2 composite. *Journal of Hazardous*

*Materials*, *390*. https://doi.org/10.1016/j.jhazmat.2019.121623

Ganguli, A., Ganguly, P., Das, P., & Saha, A. (2020). Integral approach for the treatment of phenolic wastewater using gamma irradiation and graphene oxide. *Groundwater for Sustainable Development*, *10*. https://doi.org/10.1016/j.gsd.2020.100355

Ganguly, P., Sarkhel, R., Bhattacharya, S., Das, P., Saha, A., & Bhowal, A. (2020). Integral approach of treatment of phenolic wastewater using nano-metal coated graphene oxide in combination with advanced oxidation. *Surfaces and Interfaces*, *21*. https://doi.org/10.1016/j.surfin.2020.100660

Garikoé, I., Sorgho, B., Yaméogo, A., Guel, B., & Andala, D. (2020). Removal of bisphenol A by adsorption on organically modified clays from Burkina Faso. *Bioremediation Journal*, *25*(1), 22–47. https://doi.org/10.1080/10889868.2020.1842321

Gimbert, F., Morin-Crini, N., Renault, F., Badot, P.-M., & Crini, G. (2008). Adsorption isotherm models for dye removal by cationized starch-based material in a single component system : Error analysis. *Journal of Hazar*, *157*, 34–46. https://doi.org/10.1016/j.jhazmat.2007.12.072

Gogoi, A., Mazumder, P., Kumar, V., Chaminda, G. G. T., Kyoungjin, A., & Kumar, M. (2018). Groundwater for Sustainable Development Occurrence and fate of emerging contaminants in water environment : A review. *Groundwater for Sustainable Development*, *6*(January), 169–180. https://doi.org/10.1016/j.gsd.2017.12.009

Górny, D., Guzik, U., Hupert-kocurek, K., & Wojcieszy, D. (2019). *A new pathway for naproxen utilisation by Bacillus thuringiensis B1 ( 2015b ) and its decomposition in the presence of organic and inorganic contaminants*. *239*(August 2018), 1–7. https://doi.org/10.1016/j.jenvman.2019.03.034

Goswami, S., Banerjee, P., Datta, S., Mukhopadhayay, A., & Das, P. (2017). Graphene oxide nanoplatelets synthesized with carbonized agro-waste biomass as green precursor and its application for the treatment of dye rich wastewater. *Process Safety and Environmental Protection*, *106*, 163–172. https://doi.org/10.1016/j.psep.2017.01.003

Grenni, P., Patrolecco, L., Ademollo, N., Tolomei, A., & Barra, A. (2013). Degradation of Gem fi brozil and Naproxen in a river water ecosystem. *Microchemical Journal*, *107*, 158–164. https://doi.org/10.1016/j.microc.2012.06.008

Guo, R., Xie, X., & Chen, J. (2014). The degradation of antibiotic amoxicillin in the Fenton-activated sludge combined system. *Environmental Technology*, *December*, 37–41. https://doi.org/10.1080/09593330.2014.963696

Hai, F. I., Yang, S., Id, M. B. A., Id, V. S., Shawkat, S., Sanderson-smith, M., Gorman, J., Xu, Z., & Yamamoto, K. (2018). Carbamazepine as a Possible Anthropogenic Marker in Water : Occurrences , Toxicological Effects , Treatment Technologies. *Water*, *10*(2), 1–32. https://doi.org/10.3390/w10020107

Hao, Z., Wang, C., Yan, Z., Jiang, H., & Xu, H. (2018). SC. *ECSN*. https://doi.org/10.1016/j.chemosphere.2018.08.038

Hashim, A. M., Kundu, A., Mukherjee, S., Ng, Y., Mukhopadhaya, S., Redzwan, G., & Gupta, B. Sen. (2019). Arsenic removal by adsorption on activated carbon in a rotating packed bed. *Journal of Water Process Engineering*, *30*, 1–19.

Hassani, A., Khataee, A., Karaca, S., Karaca, C., & Gholami, P. (2017). Sonocatalytic degradation of ciprofloxacin using synthesized TiO2 nanoparticles on montmorillonite. *Ultrasonics Sonochemistry*, *35*, 251–262. https://doi.org/10.1016/j.ultsonch.2016.09.027

Hossain, M. A., Ngo, H. H., Guo, W. S., & Setiadi, T. (2012). Bioresource Technology Adsorption and desorption of copper ( II ) ions onto garden grass. *BIORESOURCE TECHNOLOGY*, *121*, 386–395. https://doi.org/10.1016/j.biortech.2012.06.119

Hummers Jr., W. S., & Offeman, R. E. (1957). *Preparation of Graphitic Oxide*. *208*(1937), 1937. https://doi.org/10.1021/ja01539a017

I˙lbay, Z., Ahin, S. S., Kerkez, O. ., & Bayazit, S. . S. (2015). Isolation of naproxen from wastewater using carbon-based magnetic adsorbents. *International Journal of Environmentall Science and Tec Hnology*, *12*, 3451–3550. https://doi.org/10.1007/s13762-015-0775-4

Isidori, M., Parrella, A., Pistillo, P., & Temussi, F. (2009). *Effects of ranitidine and its photoderivatives in the aquatic environment*. *35*, 821–825. https://doi.org/10.1016/j.envint.2008.12.002

Jo, W. K., & Kang, H. J. (2013). Titanium dioxide-graphene oxide composites with different ratios supported by pyrex tube for photocatalysis of toxic aromatic vapors. *Powder Technology*, *250*, 115–121. https://doi.org/10.1016/j.powtec.2013.10.017

Kanakaraju, D., Glass, B. D., & Oelgem, M. (2018). *Advanced oxidation process-mediated removal of pharmaceuticals from water : A review*. *219*. https://doi.org/10.1016/j.jenvman.2018.04.103

Katsumata, H., Kawabe, S., Kaneco, S., Suzuki, T., & Ohta, K. (2004). *Degradation of bisphenol A in water by the photo-Fenton reaction*. *162*, 297–305. https://doi.org/10.1016/S1010-6030(03)00374-5

Kavitha, V., & Palanivelu, K. (2005). Destruction of cresols by Fenton oxidation process. *Water*

*Research*, *39*(13), 3062–3072. https://doi.org/10.1016/j.watres.2005.05.011

Kayaalp, N., Ersahin, M. E., & Ozgun, H. (2010). *RESEARCH ARTICLE A new approach for chemical oxygen demand ( COD ) measurement at high salinity and low organic matter samples*. 1547–1552. https://doi.org/10.1007/s11356-010-0341-z

Khalid, N. R., Majid, A., Tahir, M. B., Niaz, N. A., & Khalid, S. (2017). *pollutants : A review. June*. https://doi.org/10.1016/j.ceramint.2017.08.143

Khalil, A. M. E., Memon, F. A., Tabish, T. A., Salmon, D., Zhang, S., & Butler, D. (2020). Nanostructured porous graphene for efficient removal of emerging contaminants ( pharmaceuticals ) from water. *Chemical Engineering Journal*, *398*(March), 125440. https://doi.org/10.1016/j.cej.2020.125440

Khalil, U., Bilal, M., Ali, S., Rizwan, M., Nasser, M., & Wijaya, L. (2020). Adsorption-reduction performance of tea waste and rice husk biochars for Cr ( VI ) elimination from wastewater. *Journal of Saudi Chemical Society*. https://doi.org/10.1016/j.jscs.2020.07.001

Khan, A., Wang, J., Li, J., Wang, X., & Chen, Z. (2017). The role of graphene oxide and graphene oxide-based nanomaterials in the removal of pharmaceuticals from aqueous media : a review. *Environmental Science and Pollution Research*, *March*. https://doi.org/10.1007/s11356-017-8388-8

Kim, H., & Lee, J. (2014). Sensors and Actuators B : Chemical Highly sensitive and selective gas sensors using p-type oxide semiconductors : Overview. *Sensors & Actuators: B. Chemical*, *192*, 607–627. https://doi.org/10.1016/j.snb.2013.11.005

Kim, J. R., & Kan, E. (2016). *Heterogeneous Photocatalytic Degradation of Sulfamethoxazole in Water Using a Biochar- Supported TiO2 Photocatalyst Jihyun*.

Kolpin, D. W., Edward T, F., T.Meyer, M., Thurman, E. M., Zaugg, S. D., Barber, L. B., & T.Buxton, H. (2002). Pharmaceuticals, hormones, and other organic wastewater contaminants in U.S. streams, 1999-2000: a national reconnaissance. *Environmental Science & Technology*, *36*(18), 1202–1211. https://doi.org/10.1021/es0200903

Kortejarvi, H., Yliperttula, M., Dressman, J. B., Junginger, H. E., & Midha, K. K. (2005). *Biowaiver Monographs for Immediate Release Solid Oral Dosage Forms : Ranitidine Hydrochloride*. *94*(8), 1617–1625. https://doi.org/10.1002/jps.20392

Ku¨mmerer, K. (2009). The presence of pharmaceuticals in the environment due to human use – present knowledge and future challenges. *Journal of Environmental Management*, *90*, 2354–2366. https://doi.org/10.1016/j.jenvman.2009.01.023

Kundu, A., Hassan, L. S., Redzwan, G., Robinson, D., Ali, M., & Sengupta, B. (2015). Application of a rotating packed bed contactor for removal of Direct Red 23 by adsorption. *Desalination A*, *August*, 1–9. https://doi.org/10.1080/19443994.2015.1060165

Kwon, J., & Lee, B. (2015). Bisphenol A adsorption using reduced graphene oxide prepared by physical and chemical reduction methods. *Chemical Engineering Research and Design*, *104*, 519–529. https://doi.org/10.1016/j.cherd.2015.09.007

Largitte, L., & Pasquier, R. (2016). Chemical Engineering Research and Design A review of the kinetics adsorption models and their application to the adsorption of lead by an activated carbon. *Chemical Engineering Research and Design*, *109*, 495–504. https://doi.org/10.1016/j.cherd.2016.02.006

Lazarotto, J. S., de Lima Brombilla, V., Silvestri, S., & Foletto, E. L. (2020). Conversion of spent coffee grounds to biochar as promising TiO2 support for effective degradation of diclofenac in water. *Applied Organometallic Chemistry*, *34*(12), 1–11. https://doi.org/10.1002/aoc.6001

Li, B., Cui, Y., Japip, S., Thong, Z., & Chung, T. (2018). Graphene Oxide (GO) laminar membranes for concentrating pharmaceuticals and food additives in organic solvents. *Carbon*, *130*, 503–514. https://doi.org/10.1016/j.carbon.2018.01.040

Li, F., Gao, X., Chen, M., & Wang, W. (2016). Photocatalytic removal of phenol over titanium dioxide- reduced graphene oxide photocatalyst Photocatalytic removal of phenol over titanium dioxide- reduced graphene oxide photocatalyst. *Materials Science and Engineering*, *107*. https://doi.org/10.1088/1757-899X/107/1/012001

Li, M. J., Liu, C. M., Xie, Y. B., Cao, H. Bin, Zhao, H., & Zhang, Y. (2014). The evolution of surface charge on graphene oxide during the reduction and its application in electroanalysis. *Carbon*, *66*, 302–311. https://doi.org/10.1016/j.carbon.2013.09.004

Li, M., & Liu, C. (2013). The evolution of surface charge on graphene oxide during the reduction and its application in electroanalysis. *Carbon*, *66*, 302–311. https://doi.org/10.1016/j.carbon.2013.09.004

Li, Q., Wang, P., Chen, L., Gao, H., & Wu, L. (2016). Acute toxicity and histopathological effects of naproxen in zebrafish ( Danio rerio ) early life stages. *Environmental Science and Pollution Research*, 18832–18841. https://doi.org/10.1007/s11356-016-7092-4

Li, Y., Cui, W., Liu, L., Zong, R., Yao, W., & Liang, Y. (2016). Applied Catalysis B : Environmental Removal of Cr ( VI ) by 3D TiO 2 -graphene hydrogel via adsorption enriched with photocatalytic reduction. *"Applied Catalysis B, Environmental," 199*, 412–423. https://doi.org/10.1016/j.apcatb.2016.06.053

Lima, H. H. C. de, Maria Eugˆenia Grego Llop, R. dos S. M., Moises, M. P., Janeiro, V., Arroyo, P. A., & Rinaldi, M. R. G. A. W. (2021). Enhanced removal of bisphenol A using pine-fruit shell-derived hydrochars : Adsorption mechanisms and reusability. *Journal of Hazardous Materials*, *416*(December 2020), 126167. https://doi.org/10.1016/j.jhazmat.2021.126167

Lin, L., Lin, L., Wang, H., & Xu, P. (2016). *Immobilized TiO2-reduced Graphene Oxide Nanocomposites on Optical Fibers as High Performance Photocatalysts for Degradation of Pharmaceuticals Immobilized TiO 2 -reduced graphene oxide nanocomposites on optical fibers as high performance photocatalysts fo*. *April*. https://doi.org/10.1016/j.cej.2016.04.024

Liu, K., Li, F., Cui, J., Yang, S., & Fang, L. (2020). Simultaneous removal of Cd ( II ) and As ( III ) by graphene-like biochar- supported zero-valent iron from irrigation waters under aerobic conditions : Synergistic effects and mechanisms. *Journal of Hazardous Materials*, *395*(March), 122623. https://doi.org/10.1016/j.jhazmat.2020.122623

Liu, L., Li, C., Bao, C., Jia, Q., Xiao, P., Liu, X., & Zhang, Q. (2012). Talanta Preparation and characterization of chitosan / graphene oxide composites for the adsorption of Au ( III ) and Pd ( II ). *Talanta*, *93*, 350–357. https://doi.org/10.1016/j.talanta.2012.02.051

Luo, L., Yang, Y., Xiao, M., Bian, L., Yuan, B., Liu, Y., Jiang, F., & Pan, X. (2015). A novel biotemplated synthesis of TiO2/wood charcoal composites for synergistic removal of bisphenol A by adsorption and photocatalytic degradation. *Chemical Engineering Journal*, *262*, 1275–1283. https://doi.org/10.1016/j.cej.2014.10.087

Ma, J., Wang, H., Wang, F., Ma, J., Wang, H., Wang, F., & Huang, Z. (2010). Adsorption of 2 , 4-dichlorophenol from Aqueous Solution by a New Low-Cost Adsorbent – Activated Bamboo Charcoal Adsorption of 2 , 4-dichlorophenol from Aqueous Solution by a New Low-Cost Adsorbent – Activated Bamboo Char. *Separation Science and Technology*, *45*(January 2015), 2329–2336. https://doi.org/10.1080/01496395.2010.504482

Ma, Y., Liu, H., Wu, J., Yuan, L., Wang, Y., Du, X., Wang, R., Marwa, P. W., Petlulu, P., Chen, X., & Zhang, H. (2019). The adverse health effects of bisphenol A and related toxicity mechanisms. *Environmental Research*, *176*(April). https://doi.org/10.1016/j.envres.2019.108575

Mirzaei, A., Chen, Z., Haghighat, F., & Yerushalmi, L. (2017). Chemosphere Removal of pharmaceuticals from water by homo / heterogonous Fenton-type processes e A review. *Chemosphere*, *174*, 665–688. https://doi.org/10.1016/j.chemosphere.2017.02.019

Mohammed, M., Aziz, A., Raman, A., & Asghar, A. (2019). A review on approaches for addressing the limitations of Fenton oxidation for recalcitrant wastewater treatment. *Process Safety and Environmental Protection*, *126*, 119–140. https://doi.org/10.1016/j.psep.2019.03.028

Mondal, Sandip, Aikat, K., Siddharth, K., & Sarkar, K. (2017). Optimizing ranitidine hydrochloride uptake of Parthenium hysterophorus derived N-biochar through response surface methodology and. *Process Safety and Environmental Protection*, *107*, 388–401. https://doi.org/10.1016/j.psep.2017.03.011

Mondal, Sandip, Sinha, K., Aikat, K., & Halder, G. (2015). Journal of Environmental Chemical Engineering Adsorption thermodynamics and kinetics of ranitidine hydrochloride onto superheated steam activated carbon derived from mung bean husk. *Biochemical Pharmacology*, *3*(1), 187–195. https://doi.org/10.1016/j.jece.2014.11.021

Mondal, Somen, Patel, S., & Majumder, S. K. (2020). Bio-extract assisted in-situ green synthesis of Ag-RGO nanocomposite film for enhanced naproxen removal. *Korean Journal of Chemical Engineering*, *37*(2), 274–289. https://doi.org/10.1007/s11814-019-0435-3

Mosleh, S., Reza, M., Ghaedi, M., & Dashtian, K. (2018). Ultrasonics - Sonochemistry Sonochemical-assisted synthesis of CuO / Cu 2 O / Cu nanoparticles as e ffi cient photocatalyst for simultaneous degradation of pollutant dyes in rotating packed bed reactor : LED illumination and central composite design optim. *Ultrasonics - Sonochemistry*, *40*(July 2017), 601–610. https://doi.org/10.1016/j.ultsonch.2017.08.007

Mukherjee, M., Goswami, S., Banerjee, P., Sengupta, S., Das, P., Banerjee, P. K., & Datta, S. (2019). Ultrasonic assisted graphene oxide nanosheet for the removal of phenol containing solution. *Environmental Technology and Innovation*, *13*, 398–407. https://doi.org/10.1016/j.eti.2016.11.006

Naghdi, M., Taheran, M., Pulicharla, R., & Rouissi, T. (2019). Pine-wood derived nanobiochar for removal of carbamazepine from aqueous media : Adsorption behavior and influential parameters. *Arabian Journal of Chemistry*, *12*(8), 5292–5301. https://doi.org/10.1016/j.arabjc.2016.12.025

Nawaz, M., Miran, W., Jang, J., & Lee, D. S. (2017). One-step hydrothermal synthesis of porous 3D reduced graphene oxide/TiO2 aerogel for carbamazepine photodegradation in aqueous solution. *Applied Catalysis B: Environmental*, *203*, 85–95. https://doi.org/10.1016/j.apcatb.2016.10.007

Neyens, E., & Baeyens, J. (2003). *A review of classic Fenton ' s peroxidation as an advanced oxidation technique*. *98*, 33–50.

Park, Y., Ayoko, G. A., Kurdi, R., Horváth, E., Kristóf, J., & Frost, R. L. (2013). Journal of Colloid and Interface Science Adsorption of phenolic compounds by organoclays : Implications for the removal of organic pollutants from aqueous media. *Journal of Colloid And Interface Science*, *406*, 196–208. https://doi.org/10.1016/j.jcis.2013.05.027

Perera, F., Roen, E. L., Wang, Y., Margolis, A. E., Calafat, A. M., Wang, S., Garcia, W., Hoepner, L. A., Peterson, B. S., Rauh, V., & Herbstman, J. (2016). Bisphenol A exposure and symptoms of anxiety and depression among inner city children at 10 – 12 years of age. *Environmental Research*, *151*, 195–202. https://doi.org/10.1016/j.envres.2016.07.028

Phatthanakittiphong, T., & Seo, G. T. (2016). Characteristic evaluation of graphene oxide for bisphenol a adsorption in aqueous solution. *Nanomaterials*, *6*(7). https://doi.org/10.3390/nano6070128

Poerschmann, J., Trommler, U., & Górecki, T. (2010). Chemosphere Aromatic intermediate formation during oxidative degradation of Bisphenol A by homogeneous sub-stoichiometric Fenton reaction. *Chemosphere*, *79*(10), 975–986. https://doi.org/10.1016/j.chemosphere.2010.03.030

Prado, A. G. S., Torres, J. D., Faria, E. A., & Dias, S. C. L. (2004). *Comparative adsorption studies of indigo carmine dye on chitin and chitosan*. *277*, 43–47. https://doi.org/10.1016/j.jcis.2004.04.056

Rahbar, M. H., Swingle, H. M., Christian, M. A., Krone, R., Loveland, K. A., & Jr, D. G. P. (2017). *Environmental Exposure to Dioxins , Dibenzofurans , Bisphenol A , and Phthalates in Children with and without Autism Spectrum Disorder Living near the Gulf of Mexico*. https://doi.org/10.3390/ijerph14111425

Reynel-avila, H. E., Mendoza-castillo, D. I., Bonilla-petriciolet, A., & Silvestre-albero, J. (2015). Assessment of naproxen adsorption on bone char in aqueous solutions using batch and fi xed-bed processes. *Journal of Molecular Liquids*, *209*, 187–195. https://doi.org/10.1016/j.molliq.2015.05.013

Richmond, E. K., Grace, M. R., Kelly, J. J., Reisinger, A. J., Rosi, E. J., & Walters, D. M. (2017). *Pharmaceuticals and personal care products ( PPCPs ) are ecological disrupting compounds ( EcoDC )*.

Roy, S., Sengupta, S., Manna, S., & Das, P. (2018). Chemically reduced tea waste biochar and its application in treatment of fluoride containing wastewater: Batch and optimization using response surface methodology. *Process Safety and Environmental Protection*, *116*, 553–563. https://doi.org/10.1016/j.psep.2018.03.009

Saha, N., Das, L., Das, P., Bhowal, A., & Bhattacharjee, C. (2021). Comparative experimental and mathematical analysis on removal of dye using raw rice husk, rice husk charcoal and activated rice husk charcoal: batch, fixed-bed column, and mathematical modeling. *Biomass Conversion and Biorefinery*. https://doi.org/10.1007/s13399-021-01996-8

Sahoo, T. R., & Prelot, B. (2020). Chapter 7 - Adsorption processes for the removal of contaminants from wastewater: the perspective role of nanomaterials and nanotechnology. In *Nanomaterials for the Detection and Removal of Wastewater Pollutants*. Elsevier Inc. https://doi.org/10.1016/B978-0-12-818489-9.00007-4

Saleem, H., Haneef, M., & Abbasi, H. Y. (2018). Synthesis route of reduced graphene oxide via thermal reduction of chemically exfoliated graphene oxide. *Materials Chemistry and Physics*, *204*, 1–7. https://doi.org/10.1016/j.matchemphys.2017.10.020

Saryel-deen, R. A., Mahmoud, A. S., Mahmoud, M. S., & Mostafa, M. K. (2017). *Adsorption and Kinetic Studies of using Entrapped Sewage Sludge Ash in the Removal of Chemical Oxygen Demand from Domestic Wastewater , with Artificial Intelligence Approach Adsorption and Kinetic Studies of using Entrapped Sewage Sludge Ash in the Remova*. *November*.

Schneider, J., Matsuoka, M., Takeuchi, M., Zhang, J., Horiuchi, Y., Anpo, M., & Bahnemann, D. W. (2014). *Understanding TiO 2 Photocatalysis : Mechanisms and Materials*.

Shankar, A., & Teppala, S. (2012). *Urinary Bisphenol A and Hypertension in a Multiethnic Sample of US Adults*. *2012*. https://doi.org/10.1155/2012/481641

Sharma, N., Arif, M., Monga, S., Shkir, M., Mishra, Y. K., & Singh, A. (2020). Applied Surface Science Investigation of bandgap alteration in graphene oxide with different reduction routes. *Applied Surface Science*, *513*(December 2019), 145396. https://doi.org/10.1016/j.apsusc.2020.145396

Shen, Y., Zhu, C., Chen, B., Chen, J., Fang, Q., Wang, J., He, Z., & Song, S. (2020). Novel photocatalytic performance of nanocage-like MIL-125-NH2induced by adsorption of phenolic pollutants. In *Environmental Science: Nano* (Vol. 7, Issue 5). https://doi.org/10.1039/d0en00120a

Shen, Y., Zhu, C., Chen, J., Fang, Q., Chen, W., He, Z., & Xu, H. (2020). A hybrid block consisting of covalent triazine frameworks and GO aerogel with switchable selectivity between adsorption of UV fi lters and regeneration under sunlight. *Chemical Engineering Journal*, *395*(January), 125074. https://doi.org/10.1016/j.cej.2020.125074

Shen, Y., Zhu, C., Song, S., Zeng, T., Li, L., & Cai, Z. (2019). Defect-Abundant Covalent Triazine Frameworks as Sunlight-Driven Self-Cleaning Adsorbents for Volatile Aromatic Pollutants in Water. *Environmental Science and Technology*, *53*(15), 9091–9101. https://doi.org/10.1021/acs.est.9b02222

Shu, X., Tang, S., Peng, C., Gao, R., Yang, S., Luo, T., Cheng, Q., & Wang, Y. (2018). Bisphenol A is not associated with a 5 - year incidence of type 2 diabetes : a prospective nested case – control

study. *Acta Diabetologica*. https://doi.org/10.1007/s00592-018-1104-4

Shukla, N., Sahoo, D., & Remya, N. (2019). Biochar from microwave pyrolysis of rice husk for tertiary wastewater treatment and soil nourishment. *Journal of Cleaner Production*, *235*, 1073–1079. https://doi.org/10.1016/j.jclepro.2019.07.042

Siew, A., Le, H., Thiovolet, M., Gellert, P., Schatzlein, A., & Uchegbu, I. (2012). Enhanced Oral Absorption of Hydrophobic and Hydrophilic Drugs Using Quaternary Ammonium Palmitoyl Glycol Chitosan Nanoparticles. *Molecular Pharmaceuticals*, *9*, 14–28.

Silva, C. P., Pereira, D., Calisto, V., Martins, M. A., Otero, M., Esteves, V. I., & Lima, D. L. D. (2021). Biochar-TiO2 magnetic nanocomposites for photocatalytic solar-driven removal of antibiotics from aquaculture effluents. *Journal of Environmental Management*, *294*(April). https://doi.org/10.1016/j.jenvman.2021.112937

Singh, B., & Sharma, N. (2008). *Development of novel hydrogels by functionalization of sterculia gum for use in anti-ulcer drug delivery*. *74*, 489–497. https://doi.org/10.1016/j.carbpol.2008.04.003

Singh, M. K., & Mehata, M. S. (2019). Phase-dependent optical and photocatalytic performance of synthesized titanium dioxide (TiO2) nanoparticles. *Optik*, *193*, 163011. https://doi.org/10.1016/j.ijleo.2019.163011

Sophia, A. C., Lima, E. C., Allaudeen, N., Rajan, S., Sophia, A. C., Lima, E. C., Allaudeen, N., & Rajan, S. (2016). Application of graphene based materials for adsorption of pharmaceutical traces from water and wastewater- a review. *Desalination and Water Treatment*, *3994*, 1–14. https://doi.org/10.1080/19443994.2016.1172989

Sun, S., Li, C., Sun, J., & Shi, S. (2009). *Decolorization of an azo dye Orange G in aqueous solution by Fenton oxidation process : Effect of system parameters and kinetic study*. *161*, 1052–1057. https://doi.org/10.1016/j.jhazmat.2008.04.080

Tan, G., Wu, Y., Liu, Y., & Xiao, D. (2018). *Removal of Pb ( II ) ions from aqueous solution by manganese oxide coated rice straw biochar – A low-cost and highly effective sorbent*. *0*, 1–8. https://doi.org/10.1016/j.jtice.2017.12.031

Tan, X., Liu, Y., Zeng, G., Wang, X., Hu, X., & Gu, Y. (2015). Chemosphere Application of biochar for the removal of pollutants from aqueous solutions. *CHEMOSPHERE*. https://doi.org/10.1016/j.chemosphere.2014.12.058

Tan, Z., Wang, Y., Huang, C., & Ai, P. (2016). *Cadmium removal potential by rice straw-derived magnetic biochar*. *2*(Marousek 2014). https://doi.org/10.1007/s10098-016-1264-2

Tebeje, A., Worku, Z., Nkambule, T. T. I., & Fito, J. (2020). Adsorption of Methylene Blue from Textile Industrial Wastewater onto Activated Carbon of Parthenium hysterophorus Adsorption of chemical oxygen demand from textile industrial wastewater through locally prepared bentonite adsorbent. *International Journal of Environmental Science and Technology*, *May 2021*. https://doi.org/10.1007/s13762-021-03230-4

Thalla, A. K. (2020). *Occurrence and environmental risks of nonsteroidal anti-inflammatory drugs in urban wastewater in the southwest monsoon region of India*.

Tian, Y., Xia, X., Wang, J., Zhu, L., Wang, J., Zhang, F., & Ahmad, Z. (2019). Chronic Toxicological Effects of Carbamazepine on Daphnia magna Straus : Effects on Reproduction Traits , Body Length , and Intrinsic Growth. *Bulletin of Environmental Contamination and Toxicology*, *103*(5), 723–728. https://doi.org/10.1007/s00128-019-02715-w

Tomul, F., Arslan, Y., Kabak, B., Kendüzler, E., Lima, E. C., & Nguyen, H. (2020). *Science of the Total Environment Peanut shells-derived biochars prepared from different carbonization processes : Comparison of characterization and mechanism of naproxen adsorption in water*. *726*. https://doi.org/10.1016/j.scitotenv.2020.137828

Trojanowicz, M., Bojanowska-czajka, A., Szreder, T., Bobrowski, K., & Fornal, E. (2020). Application of ionizing radiation for removal of endocrine disruptor bisphenol A from waters and wastewaters. *Chemical Engineering Journal*, 126169. https://doi.org/10.1016/j.cej.2020.126169

Trovo, A. G., Hassan, A. K., Sillanpa¨a¨, M., & Tang, W. Z. (2016). Degradation of Acid Blue 161 by Fenton and photo-Fenton processes. *International Journal of Environmental Science and Technology*, *13*, 147–158. https://doi.org/10.1007/s13762-015-0854-6

Tshangana, C. S., Muleja, A. A., Kuvarega, A. T., Malefetse, T. J., & Mamba, B. B. (2021). Journal of Water Process Engineering The applications of graphene oxide quantum dots in the removal of emerging pollutants in water : An overview. *Journal of Water Process Engineering*, *43*(July), 102249. https://doi.org/10.1016/j.jwpe.2021.102249

Vasquez-Medrano, R., Prato-garcia, D., & Vedrenne, M. (2018). *Ferrioxalate-Mediated Processes*. https://doi.org/10.1016/B978-0-12-810499-6.00004-8

Velásquez, M., Santander, I. P., Contreras, D. R., Yáñez, J., Salazar, R. A., & Mansilla, H. D. (2014). Oxidative degradation of sulfathiazole by Fenton and photo-Fenton reactions Oxidative degradation of sulfathiazole by Fenton and photo-Fenton reactions. *Journal of Environmental Science and Health, Part A: Toxic/Hazardous Substances and Environmental Engineering*, *49*(September), 37–41. https://doi.org/10.1080/10934529.2014.865447

Wang, H., Shen, H., Shen, C., Li, Y., Ying, Z., & Duan, Y. (2019). Kinetics and Mechanism Study of Mercury Adsorption by Activated Carbon in Wet Oxy-Fuel Conditions [Research-article]. *Energy & Fuels*, *33*, 1344–1353. https://doi.org/10.1021/acs.energyfuels.8b03610

Wang, Jinfeng, Tsuzuki, T., Tang, B., Hou, X., Sun, L., & Wang, X. (2012). Reduced graphene oxide/ZnO composite: Reusable adsorbent for pollutant management. *ACS Applied Materials and Interfaces*, *4*(6), 3084–3090. https://doi.org/10.1021/am300445f

Wang, Jun, Chen, Z., & Chen, B. (2014). Adsorption of polycyclic aromatic hydrocarbons by graphene and graphene oxide nanosheets. *Environmental Science and Technology*, *48*(9), 4817–4825. https://doi.org/10.1021/es405227u

Wang, S., Cole, I., & Li, Q. (2016). Quantum-confined bandgap narrowing of TiO2 nanoparticles by graphene quantum dots for visible-light-driven applications. *Chemical Communications*, *52(59)*, 9208–9211. https://doi.org/10.1039/x0xx00000x

Wang, Y., Wei, X., Qi, Y., & Huang, H. (2021). Efficient removal of bisphenol-A from water and wastewater by Fe2O3-modified graphene oxide. *Chemosphere*, *263*. https://doi.org/10.1016/j.chemosphere.2020.127563

Williams, G., Seger, B., & Kamat, P. V. (2008). *UV-Assisted Photocatalytic Reduction of Graphene Oxide*. *2*(7), 1487–1491.

Wisniewski, P., Romano, R. M., Kizys, M. M. L., Oliveira, K. C., Kasamatsu, T., Giannocco, G., Chiamolera, M. I., Dias-da-silva, M. R., & Romano, M. A. (2015). Adult exposure to bisphenol A ( BPA ) in Wistar rats reduces sperm quality with disruption of the hypothalamic – pituitary – testicular axis. *Toxicology*, *329*, 1–9. https://doi.org/10.1016/j.tox.2015.01.002

Wojcieszyńska, D., & Guzik, U. (2020). *Naproxen in the environment : its occurrence , toxicity to nontarget organisms and biodegradation*. 1849–1857.

Wu, S., Yang, D., Zhou, Y., Zhou, H., Ai, S., Yang, Y., Wan, Z., Luo, L., Tang, L., & Tsang, D. C. W. (2020). Simultaneous degradation of p-arsanilic acid and inorganic arsenic removal using M-rGO/PS Fenton-like system under neutral conditions. *Journal of Hazardous Materials*, *399*, 123032. https://doi.org/10.1016/j.jhazmat.2020.123032

Xiang, C., Li, M., Zhi, M., Manivannan, A., & Wu, N. (2012). Reduced graphene oxide/titanium dioxide composites for supercapacitor electrodes: Shape and coupling effects. *Journal of Materials Chemistry*, *22*(36), 19161–19167. https://doi.org/10.1039/c2jm33177b

Xu, C., Cui, A., Xu, Y., & Fu, X. (2013). Graphene oxide – TiO 2 composite filtration membranes and their potential application for water purification. *Carbon*, *62*, 465–471.

https://doi.org/10.1016/j.carbon.2013.06.035

Xu, J., Wang, L., & Zhu, Y. (2012). Decontamination of bisphenol A from aqueous solution by graphene adsorption. *Langmuir*, *28*(22), 8418–8425. https://doi.org/10.1021/la301476p

Xu, L., Yang, L., Johansson, E. M. J., Wang, Y., & Jin, P. (2018). Photocatalytic activity and mechanism of bisphenol a removal over TiO2−x/rGO nanocomposite driven by visible light. *Chemical Engineering Journal*, *350*, 1043–1055. https://doi.org/10.1016/j.cej.2018.06.046

Yang, X., Qin, J., Li, Y., Zhang, R., & Tang, H. (2013). Graphene-spindle shaped TiO2 mesocrystal composites: Facile synthesis and enhanced visible light photocatalytic performance. *Journal of Hazardous Materials*, *261*, 342–350. https://doi.org/10.1016/j.jhazmat.2013.07.044

Ye, F., Wang, Z., Mi, Y., Kuang, J., Jiang, X., Huang, Z., Luo, Y., Shen, L., Yuan, H., & Zhang, Z. (2020). Preparation of reduced graphene oxide/titanium dioxide composite materials and its application in the treatment of oily wastewater. In *Colloids and Surfaces A: Physicochemical and Engineering Aspects* (Vol. 586). Elsevier B.V. https://doi.org/10.1016/j.colsurfa.2019.124251

Ye, Y., Zhou, Q., Feng, L., Wu, J., Xiong, Y., & Li, X. (2018). *Maternal serum bisphenol A levels and risk of pre-eclampsia : a nested case – control study*. *27*(6), 1102–1107. https://doi.org/10.1093/eurpub/ckx148

Yu, F., Bai, X., Yang, C., Xu, L., & Ma, J. (2019). Reduced graphene oxide–P25 nanocomposites as efficient photocatalysts for degradation of bisphenol a in water. *Catalysts*, *9*(7). https://doi.org/10.3390/catal9070607

Zhang, Hanyu, Wang, Z., Li, R., Guo, J., Li, Y., Zhu, J., & Xie, X. (2017). TiO2 supported on reed straw biochar as an adsorptive and photocatalytic composite for the efficient degradation of sulfamethoxazole in aqueous matrices. *Chemosphere*, *185*, 351–360. https://doi.org/10.1016/j.chemosphere.2017.07.025

Zhang, Hao, Peng, L., Chen, A., Shang, C., Lei, M., He, K., Luo, S., Shao, J., & Zeng, Q. (2019). Chitosan-stabilized FeS magnetic composites for chromium removal : Characterization , performance , mechanism , and stability. *Carbohydrate Polymers*, *214*(March), 276–285. https://doi.org/10.1016/j.carbpol.2019.03.056

Zhang, K., Sun, P., Faye, M. C. A. S., & Zhang, Y. (2018). Characterization of biochar derived from rice husks and its potential in chlorobenzene degradation. *Carbon*, *130*, 730–740. https://doi.org/10.1016/j.carbon.2018.01.036

Zhang, M., Dong, H., Zhao, L., Wang, D., & Meng, D. (2019). Science of the Total Environment A

review on Fenton process for organic wastewater treatment based on optimization perspective. *Science of the Total Environment*, *670*, 110–121. https://doi.org/10.1016/j.scitotenv.2019.03.180

Zhang, Yongjun, Geißen, S., & Gal, C. (2008). Carbamazepine and diclofenac : Removal in wastewater treatment plants and occurrence in water bodies. *Chemosphere*, *73*(8), 1151–1161. https://doi.org/10.1016/j.chemosphere.2008.07.086

Zhang, Yu, Cui, W., An, W., Liu, L., Liang, Y., & Zhu, Y. (2018). Combination of photoelectrocatalysis and adsorption for removal of bisphenol A over TiO2-graphene hydrogel with 3D network structure. *Applied Catalysis B: Environmental*, *221*(June 2017), 36–46. https://doi.org/10.1016/j.apcatb.2017.08.076

Zhou, A., Wu, X., Chen, W., Liao, L., & Xie, P. (2020). Fabrication of Hydrophobic/Hydrophilic Bifunctional Adsorbent for the Removal of Sulfamethoxazole and Bisphenol A in Water. *Biochemical Pharmacology*, *June*, 104161. https://doi.org/10.1016/j.jece.2020.104161

Zhou, Y., Cao, S., Xi, C., Li, X., Zhang, L., Wang, G., & Chen, Z. (2019). Bioresource Technology A novel Fe 3 O 4 / graphene oxide / citrus peel-derived bio-char based nanocomposite with enhanced adsorption a ffi nity and sensitivity of cipro fl oxacin and spar fl oxacin. *Bioresource Technology*, *292*(July), 121951. https://doi.org/10.1016/j.biortech.2019.121951

Zhu, C., Xu, J., Song, S., Wang, J., Li, Y., Liu, R., & Shen, Y. (2020a). Science of the Total Environment TiO 2 quantum dots loaded sulfonated graphene aerogel for effective adsorption-photocatalysis of PFOA. *Science of the Total Environment*, *698*, 134275. https://doi.org/10.1016/j.scitotenv.2019.134275

Zhu, C., Xu, J., Song, S., Wang, J., Li, Y., Liu, R., & Shen, Y. (2020b). TiO2 quantum dots loaded sulfonated graphene aerogel for effective adsorption-photocatalysis of PFOA. *Science of the Total Environment*, *698*, 134275. https://doi.org/10.1016/j.scitotenv.2019.134275

Ziegmann, M., & Frimmel, F. H. (2010). Photocatalytic degradation of clofibric acid, carbamazepine and iomeprol using conglomerated TiO2 and activated carbon in aqueous suspension. *Water Science and Technology*, *61*(1), 273–281. https://doi.org/10.2166/wst.2010.812

# LIST OF PUBLICATIONS

1. **List of papers published in journals :-**

**1.1.>** Manna, S., **Bhattacharya, S.,** Sengupta, S., & Das, P. (2018). Synthesis of graphene oxide dots coated biomatrices and its application for the removal of multiple pollutants present in wastewater. *Journal of Cleaner Production*, *203*, 83-88. https://doi.org/10.1016/j.jclepro.2018.08.261

**1.2.>** Bhattacharyya, S., Banerjee, P., **Bhattacharya, S.,** Rathour, R. K. S., Majumder, S. K., Das, P., & Datta, S. (2018). Comparative assessment on the removal of ranitidine and prednisolone present in solution using graphene oxide (GO) nanoplatelets. *Desalin Water Treat*, *132*, 287-296. doi:10.5004/dwt.2018.23170

**1.3.>** **Bhattacharya, S.,** Banerjee, P., Das, P., Bhowal, A., Majumder, S. K., & Ghosh, P. (2020). Removal of aqueous carbamazepine using graphene oxide nanoplatelets: process modelling and optimization. *Sustainable Environment Research*, *30*(1), 1-12. https://doi.org/10.1186/s42834-020-00062-8

**1.4.>** Ganguly, P., Sarkhel, R., **Bhattacharya, S.,** Das, P., Saha, A., & Bhowal, A. (2020). Integral approach of treatment of phenolic wastewater using nano-metal coated graphene oxide in combination with advanced oxidation. *Surfaces and Interfaces*, *21*, 100660. https://doi.org/10.1016/j.surfin.2020.100660

**1.5.>** **Bhattacharya, S.,** Das, P., Bhowal, A., & Saha, A. (2021). Thermal, Chemical and ultrasonic assisted synthesis of carbonized Biochar and its application for reducing Naproxen: Batch and Fixed bed study and subsequent optimization with response surface methodology (RSM) and artificial neural network (ANN). *Surfaces and Interfaces*, *26*, 101378. https://doi.org/10.1016/j.surfin.2021.101378

**1.6.>** **Bhattacharya, S.,** Das, P., Bhowal, A., & Majumder, S. K. (2022). Metal-oxide coated Graphene oxide nano-composite for the treatment of pharmaceutical compound in photocatalytic reactor: Batch, Kinetics and Mathematical Modeling using Response Surface Methodology and Artificial Neural Network. *Environmental Science and Pollution Research*, 1-16. http://10.1007/s11356-021-18227-2

**1.7 .>** Das, S., **Bhattacharya, S.,** & Das, P. (2022). Titanium oxide–coated coconut husk–derived biochar composite and its application for removal of crystal violet dye. *Biomass Conversion and Biorefinery*, 1-17. http:// 10.1007/s13399-022-02956-6

**2. List of Book Chapters**

**2.1.>** Banerjee, P., **Bhattacharya, S.,** Das, R., Das, P., & Mukhopadhyay, A. (2021). Microfiltration and Ultrafiltration Membranes for Water Purification. *Polymeric Membranes for Water Purification and Gas Separation*, *113*, 33-68. https://doi.org/10.21741/9781644901632-3.

**2.2.>** **Bhattacharya, S**., Banerjee, P., & Das, P. (2023). Graphene Oxide-Based Nanocomposites for Wastewater Treatment. *Carbon Composites: Composites with Nanotubes, Nanomaterials, and Graphene Oxide*, 79

**List of Patents :** Nil

# LIST OF CONFERENCE PRESENTATION

1. **Sandipan Bhattacharya**, Papita Das, Avijit Bhowal. Removal of Chlorothiazide from its aqueous solution using graphene oxide as an adsorbent, 12th All India Peoples' technology congress organised by forum of scientists, engineers & technologists (FOSET) held at:- National Institute of Technical Teachers' Training and Research, Kolkata on 16th and 17th February, 2019.

2. **Sandipan Bhattacharya**, Papita Das, Avijit Bhowal. Removal of Cetrizine with Graphene Oxide as an Adsorbent, International Conference on "Emerging Trends for Sustainable Development, 2019", Organized By: Government College Of Engineering And Leather Technology. Date :- 5th - 6th March, 2019 (Oral)

3. **Sandipan Bhattacharya**, Papita Das, Avijit Bhowal, Subrata Majumdar and Pallab Ghosh. The Use Of GO-TiO$_2$ Nanocomposite For The Purpose Of Removing Rantidine From Its Aqueous Solution Under UVA Radiation. International ConferenceOn Sustainable Water Resources Management under Changed Climate. Organized By:- School of Water Resources Engineering, Jadavpur Universityu. In Joint Collaboration with Women's College Calcutta (Department of Geography)& National Institute of Technology, Durgapur. Held at :- Jadavpur University on 13$^{th}$ -15$^{th}$ March, 2020.

4. **Sandipan Bhattacharya**, Papita Das, and Avijit Bhowal. Synthesis of activated biochar from rice straw for the purpose of removing Bisphenol A from water, International Conference on Chemical Engineering Innovations and Sustainability. Organized By :- Chemical Engineering Department, Jadavpur University. Held during 26$^{th}$-27$^{th}$ February, 2023 at Jadavpur University, Kolkata, India.

**RESEARCH**                                                                                          **Open Access**

# Removal of aqueous carbamazepine using graphene oxide nanoplatelets: process modelling and optimization

Sandipan Bhattacharya[1], Priya Banerjee[2], Papita Das[1,3]* , Avijit Bhowal[1,3], Subrata K. Majumdar[4] and Pallab Ghosh[4]

## Abstract

Unplanned and unmonitored developmental activities have resulted in a rapid emergence of pollutants like pharmaceuticals and personal care products (PPCPs) in the environment. These PPCPs are considered as potential health hazards. A wide variety of physical, biological and chemical processes are presently being investigated for ensuring the efficient removal of such pollutants from effluents. The present study investigates the potential of graphene oxide nanoplatelets (GONPs) for removal of a common and extensively used drug, Carbamazepine (CBZ) from aqueous solutions. Batch studies were performed to assess the potential of graphene oxide for adsorption of CBZ under different conditions of initial CBZ concentration, adsorbent dosage, temperature and solution pH. Process optimization was performed using Response Surface Methodology and Artificial Neural Network modelling. Results obtained indicated 99% CBZ removal under optimum solution pH, adsorbent dosage and treatment duration of 6, 1 g $L^{-1}$ and 120 min respectively. Results revealed that CBZ adsorption by GONPs followed Temkin isotherm and pseudo second order kinetics. A subsequent reusability study established that the GONPs could be reused for up to 8 times without any loss of adsorption efficiency. Therefore, it can be concluded that graphene oxide reported herein has immense potential for adsorption of trace organic pollutants from aqueous phases.

**Keywords:** Emerging pollutants, Graphene oxide, Carbamazepine, Adsorption, Wastewater treatment

## Introduction

Pharmaceutical wastes present in effluents are rapidly becoming issues of immense concern on a global scale [1]. Wide use and disposal of these products have resulted in a rapid rate of accumulation of the same in adjacent aquatic environments [2, 3]. Carbamazepine (CBZ; $C_{15}H_{12}N_2O$) is one such widely consumed antiepileptic drug which is primarily prescribed as sedative to patients suffering from depression, post-traumatic stress disorder, restless leg syndrome, diabetes insipidus, pain and neurological syndromes [4–6].

Previous studies have reported a global yearly CBZ usage of approximately 1.01 kt. Such substantial usage of CBZ has resulted in its appearance in different sources of water including surface water, ground water, wastewater treatment plants and even drinking water. Therefore, presence of CBZ in different water resources is being considered as an issue of global concern [7–14]. CBZ reportedly exerts toxic effects on aquatic life including bacteria, algae, invertebrates and fish [15]. Permissible limit of CBZ in drinking water sources varies in different countries and is found to be 40 and 100 µg $L^{-1}$ in Minnesota, U.S and Australia respectively [16]. Moreover, use of water bearing CBZ for irrigation results in accumulation of the same in soil [17]. The standard concentration of CBZ in soils irrigated using wastewaters has been found to be 0.02–15 µg $kg^{-1}$ [18]. According to the US Food and Drug Administration, an environment

* Correspondence: papitasaha@gmail.com
[1]Department of Chemical Engineering, Jadavpur University, Kolkata 700032, India
[3]School of Advanced Studies in Industrial Pollution Control Engineering, Jadavpur University, Kolkata 700032, India
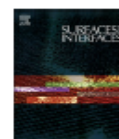Full list of author information is available at the end of the article

# Thermal, Chemical and ultrasonic assisted synthesis of carbonized Biochar and its application for reducing Naproxen: Batch and Fixed bed study and subsequent optimization with response surface methodology (RSM) and artificial neural network (ANN)

Sandipan Bhattacharya[a], Papita Das[a,b,*], Avijit Bhowal[a,b], Abhijit Saha[c]

[a] Department of Chemical Engineering, Jadavpur University, Kolkata, India
[b] School of Advanced Studies in Industrial Pollution Control Engineering, Jadavpur University, Kolkata, India
[c] UGC-DAE Consortium for Scientific Project, Kolkata, India

## ARTICLE INFO

## ABSTRACT

An adsorbent was synthesized using a cheap and locally available raw material, rice straw which was treated thermally and then chemically to form an activated rice straw biochar (ARSB). The ARSB was used for removing Naproxen, a widely used pharmaceutical compound. ARSB was used for the removing of Naproxen using both a batch and column study. The batch study was further optimised with using optimizing tools like artificial neural network (ANN) and response surface methodology (RSM). The isotherm, kinetics and thermodynamics of the adsorption process was analysed using the data of the batch study. A detailed analysis of the characteristics of ARSB was done by different characterization methods in order to acquire an in depth knowledge of its structural and functional characteristics. The highest removal was observed as 89.78% from batch study and 97.54% from Optimization study at pH 4, dose of 2.8 g/L using RSM. The adsorption of Naproxen on the ARSB was deduced to be following the Tempkin Isotherm and Pseudo second order kinetics. In case of the column study the highest efficiency was exhibited by the bed height of 7.62 cm and adsorbate concentration of 10 mg/L. The column study data was best explained by the Thomas model of column kinetics. From the regeneration study, it was found that the ARSB was able to maintain its effectivity even after repeated cycles of reuse.

## 1. Introduction

In the contemporary era, different type of emerging pollutants has become a major issue for the environment due to their ubiquitous and pervasive nature. Trace pharmaceuticals residues mainly found in the aquatic environment forms a major group of these emerging pollutants and are a cause of major concern due to their chemically active and persistent nature. Pharmaceuticals contaminants enter the environment mainly by the four probable routes:- (1) As an non metabolized component of human and animal waste, (2) Inadequate disposal of unused or expired medicine, (3) In the form of effluent generated from hospital (4) Waste effluent generated from pharmaceutical industry [46]. Naproxen ($C_{14}H_{14}O_3$) is a well-known and widely used broad range, NSAID (non-steroidal anti-inflammatory drug) [48]. Naproxen is widely prescribed for the remediation of pain and swelling [13] and as

per ClinCalc [18] it is the 67th most popular drug in USA with 11,942,765 annual prescriptions. And as a consequence of its widespread utilization, Naproxen has been found in a range of locations consisting of both natural and man-made aquatic environments and thereby poses a health risk to any organisms which consumes water from these resources, including the organisms that live in these ecosystems [1, 31, 47, 49]. Also in reference to previous literature regarding the toxicity of Naproxen, it was noted that Naproxen can cause some oxidative stress and genotoxic effect in microorganisms [2, 25]. Therefore, it is very much important to make the necessary arrangements in order to remove the Naproxen from water at the earliest opportunity. There are many methods which has been explored for the purpose of removing Naproxen from the aquatic environments namely, photodegradation, photocatalysis, biodegradation, phytoremediation, membrane bioreactor, electrochemical oxidation, Fenton like oxidation, catalytic wet peroxide

---

**CURRENT TRENDS AND RESEARCH IN INDUSTRIAL WASTEWATER TREATMENT THROUGH BIOREACTOR APPROACH**

# Metal-oxide coated Graphene oxide nano-composite for the treatment of pharmaceutical compound in photocatalytic reactor: Batch, Kinetics and Mathematical Modeling using Response Surface Methodology and Artificial Neural Network

Sandipan Bhattacharya[1] · Papita Das[1,2] · Avijit Bhowal[1,2] · Subrata Kumar Majumder[3]

## Abstract

Titanium dioxide ($TiO_2$) photocatalyst has gained constant interest in the treatment of wastewater because of its greater stability, lower cost, low-toxicity, high efficiency, and more reactivity under UV radiation. On the other hand, Graphene oxide (GO) possesses high electron mobility, and therefore when GO is combined with $TiO_2$ the photocatalytic activity of $TiO_2$ is increased. In this study, nano-composite was synthesized in a hydrothermal reactor using two types of $TiO_2$ nanoparticles ($TiO_2$ consisting of a mixture of rutile and anatase phase (**Type 1**) and bioreduced $TiO_2$ (**Type 2**)) and the efficiency of both the $TiO_2$-GO nanocomposite to remove the drug Carbamazepine (CBZ) was investigated. The $TiO_2$-GO nanocomposite with the **Type 1** $TiO_2$ exhibited greater efficiency hence further studies were conducted with that composite. The efficiency of $TiO_2$-GO nanocomposite for the purpose of removing CBZ were investigated in presence of different types of incident radiation like Solar radiation, white light and three type of Ultraviolet radiation (A, B, C). The removal of the drug by $TiO_2$-GO composite has been optimized using response surface methodology and artificial neural network. From this study, the maximum reduction was observed was 91.2% and whereas in case of the RSM optimization study the maximum removal that was observed was 91.7%. The validation of the RSM model was done using the mathematical analysis of the model equation of RSM. Different kinetics models was also analyzed using the experimental data and it was observed that it followed pseudo-second-order kinetics. The optimization using ANN also showed a close interaction with the experimental results.

**Keywords** Graphene Oxide (GO) · Titanium Dioxide ($TiO_2$) · Nanocomposite · Photocatalytic reactor · RSM · ANN

## INTRODUCTION

Addressing the effect of pollution on the environment and finding the necessary solutions should be a global objective of topmost priority (Schneider et al. 2014). In the recent times, mostly due to intense anthropogenic activities, more and more pollutants are being introduced into the environment mostly in the water bodies which have negative consequences for human health and environment (Wu et al. 2020a). Rate of consumption of pharmaceuticals has rapidly gone up in the last few decades. These pharmaceutical products, if not disposed properly make their way back in the environment as persistent pollutants of the aquatic system. The level of the pharmaceutical compounds in the water remains in the range of μg/L to ng/L, but still, the continuous influx of these materials has a deleterious effect on the environment (Nawaz et al. 2017). Therefore, exploring environmentally friendly and efficient techniques to remove this type of trace organic pollutants from the environment should be a priority concern.

✉ Papita Das
  papitasaha@gmail.com

1   Department of Chemical Engineering, Jadavpur University, 188, Raja S. C. Mullick Road, Kolkata 700032, India

2   School of Advanced Studies in Industrial Pollution Control Engineering, Jadavpur University, Kolkata, India

3   Department of Chemical Engineering, Indian Institute of Technology, Guwahati, India

🌀 Springer

## CHAPTER 4

# Graphene Oxide-Based Nanocomposites for Wastewater Treatment

SANDIPAN BHATTACHARYA,[1] PRIYA BANERJEE,[2] and PAPITA DAS[1,3]

[1]Department of Chemical Engineering, Jadavpur University, Kolkata – 700032, West Bengal, India

[2]Department of Environmental Studies, CDOE Rabindra Bharati University, Kolkata – 700091, West Bengal, India

[3]School of Advanced Studies in Industrial Pollution Control Engineering, Jadavpur University, Kolkata – 700032, West Bengal, India

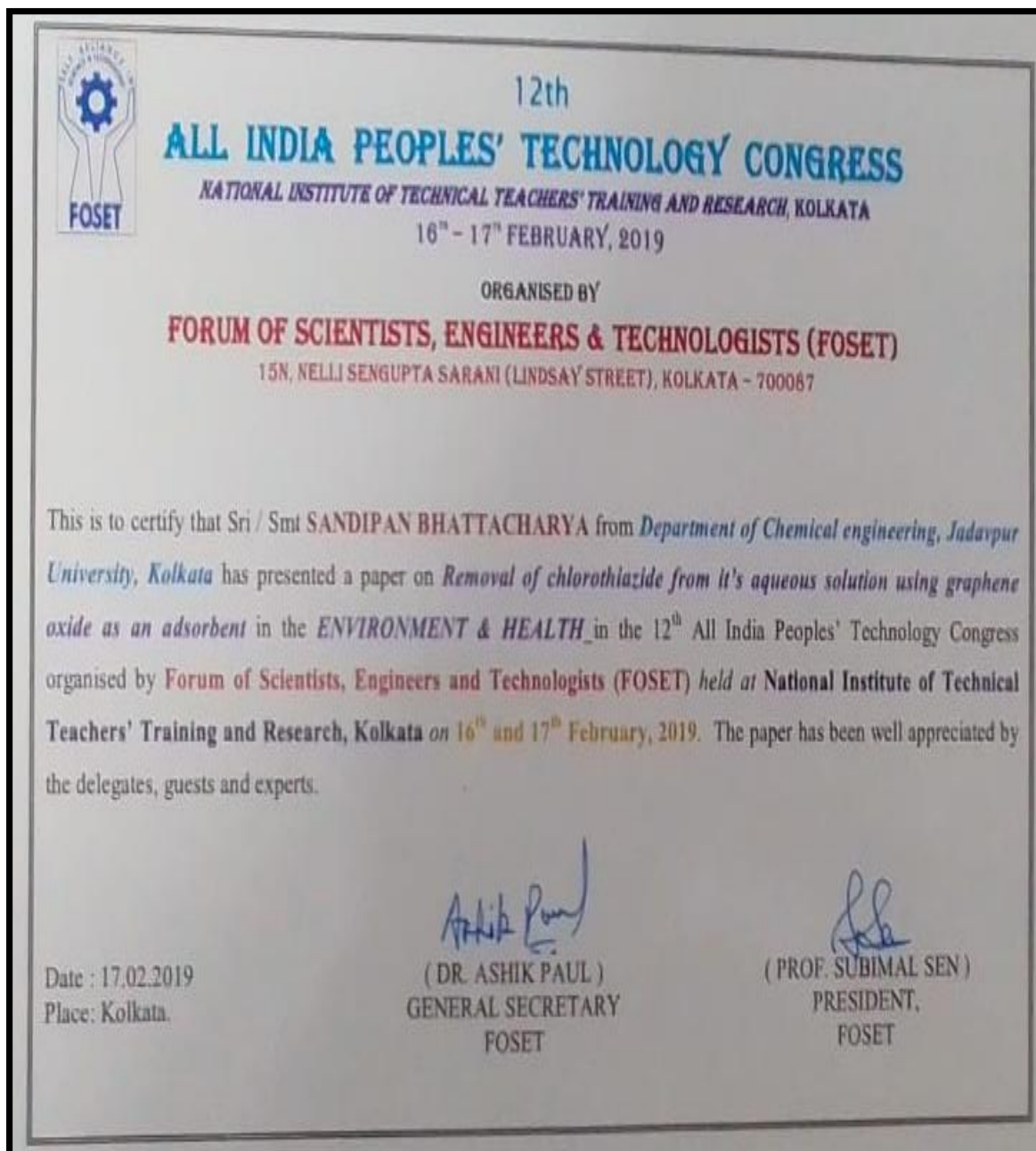*Corresponding author. E-mail: prya_bnrje@yahoo.com

### ABSTRACT

Pharmaceuticals and personal care products (PPCP) are widely used for medicinal and cosmetic purposes. Due to their extensive use in recent times, PPCPs are emerging as a prominent group of micropollutants with near universal presence. PPCPs are frequently encountered as a trace pollutant in almost every water body (lakes, rivers, and oceans). PPCPs are considered to be a reason for concern due to their persistent nature, ability to bioaccumulate in bodies of the organism, and their ability to induce a physiological effect even at a very low concentration. Recent studies have reported the adverse effects of PPCPs on different forms of life. Traditional water treatment plants are not capable of complete removal of these PPCPs from contaminated water. Therefore, advanced water

# CERTIFICATES OF CONFERENCE ATTENDED



12th

## ALL INDIA PEOPLES' TECHNOLOGY CONGRESS
*NATIONAL INSTITUTE OF TECHNICAL TEACHERS' TRAINING AND RESEARCH, KOLKATA*
16ᵗʰ – 17ᵗʰ FEBRUARY, 2019

ORGANISED BY

## FORUM OF SCIENTISTS, ENGINEERS & TECHNOLOGISTS (FOSET)
15N, NELLI SENGUPTA SARANI (LINDSAY STREET), KOLKATA – 700087

This is to certify that Sri / Smt **SANDIPAN BHATTACHARYA** from *Department of Chemical engineering, Jadavpur University, Kolkata* has presented a paper on *Removal of chlorothiazide from it's aqueous solution using graphene oxide as an adsorbent* in the *ENVIRONMENT & HEALTH* in the 12ᵗʰ All India Peoples' Technology Congress organised by Forum of Scientists, Engineers and Technologists (FOSET) *held at* **National Institute of Technical Teachers' Training and Research, Kolkata** *on* 16ᵗʰ and 17ᵗʰ February, 2019. The paper has been well appreciated by the delegates, guests and experts.

Date : 17.02.2019
Place: Kolkata.

( DR. ASHIK PAUL )
GENERAL SECRETARY
FOSET

( PROF. SUBIMAL SEN )
PRESIDENT,
FOSET

# ICETSD '19

International Conference on Emerging Technologies for Sustainable Development

Certificate of Presentation

This is to certify that......Sandipan Bhattacharya......has presented the paper (oral/poster) entitled......Removal of Cetrizine using Graphene Oxide as an Adsorbent......in the "International Conference on Emerging Technologies for Sustainable Development" held at Eastern Zonal Cultural Centre & GCELT, Kolkata, India on 5th & 6th March, 2019.

Organized by
Government College of Engineering and Leather Technology, Kolkata, India

| Professor Sanjoy Chakraborty | Dr. Anup Dey | Sarit Chakraborty | Dr. Nayan Ranjan Singha |
| OIC, GCELT & Patron, | General Chair, | General Co-Chair, | Coordinator, |
| ICETSD '19 | ICETSD '19 | ICETSD '19 | ICETSD '19 |

274

CERTIFICATE OF PARTICIPATION

**International Conference on Chemical Engineering
Innovations and Sustainability (ICEIS-2023)**

**Chemical Engineering Department, Jadavpur University**

This is to certify that

# Sandipan Bhattacharya

*Jadavpur University, Kolkata, India*

Orally presented technical paper entitled "Synthesis of activated biochar from rice straw for the purpose of removing Bisphenol A from water" in ICEIS-2023 held during 26th-27th February, 2023 at Jadavpur University, Kolkata, India

PROF. RAJAT CHAKRABORTY

Chairman, ICEIS 2023

PROF. RANJANA CHOWDHURY     PROF. KAJARI KARGUPTA     PROF. PAPITA DAS

Joint Conveners, ICEIS 2023